NATIONAL ENERGY AUTHORITY
Geoscience Division

Short report SÞG 01/00
Project No. 720 105

An unusual permeability anomaly in a Pleistocene shield-lava in Öskjuhlíð, Iceland - A study based on empirical relationships between petrophysical parameters, mineralogy and chemical composition

by

Steinar Þór Guðlaugsson

ABSTRACT

The permeability of an olivine tholeiite lava flow of Pleistocence age in Öskjuhlíð, Iceland, shows a peculiar distribution: In the highly porous margins of the flow, the permeability is an order of magnitude lower than in the less porous inner part. This behavior is opposite to the general trend in a very loose empirical relationship between permeability and porosity in Icelandic rocks. It demonstrates that the distribution of non-fracture-related permeabilities in the basaltic rock sequences, which host the geothermal systems of Iceland, cannot be fully understood unless studied at the level of the individual building blocks of the the lava pile. A large number of core samples were taken from the flow and the petrophysical properties, geometry of the pore space, mineralogy and geochemical composition studied in detail in order to determine the reason for the unusual permeability distribution. Analysis of petrophysical measurements revealed that the permeability-vs-porosity anomaly is only one aspect of the anomalous behavior of the Öskjuhlíð samples. The high permeability - low porosity samples are also characterized by low seismic velocity and high grain density. The preferred explanation of the permeability anomaly is that the presence of an extensive, connected network of grain-boundary microcracks is the feature that causes high permability in the coarse-grained inner part of the flow. Changes in the ratio of vesicular to intercrystalline porosity and the influence of a low-permeability glass coating around vesicles are unlikely to be the primary causes of the anomaly. An attractive feature of the microcrack model is that it potentially provides an explanation for the simultaneous jump not only in permability and sonic velocity between the margins and inner part of the flow, but also for the corresponding jump in grain density. According to the model, the absence of a network of microcracks allows a greater number of isolated pores to exist within the margins of the flow than in its inner part, thus lowering the apparent grain density. Testing of this hypothesis is possible by further measurements, but to date too few samples have been tested to provide conclusive results.

Prepared for the National Energy Authority, Resource Division, January 2000

CONTENTS

LIST OF FIGURES

Figures 3.1-3.5 **Comparison of gas porosity and porosity measured in thin section**

Scatter plots with supergroups shown

3.1 Porosity measured in thin section vs gas porosity. Best line fit
3.2 Gas porosity and thin section porosity vs permeability
3.3 Gas porosity and thin section porosity vs sonic velocity
3.4 Gas porosity and thin section porosity vs thermal conductivity
3.5 Gas porosity and thin section porosity vs grain density

Figures 3.6-3.11 **Components of thin section porosity compared with petrophysical parameters**

Scatter plots with supergroups shown. Porosity in vesicles distinguished from intercrystalline porosity

3.6 Vesicle porosity and intercrystalline porosity vs gas porosity.
3.7 Vesicle porosity and intercrystalline porosity vs total thin section porosity
3.8 Vesicle porosity and intercrystalline porosity vs permeability
3.9 Vesicle porosity and intercrystalline porosity vs sonic velocity
3.10 Vesicle porosity and intercrystalline porosity vs thermal conductivity
3.11 Vesicle porosity and intercrystalline porosity vs grain density

Figures 3.12-3.17 **Ratios of vesicle porosity and intercrystalline porosity to total thin section porosity compared with petrophysical parameters**

Scatter plots with supergroups shown. Porosity in vesicles distinguished from intercrystalline porosity

3.12 Vesicle-to-total and intercrystalline-to-total thin section porosity ratios vs gas porosity
3.13 Vesicle-to-total and intercrystalline-to-total thin section porosity ratios vs total thin section porosity
3.14 Vesicle-to-total and intercrystalline-to-total thin section porosity ratios vs permeability
3.15 Vesicle-to-total and intercrystalline-to-total thin section porosity ratios vs sonic velocity
3.16 Vesicle-to-total and intercrystalline-to-total thin section porosity ratios vs thermal conductivity
3.17 Vesicle-to-total and intercrystalline-to-total thin section porosity ratios vs grain density

Figures 3.18-3.24 **Grain size compared with components of thin section porosity and petrophysical parameters**

Scatter plots with supergroups shown. Porosity in vesicles distinguished from intercrystalline porosity

3.18 Vesicle porosity and intercrystalline porosity vs grain size
3.19 Vesicle-to-total and intercrystalline-to-total thin section porosity ratios vs grain size
3.20 Grain size vs permeabilty
3.21 Grain size vs sonic velocity
3.22 Grain size vs thermal conductivity
3.23 Grain size vs grain density
3.24 Grain size vs gas porosity

Figures 4.1-4.20 **Mineral components compared with petrophysical properties**

Scatter plots with supergroups shown

4.1 Plagioclase and pyroxene vs permeability
4.2 Plagioclase and pyroxene vs sonic velocity
4.3 Plagioclase and pyroxene vs thermal conductivity
4.4 Plagioclase and pyroxene vs grain density
4.5 Plagioclase and pyroxene vs porosity
4.6 Olivine and opaque minerals vs permeability
4.7 Olivine and opaque minerals vs sonic velocity
4.8 Olivine and opaque minerals vs thermal conductivity
4.9 Olivine and opaque minerals vs grain density
4.10 Olivine and opaque minerals vs porosity
4.11 Glass rim vs permability
4.12 Glass rim vs sonic velocity
4.13 Glass rim vs thermal conductivity
4.14 Glass rim vs grain density
4.15 Glass rim vs porosity
4.16 Opaline silica vs permeability
4.17 Opaline silica vs sonic velocity
4.18 Opaline silica vs thermal conductivity
4.19 Opaline silica vs grain density
4.20 Opaline silica vs porosity

Figures 5.1--5.35 **Mineral components compared with petrophysical properties**

Scatter plots with supergroups shown

5.1 SiO2 vs permeability
5.2 SiO2 vs sonic velocity
5.3 SiO2 vs thermal conductivity
5.4 SiO2 vs grain density
5.5 SiO2 vs porosity
5.6 Al_2O_3, Fe2O3, MgO, CaO vs permeability
5.7 Al_2O_3, Fe2O3, MgO, CaO vs sonic velocity
5.8 Al_2O_3, Fe2O3, MgO, CaO vs thermal conductivity
5.9 Al_2O_3, Fe2O3, MgO, CaO vs grain density
5.10 Al_2O_3, Fe2O3, MgO, CaO vs porosity
5.11 MnO, K_2O, P_2O_5 vs permeability
5.12 MnO, K_2O, P_2O_5 vs sonic velocity
5.13 MnO, K_2O, P_2O_5 vs thermal conductivity
5.14 MnO, K_2O, P_2O_5 vs grain density
5.15 MnO, K_2O, P_2O_5 vs porosity
5.16 TiO_2, Na_2O vs permeability
5.17 TiO_2, Na_2O vs sonic velocity
5.18 TiO_2, Na_2O vs thermal conductivity
5.19 TiO_2, Na_2O vs grain density
5.20 TiO_2, Na_2O vs porosity
5.21 Cu, V, Zn, Sr, Zr vs permeability
5.22 Cu, V, Zn, Sr, Zr vs sonic velocity
5.23 Cu, V, Zn, Sr, Zr vs thermal conductivity
5.24 Cu, V, Zn, Sr, Zr vs grain density
5.25 Cu, V, Zn, Sr, Zr vs porosity
5.26 BaO, Ce, Ga, Nb, Y vs permeability
5.27 BaO, Ce, Ga, Nb, Y vs sonic velocity
5.28 BaO, Ce, Ga, Nb, Y vs thermal conductivity
5.29 BaO, Ce, Ga, Nb, Y vs grain density
5.30 BaO, Ce, Ga, Nb, Y vs porosity
5.31 Pb, Rb, Th, As vs permeability
5.32 Pb, Rb, Th, As vs sonic velocity
5.33 Pb, Rb, Th, As vs thermal conductivity
5.34 Pb, Rb, Th, As vs grain density
5.35 Pb, Rb, Th, As vs porosity

LIST OF TABLES

In the Appendix:

1 INTRODUCTION

1.1 TCP-project

The mineralogy, geochemistry and petrophysics of a single lava flow in Öskjuhlíð, Reykjavík, are being studied in detail in the Thermal Conductivity Project (TCP), a cooperative research project, between several Nordic institutions. The institutions are:

-Orkustofnun (OS), Iceland
-Orkuveita Reykjavíkur, Iceland
-Chalmers Tekniska Högskola (CTH), Sweden
-GEUS, Denmark, and
-Rogaland Research, Norway.

The original purpose of the project, was to obtain empirical constraints on possible theoretical functional relationships between the thermal conductivity and porosity of rocks. The approach chosen was to make a large number of measurements of the two parameters in a homogenous rock spanning a wide range of porosities. The Öskjuhlíð lava flow was selected for the study, because olivine tholeiite shield lavas were thought to meet these criteria, and about 100 samples were obtained for analysis.

In order to make sure that the lava flow was homogenous, the mineralogy was studied in thin sections and the chemical composition analysed. In addition to thermal conductivity and porosity, measurements were also made of the permeability, sonic P-wave velocity and grain density. This was done partly to expand the growing database on the petrophysical properties of Icelandic geothermal reservoir rocks, and also to check that the Öskjuhlíð samples were petrophysically well-behaved, i.e. did not show any unusual petrophysical behavor that might affect the study of the conductivity-porosity relationship.

During analysis of the data, however, unusual interrelationships between the petrophysical parameters emerged. In short, it was discovered that permeabilities in the core of the lava flow, where the porosity is at a minimum, were more than an order of magnitude higher than at the vesicular top and bottom of the flow. Since permeability is perhaps the key physical parameter affecting geothermal reservoirs and olivine tholeiite lava sequences commonly occur as geothermal reservoir rocks in Iceland, it was decided to expand the scope of the research project and investigate this unexpected behavior further.

1.2 Öskjuhlíð samples

The sampled lava flow is one of a composite sequence of flows originating in a single olivine tholeiite lava shield of Pleistocene age in the Reykjavík area. The Öskjuhlíð site was chosen because the lava is almost unaltered and spans a wide range of porosities. In addition, there is a quarry at the site, which makes it easy to obtain samples. The flow is coarse grained in the centre, but glassy and vesicular at the top and bottom. Some infilling of pores by light coloured opaline silica occurs at the margins, perhaps resulting from percolation of cold groundwater in glacial time.

A total of 104 core samples were taken from the lava flow. In order to span the entire porosity range, and yet be able to evaluate statistical variation in properties on a small-scale, the samples were taken in closely spaced groups at 9 different locations within the flow. A description of the site and the sampling method is available in a short report (OS Short Report, GÓF-HF-STG-SSJO - 97/06).

1.3 Permeability enigma

A general problem in both surface hydrology and geothermal reservoir studies is the dual porosity nature of Icelandic rocks and the bipolar distribution of permeabilities. Experience shows that most of the fluid circulating in geothermal reservoirs flows through a few widely spaced (tens, hundreds of meters) tectonic fractures and the flow through the intervening rock sequences, which probably occurs through a connected network of pores and microcracks, is in most cases insignificant by comparison. Fracture porosity and fracture permeability are difficult to study in the laboratory and in small cores, because fractures are frequently underrepresented in the samples. Fractured samples often fall apart and are discarded. The study of the Öskjuhlíð samples is on the other hand directed more towards the rock matrix permeabilities of geothermal systems.

In Icelandic rocks, matrix permeabilities range from $1 \cdot 10^{-3}$ to $5 \cdot 10^{4}$ mD. The corresponding range in porosities is 0-50%, and a general dependence of permeability on porosity is expected for theoretical reasons. This is also born out by measurements, which demonstrate that permeabilities generally increase with increasing porosity, at least for porosities above 15-20 %. However, the relationship is weak as the range of permeabilities measured at a given porosity can span approximately 5 orders of magnitude. A number of geological factors contribute to this scatter, including vatiations in lithology, degree of alteration, fracturing and state of stress. These factors operate through their effect on the geometry of the pore space. Studies of the permeability of Icelandic rocks have shown that the scatter may be reduced considerably if an additional (simple) parameter describing the geometry of the pore space were known.

This is what the Öskjuhlíð samples revealed: The coarse-grained inner part of the flow, which has a porosity of about 11-13 %, has permeabilities on the order of 10 mD, whereas the vesicular flow margins with a porosity of 14 - 40%, exhibit permeabilities of only 1 mD or less. This shape of the permeability-porosity relationship for the Öskjuhlíð lava flow came as a total surprise. The transition is so sharp that it indicates the presence of two different types of pore geometry in the lava flow, one type in the vesicular margins of the flow and another in the less porous core, the two seperated by an abrupt transition. Furthermore, the lack of porosity dependence on permeability within the porous margins of the flow also indicates that the pores do not become better connected with increasing porosity.

The Öskjuhlíð samples demonstrate that a large part of the scatter in the permeability-porosity relationship may arise at the level of the smallest building blocks of Icelandic stratigraphy, the single lava flow and that at this scale the relationship between porosity and permeability may be entirely different from the large-scale relationship based on a collection of all types of rock. (Figure 2.36). This indicates that a good way to improve our understanding of the permeabilities of geothermal reservoir rocks in Iceland would be to study the individual building blocks, e.g different types of basaltic lithologies at different alteration states.

It should be noted, however, that because the Öskjuhlíð lava is relatively young and has not been subjected to a significant overburden, the samples are not typical of geothermal reservoir rocks. Firstly, they are almost unaffected by hydrothermal alteration. Secondly, and more importantly, they are located at the surface and may therefore contain numerous open microcracks, which are expected to be closed at typical reservoir depths. Nevertheless, they are useful in helping define the properties of the shallow part of normal rock sequences which host geothermal systems. In order to extrapolate the results to reservoir depths, it would be necessary to carry out the measurements under pressure.

1.4 Purpose of study

The purpose of this study is to search for an explanation of the permeability anomaly by exploring the multiparameter dataspace.

1.5 Outline

Chaper 2 focusses on interrelationships between the petrophysical parameters permeability, sonic velocity, thermal conductivity, grain density and porosity.

In Chapter 3 correlations are explored between the petrophysical parameters on the one hand and the structure of the pore space and the grain size of the rock skeleton on the other.

In Chapters 4 and 5 correlations between the petrophysical parameters and mineralogcial and chemical composition are investigated.

An analysis and discussion of the results is found in Chapter 6

2 PETROPYSICS

2.1 Petrophysical parameters measured

The petrophysical parameters measured in the Öskjuhlíð samples are listed in Table 1.

Table 1. *Petrophysical parameters measured in the laboratory*

Parameter	Thermal condonductivity (dry samples)	Sonic P-wave velocity (dry samples)	Grain density	Gas permeability	Gas porosity
Unit	W/m°C	m/s	g/cm^3	mD	%
Identifier	KDRY	VPDRY	MGD	GP	POR
Laboratory	CTH	CTH	GEUS	GEUS	GEUS

2.2 Petrophysical parameters as a function of location (and orientation) within the lava flow

In Figures 2.1-2.5 the petrophysical parameters are plotted against sample number. Individual measurements are also labelled with the sample number in order to facilitate the identification of individual measurements in the other figures of this report.

Figures 2.6-2.10 show the same information, but in addition emphasize the groups of closely spaced values measured at the 9 different locations within the lava flow by displaying the points belonging to different groups with different symbols and placing a box around each group.

The samples were taken both from the scoriaceous margins of the flow and the less porous middle part. For each group, this is indicated in the figures by the symbols T, M and S, which stand for top, middle, and scoriaceous part of flow. The groups marked S were taken from loose blocks, which belong to the lava flow, but could not be identified with certainty as belonging to its top or bottom.

For the groups of samples obtained in situ, the orientation of the samples relative to the weakly developed flow banding in the lava flow is also indicated in the figures.

2.3 Interrelationships between petrophysical parameters

The interrelationships between the petrophysical parameters are illustrated by two series of scatter plots in which each parameter is plotted against all the others.

The first series (Figures 2.11-2.20) shows both individual measurements and groups of closely spaced measurements in as in Figures 2.6-2.10.

The second series (Figures 2.21-2.34) shows the same information without differentiating between groups.

The data show that there is an inverse relationship between permeability and porosity, i.e. low porosities correspond to high permeabilities and visa versa. There is a sharp threshold in the permeability values at 13.5 % porosity. Above the threshold the permeabilities are less than 1 mD and seem independent of porosity. Below it permeability ranges from about 1 mD up to about 25 mD. It is possible to interpret this as two different populations, a population of low permeabilities distributed over the higher porosity range, and a second population of higher permeabilities confined to the range below 13.5 % porosity.

The sonic-velocity-vs-porosity scatter plot also shows interesting anomalous behaviour. Under normal circumstances the velocity should decrease approximately linearly with increasing porosity. In basaltic lava piles, seismic velocity is usually high in the cores of lava flows and low in the rubble at the top and base. The reverse is observed in the Öskjuhlíð samples. Sonic velocities drop to below the 3000-m/s-range at porosities below 13.5 %, whereas more normal values of 4000-4500 m/s are found above.

A similar discontinuity in the grain density values appears to be linked to these anomalies also. Grain density values above 3.0595 g/cm^3 are confined to the low end of the porosity range, below 13.5 %, whereas lower grain density values are found within the higher porosity range.

Evidence for a steplike discontinuity is also found in 3 other scatterplots:

-Permeability vs sonic velocity
-Permeability vs grain density
-Sonic velocity vs grain density

2.4 Definition of supergroups for further analysis

An interesting question at this point is whether the anomalies described above consistently define two separate populations of data. An investigation of the 4-dimensional dataspace defined by the parameters permeability, sonic velocity, grain density and porosity shows that this is in fact so. The simple partitioning of the parameter space described in Table 2 affectes a near-optimal separation of the two populations of datapoints. The two populations will be referred to as supergroups A and B, with the latter corresponding to high permeability, low seismic velocity, high grain density and low porosity. Wherever it is relevant, the boundaries between the two supergroups are shown in the figures.

Table 2. *Definition of supergroups*

Supergroup	A	B
Permeability (mD)	<1	>1
Sonic velocity (m/s)	>3000	<3000
Grain density (g/cm^3)	<3.0595	> 3.0595
Porosity (%)	>13.5	<13.5

With the exception of a few outliers, this partitioning also neatly separates the 9 data groups based on location at the Öskjuhlíð site, groups 1, 7 and 8 belonging to supergroup A and groups 2,3,4,5,6 and 9 to supergroup B.

2.5 The Öskjuhlíð samples in the context of Icelandic geothermal reservoir rocks

Permeability, grain density and porosity measurements are available for a large number of samples from Icelandic geothermal reservoir rocks exposed at the surface.

Scatter plots of permeability vs grain density, permeability vs porosity and grain density vs porosity are shown in Figures 2.35-2.37 with the samples from Öskjuhlíð highlighted.

The figures show that the grain densities of the Öskjuhlíð samples are at the high end of the distribution of values for the reservoir rocks. In view of the freshness of the Öskjuhlíð samples, this is to be expected.

The permeability of Icelandic reservoir rocks shows a general increase with increasing porosity. The relationship is very fuzzy, however, as the range of permeabilities observed at each given value of porosity extends over five orders of magnitude. Interestingly, the permeability-porosity data set from Öskjuhlíð, cuts entirely across the broad permeability-porosity trend defined by the other rocks. This could indicate that a large part of the variability of petrophysical properties in reservoir rocks may arise at the scale of a single geological bed.

3 POROSITY AND NATURE OF THE PORE SPACE

3.1 Thin section studies of the pore space

The pore space of the Öskjuhlíð lava samples was studied in thin sections by Guðmundur Ómar Friðleifsson and Elsa G. Vilmundardóttir (1998). Total porosity was estimated by point counting under the microscope. The observed pores were also classified as being either vesicles or intercrystalline pores.

The parameters obtained are listed in Table 3.

Table 3. *Pore-space parameters determined from thin sections*

Parameter	Porosity in vescicles	Intercrystalline pores	Total porosity
Unit	%	%	%
Identifier	VPOR	IPOR	TPOR
Laboratory : OS			

3.2 Comparison of total gas porosity and total porosity from thin sections

A comparison of the total porosity measured in thin section and the gas porosity described earlier is shown in Figure 3.1. In addition to a considerable random scatter in the relationship between the two types of measurement, there is also a significant systematic difference. Based on a best line fit, porosity measured in thin section is systematically higher than the gas porosity by some 5 percentage points at the low end of the porosity range. At the high end of the range the difference has narrowed to about 2.5 percentage points.

A few of the thin section analyses were carried out on dyed thin sections, which should make the analysis more accurate.The rest of the sections received no such treatment. Based on the points derived from the dyed sections, which are highlighted in the figure, it seems that the porosity has been overestimated in the untreated sections.

Gas porosity is effective porosity, i.e. the method does not detect isolated pores. It has been shown by comparison between effective and total porosity from the larger database that the difference between the two types of porosity, is generally less than 2 percentage units for porosity higher than 6 % (Ómar Sigurðsson and Valgarður Stefánsson, 1994). As the thin section count is for total porosity, the bias is smaller than indicated by Figure 3.1. The total scatter and the remaining bias are, however, mainly caused by inaccuracies in the thin section measurements.

The series of scatter plots in Figures 3.2-3.5, in which the two types of porosity are plotted against permeability, sonic velocity, thermal conductivity and grain density, shows that the sharpness of the anomalies described in Chapter 2 is considerably degraded by substituting porosity determined from thin sections for the gas porosity. In view of the inaccuracy in the thin section measurements, this is to be expected. The plot of total thin section porosity against permeability in Figure 3.2 nevertheless shows that the original permeability anomaly is still clearly discernible. The transition to high permeability values occurs at a higher value of porosity (approximately 21 %), which, at least partly, can be explained by the systematic difference between the two types of porosity measurement.

3.3 Partitioning of the pore space into vesicles and intercrystalline pores

The pore space of olivine tholeiite lavas is characterized by four types of voids:

-Smooth, round, glass-rimmed vesicles caused by gas bubbles
-Intercrystalline pores - jagged, irregular voids between the crystals constituting the rock matrix
-Microcracks within crystal grains and, especially, at grain boundaries
-Fractures cutting through the crystalline matrix caused by thermal contraction or tectonic movements

The latter two types of void are underrepresented in routine analysis of thin sections under the petrographic microscope because of incompatibilities between the length scales involved. Fractures

often cause the specimen to fall apart during handling and preparation of the thin sections and therefore may escape detection unless a special effort is made to preserve them. Yet, if a rock is pervasively fractured on a length scale corresponding to a fraction of the core diameter down to the size of crystal grains, one should expect to find fractures in a collection of thin sections. Microcracks, on the other hand, are so small that special techniques are required for effective detection.

In the study of Guðmundur Ó. Friðleifsson and Elsa G. Vilmundardóttir (1998), the preparation of thin sections proceeded without special regard to preserving fractures and no fractures were observed. In the routine analysis, in which conventional methods of microscopy were used, only two types of pores were detected, vesicles and intercrystalline pores. However, in a special study, a few thin sections were impregnated with a special fluorescent resin and observed at high magnification. This method revealed the presence of abundant microcracks at the grain boundaries within the rock matrix.

Two series of scatter plots illustrate the partitioning of the pore space into vesicles and intercrystalline pores, as well as the relationship between both types of porosity and the petrophysical parameters.

In Figures 3.6 and 3.7 the two porosity components are plotted against gas porosity and total thin section porosity. Both plots clearly show that intercrystalline porosity dominates at low total porosities whereas vesicular porosity dominates at high porosities. The plot against gas porosity also shows that the transition between the two types of pore space occurs somewhere between 17 and 22 % gas porosity. This means that the transition does not correlate with the abrupt change in permeability which occurs at 13.5 % gas porosity. On the contrary, low permeabilities occur in both types of pore space.

In Figures 3.8-3.11 the two porosity components, vesicular and intercrystalline, are plotted against the petrophysical parameters. The plots confirm that the transition between vesicule-dominated and intercrystalline-dominated porosity is displaced relative to the boundaries that separate the two populations of data, supergroups A and B (see Table 2).

Figures 3.12-3.17 show the same information as Figures 3.6-3.11 exept that the two porosity components are expressed as fractions of the total thin section porosity and not in porosity percentage units. In some cases this makes the plots easier to read.

3.4 Correlations with grain size

Grain size is expected to show strong correlation with the different porosity parameters because a quick look at the thin sections shows that the high-porosity, vesicle-dominated margins of the lava flow are more glassy and fine-grained than the central part where intercrystalline pores dominate.

An effort was made to quantify this relationship in a simple manner. In the thin section analysis the average grain size of the matrix minerals of each sample was estimated visually and classfied into 3 categories: fine, medium and coarse.

In Figures 3.18 and 3.19 the vesicular and intercrystalline porosity components are plotted against grain size. As expected, the scatter plots show that intercrystalline porosity dominates in the coarse grained part of the lava flow. However, a comparison of Figure 3.6 (porosity components vs gas porosity) and Figure 3.24 (grain size versus gas porosity) provides a sharper view of these relationships. Figure 3.24 shows that below 14.5 % porosity only coarse grained matrix is found whereas above 16% porosity the matrix is either medium or fine grained. Comparison with Figure

3.6 shows that the transition between the two types of matrix occurs above the boundary between supergroups A and B (13.5 %) but within the field dominated by intercrystalline porosity.

In Figures 3.20-3.24 grain size is plotted against the petrophysical parameters. The plots confirm that, as in the case of the transition between vesicular-dominated and intercrystalline dominated porosity (see Figures 3.8-3.11), the transition between coarse grained and middle-fine grained matrix does not correspond exactly to the supergroup boundaries as defined in Table 2.

In summary, the pore space of the Öskjuhlíð lava flow may be divided into two types according to geometry. A vesicular type pore space, characterized by smooth, round, glass-rimmed vesicles with fine to middle grained matrix that dominates the margins of the flow. By contrast, irregular intercrystalline pores, set between the grains of a coarse grained matrix, characterize the inner parts of the flow. The transition between the two states is fairly sharp but occurs at somewhat higher porosities than the transition between high and low permeabilities.

4 MINERALOGY

4.1 Thin section studies of mineralogy

The mineralogical components determined from thin sections of the Öskjuhlíð samples are listed in Table 4.

Table 4. *Mineralogical composition determined from thin sections*

Component	Plagioclase	Pyroxene	Olivine	Opaque minerals	Glass rim	Opaline silica
Unit	% of matrix	% of matrix	% of matrix	% of matrix	% of matrix	% of matrix
Identifier	PLAGMA	PYRMA	OLIMA	OPQMA	GLRMA	OPSIMA
Laboratory: OS						

Glass rim refers to a thin coating of glass surrounding vesicles. Opaline silica is a secondary mineral deposit found in some pores.

4.2 Relationship between mineralogical composition and petrophysical properties

In order to investigate whether any significant correlations are present between the petrophysical properties and mineralogical composition of the Öskjuhlíð samples, the size of each mineralogical component was plotted as a function of all the petrophysical parameters. The resulting scatter plots are shown in Figures 4.1-4.20.

An inspection of the plots shows that a marked correlation is present for only one of the mineralogical components measured, the glass rim. This is not surprising because according to the thin section study, nearly all vesicles have a glass rim, whereas none of the intercrystalline pores do. The plots show that the petrophysical boundary values used to separate the measured samples into two supergroups A and B (Table 2) also separate samples with different glass content. The presence of a higher percentage of glass rim than 3-4 % is an indicator that a sample belongs to the low-permeability supergroup A, but the distinction is not as sharp as in the case of the petrophysical properties because a small but significant minority of the samples with a lesser percentage of glass rim also falls into supergroup A.

4.3 Mineralogical homogeneity of the rock matrix

In order to evaluate the homogeneity of the rock matrix, the average and standard deviation was calculated for each of the nine sample groups as well as for the supergroups A and B and the whole collection of samples. The results are presented in the Appendix (Tables A7, A8 and A9).

Deviations of group averages from the average of all samples are small and only in two cases are they statistically significant at the level of one standard deviation (Table A7; Pyroxene, Group 7 and Olivine, Group 9). This also applies to the differences between supergroups A and B which in all cases give the same value in the statistical sense. In the case of the glass rim, however, the standard deviations give a misleading result for the two supergroups. That is because of the one-sided nature and difference in shape of the distributions of the measured values in the two groups. The difference is clear in the scatter plots (Figures 4.11-4-15).

5 CHEMICAL COMPOSITION

5.1 Chemical studies of the rock matrix

The chemical elements analysed in the Öskjuhlíð samples are listed in Tables 5 and 6.

Table 5. *Chemical composition of major elements measured in the laboratory*

Element	SiO_2	TiO_2	$A_{l2}O3$	Fe_2O_3	MnO	MgO	CaO	Na_2O	K_2O	P_2O_5	LOI	Tot. weight	CO_2	FeO	Fe_2O_3
Unit	%	%	%	%	%	%	%	%	%	%	%	%	%	%	%
Identifier	SiO2	TiO2	Al2O3	Fe2O3	MnO	MgO	CaO	Na2O	K2O	P2O5	LOI	TWP	CO2 (%)	FeO (%)	Fe2O3 (%)
Laboratory: McGill															

Table 6. *Chemical composition of minor elements measured in the laboratory*

Element	BaO	Ce	Cu	V	Zn	Ga	Nb	Pb	Rb	Sr	Th	U	Y	Zr	As	Sb	S
Unit	ppm	ppm	ppm	ppm	ppm	ppm	ppm	ppm	ppm	ppm	ppm	ppm	ppm	ppm	ppm	ppm	ppm
Identifier	BaO	Ce	Cu	V	Zn	Ga	Nb	Pb	Rb	Sr	Th	U	Y	Zr	As	Sb	S
Laboratory: McGill																	

5.2 Relationship between chemical composition and petrophysical properties

In Figures 5.1-5.35 the concentration of each chemical component is plotted against all the petrophysical parameters. Only in a few cases are visual correlations between chemical composition and petrophysical properties observed.

The major elements that show such correlations are MgO, MnO and TiO_2. The plots show that the high-permeability supergroup B is slightly enriched in MgO, and slightly depleted in MnO and TiO_2.

Minor elements showing correlations with the petrophysical parameters are As, BaO, Nb, Y and Zr. Supergroup B is slightly enriched in BaO and slightly depleted in As, Nb, Zr and Y.

5.3 Chemical homogeneity of the rock matrix

The chemical homogeneity of the rock matrix was tested by calculating the average and standard deviation for each of the nine sample groups and for the supergroups A and B. The results are given in the Appendix (Tables A10-A15).

For each of the major elements Fe_2O_3, MgO, MnO and TiO_2, one or more group average deviates significantly from the average for all samples. However, the supergroup averages are significantly different only in the case of the latter three elements.

In the case of the minor elements, the group averages of 1 to 3 groups deviate from the average for all samples in the case of 7 elements: Nb, Pb, Rb, Th, V, Y and Zr. However, the deviations are relatively small and only in the case of Nb and Zr (V and Y are at the limit) are there significant differences between the two supergroups.

6 ANALYSIS AND DISCUSSION

The main purpose of this study is to search for possible explanations for the permeability anomaly. Careful examination of the multiparameter dataspace has shown that the anomaly is only one aspect of the anomalous behaviour of the Öskjuhlíð samples. Anomalies in seismic velocity, grain density and porosity correlate with the high-permeability anomaly in a manner that (with the exception of a few outliers) makes it possible to divide the whole collection of measurements into two separate populations. In the 4-dimensional dataspace the boundaries between the two populations are unexpectedly sharp, and in the case of permeability and sonic velocity, of large magnitude.

The question that needs to be answered is why this grouping of the measured samples into two separate populations occurs. An analysis and discussion of this problem follows. But first, the main correlations between the different parameters are summarized.

6.1 Main correlations in the data set

The high-permability part of the Öskjuhlíð lava flow, as represented by the samples in supergroup B, shows several differences from the lower-permeability part represented by supergroup A. The differences are listed below for supergroup B relative to supergroup A

Physical properties:

-High permeability
-Low porosity
-Low sonic P-wave velocity
-High grain density

Pore space structure:

-High proportion of intercrystalline porosity relative to vesicular porosity
-More coarse-grained rock matrix

Mineralogical composition:

-Small proportion of glass-coating around pores

Chemical composition:

-Enrichment in MgO
-Depletion in TiO_2, MnO, Nb and Zr

6.2 Possible causes of the permeability anomaly

The permeability-vs-porosity plot (Figures 2.28) provides us with a good starting point to analyse the anomalous behaviour of the Öskjuhlíð samples. Three features of the plot are especially unusual:

(1) Inverse relationship between permeability and porosity where the margins and the inner part of the lava flow are contrasted, i.e. permeability decreases with increasing porosity. This is opposite to the general permeability-porosity trend of Icelandic geothermal reservoir rocks and implies that the changes in permeability across the entire lava flow are controlled by changes in higher-order geometric aspects of the pore space rather than in the pore volume itself.

Studies have shown that the large scale permeability-porosity relationship for the Icelandic rock database may be approximated by equations based on capillary tube models (Ómar Sigurðsson og Valgarður Stefánsson, 1994; Ómar Sigurðsson, 1998). In these models the permeability of the rock is modelled by a collection of narrow tubes. The permeability-limiting property is the average cross section of the tubes and the tortuosity of their path through the rock. The models seek to capture the essential features of a much more complicated reality in which the pore space is an irregular, connected network of large and small pores of different shape.

Assuming that a capillary tube model is valid, the increase in permeability from the margins to the core of the Öskjuhlíð lava flow must be interpreted either in terms of an increase in the average diameter of the tubes, even as the volume of the pore space falls, or as a result of a decrease in the tortuosity of the flow path.

In many types of rock, the toruosity does not vary very much and it is the size distribution of the narrow passages in the network of pores (bottlenecks, pore throats) that controls the permeability. Whether this is the case for Icelandic geothermal reservoir rocks is not yet clear, but Ómar Sigurðsson (1998) has argued that, in these rocks, the average cross section of the tubes dominates over the tortuosity in restricting permeability. Assuming that this is the case and assigning a constant value to the tortuosity factor, he demonstated that, if the average tube diameter were known, the permeability could be predicted with an error of less than an order of magnutide. This is to be compared with a scatter in permeability over 5 orders of magnitude when plotted against porosity.

(2) The fact that permeability is independent of porosity over the wide range of porosities spanned by the low-permeability rocks at the margins of the lava flow. This tells us that in this vesicle-dominated part of the lava flow, the permeability-limiting geometric features of the pore space are unaffected by the large variation in the amount of porespace taken up by large pores and any explanation must take this into account.

This appears to rule out a simple explantion for the permeability behavior that was considered at an early stage of the project. Could lower permeability in the vesicle-dominated margins of the lava flow than in the core of the flow be caused by low permeability of the vesicles ? This may seem to be

a reasonable suggestion because the vesicles constitute a large part of the bulk rock and are encapsulated by a glass rim which might well be of low permeability. This would act to partly decouple the vesicles from the rest of the pore space and reduce the space available for a connected network of pores. This can hardly be the true cause, however, because then one would expect the permeability in the vesicular part of the flow to decrease with increasing porosity, which is clearly not the case.

(3) The sharpness of the transition between the high- and low-permeability groups. This is difficult to understand in terms of gradual changes in the nature of the pore space and rather indicates a sharp transition in pore geometry although it is conceivable that a continuous change in pore space geometry may lead to a sudden change, such as when a critical threshold is passed and a new property suddenly emerges. In fact, this is a well-know property of abstract networks.

Two main models have been considered as possible explanations for the unusual permeability behavior of the Öskjuhlíð samples.

In the first model the difference in permeability between the central and the marginal parts of the lava flow is attributed to differences in the nature of the pore space as observed in thin sections. The high permeabilities associated with the inner parts of the lava flow are in this case thought to be caused by the presence of a well connected network of intercrystalline pores. As the flow margins are approached, this network disintegrates, leading to a decrease in permeability. The reason for this would be that, because the margins cooled more rapidly than the inner part of the flow, the grain size is smaller than in the centre, the glass content higher and a large number of glass-rimmed gas bubbles (vesicles) are preserved in the rock.

Plots of grain size, glass content, vesicular porosity and intercrystalline porosity vs gas porosity indeed show significant intercorrelation and seem, at first sight, to fit with the subdivision into supergroups A and B (Figures 3.6, 3.12, 3.24, 4.15). On closer inspection, however, it becomes evident that the boundary between a vesicle-dominated and intercrystalline dominated pore space does not actually coincide with the boundary between the low-permeability (A) and high-permeability (B) supergroups. The latter occurs at 13,5 % gas porosity, whereas the former occurs at 17-22 % gas porosity (Figures 3.6 and 3.12). Similarly, the marked change in grain size and amount of pore-encapsulating glass occurs within the field of intercrystalline porosity (Figures 3.6, 3.24 and 4.15). This model therefore does not seem to fit the observations. However, before it is rejected, one aspect of it has to be given further consideration.

In the analysis above it has implicitly been assumed that permeability is a slowly changing function of geometric changes in the pore space. What if the the permeability is a strongly non-linear function of changes in the pore space ? This would not be surprising in view of the sharp discontinuities observed in the petrophysical properties (see (3) above). In such a case, it is conceivable that large changes in the ratio of vesicles to intercrystalline pores, glass content and grain size, would not lead to any significant change in the critial permeability-restricting parts of the pore space until some critical threshold is crossed. Moreover, this threshold could be displaced relative to the eye-catching step changes in the properties just mentioned. For instance, it is possible that the network of intercrystalline pores does not disintegrate until the gas porosity has fallen considerably below the the 17-22 % value where the decrease in intercrystalline pore volume is greatest. It seems therefore that this possibility cannot be entirely excluded on the basis of the data discussed so far.

An alternative model is one in which the high permeabilities characterizing the inner part of the lava flow are caused by a pervasive network of microcracks. As mentioned in Chapter 3, microcracks were found in large numbers in the few cases where a special effort was made to observe them. Moreover, they seemed to be of the grain-boundary type that is common, for example, in granites (Brace et al., 1972), and have been observed in Icelandic lava flows (Kowallis et al., 1982). Since

the inner part of the lava flow has a better crystallized rock matrix with larger grains and less glass than the margins, it is resonable to expect that a more pervasive and better connected network of microcracks exists there than at the flow margins. The data on microcracks in the Öskjuhlíð samples are at present too few to allow comparison between the two parts of the flow. The sonic measurements do, however, provide an important clue.

Sonic P-wave velocity depends on the the rigidity of the rock matix through the shear modulus (μ). The presence of grain-boundary microcracks can dramatically lower the shear modulus and thus lower the sonic P-wave velocity . Velocity anomalies caused by microcracks are commonly observed in rocks exposed at or close to the surface, but are thought become less common with depth because the microcracks tend to become closed with increasing overpressure.

As described in Chapter 2, the inner, high-permeability part of the lava flow is characterized by anomalously low sonic P-wave velocities. This observation is a strong indication of the presence of microcracks. In fact, it is difficult to see how the sonic anomaly could otherwise be explained (except perhaps in terms of fractures; see section 6.3 below). Their presence could also explain the unusual features of the permeability-vs-porosity relationship discussed above.

On the other hand, it is difficult to see how the other model, based on a sudden change in the permeability of the network of intercrystalline pores, could explain the sonic anomaly. The only obvious aspect of the intercrystalline pore space that could be linked to a lowered rigidity of the rock matrix is presicely the possibility of a better developed network of microcracks where the rock matrix is coarse-grained and nearly glass free than in the more fine grained and glassy parts of the flow.

The evidence dicussed so far clearly favors an explanation of the high-permeability anomaly in terms of microcracks over one based on intercrystalline porosity, but further evidence is still needed to reach a final conclusion.

It is not clear how the high grain density associated with the high-permeability part of the lava flow should be interpreted. Two different types of explantion can be envisaged for the strong covariance between permeability and grain density across the boundary between the two supergroups.

The first type of explanation involves some mineralogical change that alters both the geometry of the pore space and the density of the minerals. Changes in the amount of low-density opaline silica precipitate in the pores and in the amount of glass in the rock matrix would be obvious candidates. However, a quick look at Figures 4.16-4.20, shows that the amount of opaline silica is very small and does not differ between the two supergroups. The presence of glass probably lowers the density of the rock matrix. However, as was discussed in Chapter 4, although the presence of a higher percentage of glass rim than 3-4% within the rock matrix correlates with low permeability, the correlation is not sharp. In fact the transition to higher glass content seems to occur at a somewhat higher gas porosity than the boundary between the low- and high-permeability groups as is also the case with the transition from intercrystalline-dominated to vesicle-dominated pore space. Changes in the content of opaline silica can therefore be ruled out as an explanation and the same probably applies to the glass content. No other mineralogical changes, that might be involved, have been identified in the thin section studies.

The second type of explanation involves a difference in the amount of isolated pores within the two parts of the lava flow. The grain density was determined from the equation

$$\rho_{gr} = W/(BV-PV)$$

where W is the weight of the sample, BV its bulk volume, and PV its pore volume as determined from measurement of gas porosity. Isolated pores are not detected in the measurement of gas porosity and this has the result of lowering the grain density obtained by the equation. The low grain density of the low-permeability margins of the lava flow can be explained by a slightly higher proportion of isolated pores in this part of the flow than in its inner part. In fact, a straightforward calculation based on the average grain density values given for the two supergroups in Table A2 shows that an increase in the volume of isolated pores of only 0.5 porosity percentage units across the supergroup boundary is enough to explain the apparent change in grain density according to this model.

This explanation seems to fit well to the microcrack hypothesis. Assume that a well connected network of microcracks only exists in the inner, high-permeability part of the flow, represented by samples in supergroup B. This may serve to increase the number of pores that are well connected to the pore network, i.e. decrease the number of pores that would otherwise be isolated. In the marginal part of the flow, where the network of microcracks is non-existent, or has disintegrated to become ineffective, isolated pores are more common. This, in turn, lowers the apparent grain density. This model provides an explanation for the jump in both permeability and grain density across the supergroup boundaries.

The remaining evidence, such as enrichment in MgO and depletion in TiO_2, MnO, Nb and Zr does not, at present, add much to the understanding of this phenomenon.

In clonclusion, the most likely explantion for the high-permeability anomaly is the presence of a connected network of grain-boundary microcracks in the rock matrix of the inner part of the Öskjuhlíð lava flow. The attractive feature of such a model is that it provides an explanation for the simultaneous jump in permeability, sonic velocity and grain density across the supergroup boundaries.

At the present stage, this model is just a hypothesis that needs to be tested. A good way to proceed would be to repeat some of the measurements of permeability, sonic P-wave velocity and grain density at higher confining pressures. If the hypothesis is correct, these petrophysical parameters should show a dependency on confining pressure, because the microcracks would become closed to some degree. Thus, one would expect that samples from the inner part of the flow would exhibit lower permeability, higher sonic velocity and lower grain density at higher confining pressures, whereas for samples from the marginal parts of the lava flow the measurements should be largely unchanged. Because of their sensitivity to microcracks, measurements of sonic S-wave velocity and resistivity could also help test the hypothesis. These measurements should be accompanied by a detailed investigation of microcraks under the microscope in a number of samples taken from each of the two supergroups.

Mesurements of petrophysical properties at different confining pressures have, in fact, been carried out for two of the samples (R34 and R43) (Johnson and Boitnott, 1998). Unfortunately, sample R34 is one of the outliers, i.e. belongs to neither of the two supergroups. Sample 43, however, belongs to the high-permeability supergroup B. It shows an increase in sonic velocity and formation factor with increasing confining pressure, as expected. On the other hand, the permeability is relatively insensitive to an increase in pressure, only a slight decrease is measured. At the present time, it is not clear how these results should be interpreted, but clearly the test will remain incomplete until the measurements have been carried out on a greater number of samples and microcracks studied at high resolution.

6.3 The question of blast damage

Blast damage has been put forth as a possible complicating factor in the interpreation of the Öskjuhlíð samples, because the samples were taken from the walls of a quarry. The question is whether the increased permeability of the inner part of the lava flow may result from fractures created by dynamite explosions. This question cannot be conclusively answered unless control mesurements are made in samples taken some distance from the quarry. It does seem unlikely, however, that the explosions would have created a pervasive network of microcracks without forming larger fractures, as may be concluded from the thin section study. Surely, some such fractures would have been seen in the thin sections, had they been formed in significant numbers.

7 SUMMARY AND CONCLUSIONS

The permeability of the Öskjuhlíð lava flow shows a peculiar distribution: In the highly porous margins of the flow, the permeability is an order of magnitude lower than in the less porous inner part. This decrease in permeability with porosity is opposite to the observed general trend in Icelandic rocks. Such behavior may, however, be one of the main reasons for the large scatter in the general trend. It demonstrates that the distribution of non-fracture related permeabilities in the basaltic rock sequences, which host the geothermal systems of Iceland, cannot be fully understood unless studied at the level of the individual building blocks of the the lava pile.

A large number of core samples were taken from the flow and the petrophysical properties, mineralogy and geochemistry studied in detail in order to determine the reason for the unusual permeability distribution. An exploration of the resulting set of petrophysical measurements revealed that the permeability-vs-porosity anomaly is only one aspect of the anomalous behavior of the Öskjuhlíð samples. Anomalies in seismic velocity and grain density also correlate with the high-permeability anomaly in a manner that (with the exception of a few outliers) makes it possible to divide the 4-dimensional dataspace defined by these parameters into two non-overlapping populations separated by relatively sharp boundaries. The high-permeability population is characterized by low porosity, low seismic velocity and high grain density.

Correlations between this partitioning of the petrophysical measurements and parameters relating to the pore geometry, mineralogy and geochemistry of the samples were explored in order to explain why this separation into two populations occurs. The high-permability part of the lava flow was found to be characterized by a higher proportion of intercrystalline porosity relative to vesicular porosity, a more coarse grained rock matrix and a lack of significant glass coating around large pores. However, a detailed comparison showed that the changes in these parameters do not occur at the population boundaries but are significantly displaced towards higher porosities. Changes in these parameters are therefore unlikely to pinpoint the underlying cause. In particular, the presence of relatively impermeable glass coating around pores and changes in the connectivity of the network of intercrystlline pores are both rejected as probable explanations of the permeability anomaly.

The preferred explanation is that the presence of an extensive, connected network of grain-boundary microcracks is the feature that causes high permability in the coarse-grained inner part of the flow. The attractive feature of such a model is that it potentially provides an explanation for the simultaneous jump not only in permability and sonic velocity across the boundary beween the two populations of measurements, but also for the corresponding jump in grain density.

Testing of this hypothesis is possible by further measurements. Such tests are presently in the initial stages and the results are not yet conclusive.

REFEERENCES

Brace, W. F., Silver, E., Hadley, K., and Goetze, C., 1972. Cracks and pores: a closer look. Science, 178, 162-163

Guðmundur Ómar Friðleifsson and Elsa G. Vilmundardóttir, 1998. Reservoir parameters. TCP-project. A thin-section study of the Öskjuhlíð samples. Orkustofnun, Report OS-98041, 15 pp.

Guðmundur Ómar Friðleifsson, Hjalti Franzson, Steinar Þór Guðlaugsson and Sigurður Sveinn Jónsson, 1997. Samples from Öskjuhlíð for TCP-project. Orkustofnun, Short Report GÓF-HF-STG-SSJO-97/06, 3 pp.

Johnson, J. and Boitnott, G. N., 1998. Velocity, permeability, resistivity and pore structure models of selected basalts from Iceland. New England Research, Inc., Vermont, U.S.A., 95 pp.

Kowallis, B. J., Roeloffs, E. A., and Wang, H. F., 1982. Microcrack studies of basalts from the Iceland Research Drilling Project. Journal of Geophysical Research, 87, 6650-6656

Ómar Sigurðsson, 1998. Forðafræðistuðlar. Lekt og hárpípulíkan. Orkustofnun, Short Report Ómar-1998/01, 10 pp.

Ómar Sigurðsson og Valgarður Stefánsson, 1994. Forðafræðistuðlar. Mælingar á bergsýnum. Orkustofnun, Report OS-94049/JHD-28 B, 35 pp.

APPENDIX : Statistical properties of groups, supergroups and the total collection of samples

Table A1. *Statistical properties of petrophysical parameters. Groups 1-9*

Parameter	Thermal conductivity	Sonic P-wave velocity	Grain density	Gas permeability	Porosity
Unit	W/m°C	m/s	g/cm^3	mD	%
Identifier	KDRY	VPDRY	MGD	GP	POR
Measured by	CTH	CTH	GEUS	GEUS	GEUS
GROUP 1					
Average	1.45	2580	3.0622	7.00	12.54
Standard deviation	0.21	257	0.0027	6.10	0.47
No. of measurements	15	16	16	16	16
GROUP2					
Average	1.24	4079	3.0516	0.30	31.39
Standard deviation	0.17	182	0.0029	0.07	4.50
No. of measurements	5	5	5	5	5
GROUP3					
Average	1.57	3768	3.0573	0.51	15.00
Standard deviation	0.07	117	0.0014	0.24	1.05
No. of measurements	3	5	5	5	5
GROUP 4					
Average	1.40	4260	3.0559	0.36	15.74
Standard deviation	0.12	199	0.0060	0.10	1.08
No. of measurements	6	7	7	7	7
GROUP 5					
Average	1.22	4377	3.0481	1.00	32.05
Standard deviation	0.13	199	0.0033	2.0	2.73
No. of measurements	5	8	8	8	8
GROUP 6					
Average	1.23	4295	3.0462	0.70	30.16
Standard deviation	0.12	250	0.0048	1.37	1.66
No. of measurements	7	17	18	18	18
GROUP 7					
Average	1.38	2442	3.0751	8.68	11.82
Standard deviation	0.18	198	0.0023	7.76	0.86
No. of measurements	6	9	9	9	9
GROUP 8					
Average	1.46	2577	3.0644	12.36	12.19
Standard deviation	0.13	154	0.0007	8.55	0.51
No. of measurements	5	12	13	13	13
GROUP 9					
Average	1.36	4126	3.0550	0.27	24.27
Standard deviation	0.34	284	0.0020	0.10	1.54
No. of measurements	5	4	5	5	5

Table A2. *Statistical properties of petrophysical parameters. Supergroups A and B*

Parameter	Thermal conductivity	Sonic P-wave velocity	Grain density	Gas permeability	Porosity
Unit	W/m°C	m/s	g/cm^3	mD	%
Identifier	KDRY	VPDRY	MGD	GP	POR
Measured by	CTH	CTH	GEUS	GEUS	GEUS
SUPERGROUP A					
Average	1.32	4208	3.0506	0.59	26.30
Standard deviation	0.20	275	0.0060	1.16	7.00
No. of measurements	31	47	48	48	48
SUPERGROUP B					
Average	1.44	2545	3.0660	9.23	12.25
Standard deviation	0.18	217	0.0056	7.58	0.64
No. of measurements	36	38	38	38	36

Table A3. *Statistical properties of petrophysical parameters. All samples*

Parameter	Thermal conductivity	Sonic P-wave velocity	Grain density	Gas permeability	Porosity
Unit	W/m°C	m/s	g/cm^3	mD	%
Identifier	KDRY	VPDRY	MGD	GP	POR
Measured by	CTH	CTH	GEUS	GEUS	GEUS
Average	1.37	3467	3.0574	4.41	20.09
Standard deviation	0.20	868	0.0096	6.66	8.75
No. of measurements	57	83	86	86	86

Table A4. *Statistical properties of pore space parameters determined from thin sections. Groups 1-9*

Parameter	Porosity in vesicles	Intercrystalline pores	Total porosity
Unit	%	%	%
Identifier	VPOR	IPOR	TPOR
Measured by	OS	OS	OS
GROUP 1			
Average	0	17	17
Standard deviation	0	5	5
No. of measurements	15	15	15
GROUP2			
Average	11	21	33
Standard deviation	7	14	8
No. of measurements	5	5	5
GROUP3			
Average	2	16	18
Standard deviation	3	6	4
No. of measurements	5	5	5
GROUP 4			
Average	1	18	19
Standard deviation	1	3	3
No. of measurements	7	7	7
GROUP 5			
Average	21	16	38
Standard deviation	15	12	8
No. of measurements	8	8	8
GROUP 6			
Average	24	8	32
Standard deviation	11	2	10
No. of measurements	18	18	18
GROUP 7			
Average	8	10	18
Standard deviation	12	3	12
No. of measurements	9	9	9
GROUP 8			
Average	1	15	15
Standard deviation	1	4	4
No. of measurements	11	11	11
GROUP 9			
Average	15	10	25
Standard deviation	13	2	11
No. of measurements	5	5	5

Table A5. *Statistical properties of pore space parameters determined from thin sections. Supergroups A and B*

Parameter	Porosity in vescicles	Intercrystalline pores	Total porosity
Unit	%	%	%
Identifier	VPOR	IPOR	TPOR
Measured by	OS	OS	OS
SUPERGROUP A			
Average	16	13	29
Standard deviation	14	8	11
No. of measurements	45	48	47
SUPERGROUP B			
Average	2	15	17
Standard deviation	7	5	7
No. of measurements	35	35	35

Table A6. *Statistical properties of pore space parameters determined from thin sections. All samples*

Parameter	Porosity in vescicles	Intercrystalline pores	Total porosity
Unit	%	%	%
Identifier	VPOR	IPOR	TPOR
Measured by	OS	OS	OS
Average	10	14	24
Standard deviation	13	7	11
No. of measurements	83	83	83

Table A7. *Statistical properties of mineralogical compositions. Groups 1-9*

Parameter	Plagioclase	Pyroxene	Olivine	Opaque minerals	Glass rim	Opaline silica	Matrix
Unit	% of matrix	% of matrix	% of matrix	% of matrix	% of matrix	% of matrix	% of section
Identifier	PLAGMA	PYRMA	OLIMA	OPQMA	GLRMA	OPSIMA	MTRX
Measured by	OS	OS	OS	OS	OS	OS	OS
GROUP 1							
Average	46	32	9	13	0	0	83
Standard deviation	5	4	3	5	0	1	5
No. of measurements	15	15	15	15	15	15	15
GROUP2							
Average	36	32	11	12	9	0	68
Standard deviation	4	4	4	3	7	0	8
No. of measurements	5	5	5	5	5	5	5
GROUP3							
Average	45	30	9	14	1	0	82
Standard deviation	7	4	2	4	2	0	4
No. of measurements	5	5	5	5	5	5	5
GROUP 4							
Average	34	36	11	18	1	0	81
Standard deviation	5	5	1	1	1	0	3
No. of measurements	7	7	7	7	7	7	7
GROUP 5							
Average	40	39	7	11	3	0	62
Standard deviation	4	4	3	3	2	1	8
No. of measurements	8	8	8	8	8	8	8
GROUP 6							
Average	38	41	9	8	5	0	64
Standard deviation	5	4	2	3	3	0	19
No. of measurements	18	18	18	18	18	18	19
GROUP 7							
Average	42	43	9	5	1	0	82
Standard deviation	4	3	3	2	1	0	12
No. of measurements	9	9	9	9	9	9	9
GROUP 8							
Average	44	38	12	5	0	0	85
Standard deviation	4	3	3	3	0	0	4
No. of measurements	11	11	11	11	11	11	11
GROUP 9							
Average	43	37	4	8	8	0	75
Standard deviation	2	2	2	3	3	0	11
No. of measurements	5	5	5	5	5	5	5

Table A8. *Statistical properties of mineralogical compositions. Supergroups A and B*

Parameter	Plagioclase	Pyroxene	Olivine	Opaque minerals	Glass rim	Opaline silica	Matrix
Unit	% of matrix	% of matrix	% of matrix	% of matrix	% of matrix	% of matrix	% of section
Identifier	PLAGMA	PYRMA	OLIMA	OPQMA	GLRMA	OPSIMA	MTRX
Measured by	OS	OS	OS	OS	OS	OS	OS
SUPERGROUP A							
Average	39	37	9	11	4	0	70
Standard deviation	5	5	3	4	4	1	15
No. of measurements	48	48	48	48	48	48	49
SUPERGROUP B							
Average	44	37	10	9	0	0	83
Standard deviation	5	6	3	5	1	0	7
No. of measurements	35	35	35	35	35	35	35

Table A9. *Statistical properties of mineralogical compositions. All samples*

Parameter	Plagioclase	Pyroxene	Olivine	Opaque minerals	Glass rim	Opaline silica	Matrix
Unit	% of matrix	% of matrix	% of matrix	% of matrix	% of matrix	% of matrix	% of section
Identifier	PLAGMA	PYRMA	OLIMA	OPQMA	GLRMA	OPSIMA	MTRX
Measured by	OS	OS	OS	OS	OS	OS	OS
Average	41	37	9	10	3	0	75
Standard deviation	6	5	3	5	4	1	14
No. of measurements	83	83	83	83	83	83	84

Table A10. *Statistical properties of major element compositions. Groups 1-9*

Parameter	SiO_2	TiO_2	Al_2O_3	Fe_2O_3	MnO	MgO	CaO	Na_2O	K_2O	P_2O_5	LOI	Tot. weight	CO_2	FeO	Fe_2O_3
Unit	%	%	%	%	%	%	%	%	%	%	%	%	%	%	%
Identifier	SiO2	TiO2	Al2O3	Fe2O3	MnO	MgO	CaO	Na2O	K2O	P2O5	LOI	TWP	CO2 (%)	FeO (%)	Fe2O3 (%)
Measured by	Mc GILL	Mc GILL	Mc GILL	Mc GILL	Mc GILL	Mc GILL	Mc GILL	Mc GILL	Mc GILL	Mc GILL	Mc GILL	Mc GILL	Mc GILL	Mc GILL	Mc GILL
GROUP 1															
Average	46.9	1.47	14.8	12.7	0.19	10.1	11.2	2.1	0.16	0.14		99.8	0.33	6.96	4.96
Standard deviation	0.2	0.00	0.1	0.2	0.00	0.2	0.2	0.0	0.01	0.00		0.2	0.04	1.24	1.20
No. of measurements	2	2	2	2	2	2	2	2	2	2	0	2	2	2	2
GROUP2															
Average	46.8	1.59	15.6	12.8	0.20	9.0	11.4	2.0	0.15	0.11	0.92	100.5	0.3	6.92	5.13
Standard deviation	0.5	0.02	0.3	0.1	0.00	0.2	0.3	0.1	0.01	0.02	0.59	0.3	0.14	0.51	0.60
No. of measurements	5	5	5	5	5	5	5	5	5	5	4	5	5	5	5
GROUP3															
Average	47.6	1.61	14.8	12.9	0.20	9.1	11.7	2.1	0.17	0.15		100.6	0.66	7.02	5.14
Standard deviation	0.5	0.17	0.3	0.3	0.01	0.9	0.3	0.2	0.01	0.02		0.2	0.03	0.06	0.23
No. of measurements	2	2	2	2	2	2	2	2	2	2	0	2	2	2	2
GROUP 4															
Average	47.4	1.58	15.1	12.9	0.20	9.3	11.6	2.2	0.16	0.15		100.7	0.19	6.89	5.26
Standard deviation	0.0	0.02	0.1	0.1	0.00	0.0	0.0	0.1	0.00	0.00		0.1	0.12	0.28	0.24
No. of measurements	2	2	2	2	2	2	2	2	2	2	0	2	2	2	2
GROUP 5															
Average	47.3	1.72	15.0	13.2	0.20	8.4	11.8	2.1	0.15	0.15	0.03	100.1	0.48	8.31	3.97
Standard deviation	0.1	0.00	0.0	0.0	0.00	0.1	0.1	0.0	0.00	0.00		0.2	0.01	0.18	0.16
No. of measurements	2	2	2	2	2	2	2	2	2	2	1	2	2	2	2
GROUP 6															
Average	47.4	1.66	15.0	13.0	0.20	8.7	11.7	2.2	0.17	0.15		100.3	0.36	8.76	3.27
Standard deviation	0.0	0.00	0.1	0.0	0.00	0.1	0.0	0.0	0.01	0.00		0.0	0.25	0.10	0.08
No. of measurements	2	2	2	2	2	2	2	2	2	2	0	2	2	2	2
GROUP 7															
Average	47.3	1.51	14.9	12.7	0.19	9.9	11.3	2.1	0.16	0.14		100.3	0.36	7.29	4.65
Standard deviation	0.2	0.01	0.1	0.0	0.00	0.2	0.0	0.1	0.01	0.00		0.5	0.02	0.11	0.08
No. of measurements	2	2	2	2	2	2	2	2	2	2	0	2	2	2	2
GROUP 8															
Average	47.3	1.51	15.1	12.6	0.19	9.4	11.5	2.2	0.16	0.14		100.3	0.34	8.57	3.08
Standard deviation	0.5	0.01	0.1	0.1	0.00	0.1	0.1	0.0	0.00	0.00		0.8	0.04	0.06	0.11
No. of measurements	2	2	2	2	2	2	2	2	2	2	0	2	2	2	2
GROUP 9															
Average	47.5	1.58	15.3	12.6	0.19	8.9	11.6	2.1	0.18	0.15		100.2	0.32	8.26	3.46
Standard deviation	0.2	0.01	0.0	0.0	0.00	0.1	0.0	0.0	0.01	0.00		0.4	0.40	0.16	0.18
No. of measurements	2	2	2	2	2	2	2	2	2	2	0	2	2	2	2

Table A11. *Statistical properties of major element compositions. Supergroups A and B*

Parameter	SiO_2	TiO_2	Al_2O_3	Fe_2O_3	MnO	MgO	CaO	Na_2O	K_2O	P_2O_5	LOI	Tot. weight	CO_2	FeO	Fe_2O_3
Unit	%	%	%	%	%	%	%	%	%	%	%	%	%	%	%
Identifier	SiO2	TiO2	Al2O3	Fe2O3	MnO	MgO	CaO	Na2O	K2O	P2O5	LOI	TWP	CO2 (%)	FeO (%)	Fe2O3 (%)
Measured by	Mc GILL	Mc GILL	Mc GILL	Mc GILL	Mc GILL	Mc GILL	Mc GILL	Mc GILL	Mc GILL	Mc GILL	Mc GILL	Mc GILL	Mc GILL	Mc GILL	Mc GILL
SUPERGROUP A															
Average	47.2	1.62	15.2	12.9	0.20	8.9	11.6	2.1	0.16	0.13	0.74	100.4	0.37	7.54	4.52
Standard deviation	0.5	0.07	0.3	0.2	0.00	0.4	0.2	0.1	0.01	0.03	0.65	0.3	0.21	0.83	0.90
No. of measurements	18	18	18	18	18	18	13	18	15	15	7	15	15	13	15
SUPERGROUP B															
Average	47.2	1.50	14.9	12.7	0.19	9.8	11.3	2.1	0.16	0.14		100.1	0.34	7.61	4.23
Standard deviation	0.3	0.02	0.2	0.1	0.00	0.3	0.2	0.1	0.01	0.00		0.5	0.03	0.94	1.05
No. of measurements	6	6	6	6	6	6	6	6	6	2	4	6	6	6	2

Table A12. *Statistical properties of major element compositions. All samples*

Parameter	SiO_2	TiO_2	Al_2O_3	Fe_2O_3	MnO	MgO	CaO	Na_2O	K_2O	P_2O_5	LOI	Tot. weight	CO_2	FeO	Fe_2O_3
Unit	%	%	%	%	%	%	%	%	%	%	%	%	%	%	%
Identifier	SiO2	TiO2	Al2O3	Fe2O3	MnO	MgO	CaO	Na2O	K2O	P2O5	LOI	TWP	CO2 (%)	FeO (%)	Fe2O3 (%)
Measured by	Mc GILL	Mc GILL	Mc GILL	Mc GILL	Mc GILL	Mc GILL	Mc GILL	Mc GILL	Mc GILL	Mc GILL	Mc GILL	Mc GILL	Mc GILL	Mc GILL	Mc GILL
Average	47.2	1.58	15.1	12.8	0.20	9.2	11.5	2.1	0.16	0.14	0.74	100.3	0.36	7.56	4.44
Standard deviation	0.4	0.08	0.3	0.2	0.004	0.6	0.2	0.1	0.01	0.02	0.65	0.4	0.17	0.84	0.93
No. of measurements	21	21	21	21	21	21	21	21	21	21	5	21	21	21	21

$\frac{\Delta y}{x} \cdot 10^3$ 8 20 20 17 4

50 15 65

Table A13. *Statistical properties of minor element compositions. Groups 1-9*

Parameter	BaO	Ce	Cu	V	Zn	Ga	Nb	Pb	Rb	Sr	Th	U	Y	Zr	As	Sb	S
Unit	ppm	ppm	ppm	ppm	ppm	ppm	ppm	ppm	ppm	ppm	ppm	ppm	ppm	ppm	ppm	ppm	ppm
Identifier	BaO	Ce	Cu	V	Zn	Ga	Nb	Pb	Rb	Sr	Th	U	Y	Zr	As	Sb	S
Measured by	Mc GILL	Mc GILL	Mc GILL	Mc GILL	Mc GILL	Mc GILL	Mc GILL	Mc GILL	Mc GILL	Mc GILL	Mc GILL	Mc GILL	Mc GILL	Mc GILL	Mc GILL	Mc GILL	Mc GILL
GROUP 1																	
Average	45	28	227	270	80	17.5	10.6	1.5	4.4	178	1.50	-	24.8	77.4	4.6	-	-
Standard deviation	3	7	9	3	1	0.4	0.4	0.4	0.1	2	0.14	-	0.4	0.2	0.8	-	-
No. of measurements	2	2	2	2	2	2	2	2	2	2	2	0	2	2	2	0	0
GROUP2																	
Average	49	28	264	293	70	18.4	11.2	1.6	4.6	249	1.38	-	25.9	85.6	4.2	-	-
Standard deviation	9	7	13	7	2	0.7	0.2	0.3	0.3	43	0.19	-	0.8	1.9	1.0	-	-
No. of measurements	5	5	5	5	5	5	5	5	5	5	4	0	5	5	5	0	0
GROUP3																	
Average	47	28	238	306	80	18.2	11.3	1.8	4.9	177	1.90	-	26.8	85.5	4.4	-	-
Standard deviation	5	1	19	33	6	0.3	0.5	0.4	0.4	0		-	2.3	8.6	0.2	-	-
No. of measurements	2	2	2	2	2	2	2	2	2	2	1	0	2	2	2	0	0
GROUP 4																	
Average	41	21	270	298	78	17.6	11.0	1.6	4.6	183	1.70	-	26.1	83.9	3.7	-	-
Standard deviation	13	4	16	7	4	0.3	0.2	0.1	0.1	2	0.00	-	0.3	1.6	0.4	-	-
No. of measurements	2	2	2	2	2	2	2	2	2	2	2	0	2	2	2	0	0
GROUP 5																	
Average	44	32	245	318	82	18.8	11.8	1.8	4.6	208	1.90	-	27.8	91.7	5.0	-	-
Standard deviation	11	4	11	8	6	0.3	0.1	0.0	0.1	12	0.00	-	0.4	0.6	2.3	-	-
No. of measurements	2	2	2	2	2	2	2	2	2	2	2	0	2	2	2	0	0
GROUP 6																	
Average	42	30	238	310	88	18.4	11.8	2.2	4.6	181	1.85	-	26.7	88.6	6.7	-	-
Standard deviation	4	4	6	2	5	0.6	0.4	0.1	0.4	4	0.21	-	0.1	0.9	0.8	-	-
No. of measurements	2	2	2	2	2	2	2	2	2	2	2	0	2	2	2	0	0
GROUP 7																	
Average	52	31	224	276	127	18.0	10.5	1.5	4.6	179	1.40	-	25.5	79.7	4.1	-	-
Standard deviation	1	12	4	6	60	0.4	0.1	0.2	0.4	2	0.14	-	0.1	0.6	2.1	-	-
No. of measurements	2	2	2	2	2	2	2	2	2	2	2	0	2	2	2	0	0
GROUP 8																	
Average	58	35	231	287	81	18.2	10.4	1.7	4.7	184	1.40	-	25.3	78.4	5.3	-	-
Standard deviation	4	4	9	6	12	0.2	0.0	0.4	0.1	0	0.14	-	0.1	0.3	0.4	-	-
No. of measurements	2	2	2	2	2	2	2	2	2	2	2	0	2	2	2	0	0
GROUP 9																	
Average	39	30	219	290	75	18.0	11.4	1.7	5.1	180	1.60	-	26.5	85.8	5.8	-	-
Standard deviation	7	0	10	1	4	0.1	0.1	0.7	0.1	0	0.14	-	0.3	1.1	1.8	-	-
No. of measurements	2	2	2	2	2	2	2	2	2	2	2	0	2	2	2	0	0

Table A14. *Statistical properties of minor element compositions. Supergroups A and B*

Parameter	BaO	Ce	Cu	V	Zn	Ga	Nb	Pb	Rb	Sr	Th	U	Y	Zr	As	Sb	S
Unit	ppm	ppm	ppm	ppm	ppm	ppm	ppm	ppm	ppm	ppm	ppm	ppm	ppm	ppm	ppm	ppm	ppm
Identifier	BaO	Ce	Cu	V	Zn	Ga	Nb	Pb	Rb	Sr	Th	U	Y	Zr	As	Sb	S
Measured by	Mc GILL	Mc GILL	Mc GILL	Mc GILL	Mc GILL	Mc GILL	Mc GILL	Mc GILL	Mc GILL	Mc GILL	Mc GILL	Mc GILL	Mc GILL	Mc GILL	Mc GILL	Mc GILL	Mc GILL
SUPERGROUP A																	
Average	45	28	249	301	77	18.2	11.3	1.7	4.7	207	1.65	-	26.5	86.6	4.8	-	-
Standard deviation	8	5	20	14	7	0.6	0.4	0.3	0.3	40	0.25	-	1.0	3.5	1.4	-	-
No. of measurements	15	15	15	15	15	15	13	15	15	15	13	2	15	15	15	2	2
SUPERGROUP B																	
Average	52	31	227	277	96	17.9	10.5	1.5	4.5	180	1.43		25.2	78.5	4.7		
Standard deviation	6	7	7	9	36	0.4	0.2	0.3	0.2	3	0.12		0.4	1.1	1.2		
No. of measurements	6	6	6	6	6	6	6	6	6	6	2	4	6	6	2	0	0

Table A15. *Statistical properties of minor element compositions. All samples*

Parameter	BaO	Ce	Cu	V	Zn	Ga	Nb	Pb	Rb	Sr	Th	U	Y	Zr	As	Sb	S
Unit	ppm	ppm	ppm	ppm	ppm	ppm	ppm	ppm	ppm	ppm	ppm	ppm	ppm	ppm	ppm	ppm	ppm
Identifier	BaO	Ce	Cu	V	Zn	Ga	Nb	Pb	Rb	Sr	Th	U	Y	Zr	As	Sb	S
Measured by	Mc GILL	Mc GILL	Mc GILL	Mc GILL	Mc GILL	Mc GILL	Mc GILL	Mc GILL	Mc GILL	Mc GILL	Mc GILL	Mc GILL	Mc GILL	Mc GILL	Mc GILL	Mc GILL	Mc GILL
Average	47	29	243	294	82	18.1	11.1	1.7	4.6	199	1.58	-	26.1	84.3	4.8	-	-
Standard deviation	8	6	20	16	21	0.5	0.5	0.3	0.3	36	0.24	-	1.0	4.8	1.3	-	-
No. of measurements	21	21	21	21	21	21	21	21	21	21	19	0	21	21	21	0	0

ÖSKJUHLÍÐ
Permeability (mD)
10
1
0.1
R40
R60
R80
R100
R120
Sample No.
A
B

Fig. 2.1

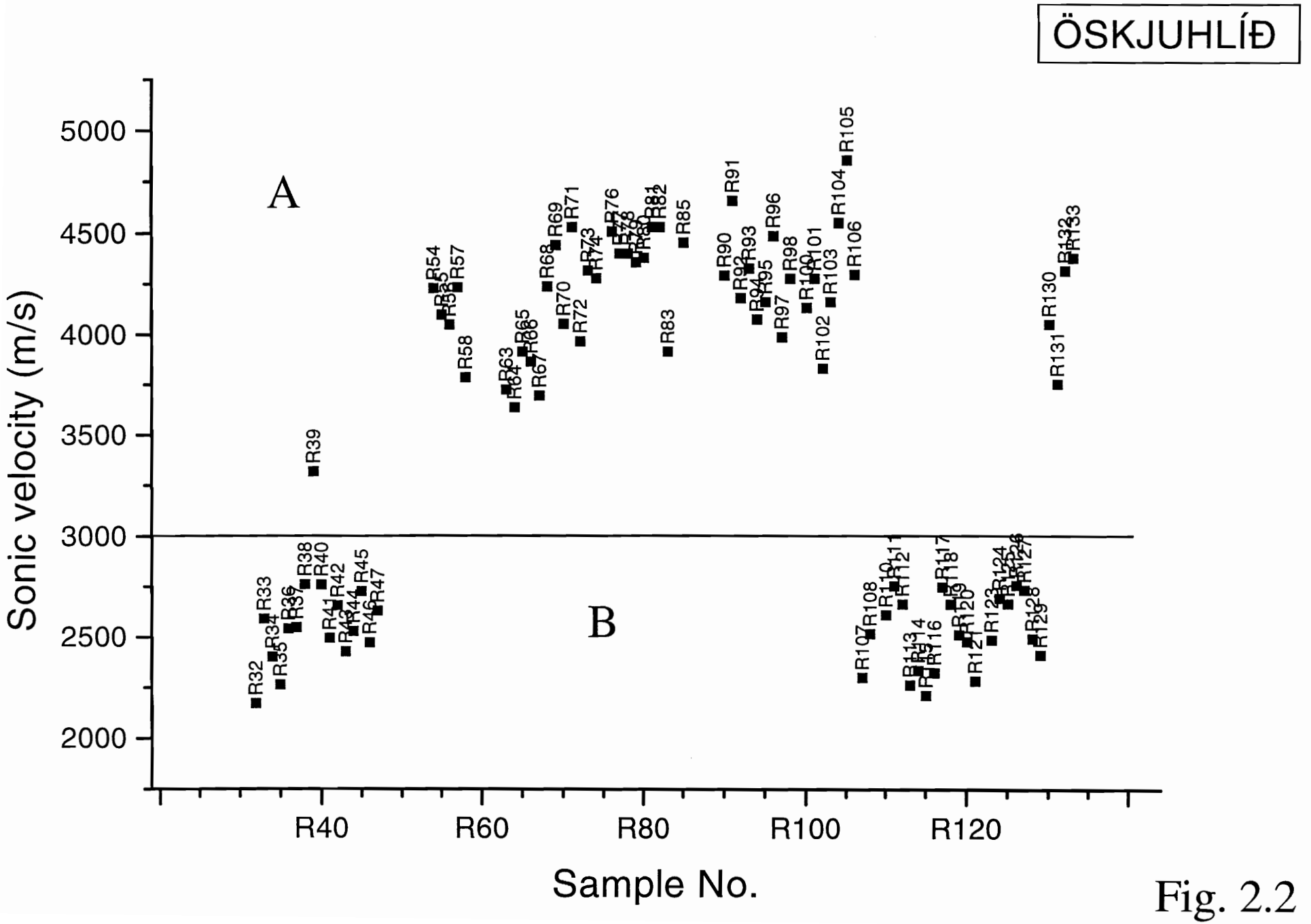
ÖSKJUHLÍÐ
A
B
Sonic velocity (m/s)
5000
4500
4000
3500
3000
2500
2000
R40
R60
R80
R100
R120
Sample No.

Fig. 2.2

ÖSKJUHLÍÐ
Thermal conductivity (W/m°C)
2.0
1.8
1.6
1.4
1.2
1.0
0.8
Sample No.
R40
R60
R80
R100
R120
R132
R130
R126
R124
R123
R120
R119
R116
R115
R114
R113
R112
R110
R102
R97
R94
R91
R90
R83
R79
R77
R76
R74
R73
R71
R70
R69
R68
R67
R66
R65
R58
R57
R56
R55
R54
R47
R46
R45
R44
R43
R42
R41
R40
R39
R38
R37
R35
R34
R33
R32

Fig. 2.3

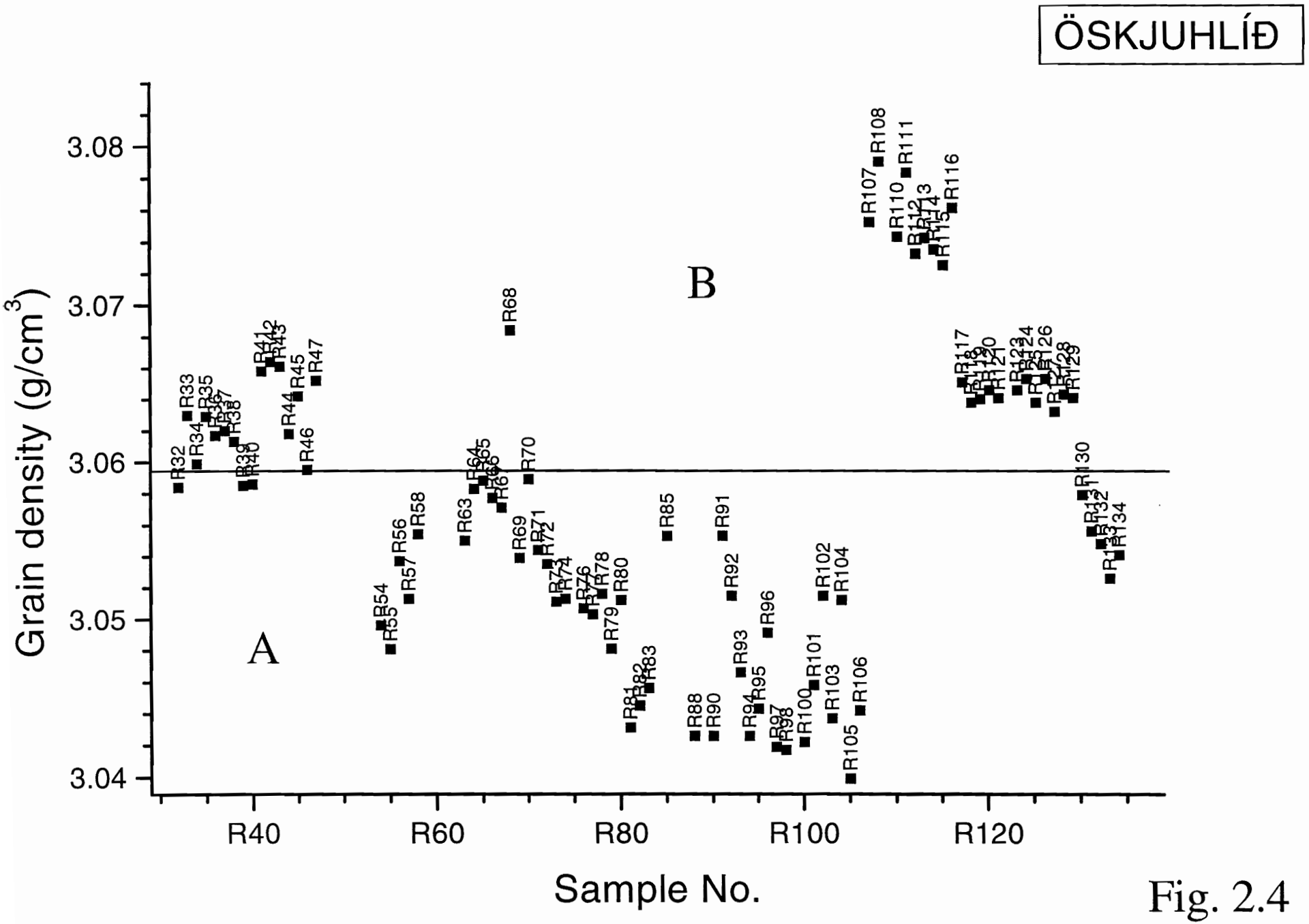
ÖSKJUHLÍÐ
Grain density (g/cm3)
3.08
3.07
3.06
3.05
3.04
A
B
R40
R60
R80
R100
R120
Sample No.

Fig. 2.4

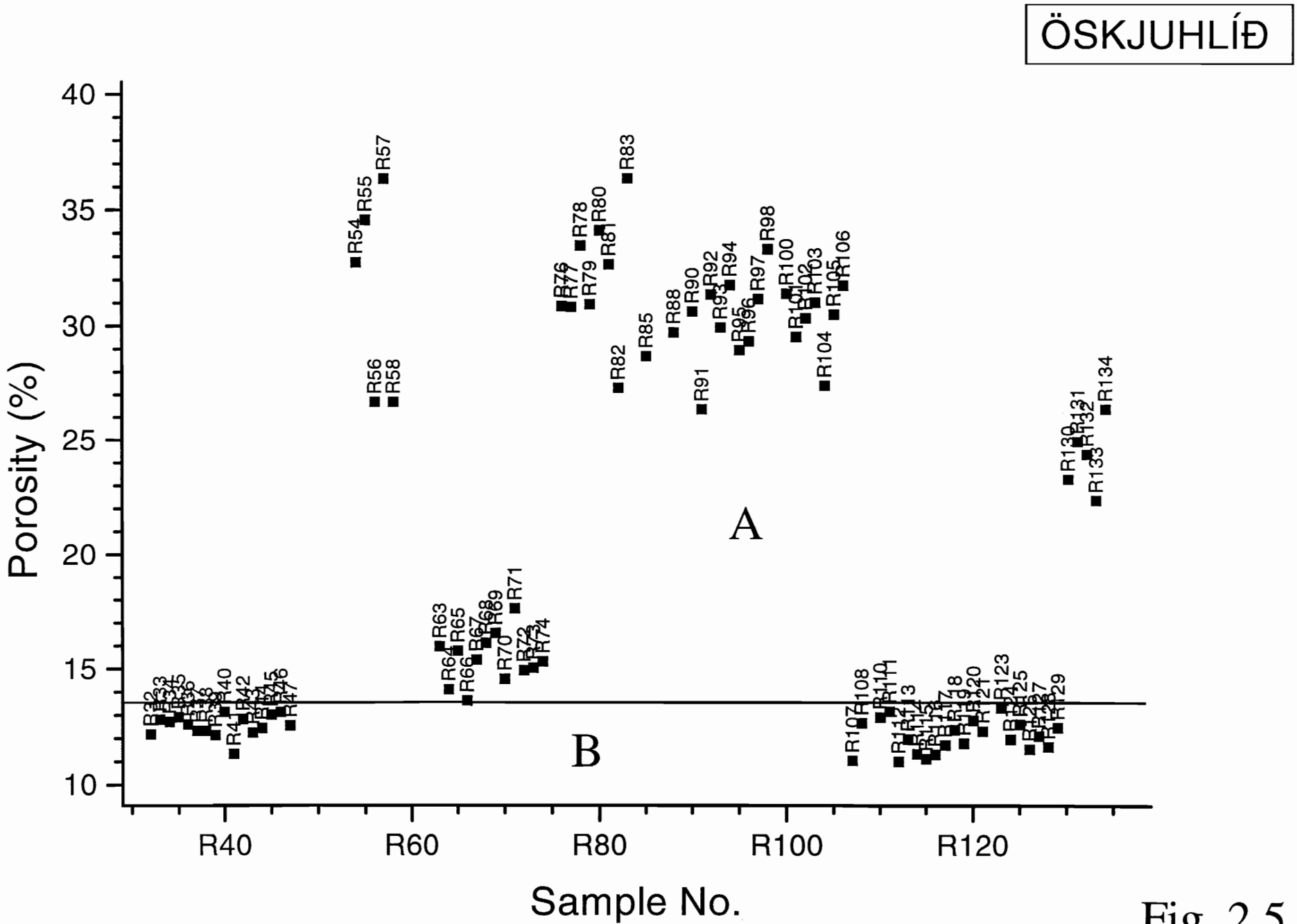
ÖSKJUHLÍÐ
Porosity (%)
Sample No.
A
B
40
35
30
25
20
15
10
R40
R60
R80
R100
R120

Fig. 2.5

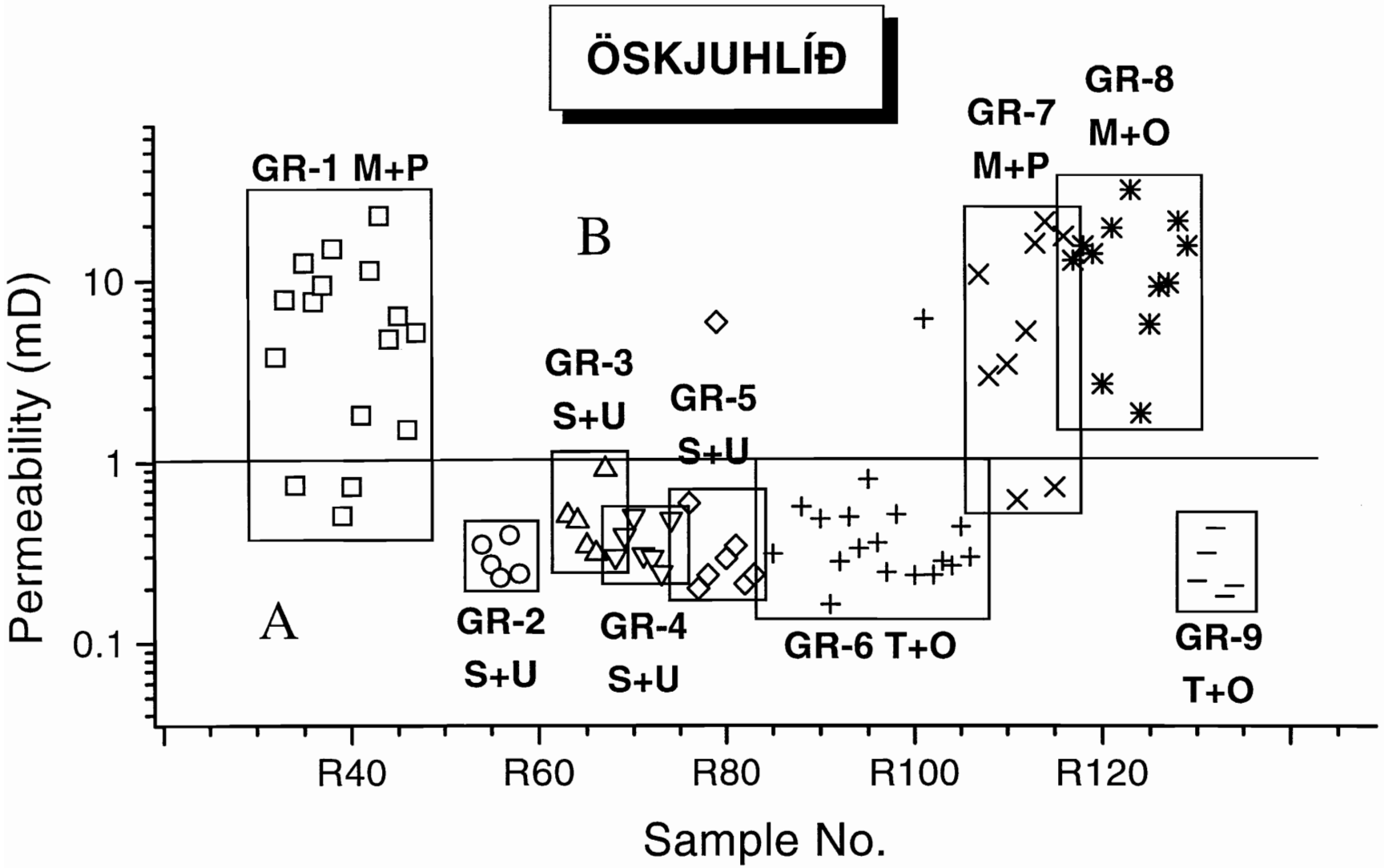

T = Top of flow
M = Middle part of flow
S = Scoriaceous part of flow
P = Parallell to flow banding
O = Orthogonal to flow banding
U = Orientation unknown

Fig. 2.6

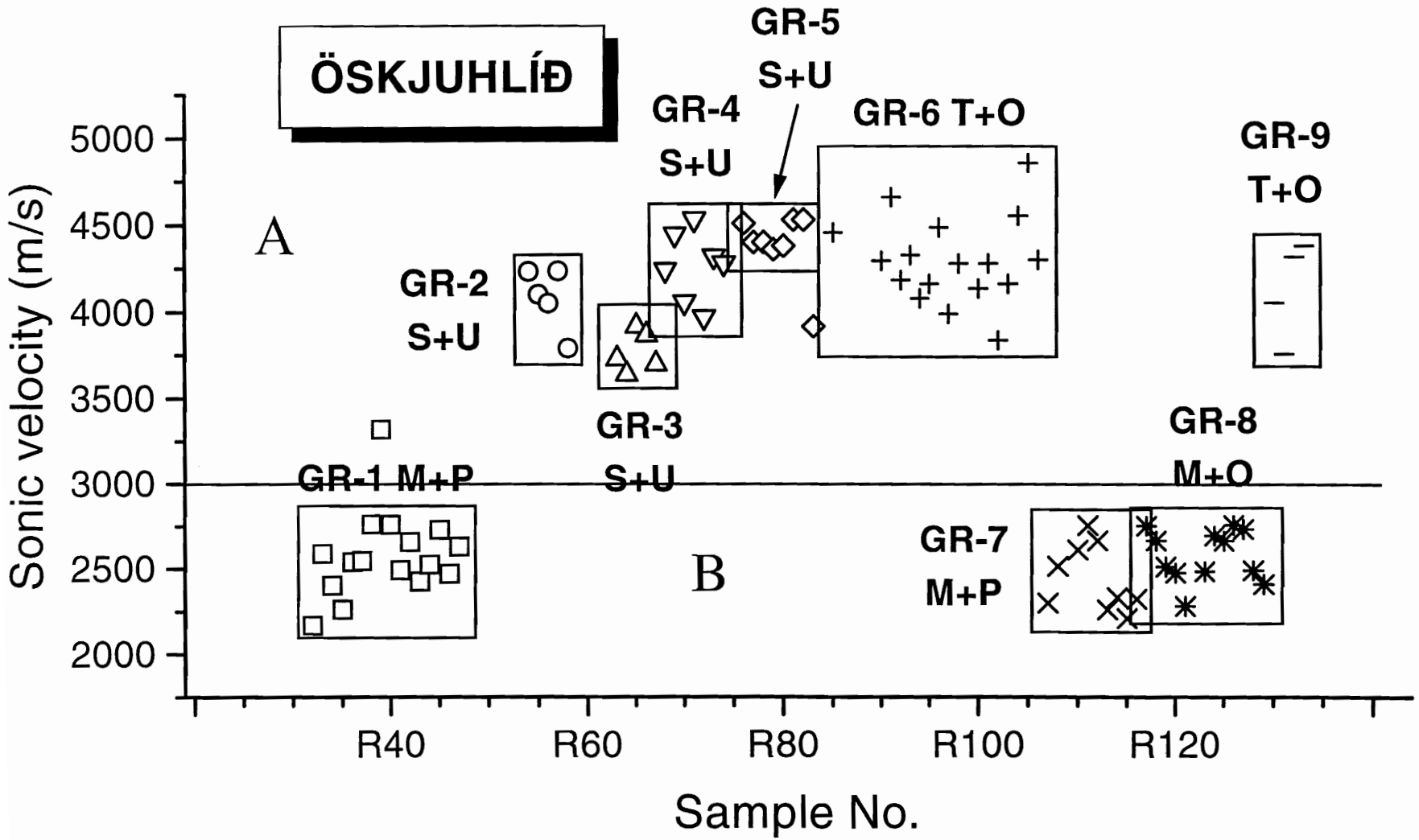

T = Top of flow
M = Middle part of flow
S = Scoriaceous part of flow
P = Parallell to flow banding
O = Orthogonal to flow banding
U = Orientation unknown

Fig. 2.7

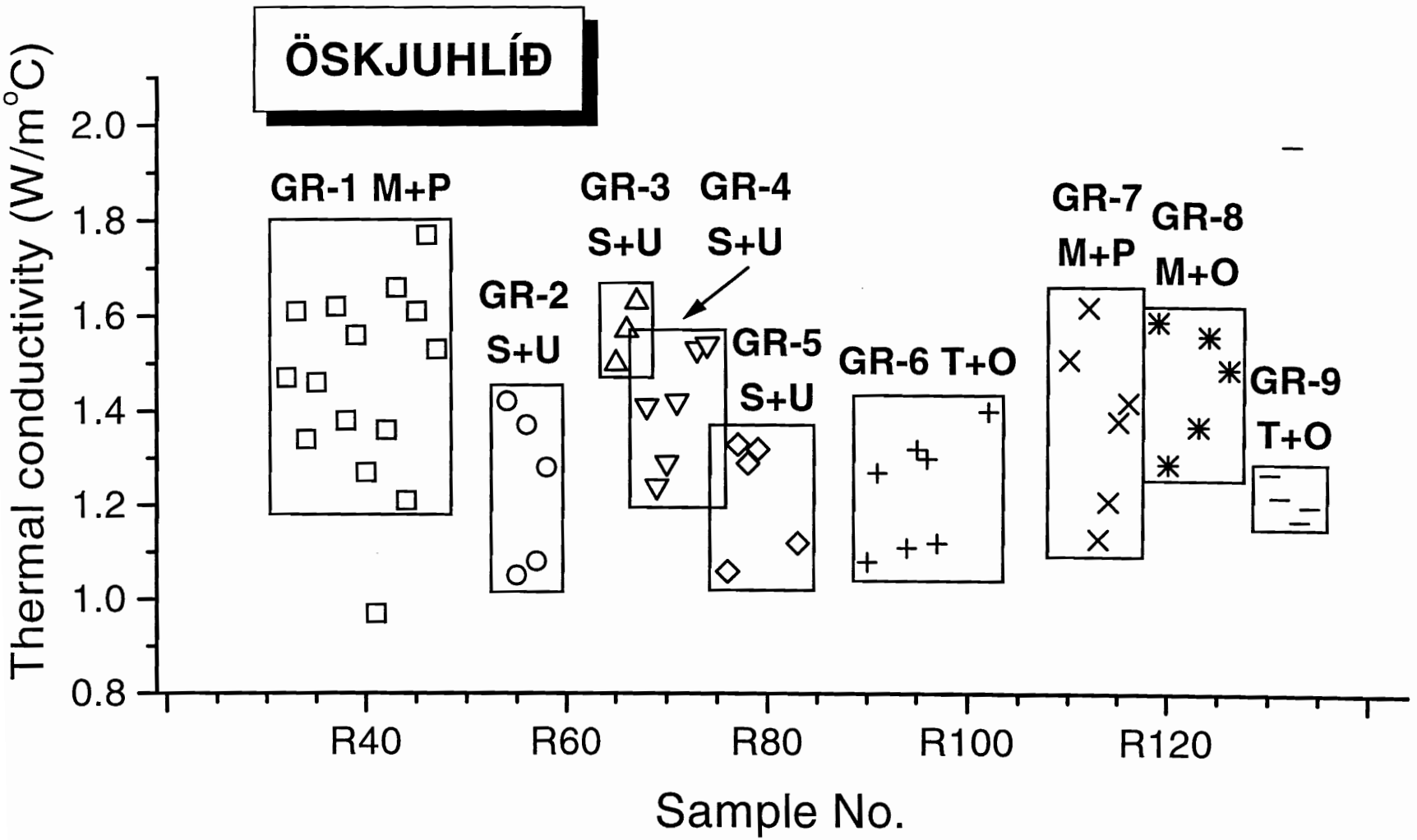

T = Top of flow
M = Middle part of flow
S = Scoriaceous part of flow

P = Parallell to flow banding
O = Orthogonal to flow banding
U = Orientation unknown

Fig. 2.8

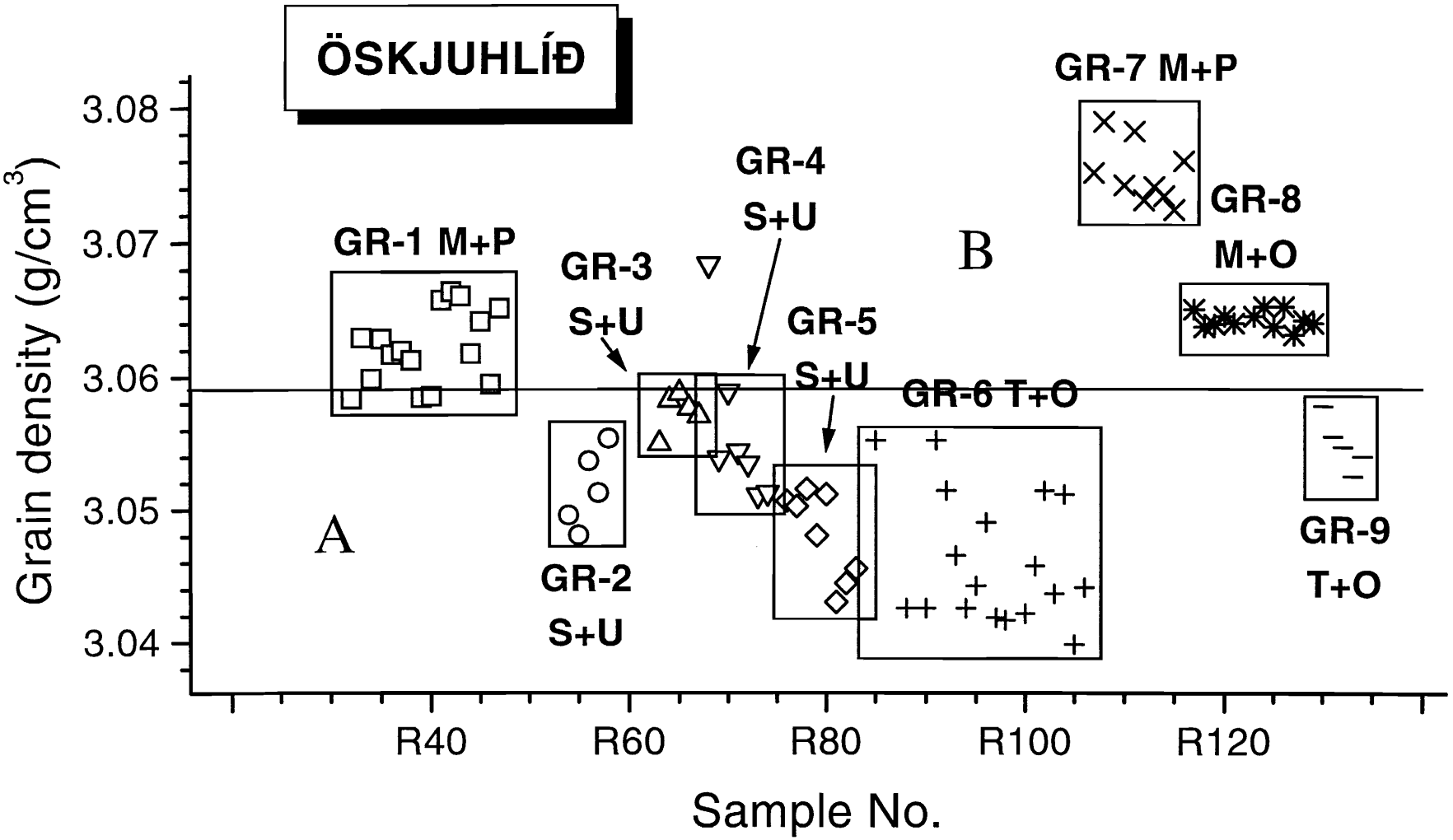

T = Top of flow
M = Middle part of flow
S = Scoriaceous part of flow
P = Parallell to flow banding
O = Orthogonal to flow banding
U = Orientation unknown

Fig. 2.9

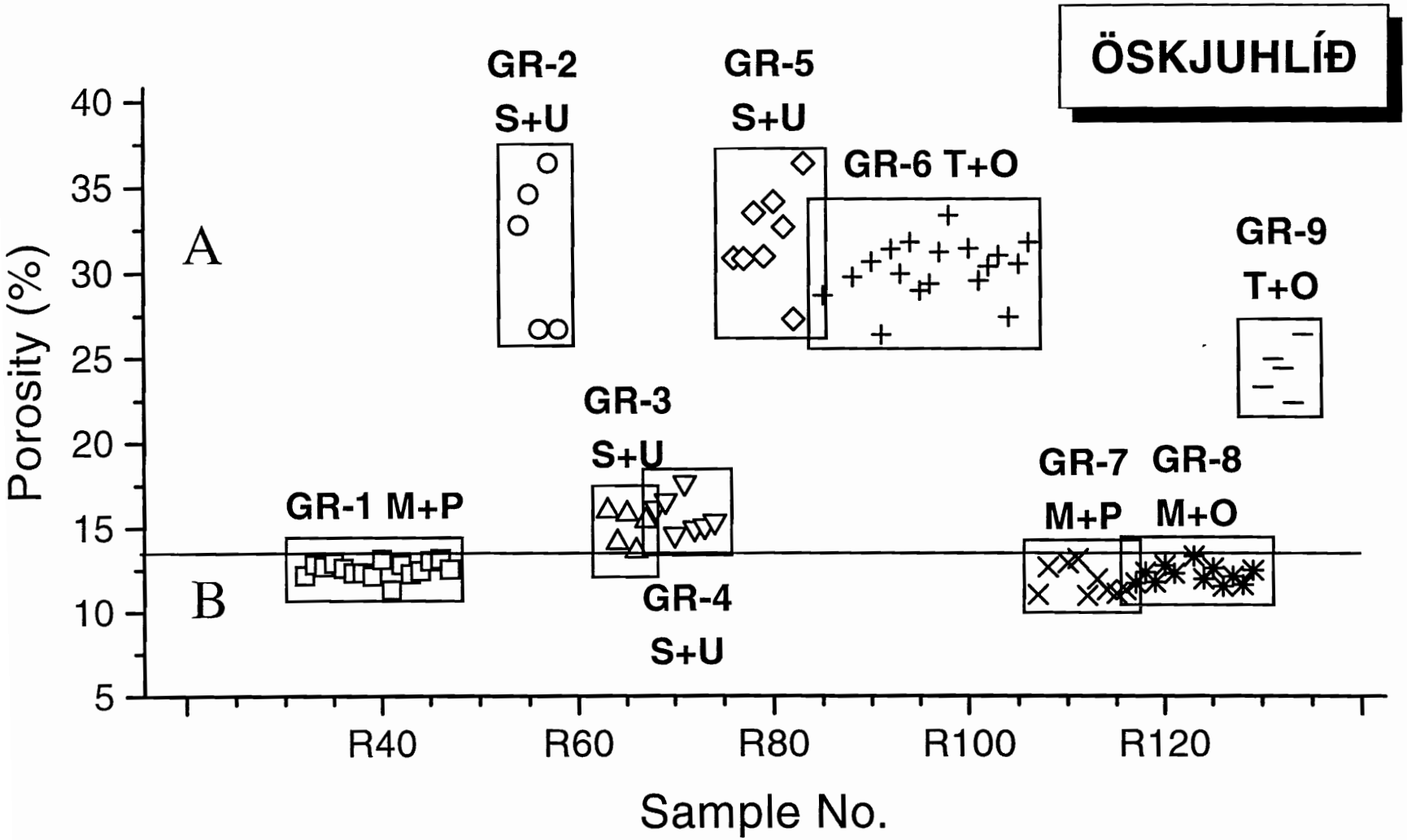

T = Top of flow
M = Middle part of flow
S = Scoriaceous part of flow
P = Parallell to flow banding
O = Orthogonal to flow banding
U = Orientation unknown

Fig. 2.10

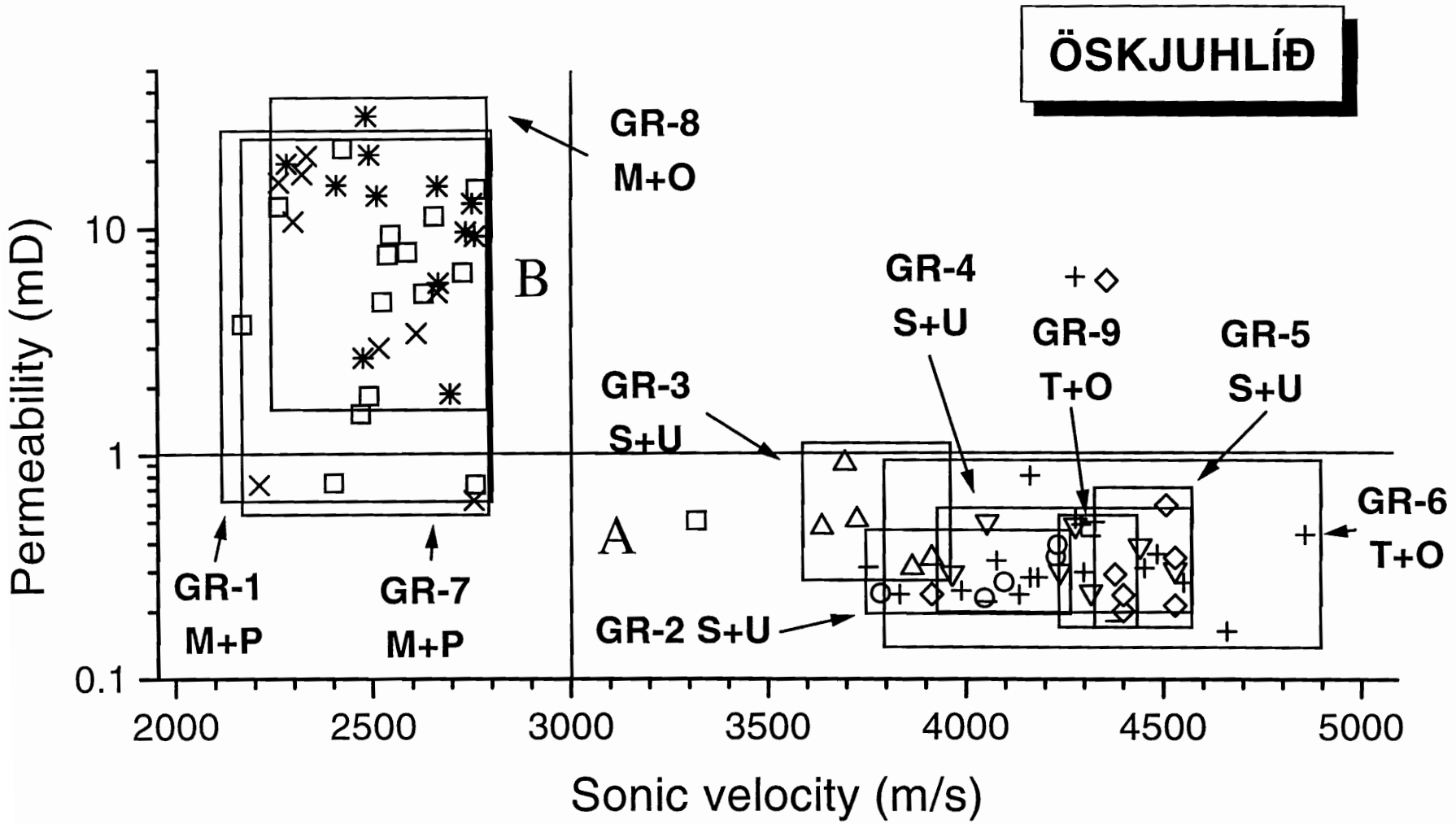

T = Top of flow
M = Middle part of flow
S = Scoriaceous part of flow

P = Parallell to flow banding
O = Orthogonal to flow banding
U = Orientation unknown

Fig. 2.11

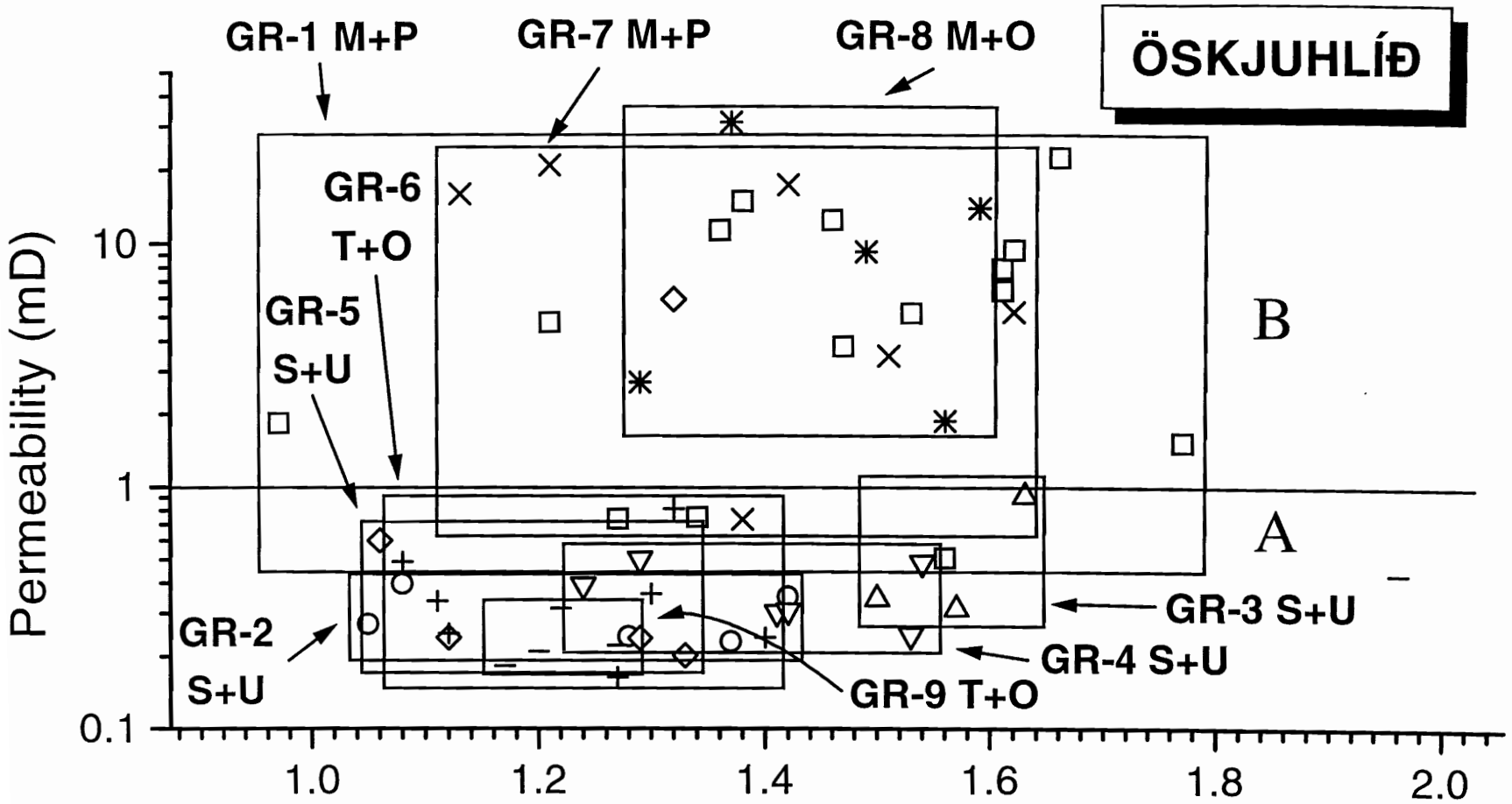

T = Top of flow
M = Middle part of flow
S = Scoriaceous part of flow

P = Parallell to flow banding
O = Orthogonal to flow banding
U = Orientation unknown

Fig. 2.12

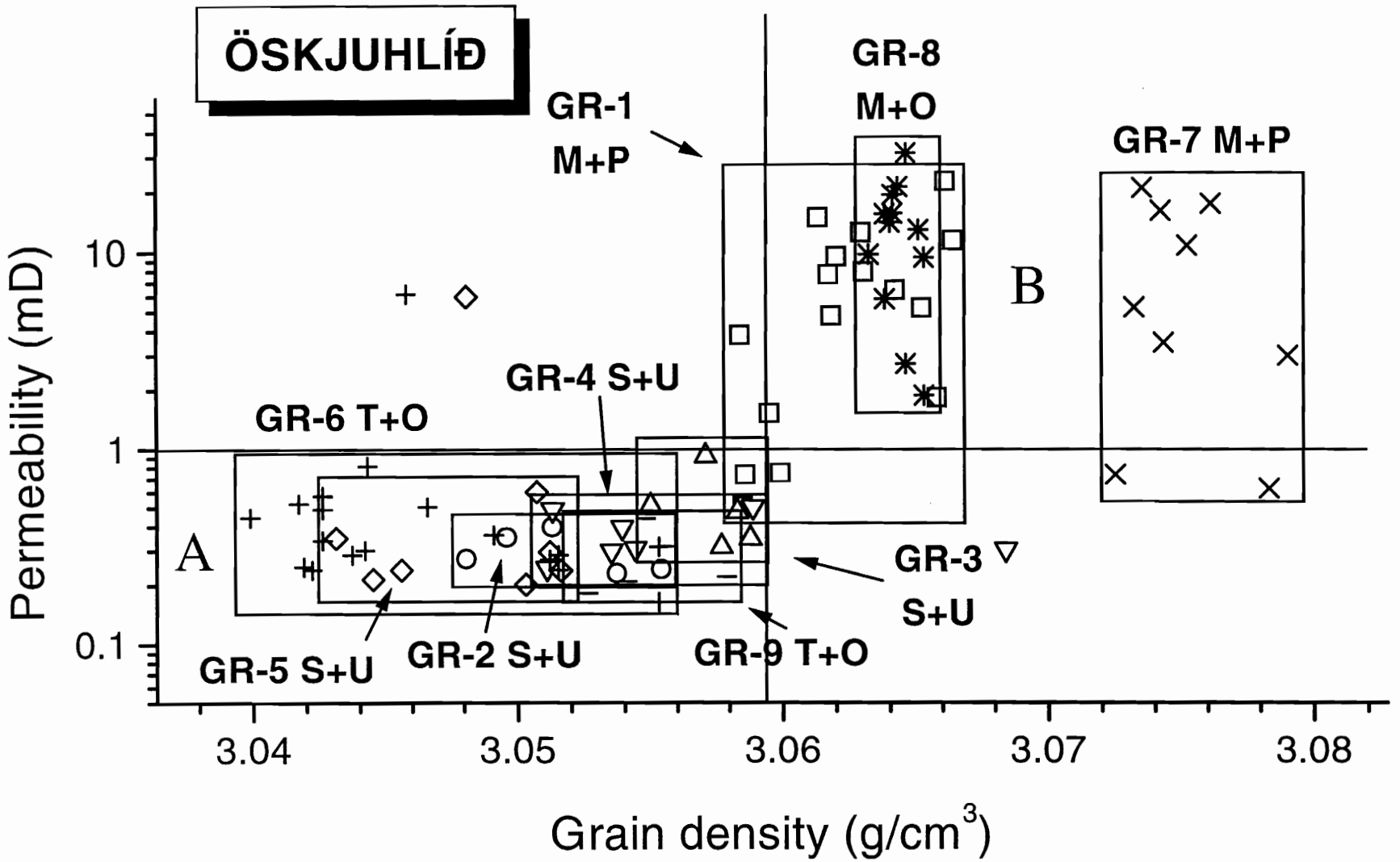

T = Top of flow
M = Middle part of flow
S = Scoriaceous part of flow
P = Parallell to flow banding
O = Orthogonal to flow banding
U = Orientation unknown

Fig. 2.13

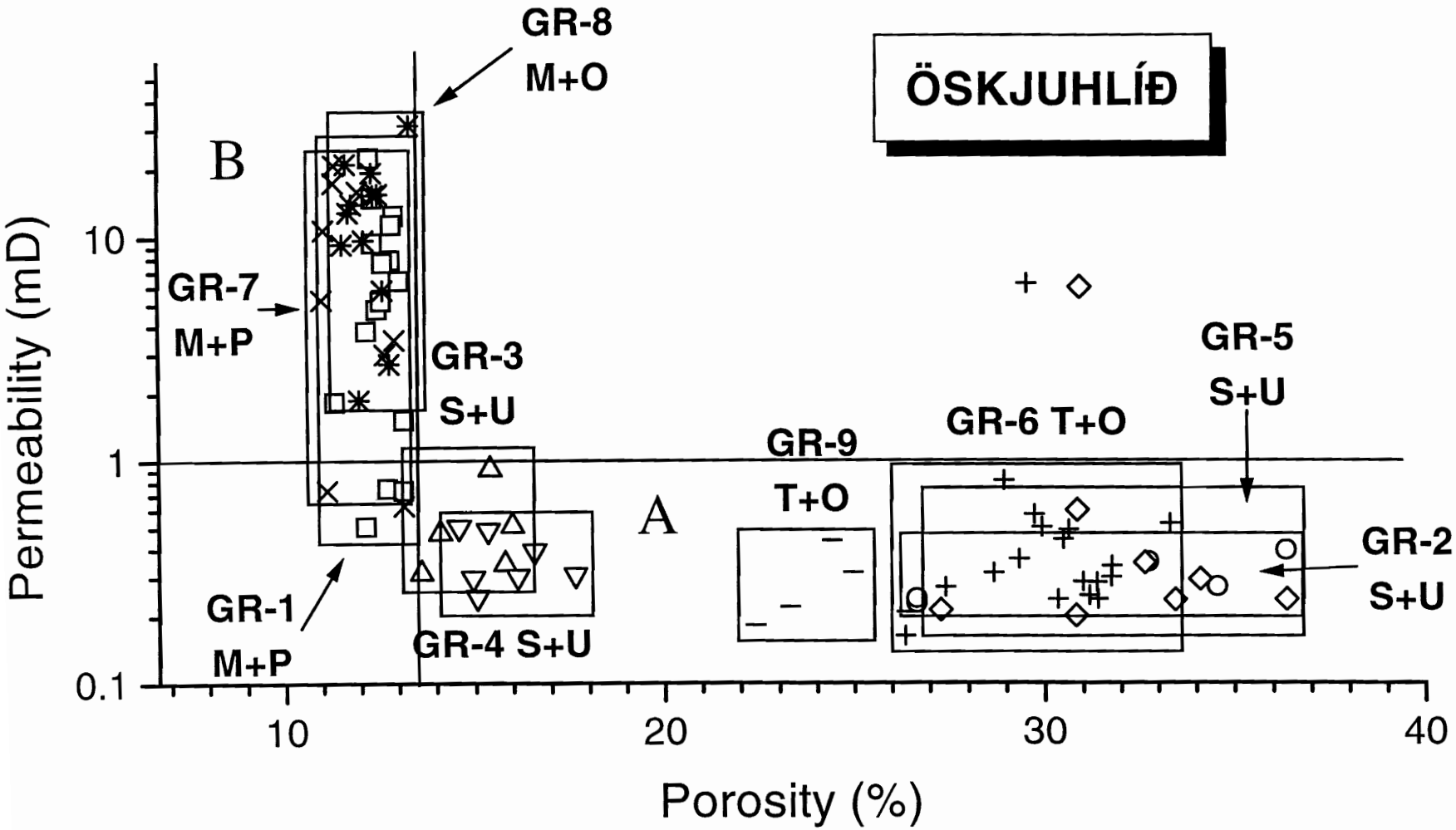

T = Top of flow
M = Middle part of flow
S = Scoriaceous part of flow

P = Parallell to flow banding
O = Orthogonal to flow banding
U = Orientation unknown

Fig. 2.14

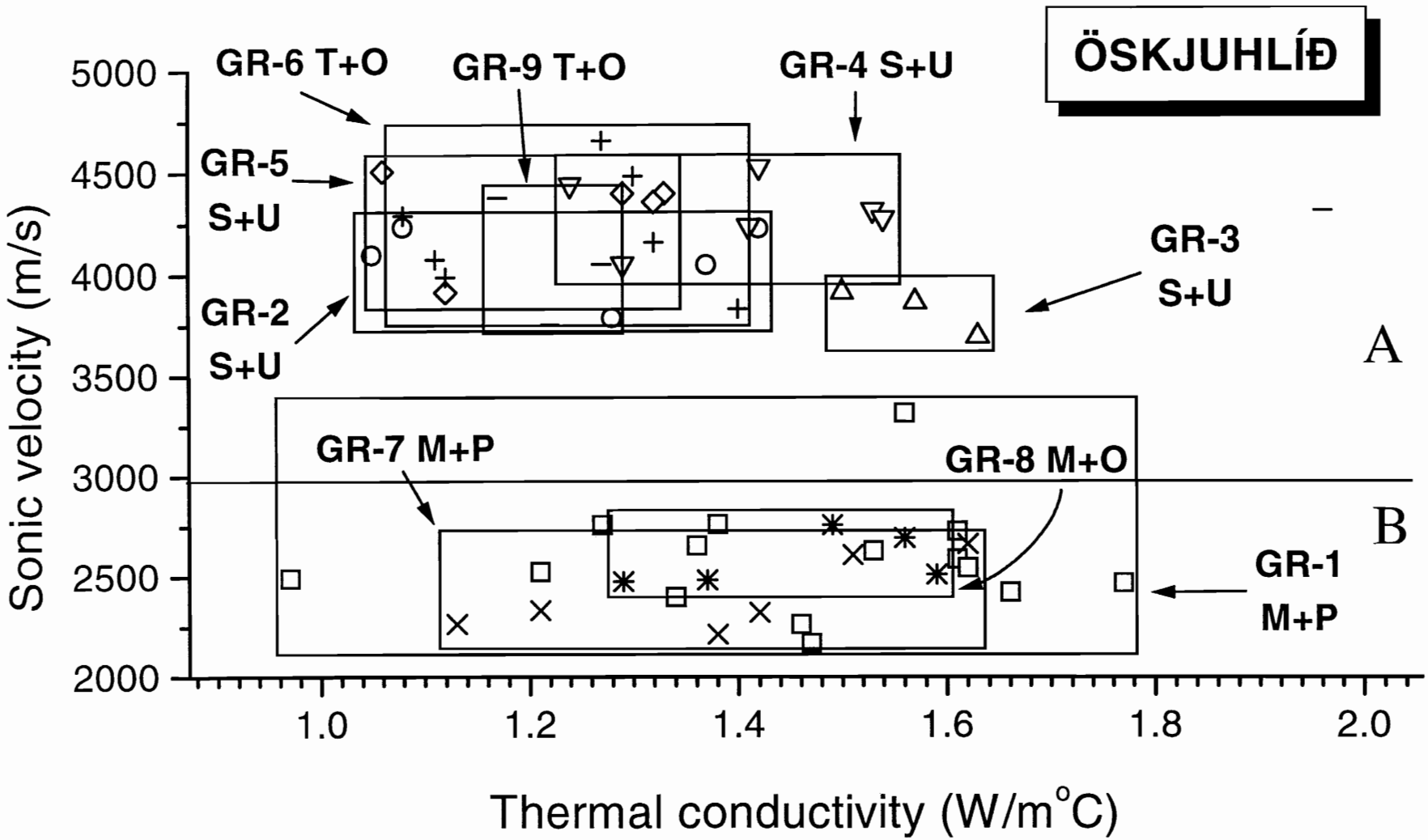

T = Top of flow

M = Middle part of flow

S = Scoriaceous part of flow

P = Parallell to flow banding

O = Orthogonal to flow banding

U = Orientation unknown

Fig. 2.15

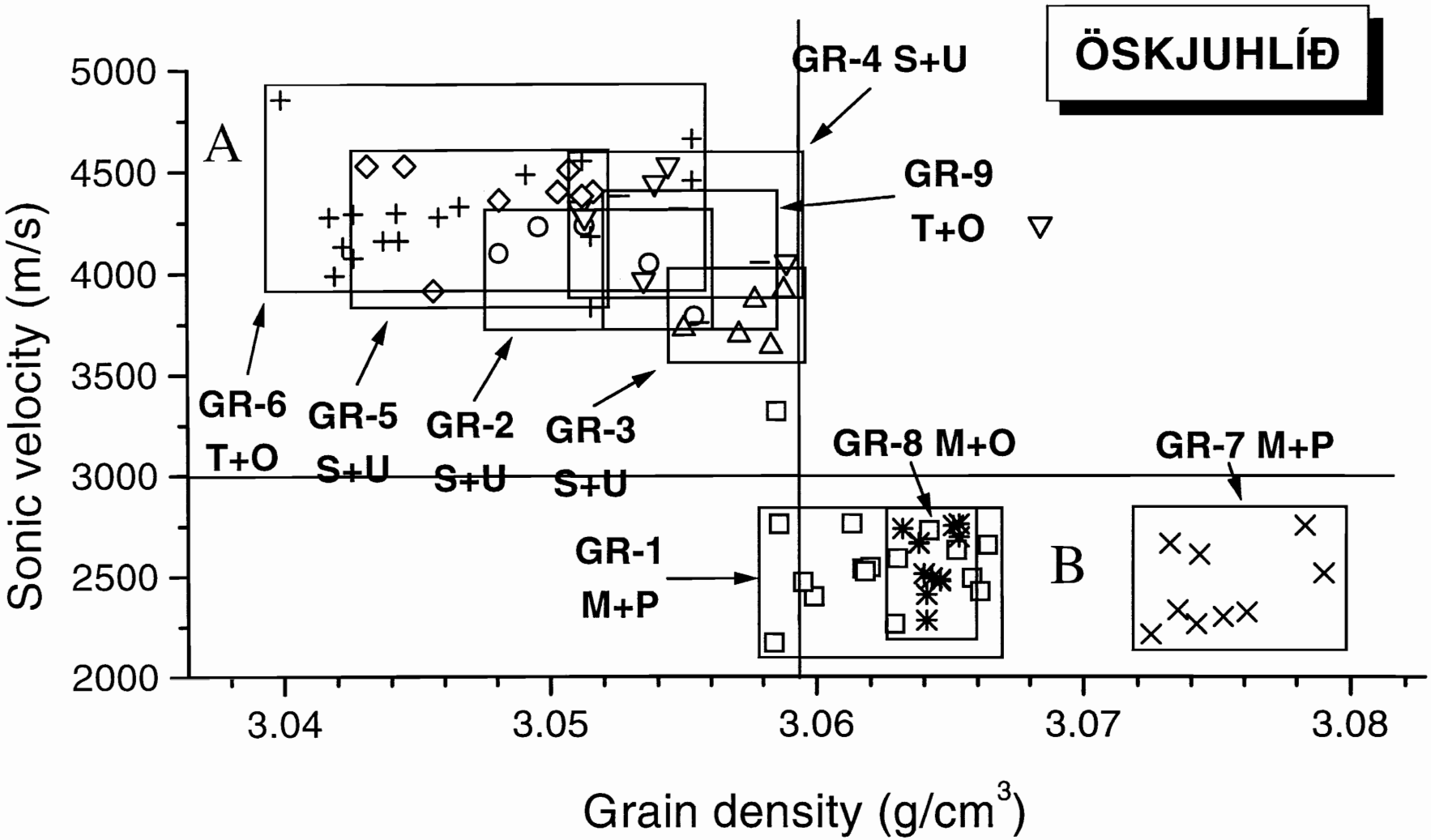

T = Top of flow
M = Middle part of flow
S = Scoriaceous part of flow
P = Parallell to flow banding
O = Orthogonal to flow banding
U = Orientation unknown

Fig. 2.16

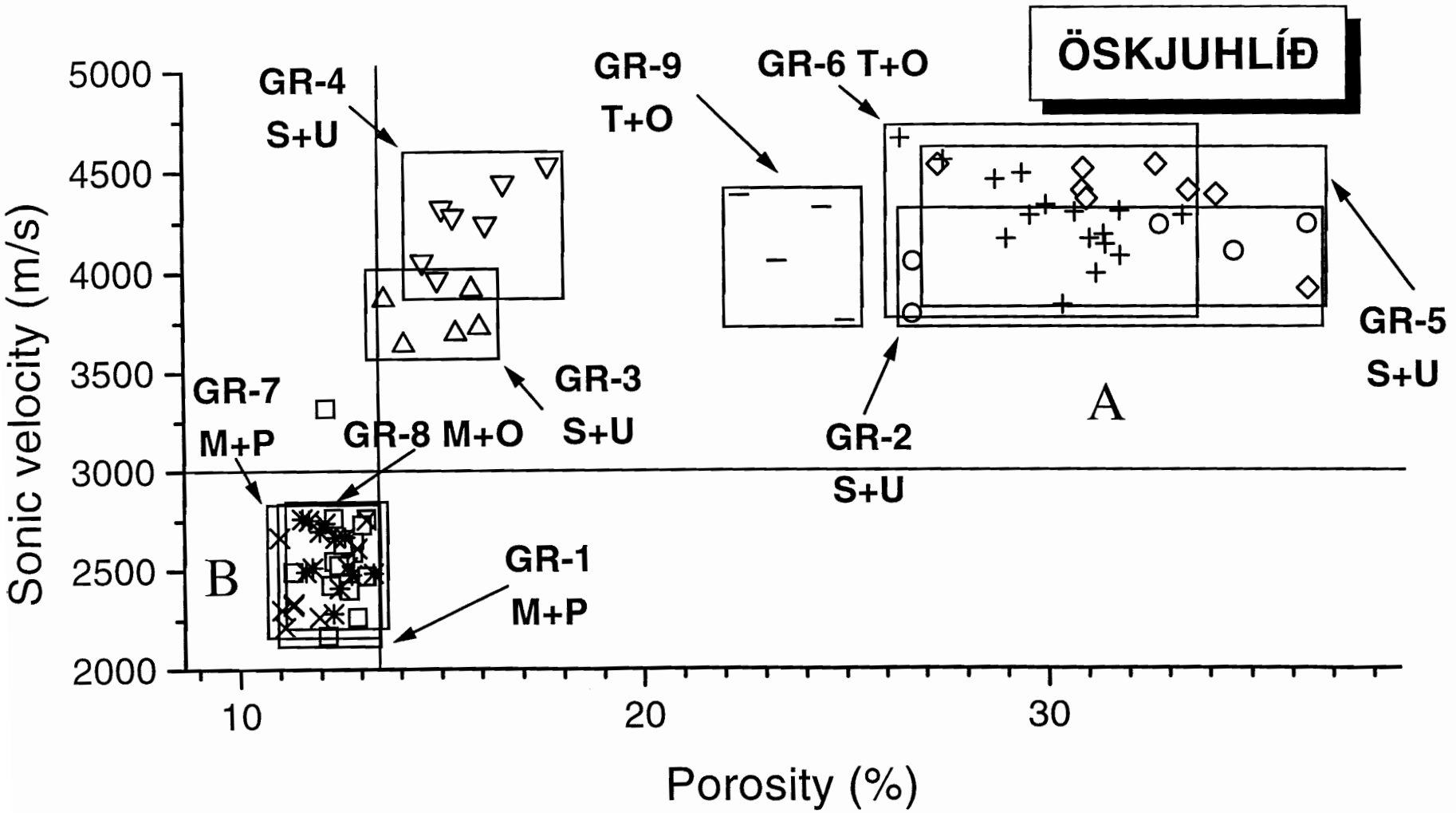

T = Top of flow
M = Middle part of flow
S = Scoriaceous part of flow

P = Parallell to flow banding
O = Orthogonal to flow banding
U = Orientation unknown

Fig. 2.17

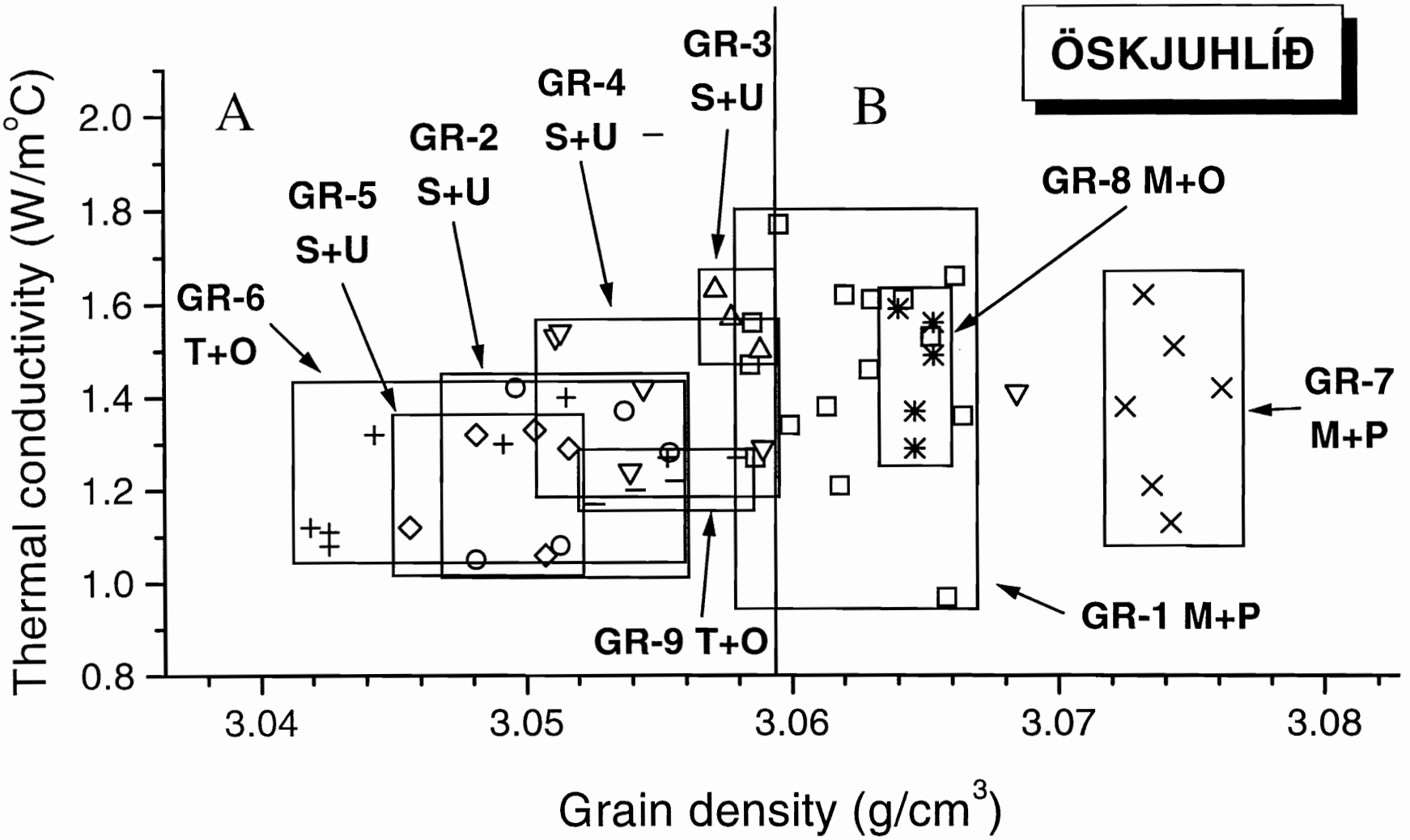

T = Top of flow
M = Middle part of flow
S = Scoriaceous part of flow

P = Parallell to flow banding
O = Orthogonal to flow banding
U = Orientation unknown

Fig. 2.18

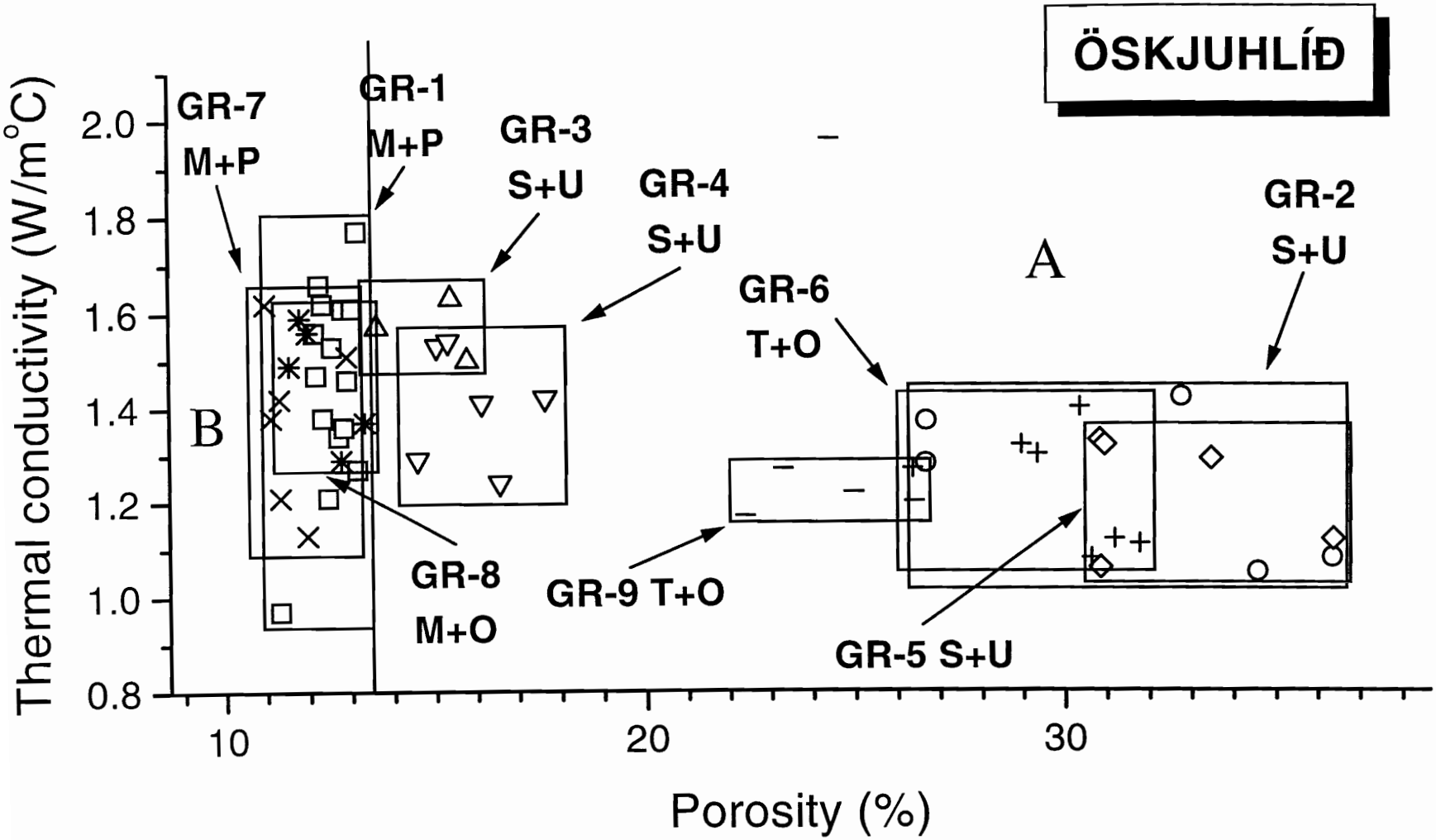

T = Top of flow
M = Middle part of flow
S = Scoriaceous part of flow

P = Parallell to flow banding
O = Orthogonal to flow banding
U = Orientation unknown

Fig. 2.19

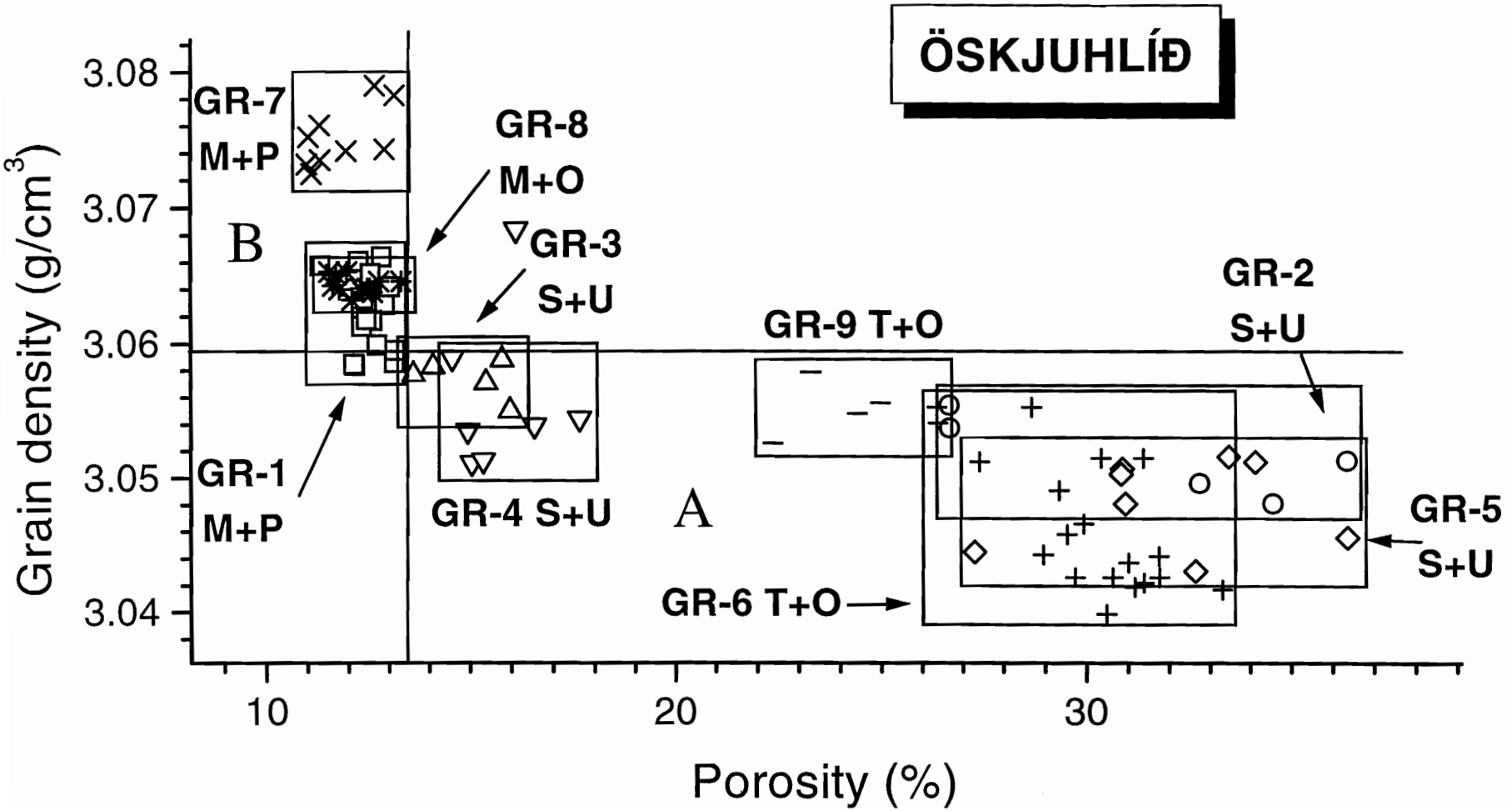

T = Top of flow
M = Middle part of flow
S = Scoriaceous part of flow

P = Parallell to flow banding
O = Orthogonal to flow banding
U = Orientation unknown

Fig. 2.20

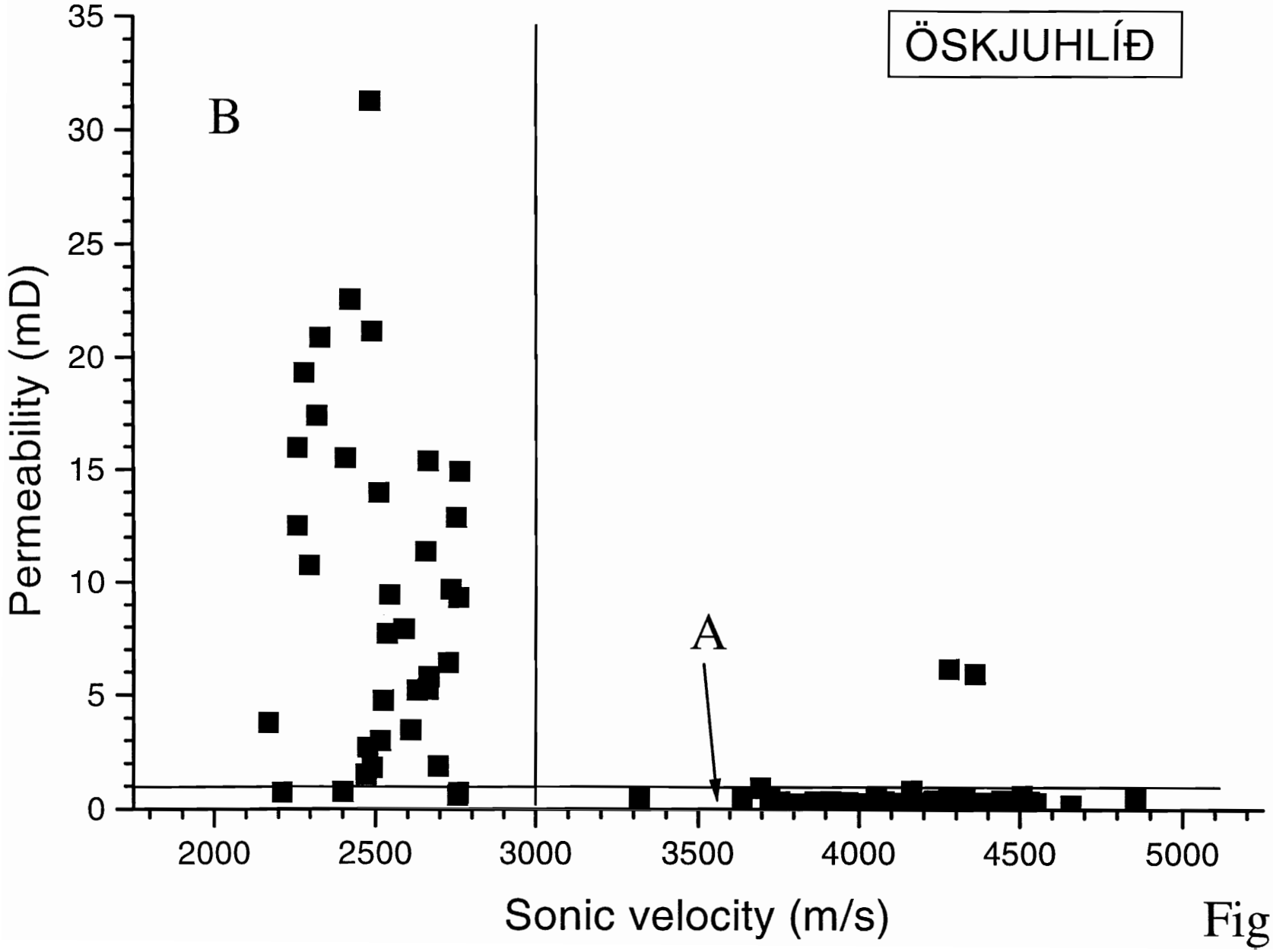
ÖSKJUHLÍÐ
B
A
Permeability (mD)
Sonic velocity (m/s)
0
5
10
15
20
25
30
35
2000
2500
3000
3500
4000
4500
5000

Fig. 2.21

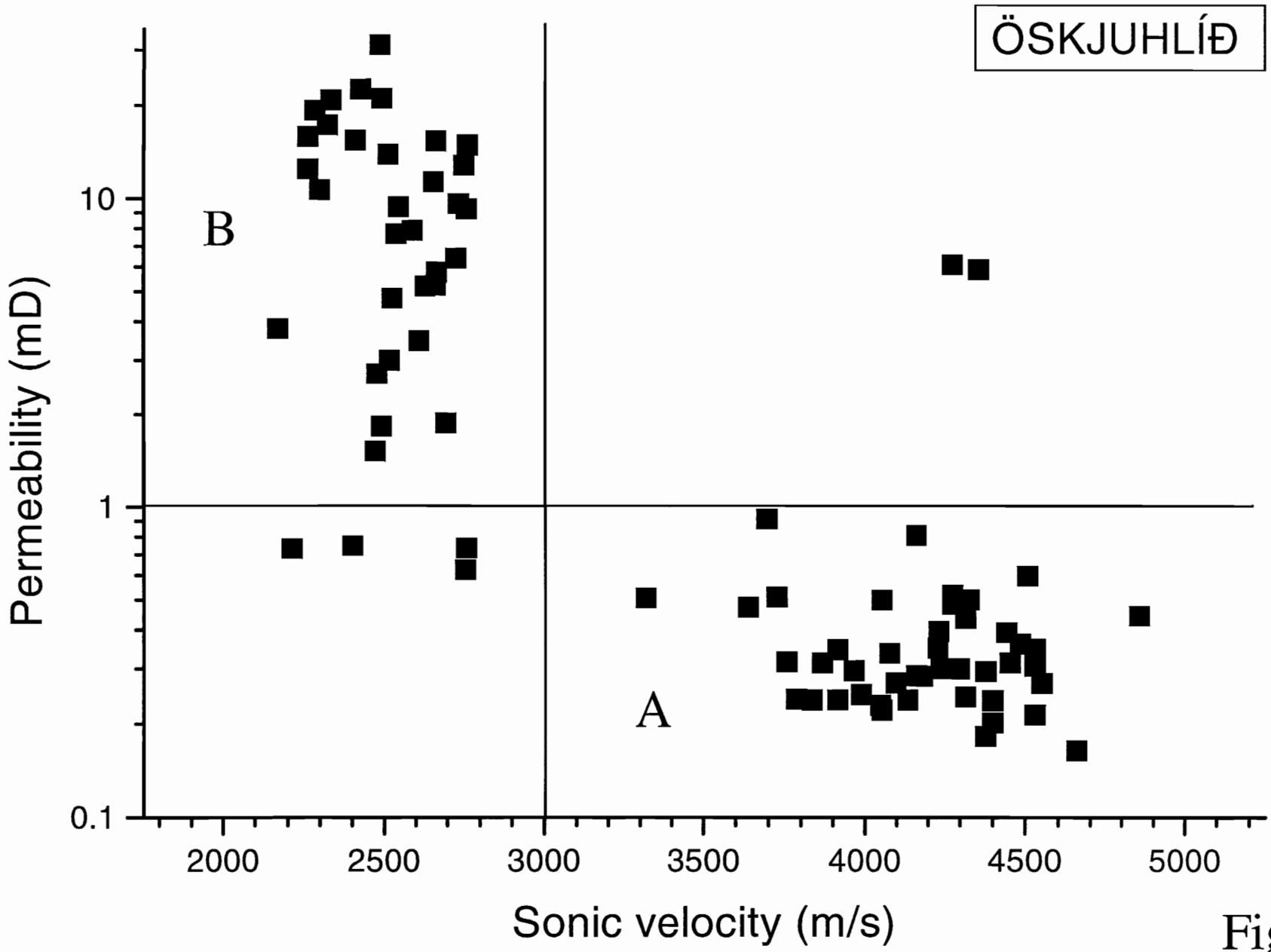
ÖSKJUHLÍÐ
Permeability (mD)
10
1
0.1
B
A
2000
2500
3000
3500
4000
4500
5000
Sonic velocity (m/s)

Fig. 2.22

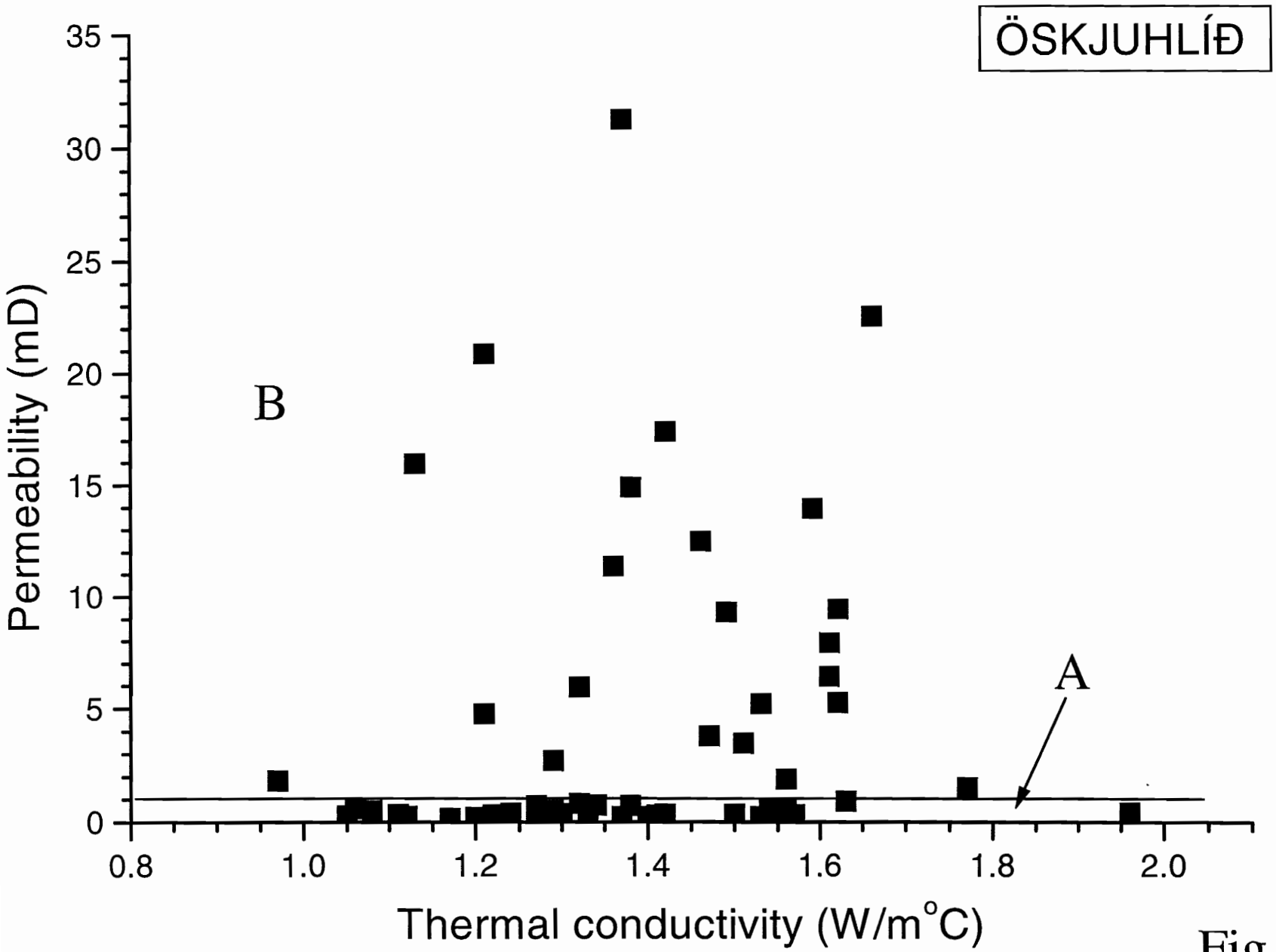
ÖSKJUHLÍÐ
Permeability (mD)
35
30
25
20
15
10
5
0
B
A
0.8
1.0
1.2
1.4
1.6
1.8
2.0
Thermal conductivity (W/m°C)

Fig. 2.23

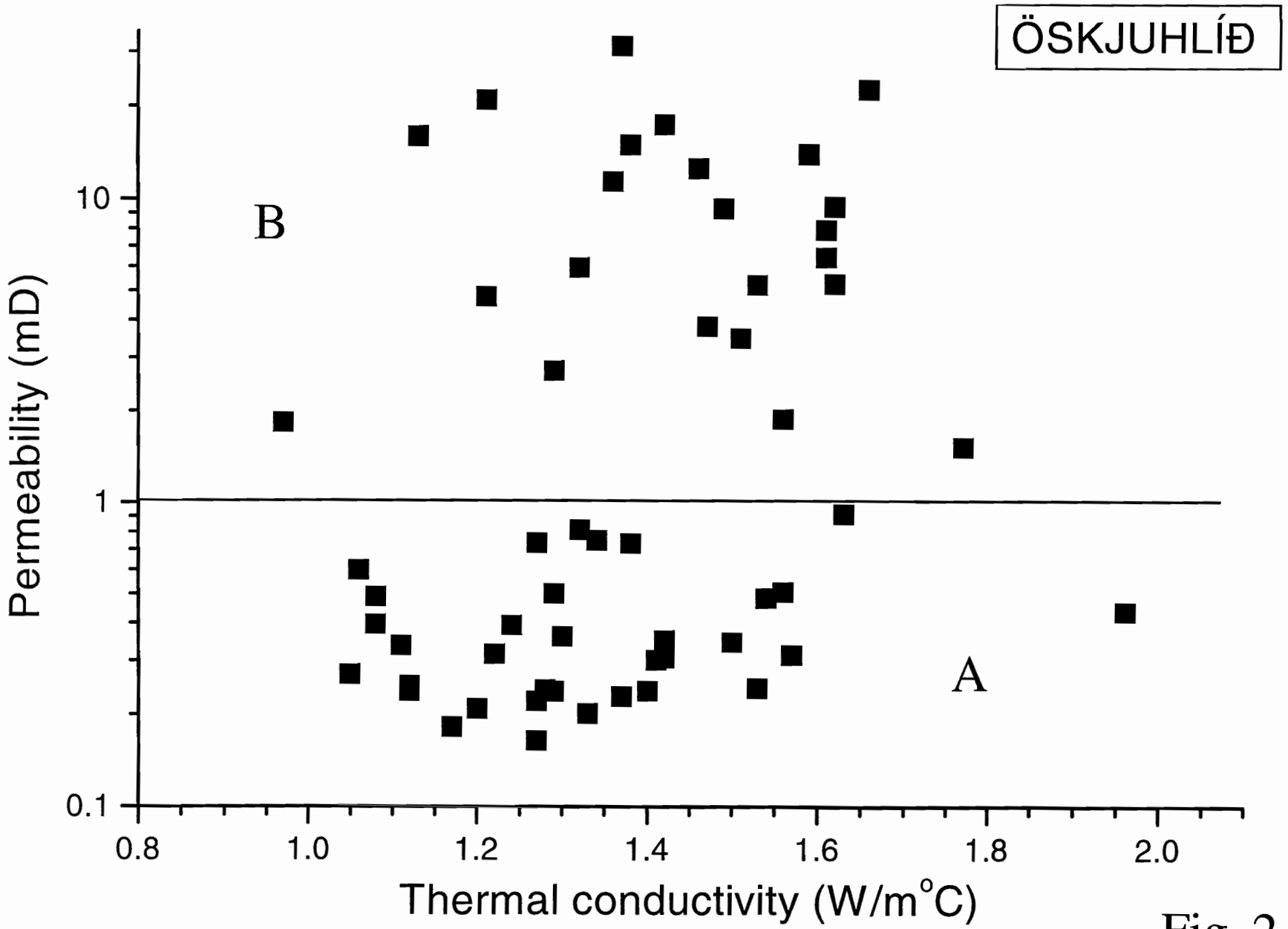
ÖSKJUHLÍÐ
B
A
10
1
0.1
Permeability (mD)
0.8
1.0
1.2
1.4
1.6
1.8
2.0
Thermal conductivity (W/m°C)

Fig. 2.24

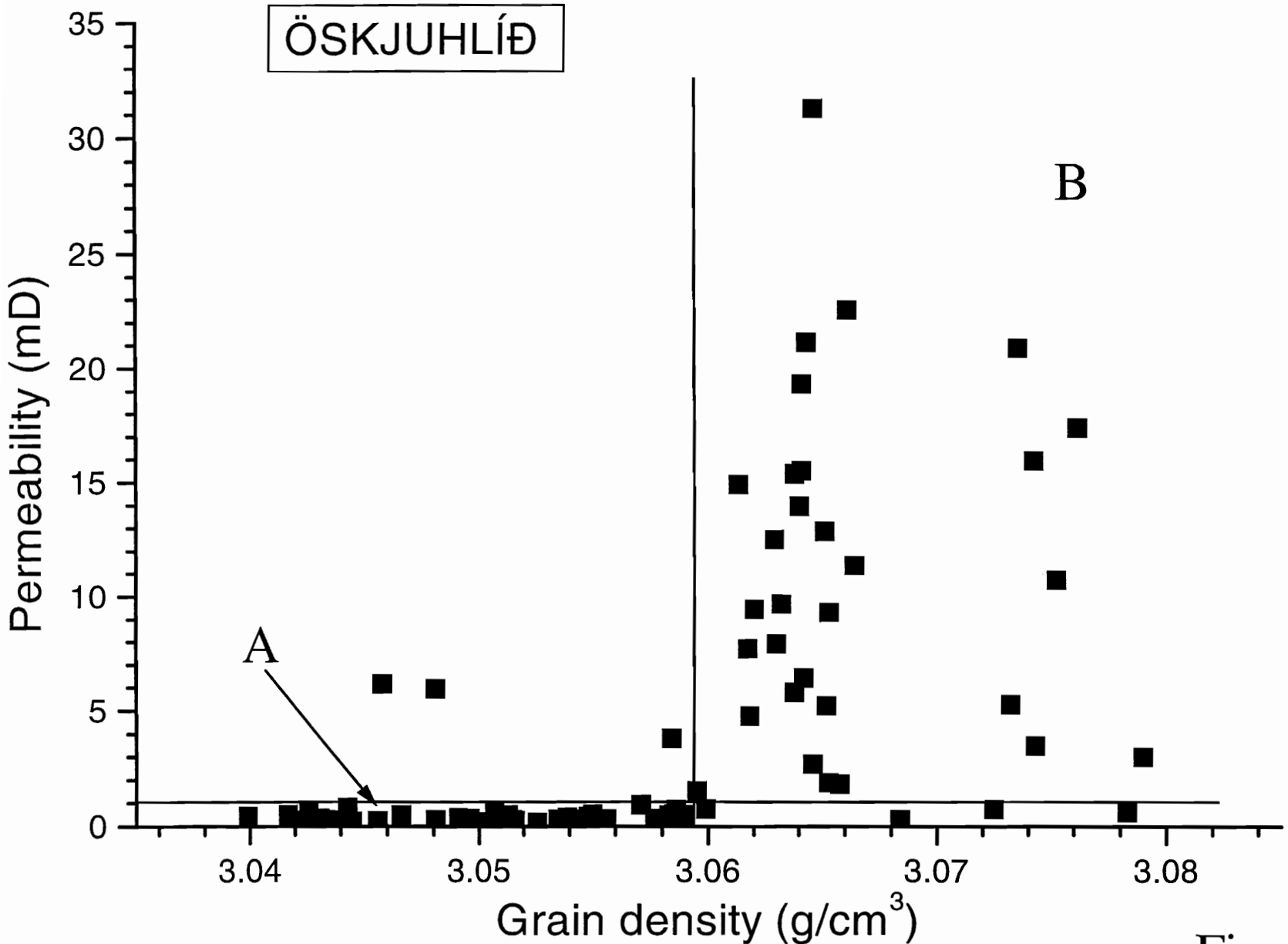
ÖSKJUHLÍÐ
Permeability (mD)
35
30
25
20
15
10
5
0
A
B
3.04
3.05
3.06
3.07
3.08
Grain density (g/cm3)

Fig. 2.25

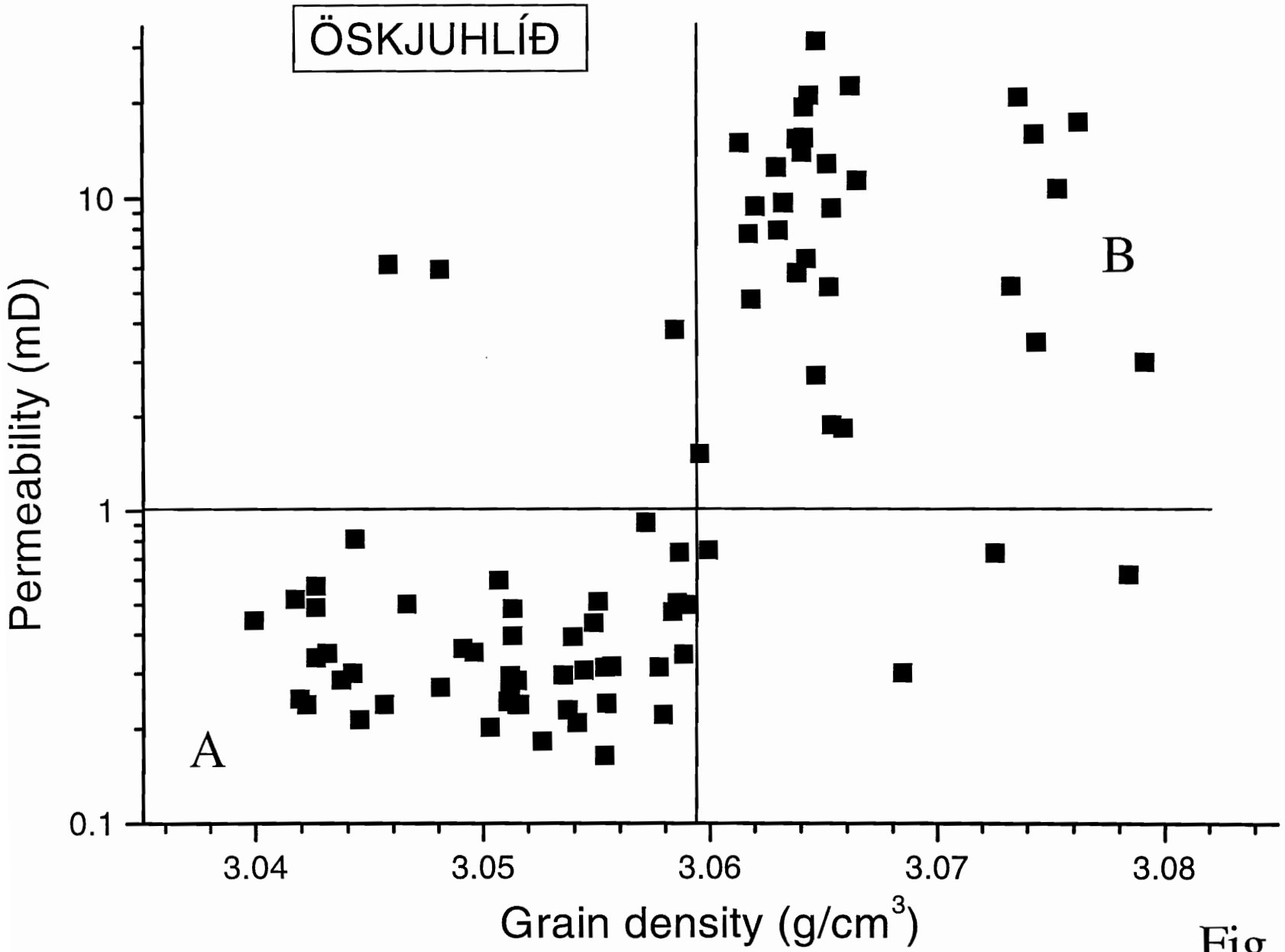
ÖSKJUHLÍÐ
Permeability (mD)
10
1
0.1
A
B
3.04
3.05
3.06
3.07
3.08
Grain density (g/cm3)

Fig. 2.26

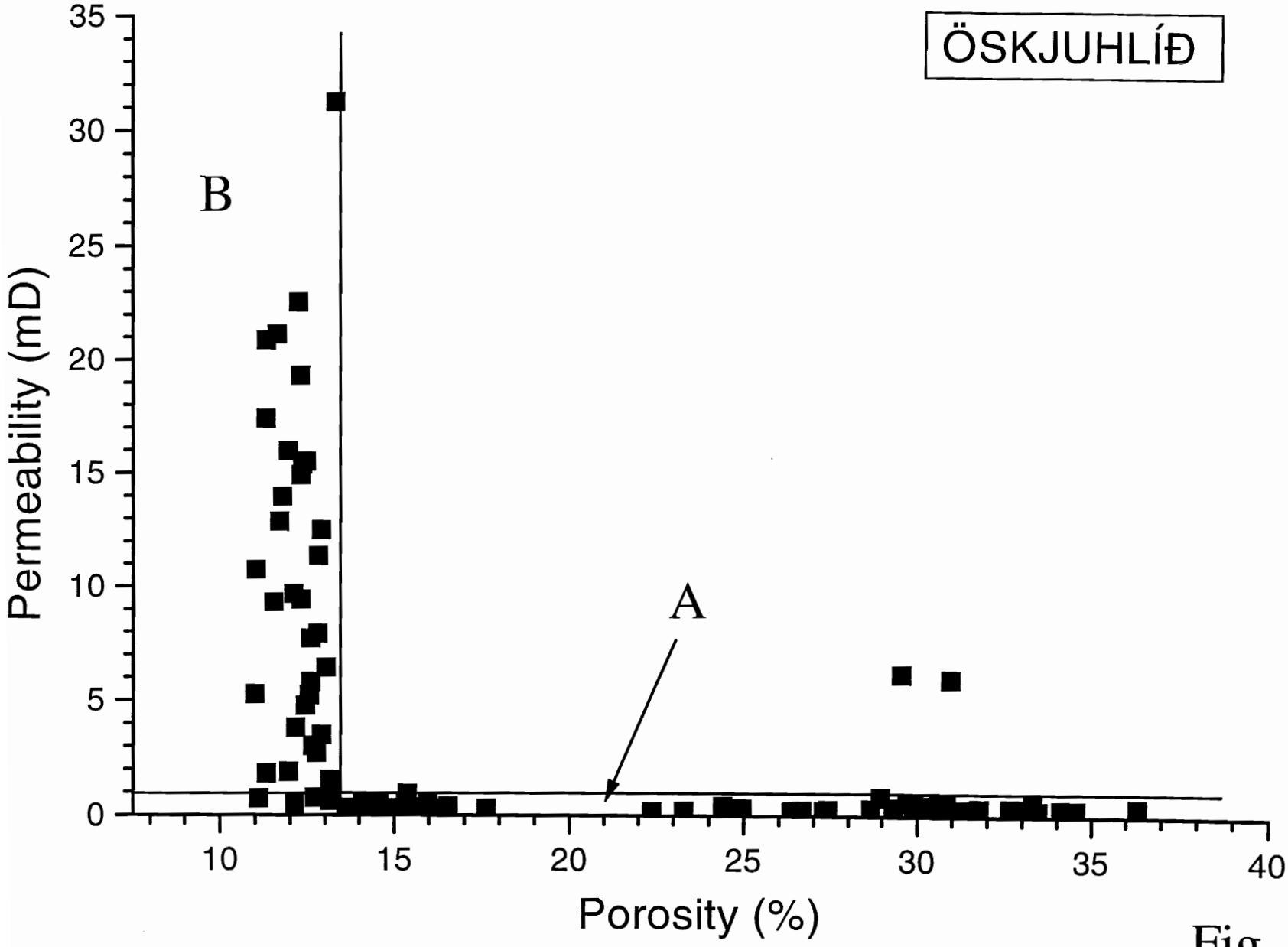
ÖSKJUHLÍÐ
B
A
Permeability (mD)
Porosity (%)
0
5
10
15
20
25
30
35
10
15
20
25
30
35
40

Fig. 2.27

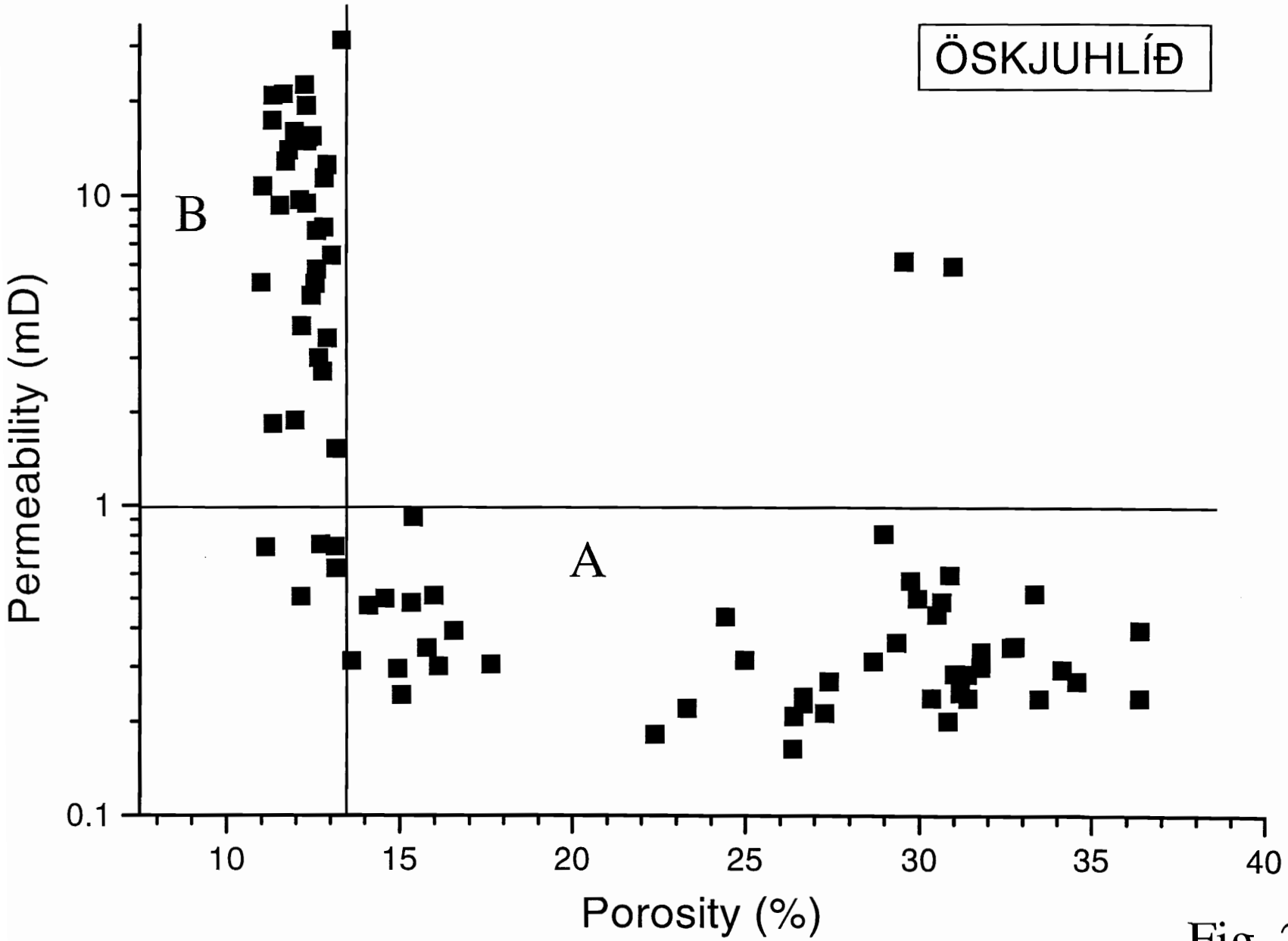
ÖSKJUHLÍÐ
B
A
Permeability (mD)
10
1
0.1
10
15
20
25
30
35
40
Porosity (%)

Fig. 2.28

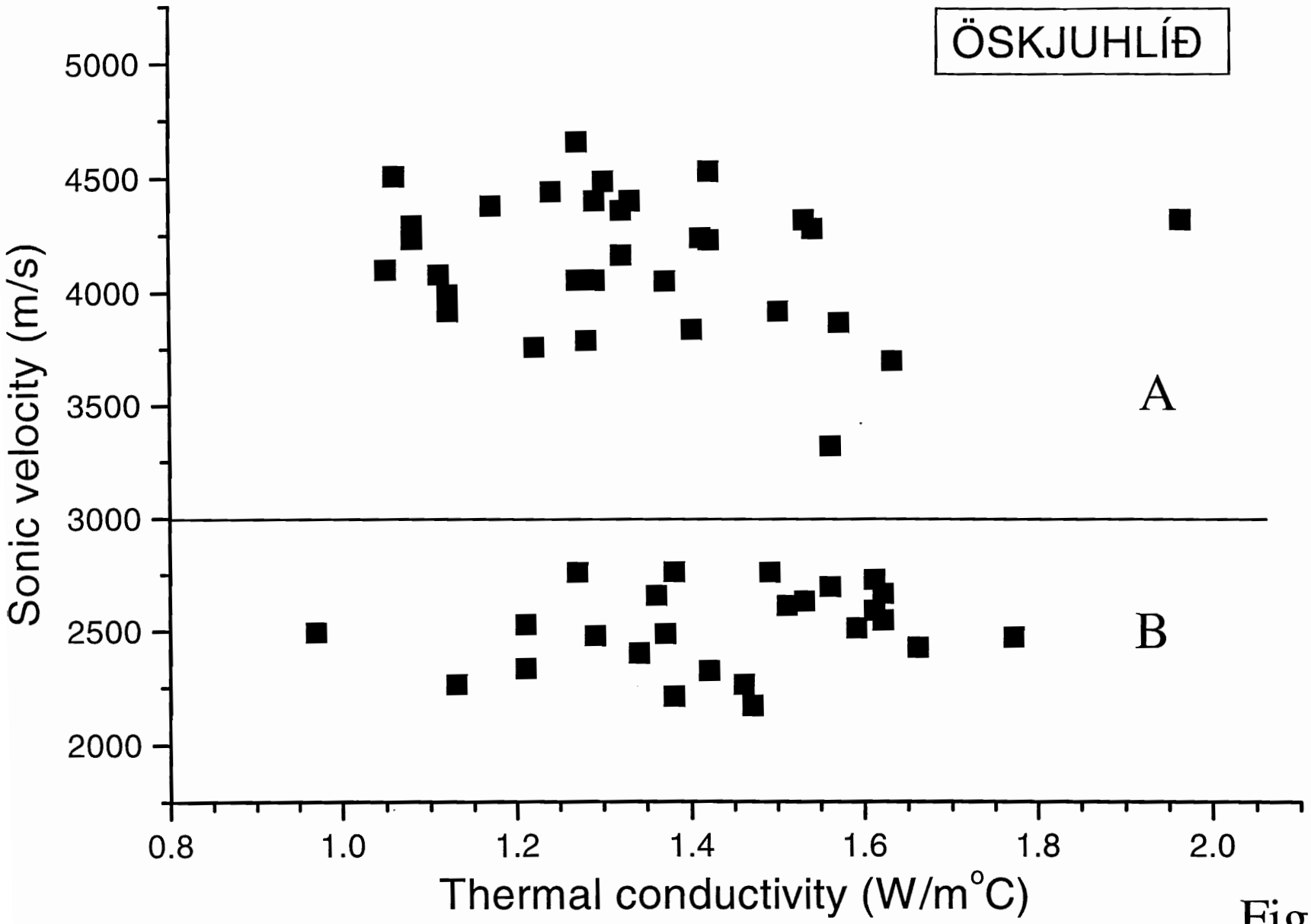
ÖSKJUHLÍÐ
5000
4500
4000
3500
3000
2500
2000
Sonic velocity (m/s)
A
B
0.8
1.0
1.2
1.4
1.6
1.8
2.0
Thermal conductivity (W/m°C)

Fig. 2.29

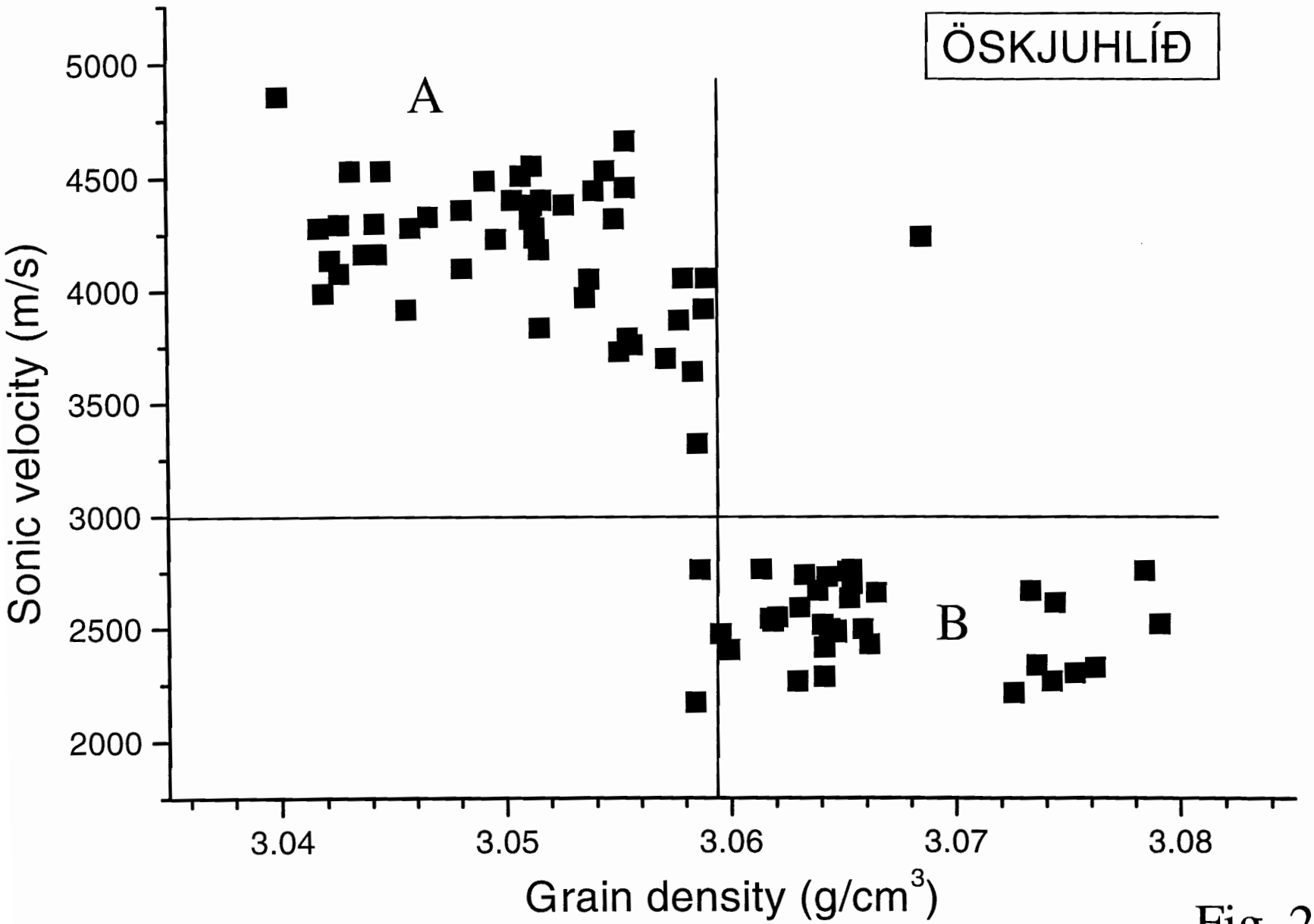
ÖSKJUHLÍÐ
A
B
5000
4500
4000
3500
3000
2500
2000
Sonic velocity (m/s)
3.04
3.05
3.06
3.07
3.08
Grain density (g/cm3)

Fig. 2.30

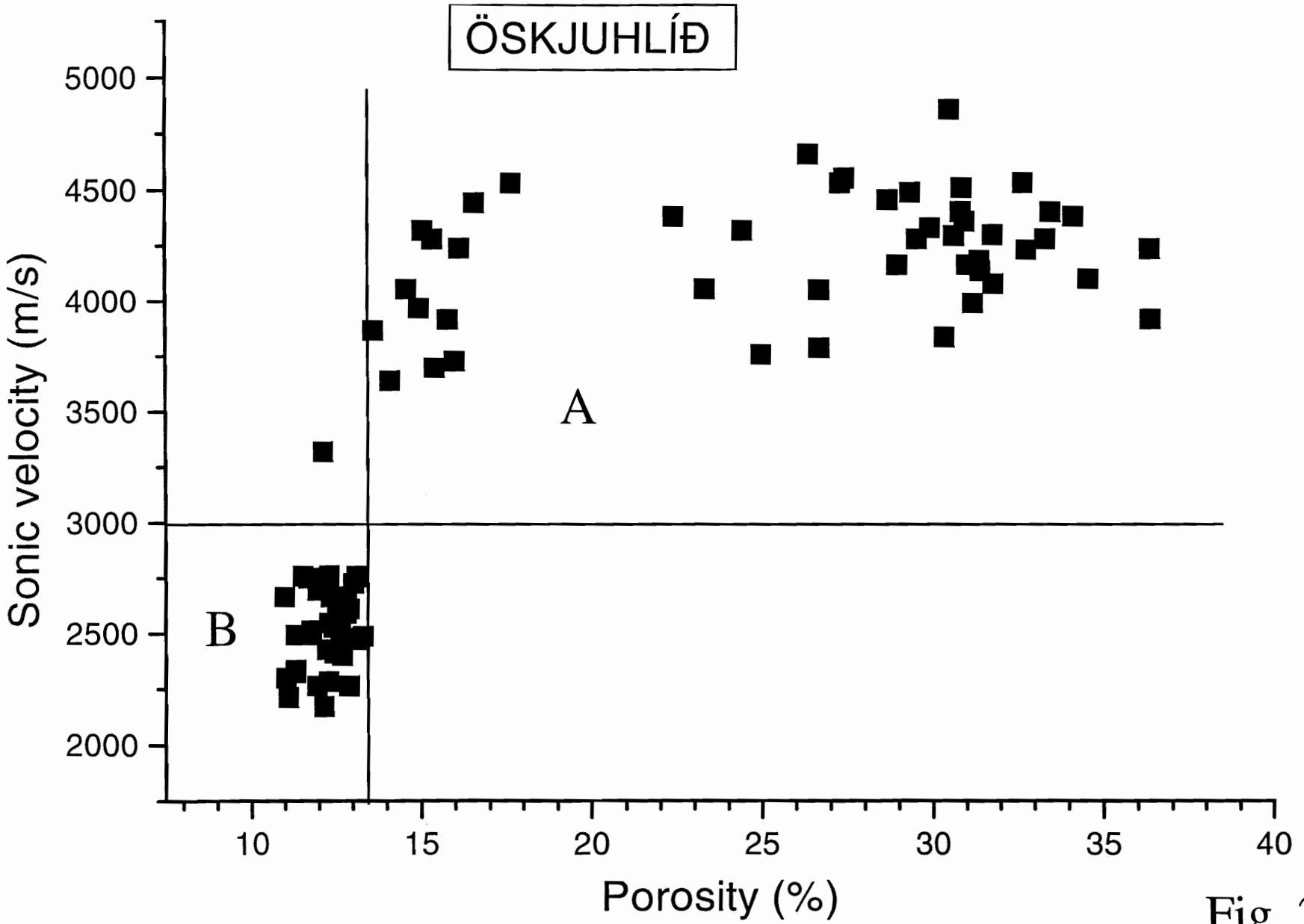
ÖSKJUHLÍÐ
Sonic velocity (m/s)
5000
4500
4000
3500
3000
2500
2000
A
B
10
15
20
25
30
35
40
Porosity (%)

Fig. 2.31

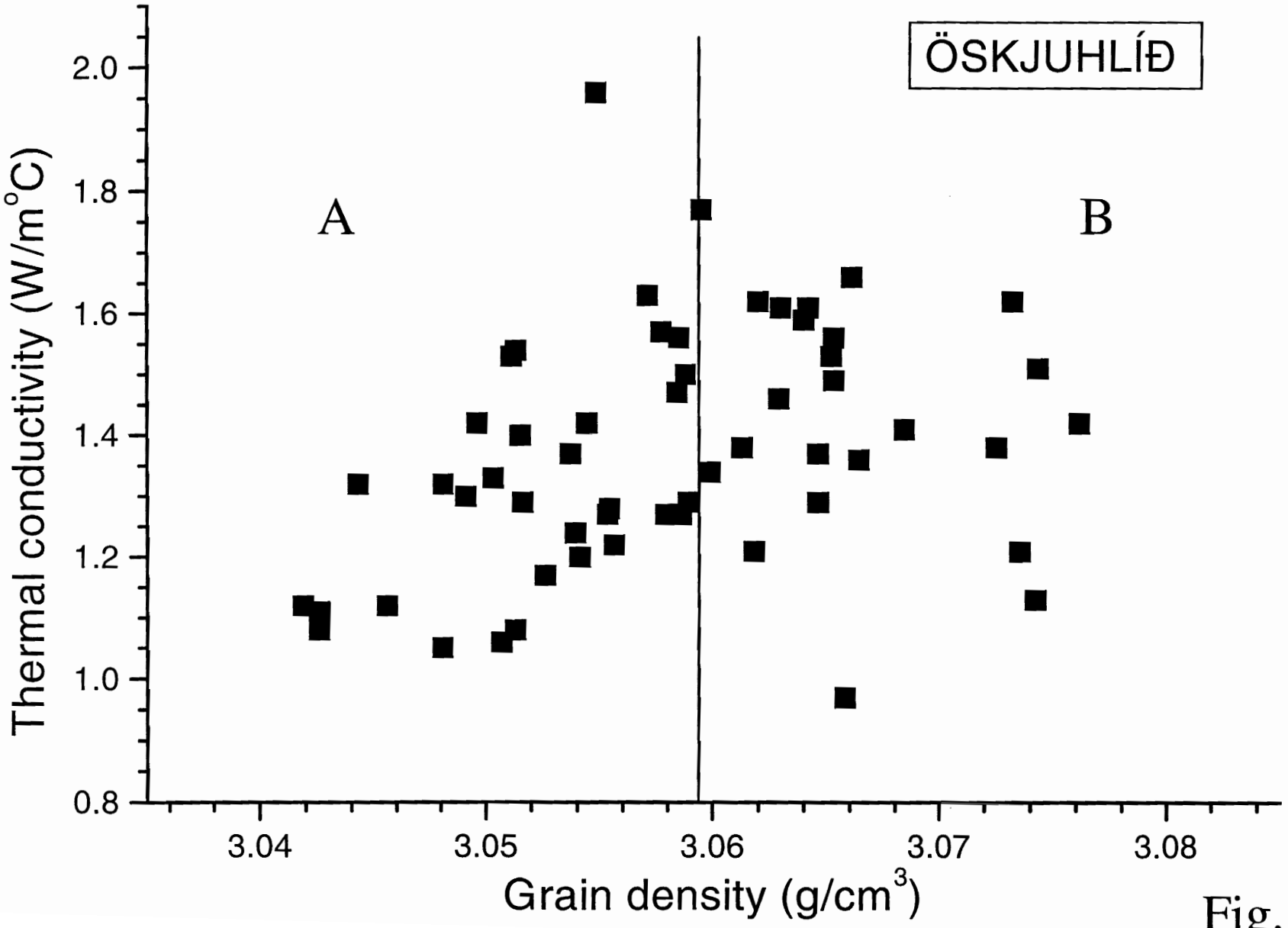
ÖSKJUHLÍÐ
A
B
Thermal conductivity (W/m°C)
2.0
1.8
1.6
1.4
1.2
1.0
0.8
3.04
3.05
3.06
3.07
3.08
Grain density (g/cm3)

Fig. 2.32

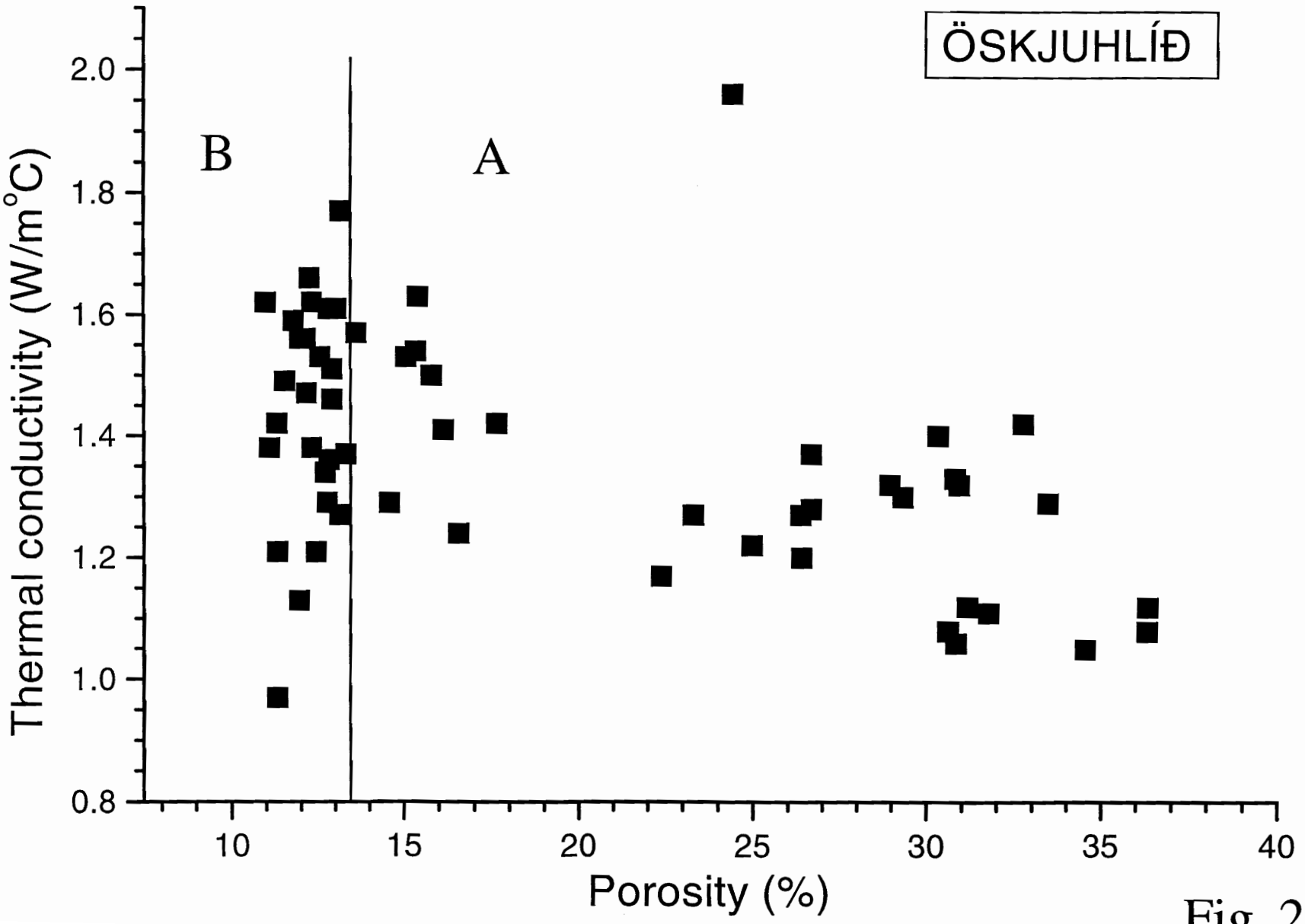
ÖSKJUHLÍÐ
B
A
Thermal conductivity (W/m°C)
2.0
1.8
1.6
1.4
1.2
1.0
0.8
10
15
20
25
30
35
40
Porosity (%)

Fig. 2.33

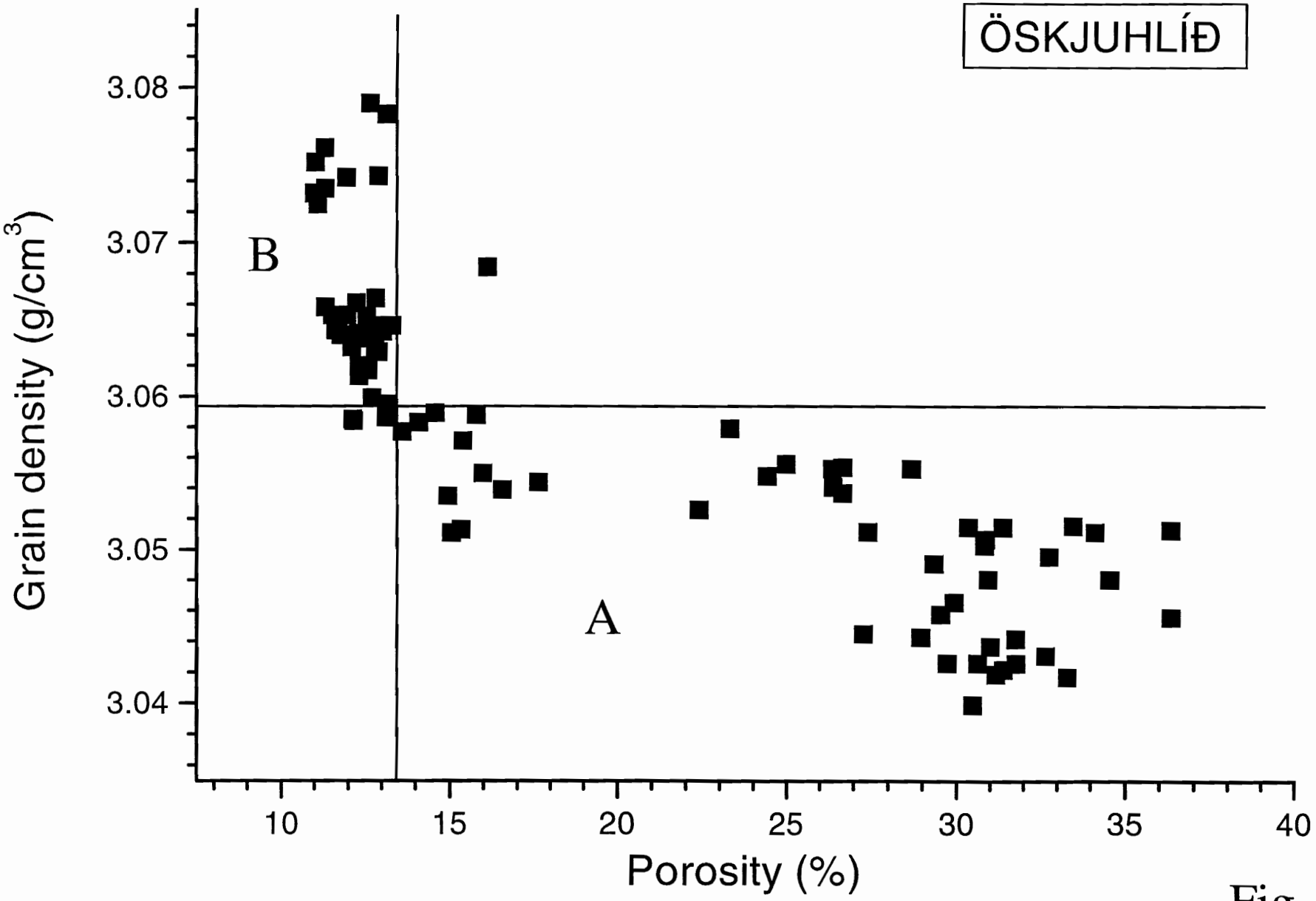
ÖSKJUHLÍÐ
Grain density (g/cm3)
3.08
3.07
3.06
3.05
3.04
B
A
10
15
20
25
30
35
40
Porosity (%)

Fig. 2.34

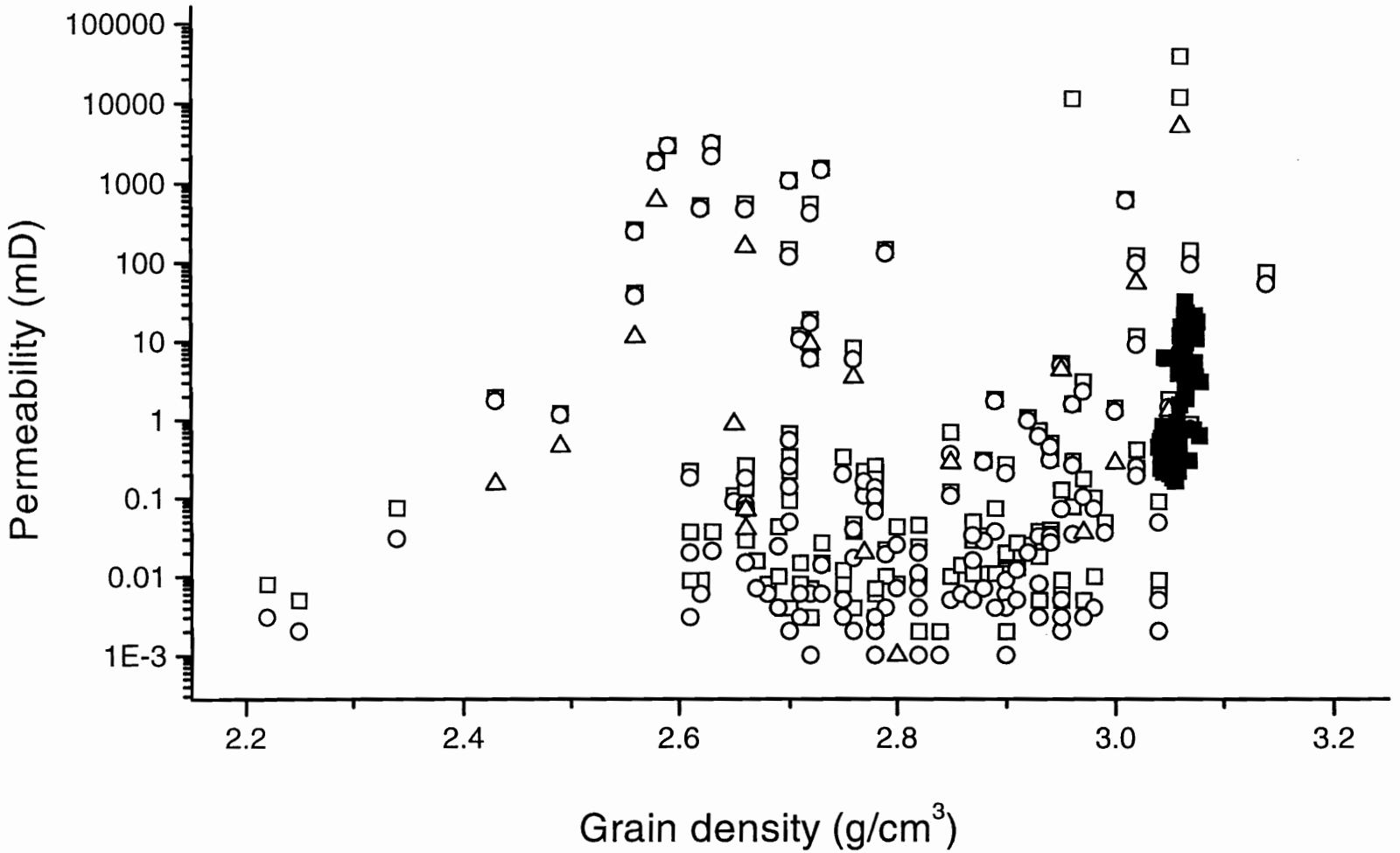
100000
10000
1000
100
10
1
0.1
0.01
1E-3
Permeability (mD)
2.2
2.4
2.6
2.8
3.0
3.2
Grain density (g/cm3)
TOTAL DATABASE
Air permeability (mD)
Klinkenberg permeability (mD)
Brine permeability (mD)
ÖSKJUHLÍÐ
Gas permeability (mD)

Fig. 2.35

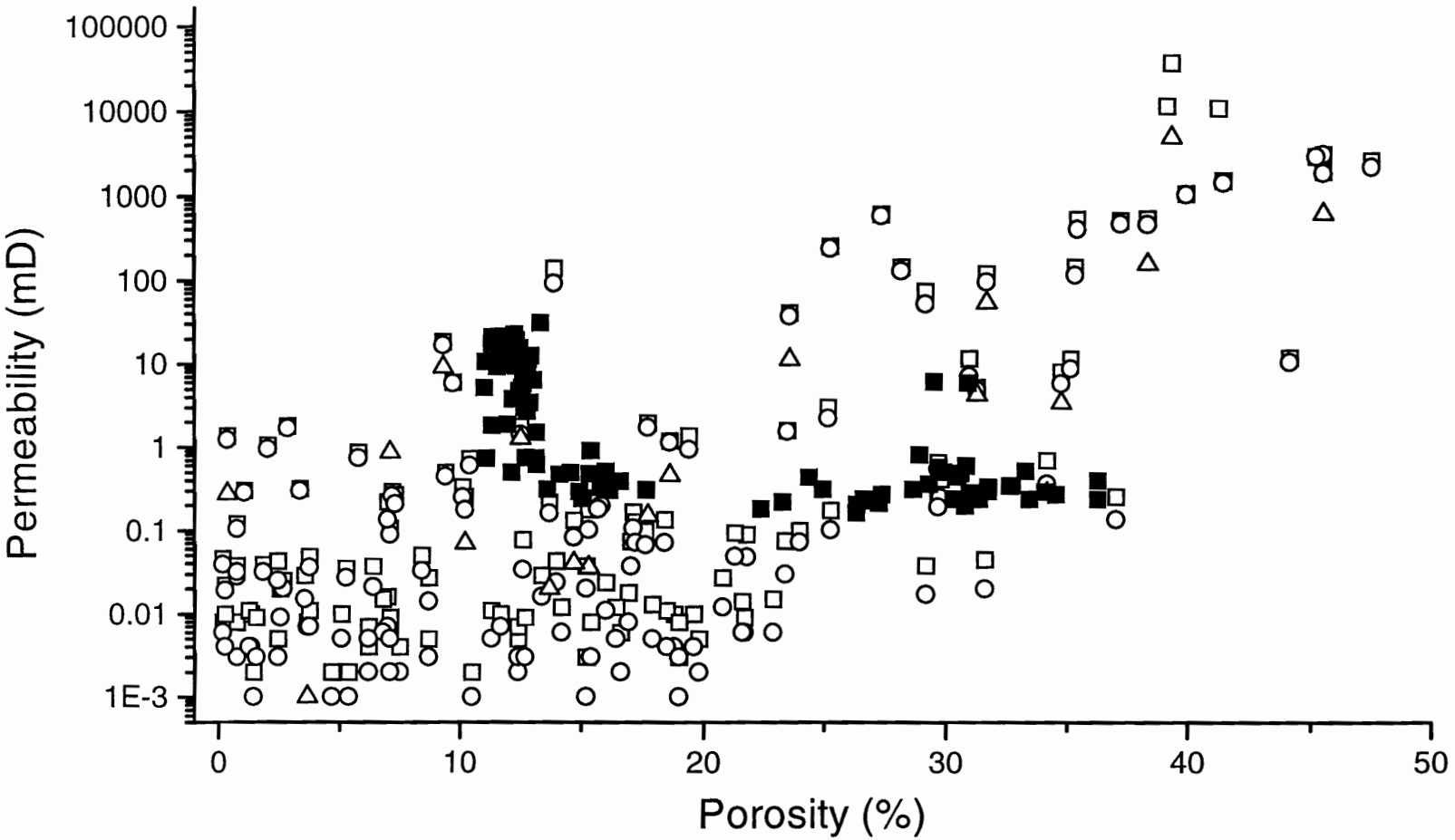
100000
10000
1000
100
10
1
0.1
0.01
1E-3
Permeability (mD)
0
10
20
30
40
50
Porosity (%)
TOTAL DATABASE
Air permeability (mD)
Klinkenberg permeability (mD)
Brine permeability (mD)
ÖSKJUHLÍÐ
Gas permeability (mD)

Fig. 2.36

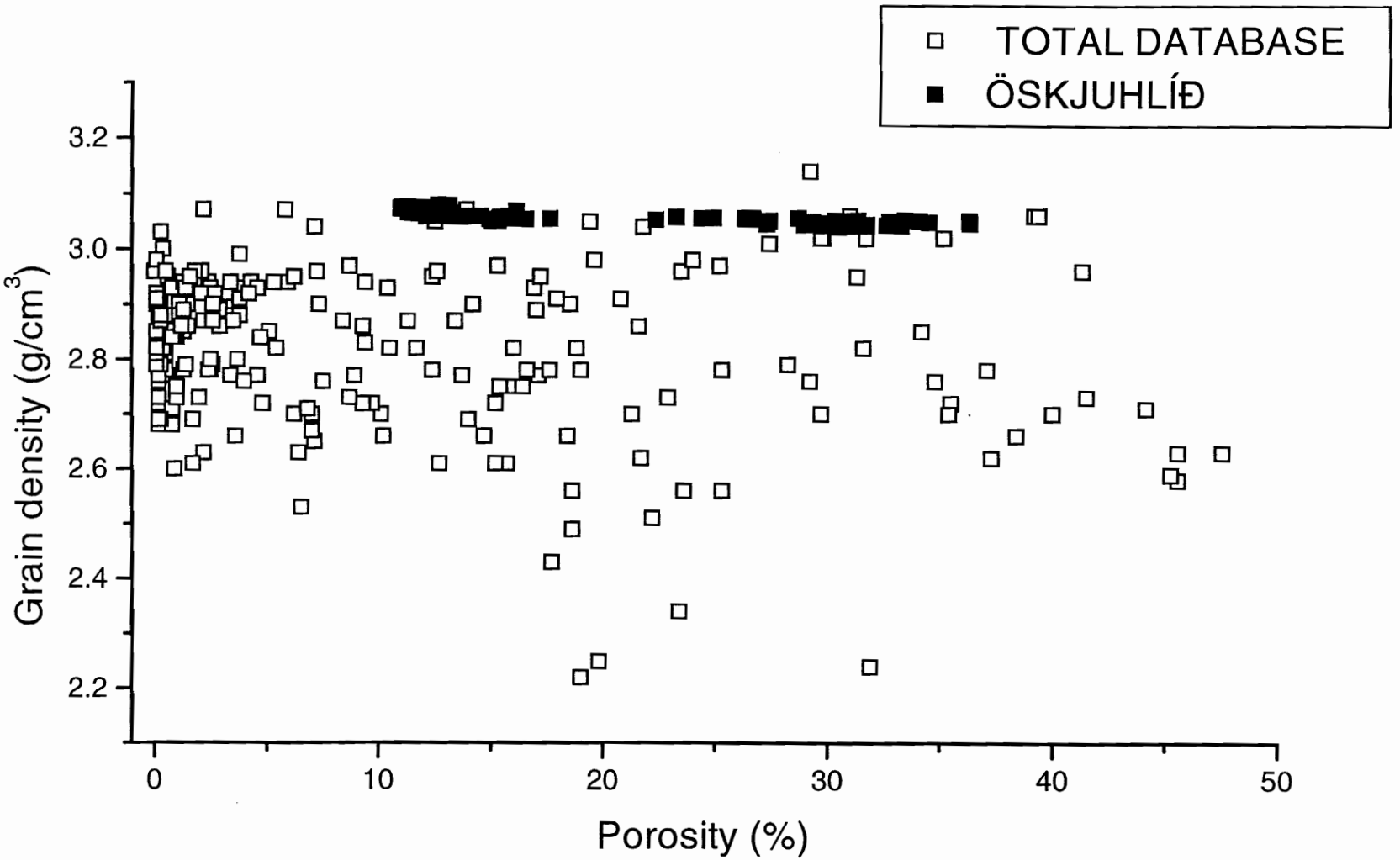
TOTAL DATABASE
ÖSKJUHLÍÐ
Grain density (g/cm3)
3.2
3.0
2.8
2.6
2.4
2.2
0
10
20
30
40
50
Porosity (%)

Fig. 2.37

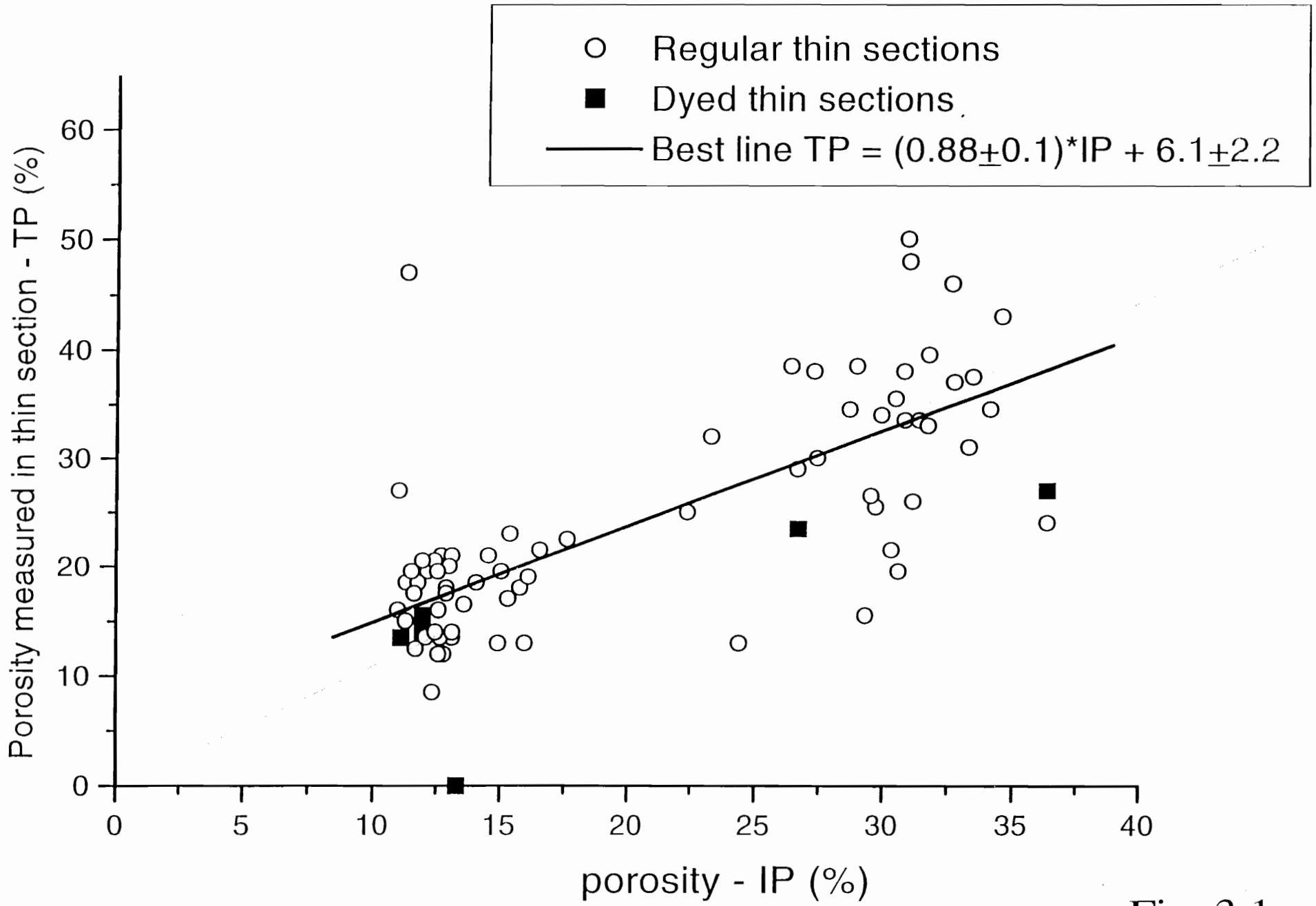
Regular thin sections
Dyed thin sections
Best line TP = (0.88±0.1)*IP + 6.1±2.2
Porosity measured in thin section - TP (%)
porosity - IP (%)
0
10
20
30
40
50
60
0
5
10
15
20
25
30
35
40

Fig. 3.1

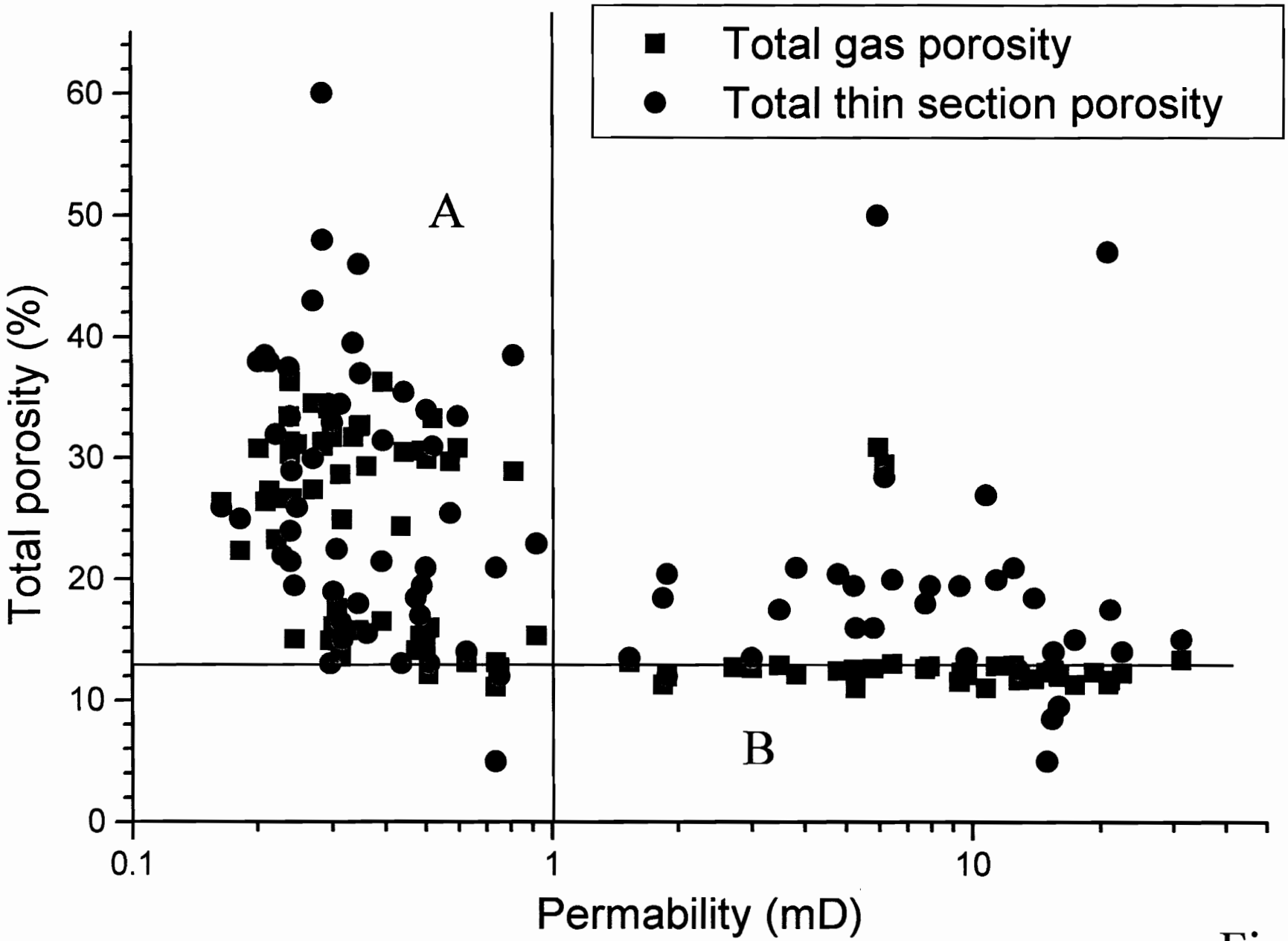
Total gas porosity
Total thin section porosity
A
B
Total porosity (%)
Permability (mD)
0
10
20
30
40
50
60
0.1
1
10

Fig. 3.2

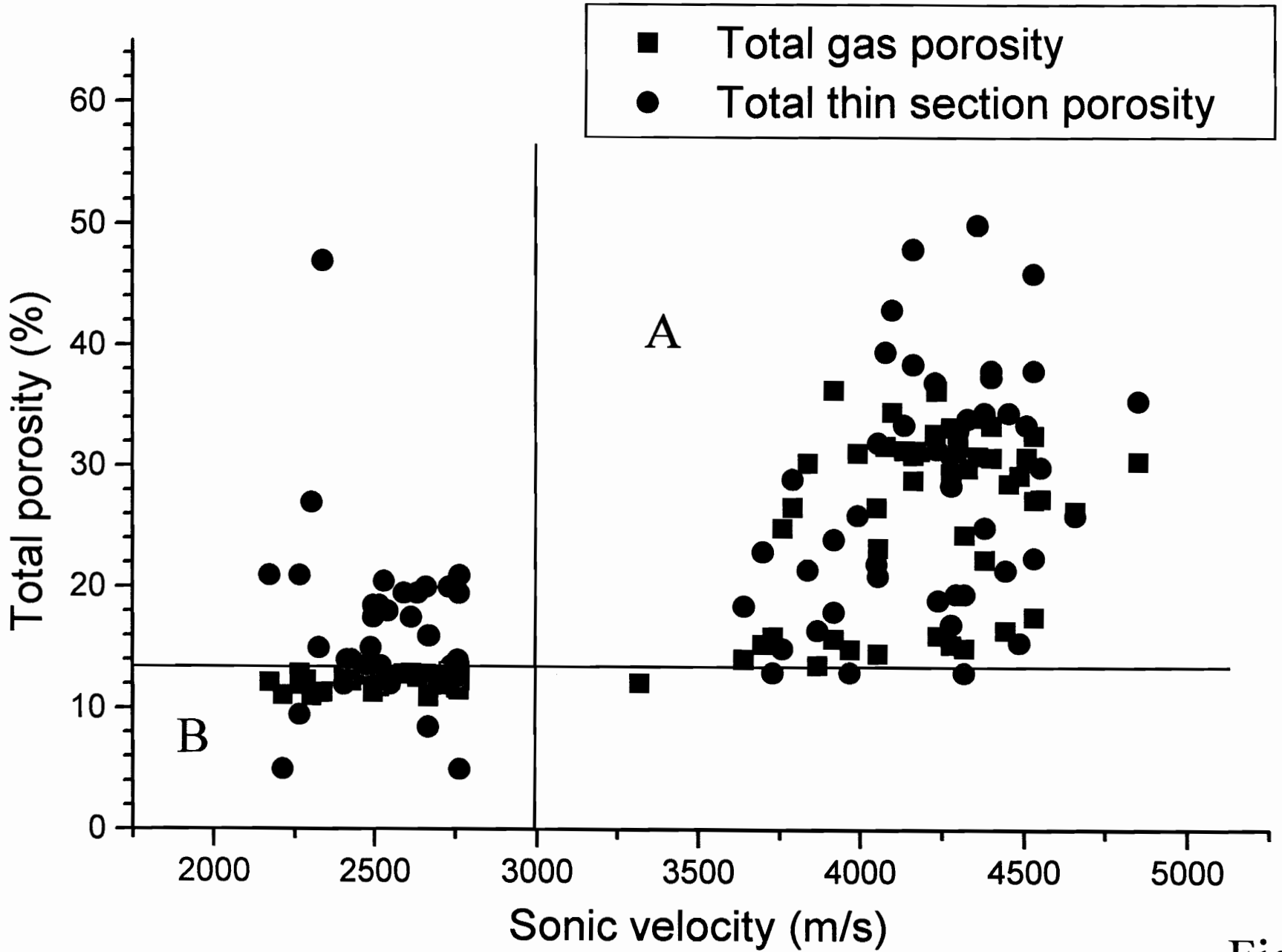
Total gas porosity
Total thin section porosity
Total porosity (%)
Sonic velocity (m/s)
A
B
0
10
20
30
40
50
60
2000
2500
3000
3500
4000
4500
5000

Fig. 3.3

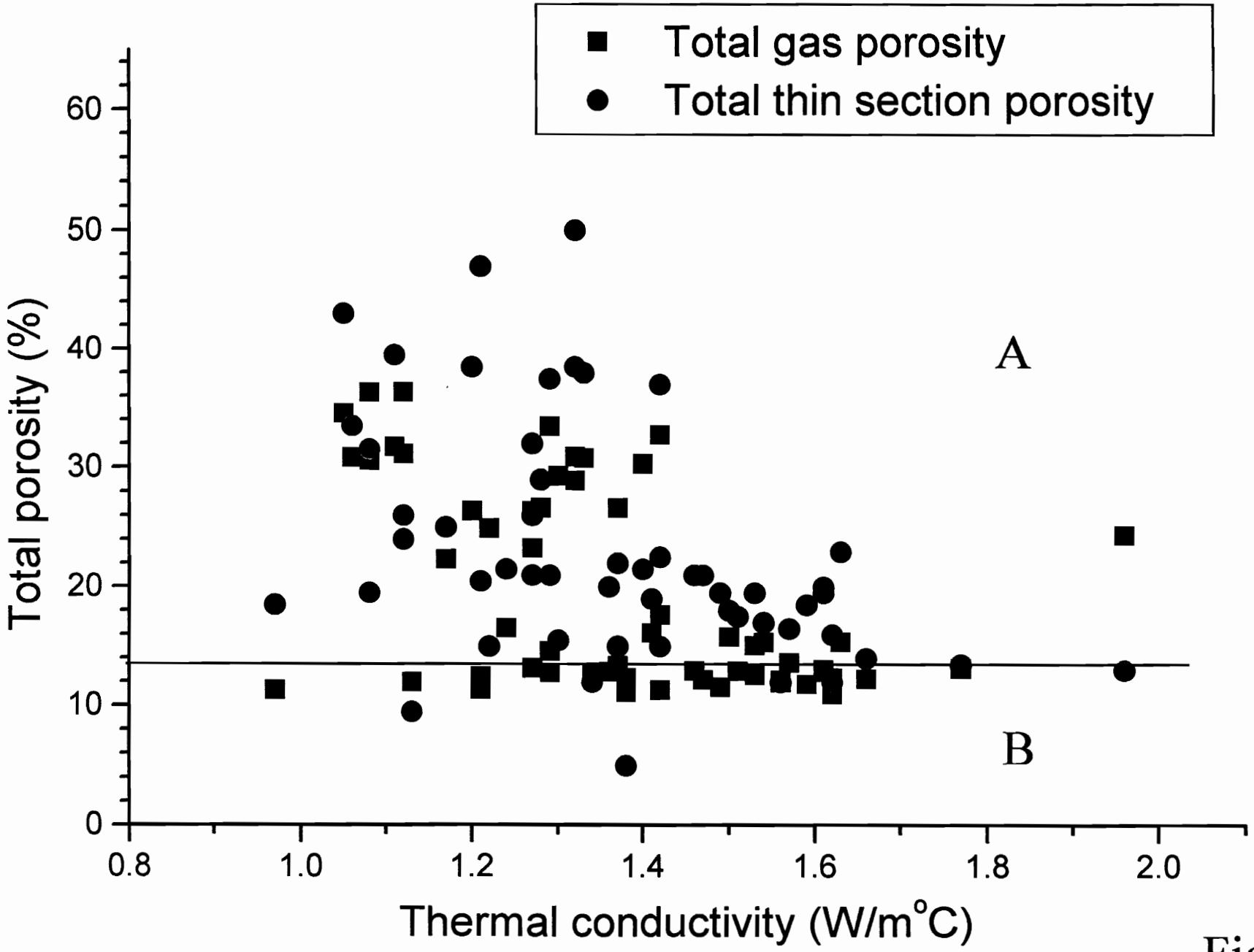
Total gas porosity
Total thin section porosity
Total porosity (%)
60
50
40
30
20
10
0
A
B
0.8
1.0
1.2
1.4
1.6
1.8
2.0
Thermal conductivity (W/m°C)

Fig. 3.4

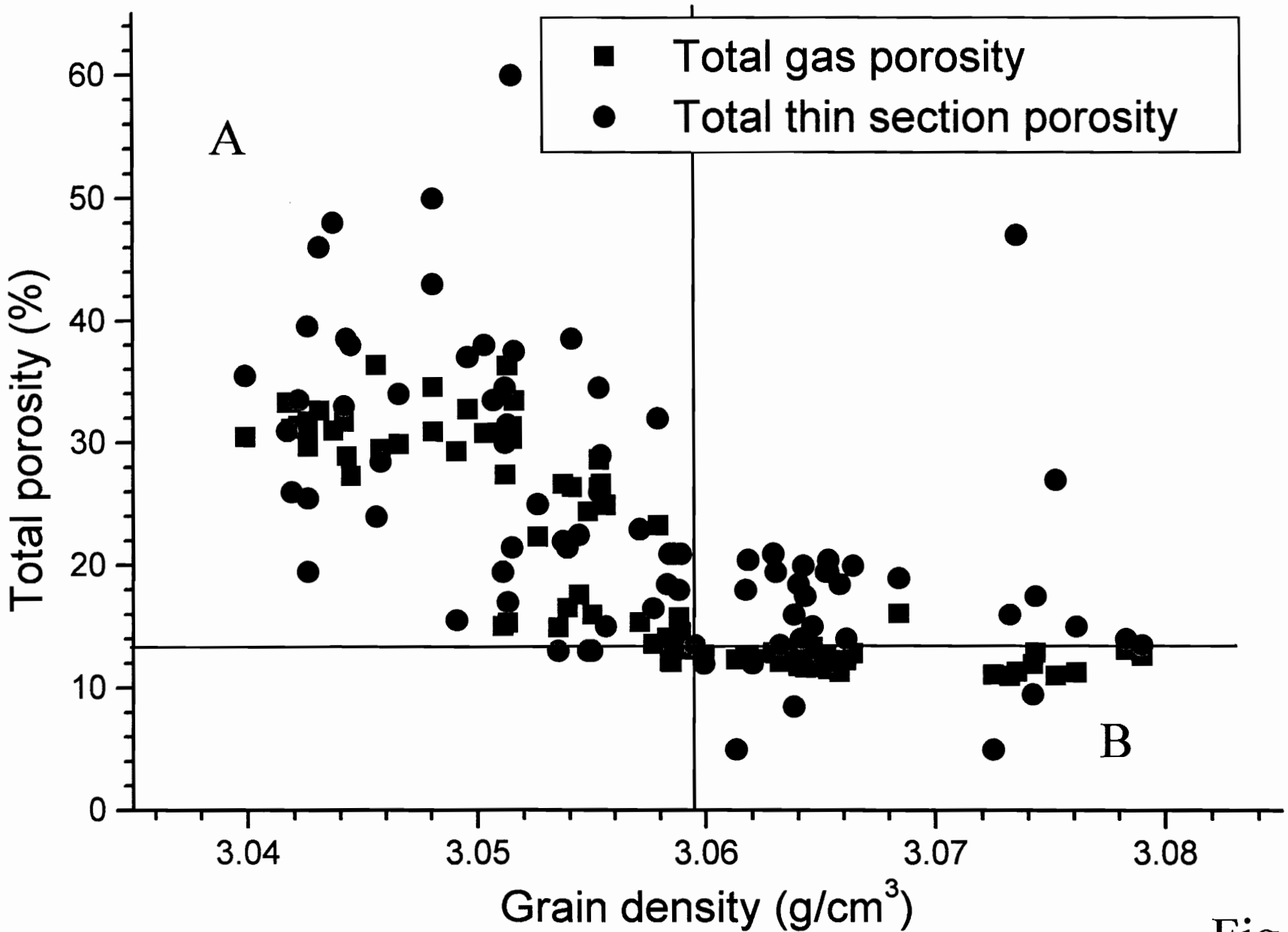
Total gas porosity
Total thin section porosity
A
B
Total porosity (%)
0
10
20
30
40
50
60
3.04
3.05
3.06
3.07
3.08
Grain density (g/cm3)

Fig. 3.5

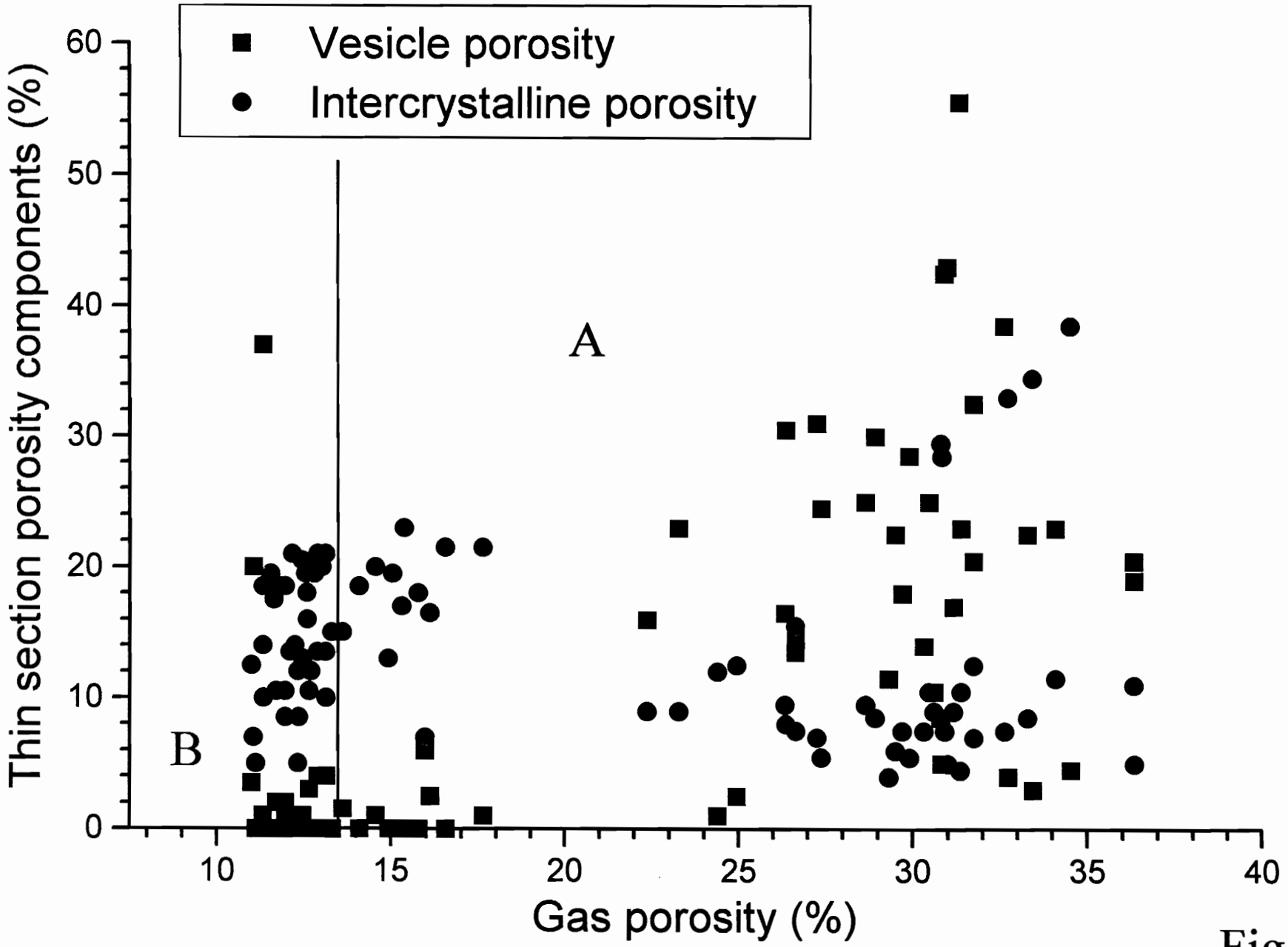
Vesicle porosity
Intercrystalline porosity
Thin section porosity components (%)
Gas porosity (%)
A
B
0
10
20
30
40
50
60
10
15
20
25
30
35
40

Fig. 3.6

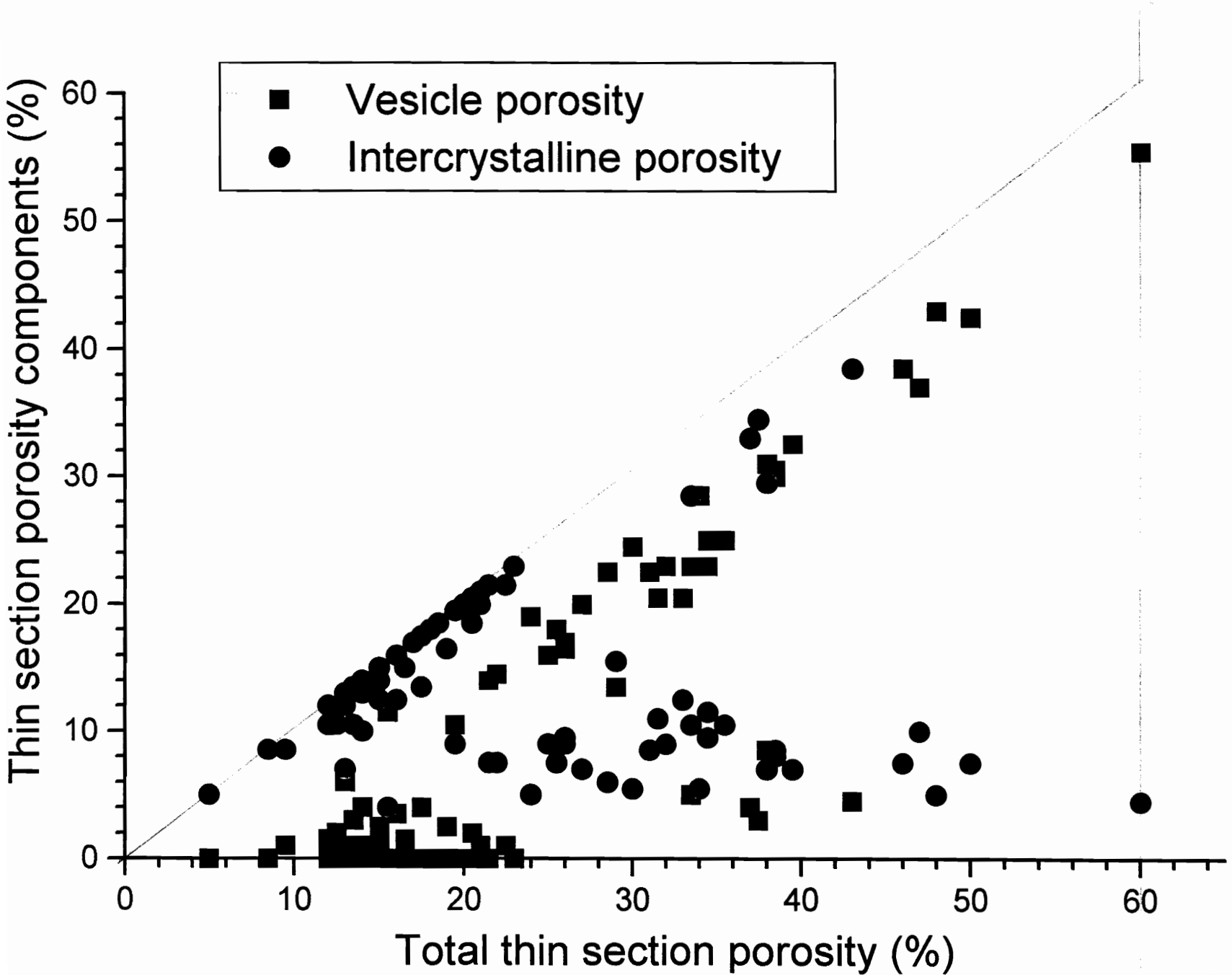
Vesicle porosity
Intercrystalline porosity
Thin section porosity components (%)
Total thin section porosity (%)
0
10
20
30
40
50
60

Fig. 3.7

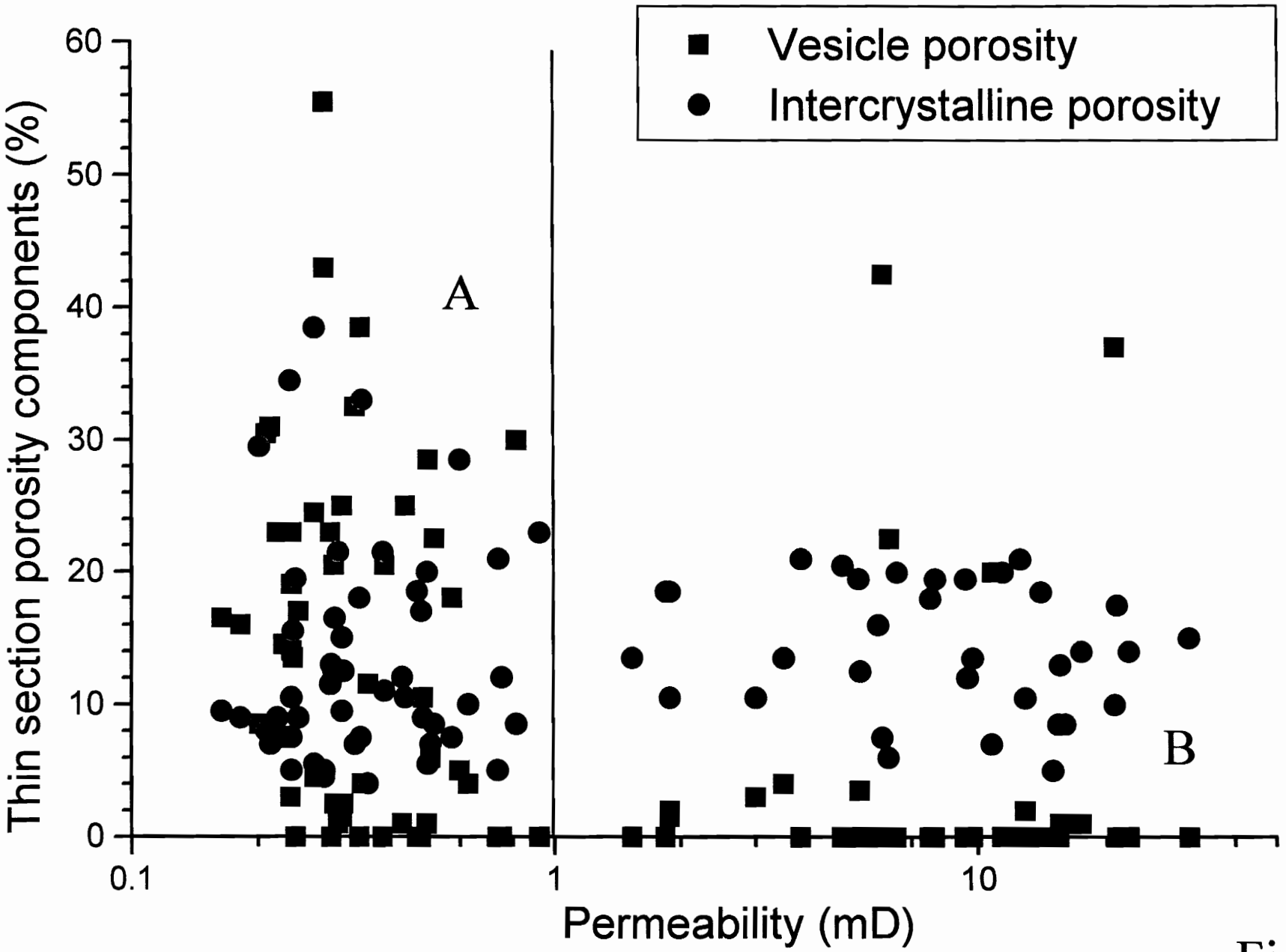
Vesicle porosity
Intercrystalline porosity
Thin section porosity components (%)
60
50
40
30
20
10
0
A
B
0.1
1
10
Permeability (mD)

Fig. 3.8

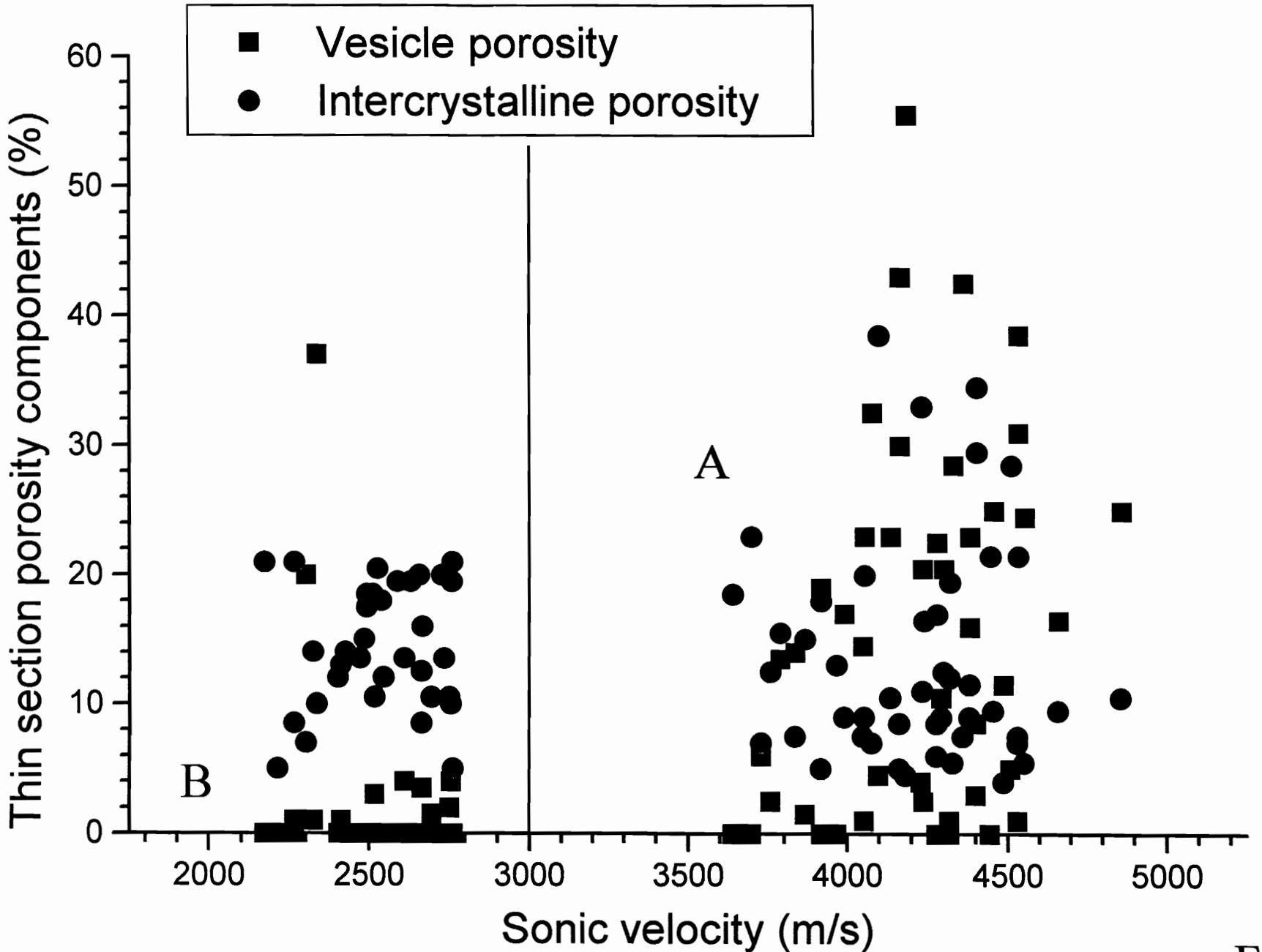
Vesicle porosity
Intercrystalline porosity
Thin section porosity components (%)
60
50
40
30
20
10
0
2000
2500
3000
3500
4000
4500
5000
Sonic velocity (m/s)
A
B

Fig. 3.9

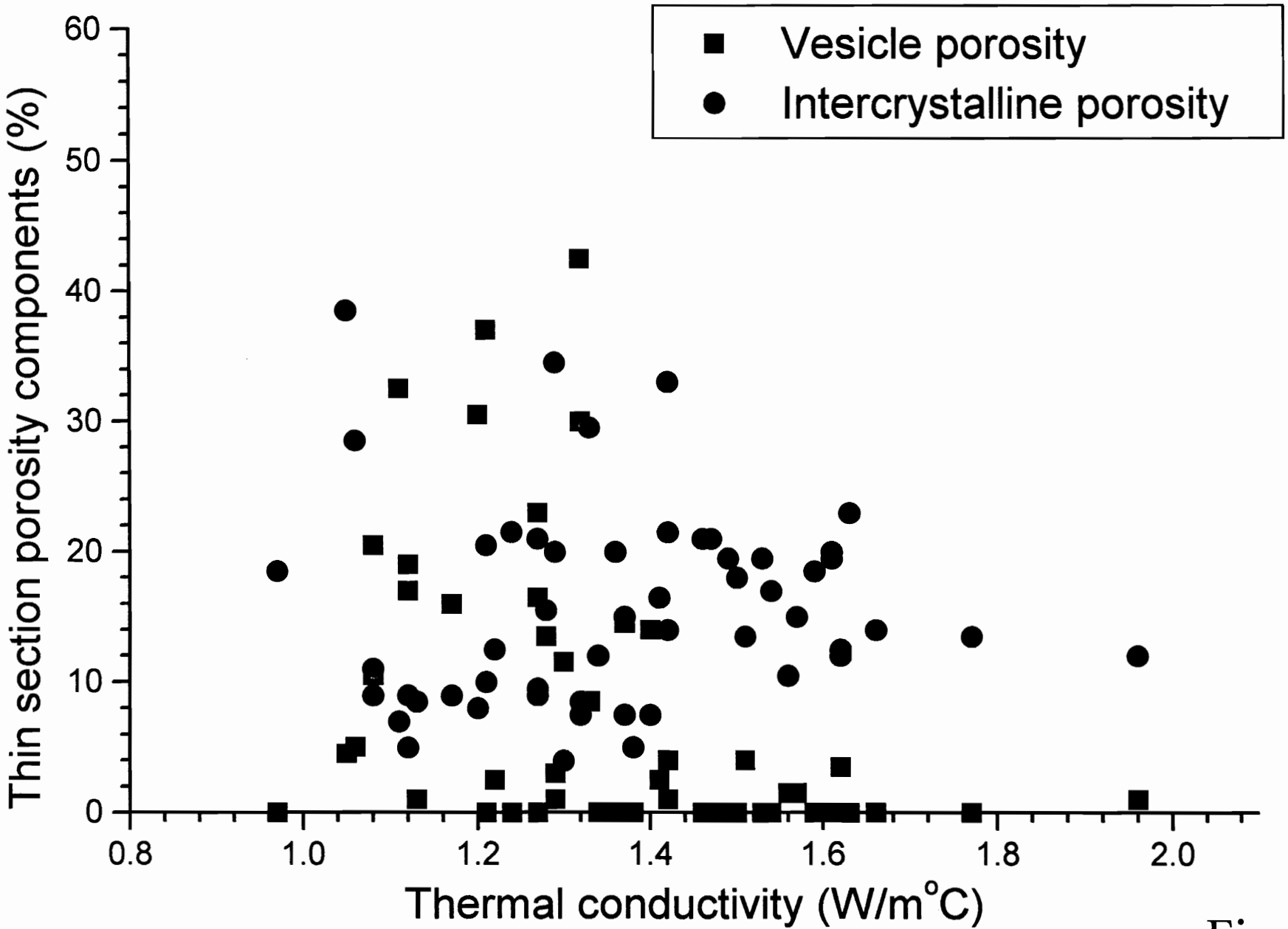
Vesicle porosity
Intercrystalline porosity
Thin section porosity components (%)
0
10
20
30
40
50
60
0.8
1.0
1.2
1.4
1.6
1.8
2.0
Thermal conductivity (W/m°C)

Fig. 3.10

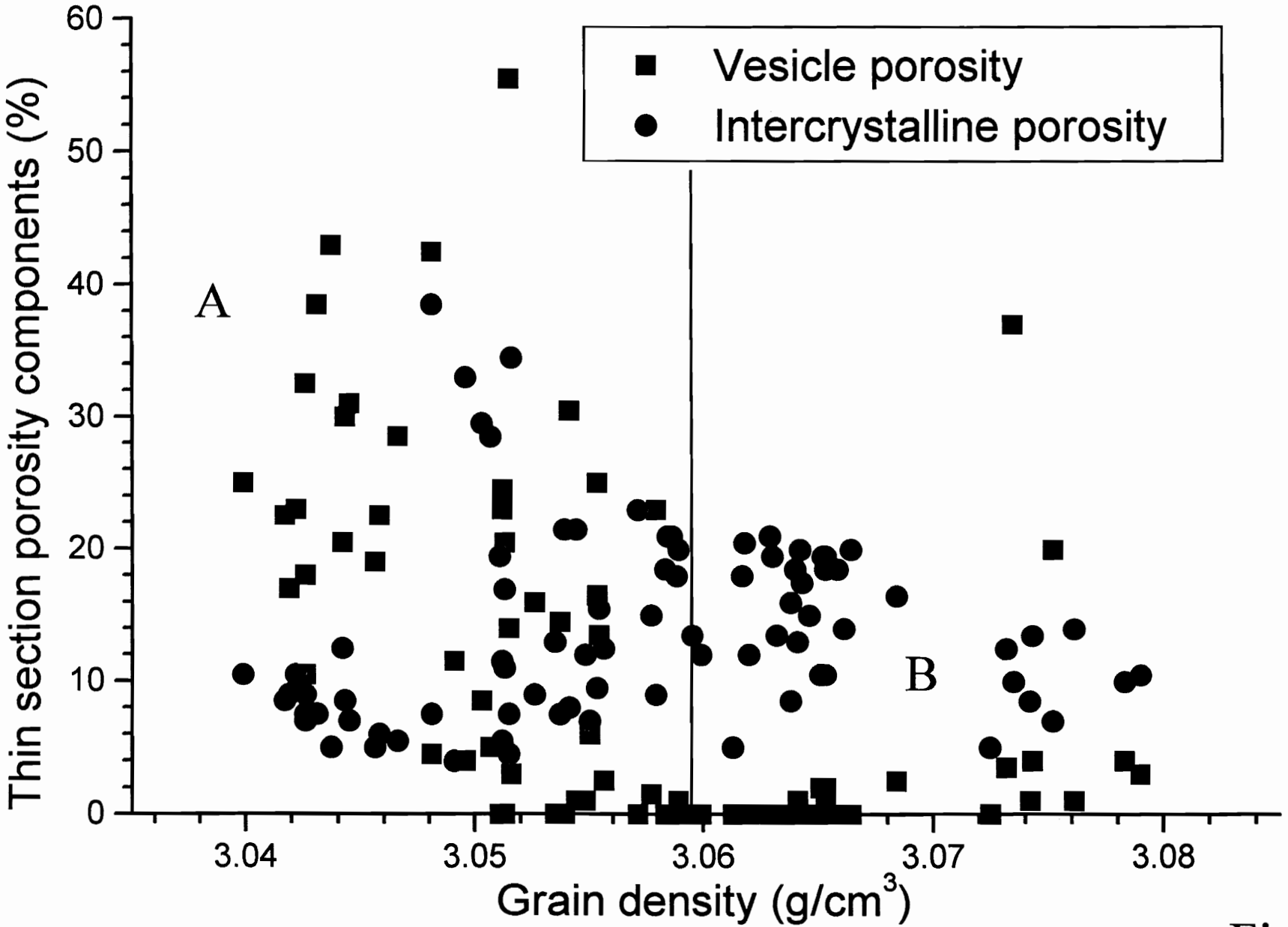
Vesicle porosity
Intercrystalline porosity
A
B
Thin section porosity components (%)
Grain density (g/cm3)
0
10
20
30
40
50
60
3.04
3.05
3.06
3.07
3.08

Fig. 3.11

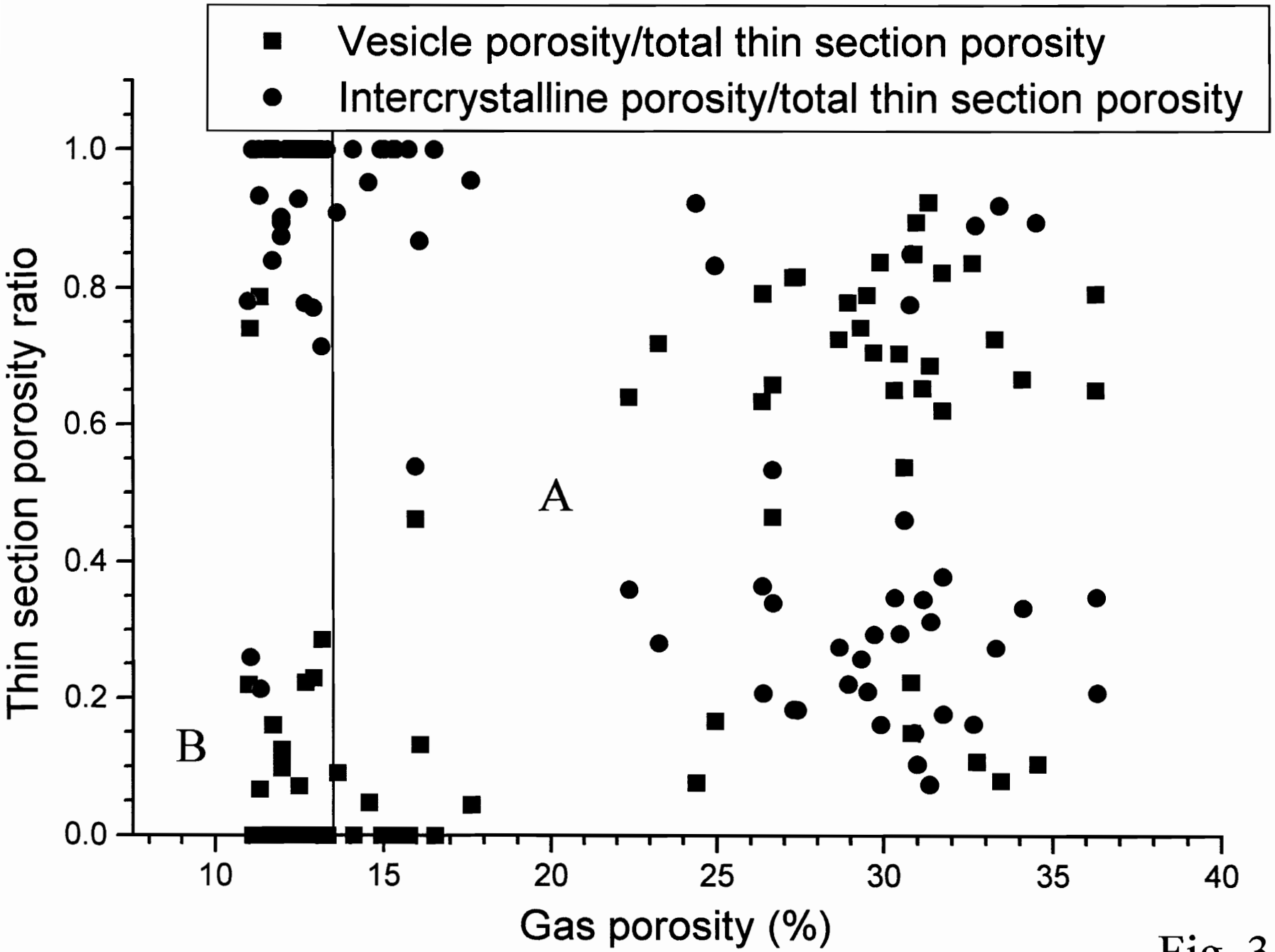
Vesicle porosity/total thin section porosity
Intercrystalline porosity/total thin section porosity
Thin section porosity ratio
0.0
0.2
0.4
0.6
0.8
1.0
10
15
20
25
30
35
40
Gas porosity (%)
A
B

Fig. 3.12

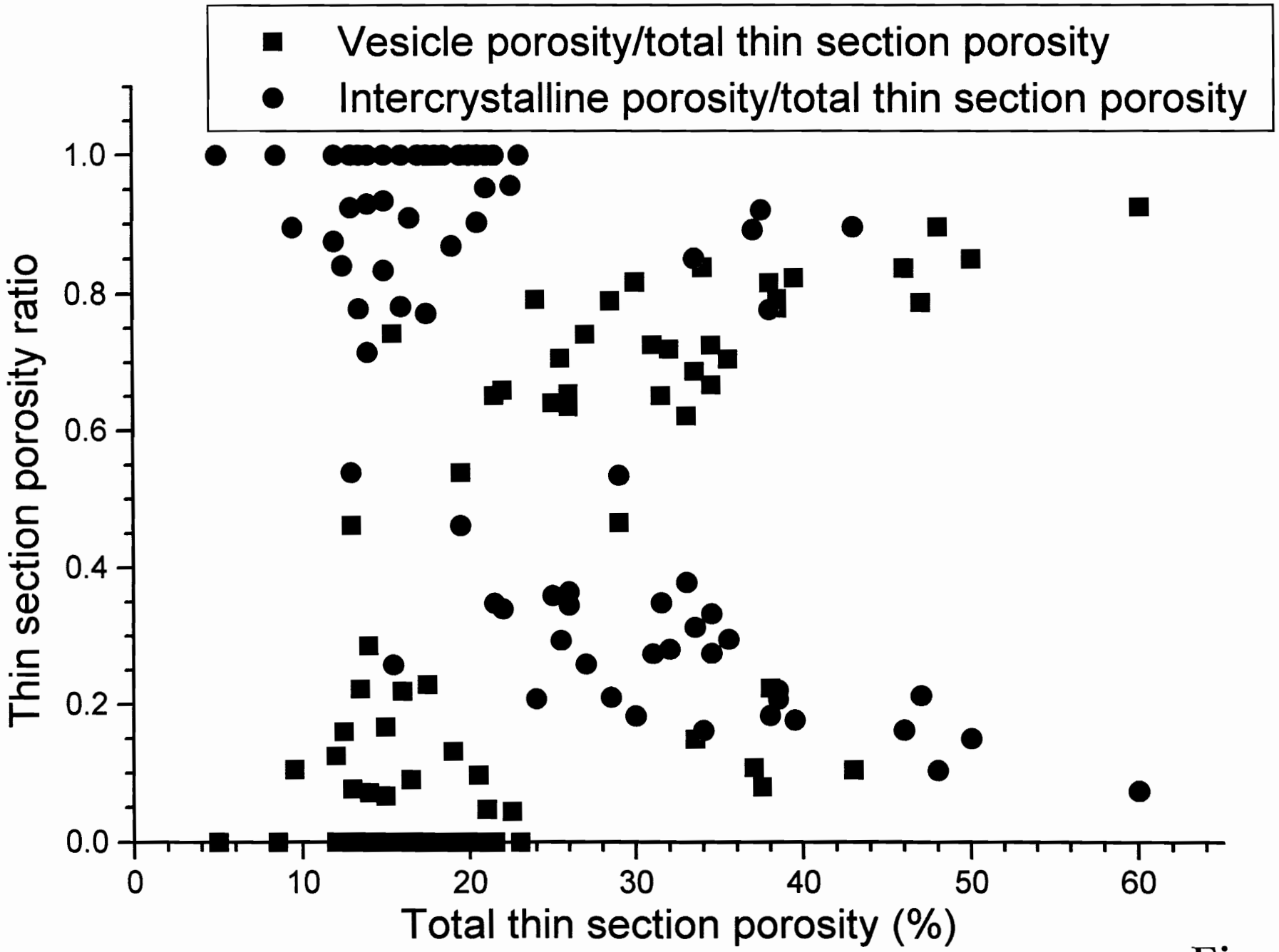
Vesicle porosity/total thin section porosity
Intercrystalline porosity/total thin section porosity
Thin section porosity ratio
1.0
0.8
0.6
0.4
0.2
0.0
0
10
20
30
40
50
60
Total thin section porosity (%)

Fig. 3.13

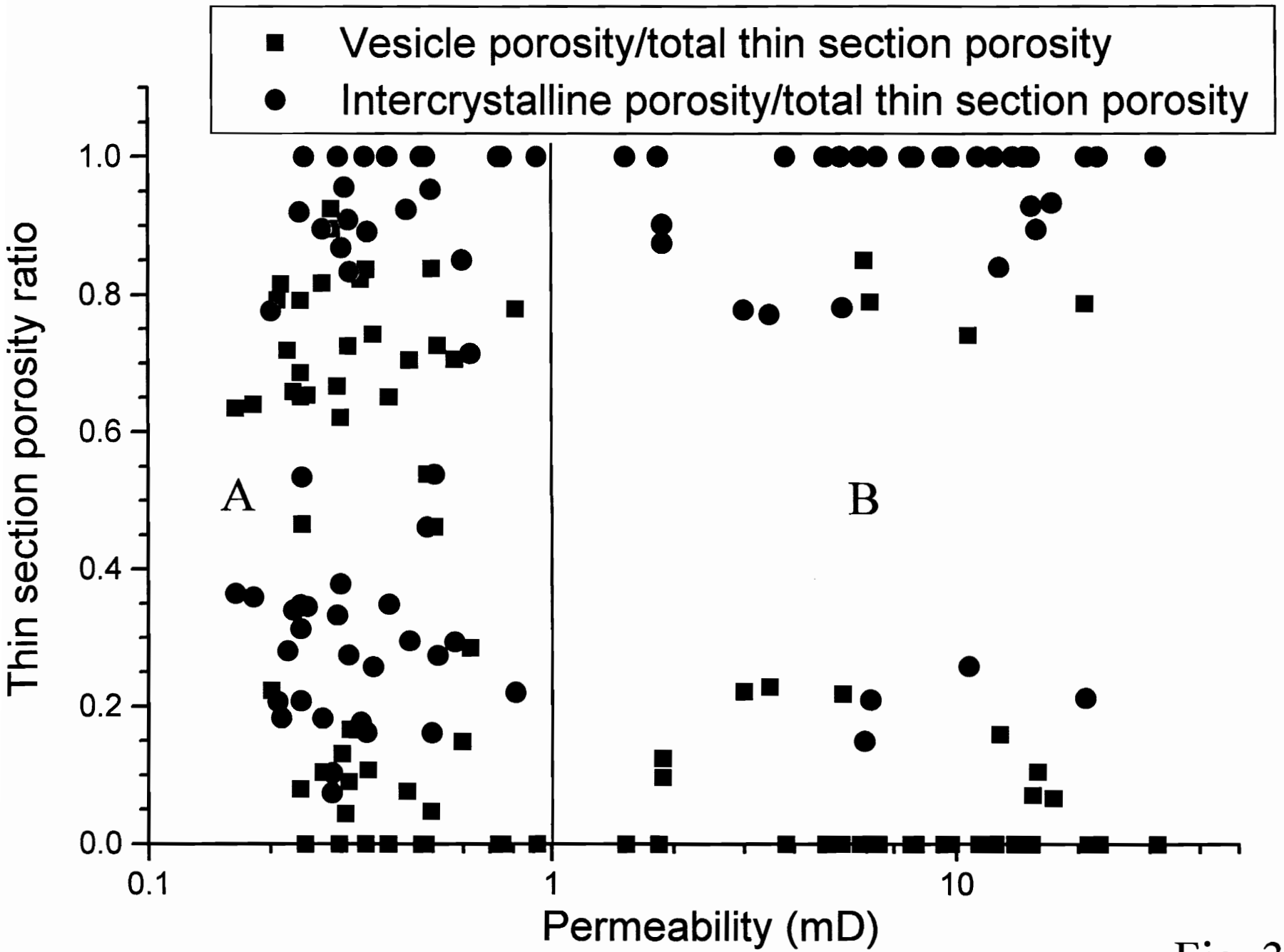
Vesicle porosity/total thin section porosity
Intercrystalline porosity/total thin section porosity
Thin section porosity ratio
1.0
0.8
0.6
0.4
0.2
0.0
A
B
0.1
1
10
Permeability (mD)

Fig. 3.14

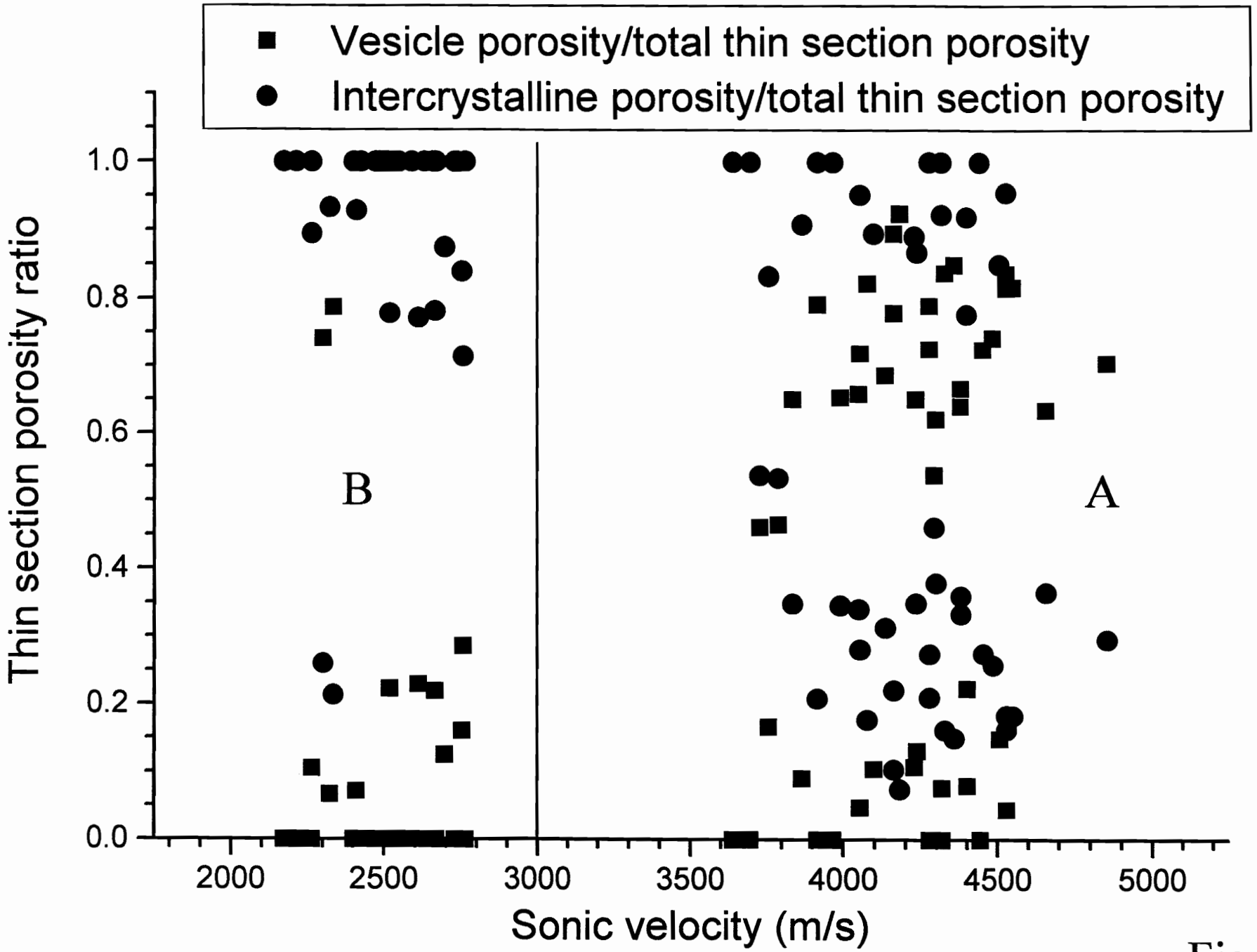
Vesicle porosity/total thin section porosity
Intercrystalline porosity/total thin section porosity
Thin section porosity ratio
1.0
0.8
0.6
0.4
0.2
0.0
B
A
2000
2500
3000
3500
4000
4500
5000
Sonic velocity (m/s)

Fig. 3.15

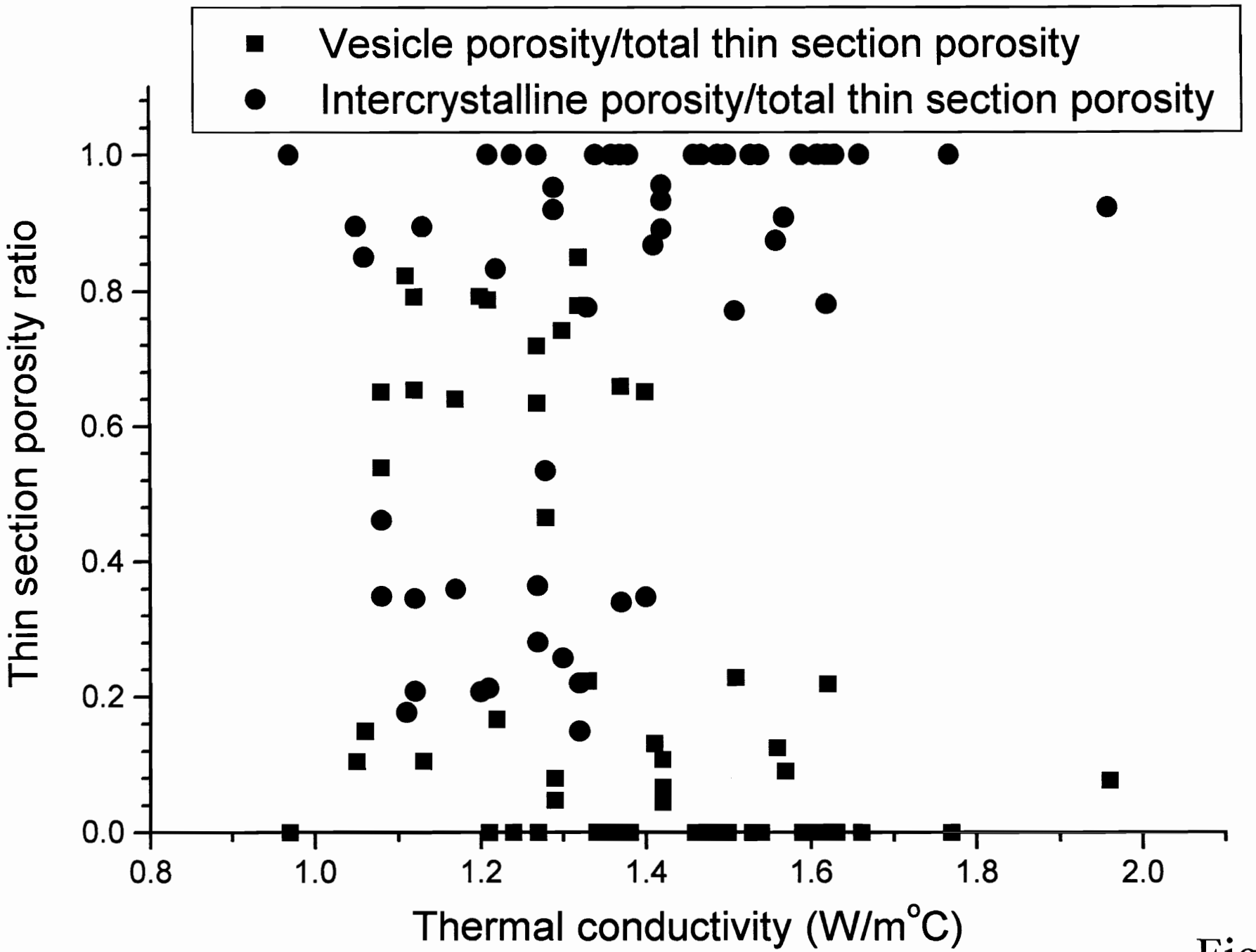
Vesicle porosity/total thin section porosity
Intercrystalline porosity/total thin section porosity
Thin section porosity ratio
0.0
0.2
0.4
0.6
0.8
1.0
0.8
1.0
1.2
1.4
1.6
1.8
2.0
Thermal conductivity (W/m°C)

Fig. 3.16

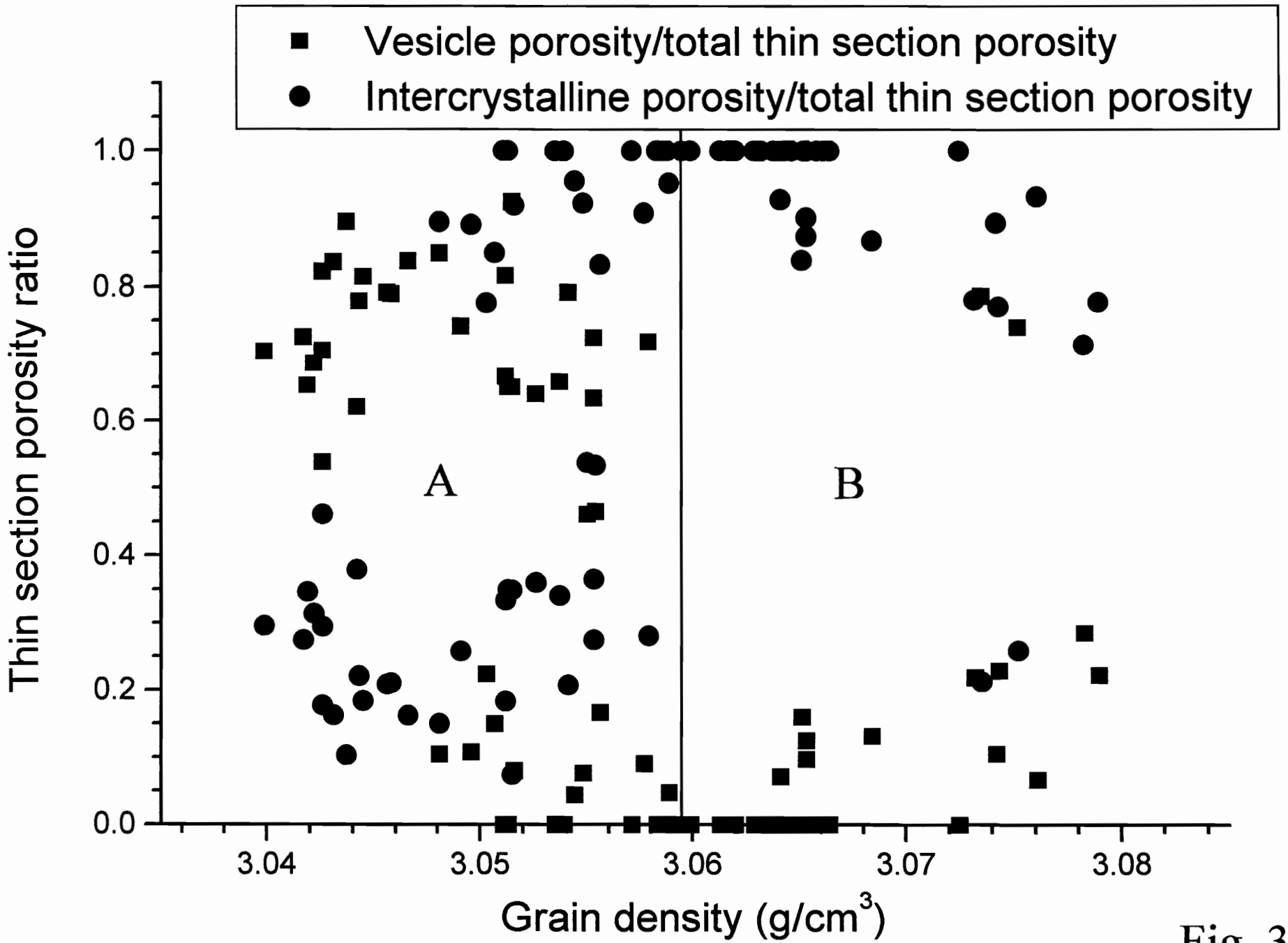
Vesicle porosity/total thin section porosity
Intercrystalline porosity/total thin section porosity
Thin section porosity ratio
1.0
0.8
0.6
0.4
0.2
0.0
A
B
3.04
3.05
3.06
3.07
3.08
Grain density (g/cm3)

Fig. 3.17

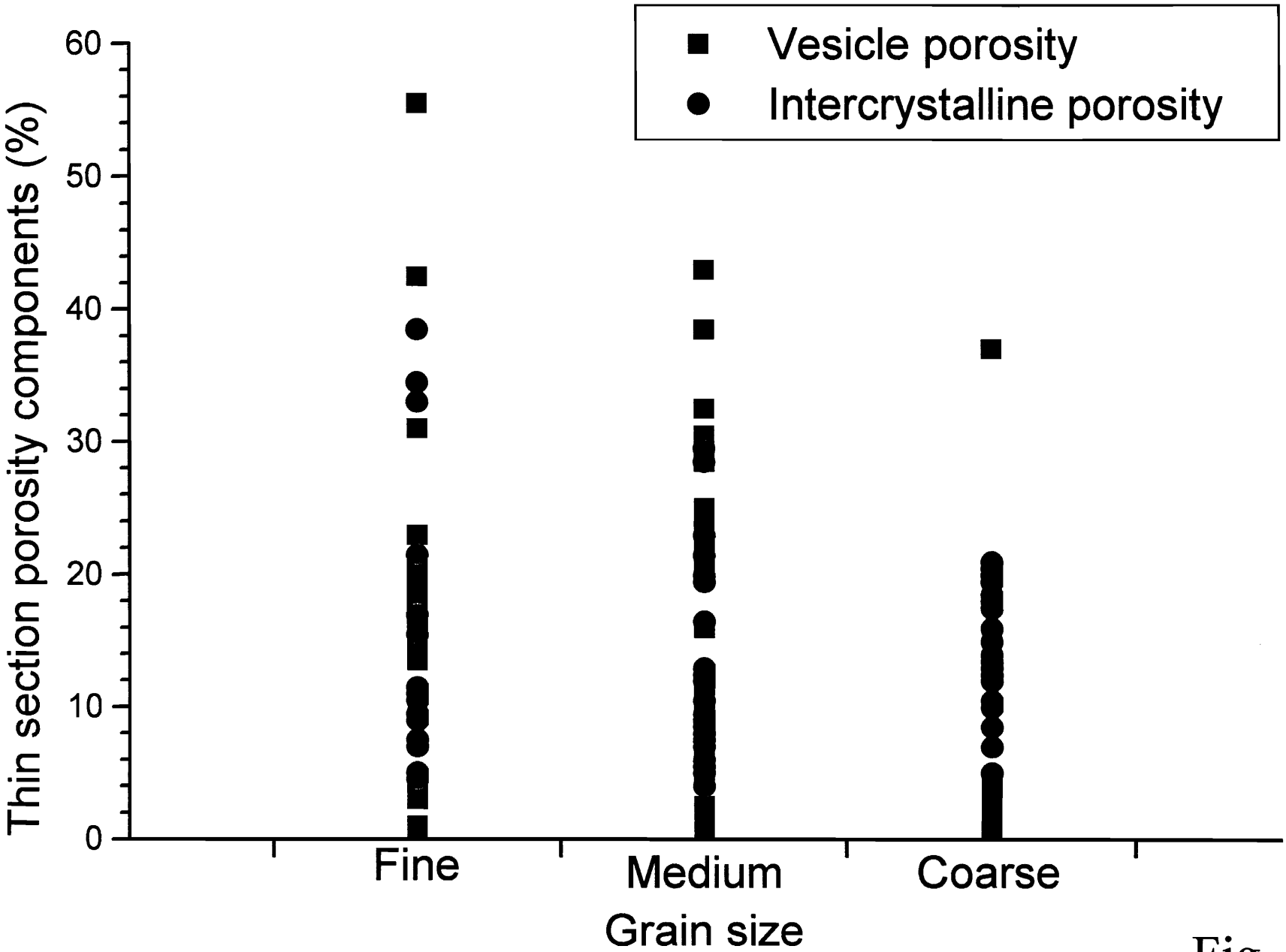
Vesicle porosity
Intercrystalline porosity
Thin section porosity components (%)
60
50
40
30
20
10
0
Fine
Medium
Coarse
Grain size

Fig. 3.18

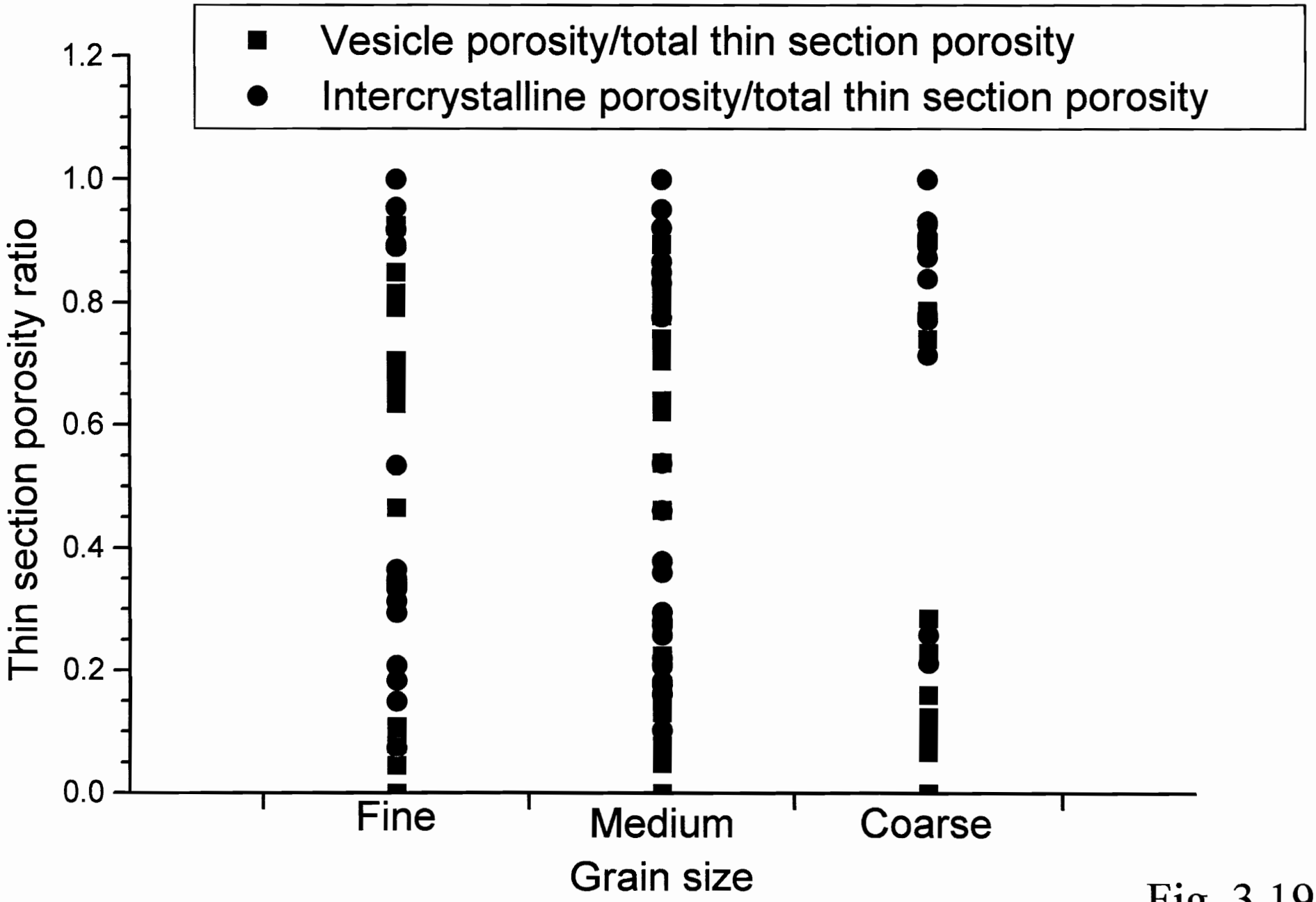
Vesicle porosity/total thin section porosity
Intercrystalline porosity/total thin section porosity
Thin section porosity ratio
1.2
1.0
0.8
0.6
0.4
0.2
0.0
Fine
Medium
Coarse
Grain size

Fig. 3.19

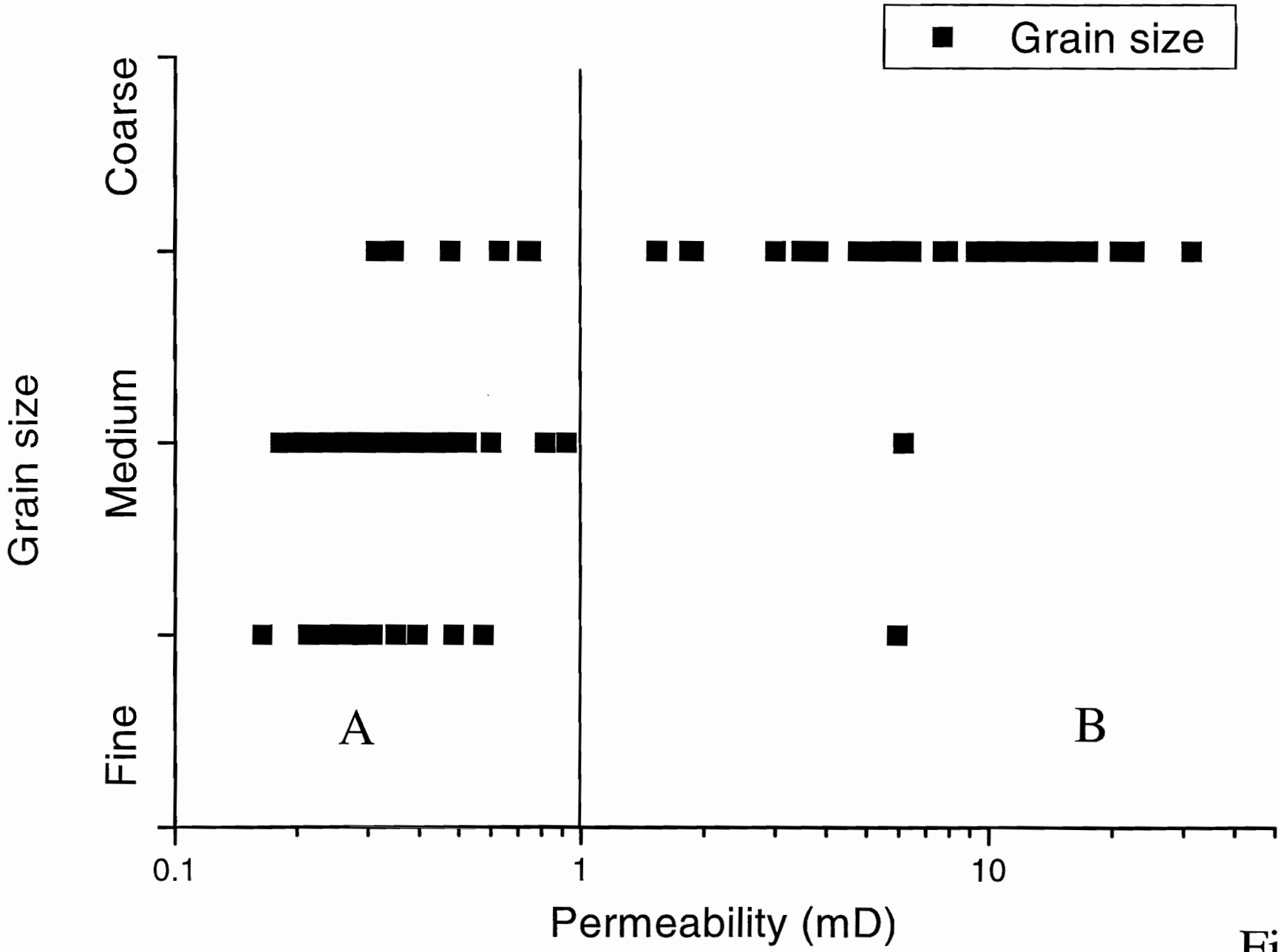
Grain size
Coarse
Medium
Fine
Grain size
A
B
0.1
1
10
Permeability (mD)

Fig. 3.20

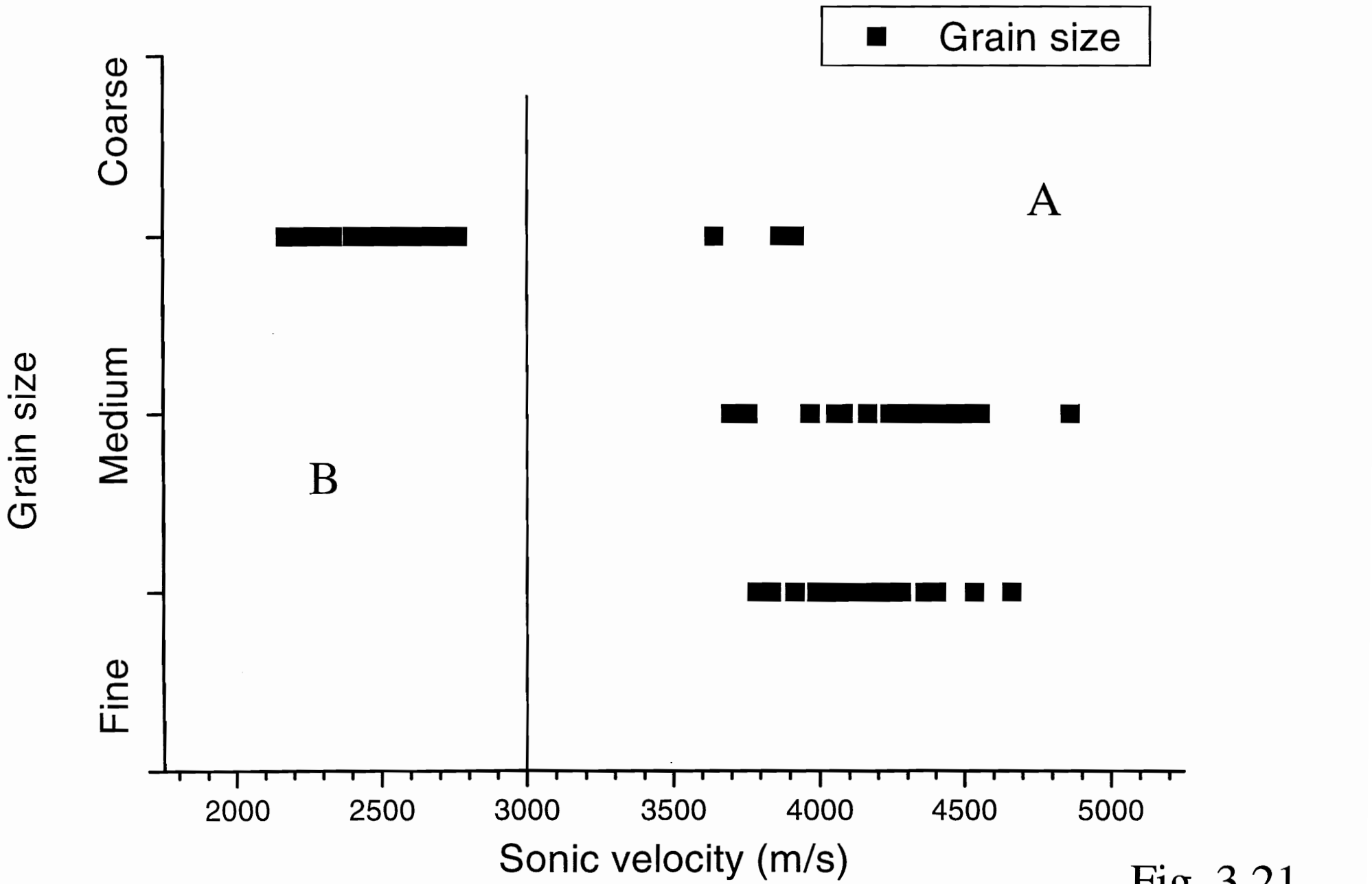
Grain size
Coarse
Medium
Fine
Grain size
A
B
2000
2500
3000
3500
4000
4500
5000
Sonic velocity (m/s)

Fig. 3.21

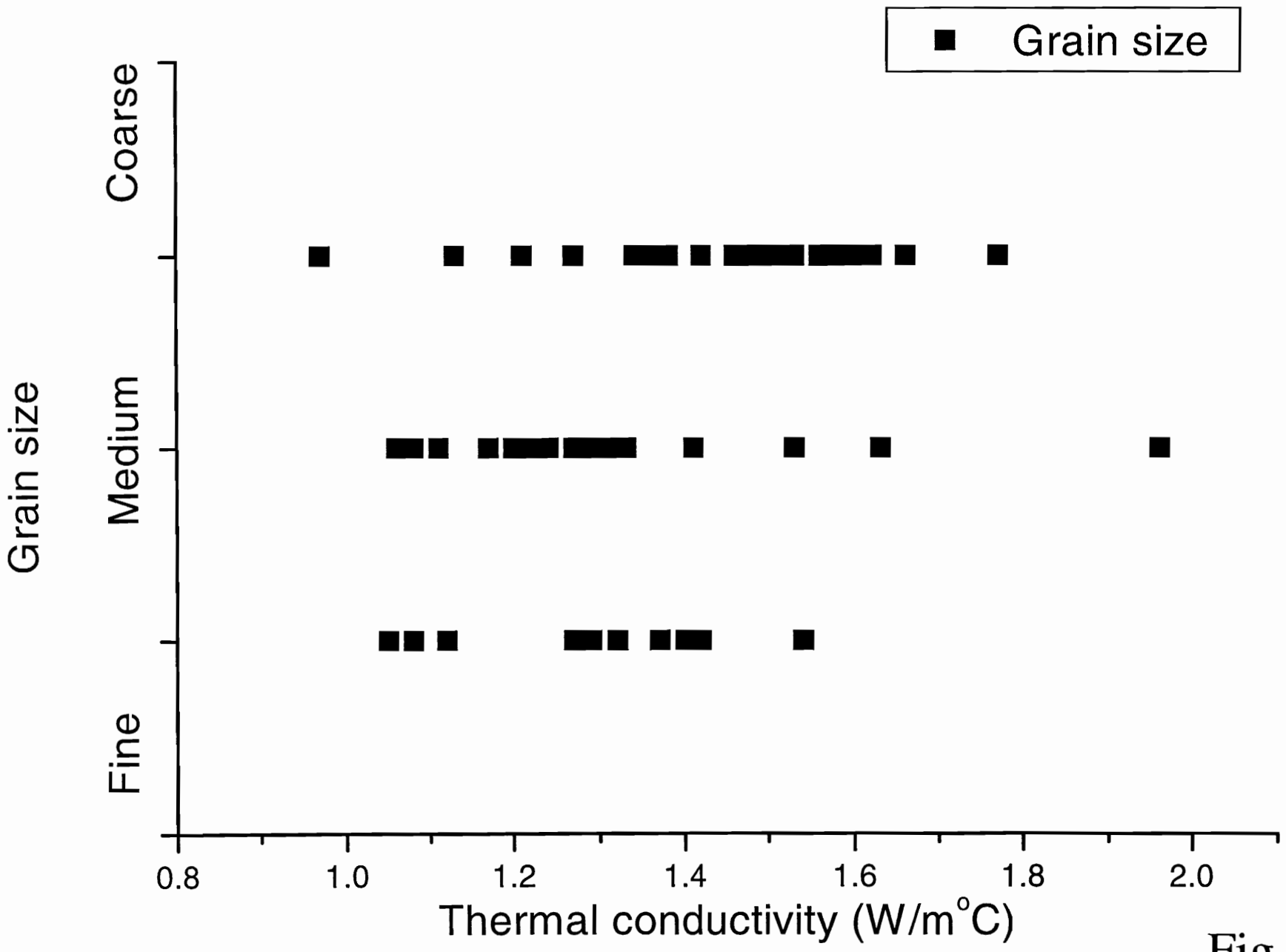
Grain size
Grain size
Coarse
Medium
Fine
0.8
1.0
1.2
1.4
1.6
1.8
2.0
Thermal conductivity (W/m°C)

Fig. 3.22

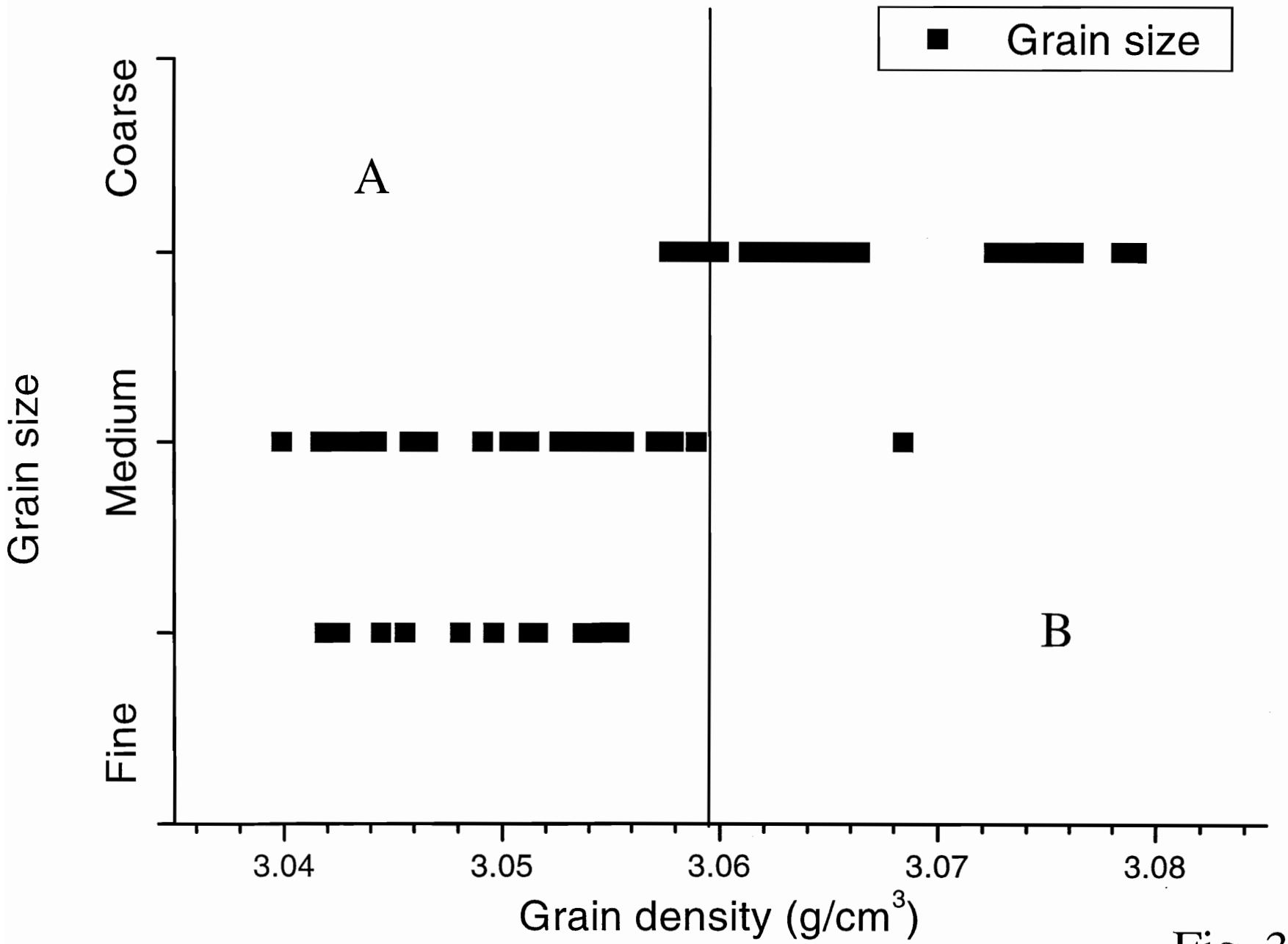
Grain size
Coarse
Medium
Fine
Grain size
A
B
3.04
3.05
3.06
3.07
3.08
Grain density (g/cm3)

Fig. 3.23

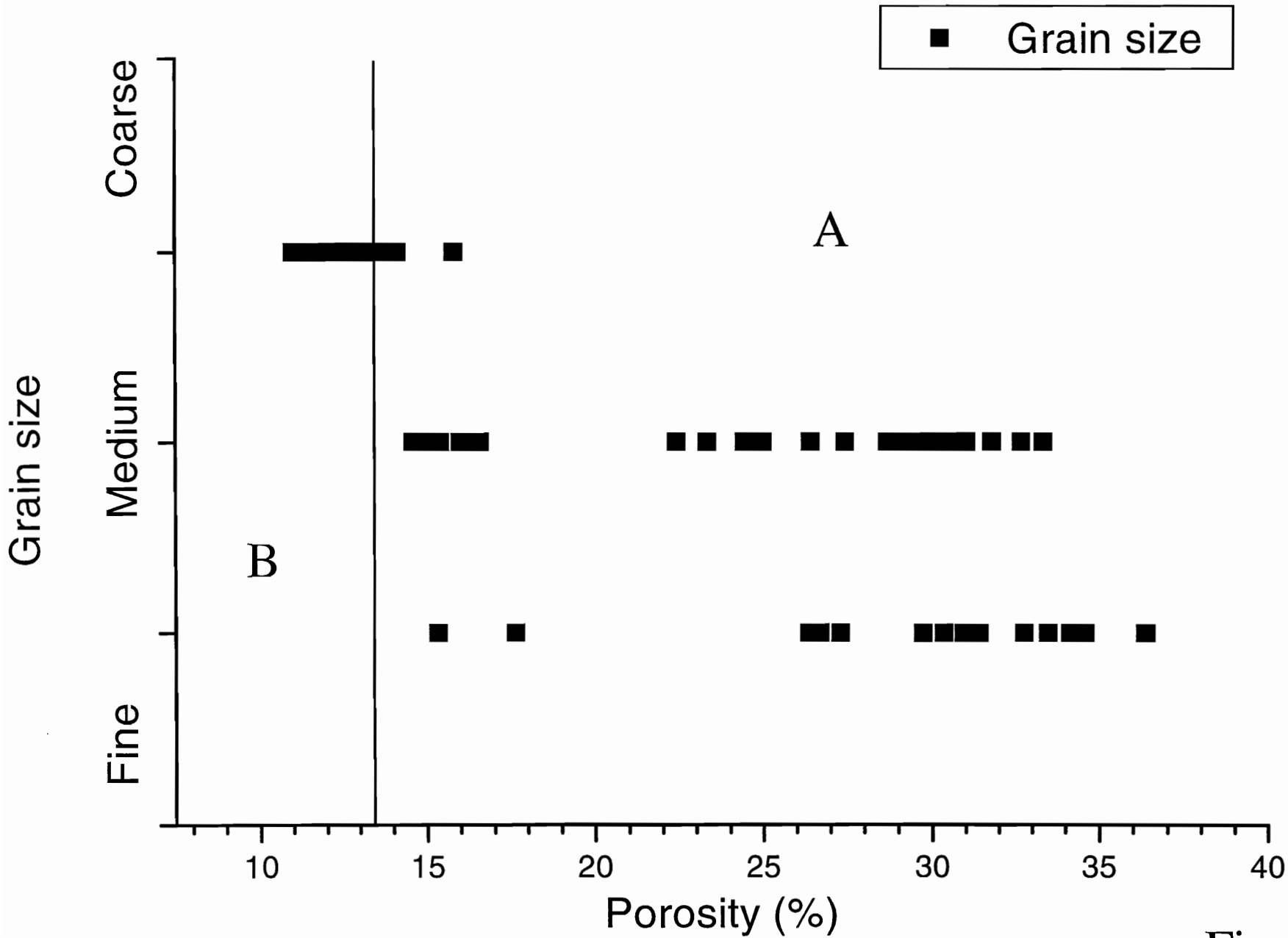
Grain size
Coarse
Medium
Fine
Grain size
A
B
10
15
20
25
30
35
40
Porosity (%)

Fig. 3.24

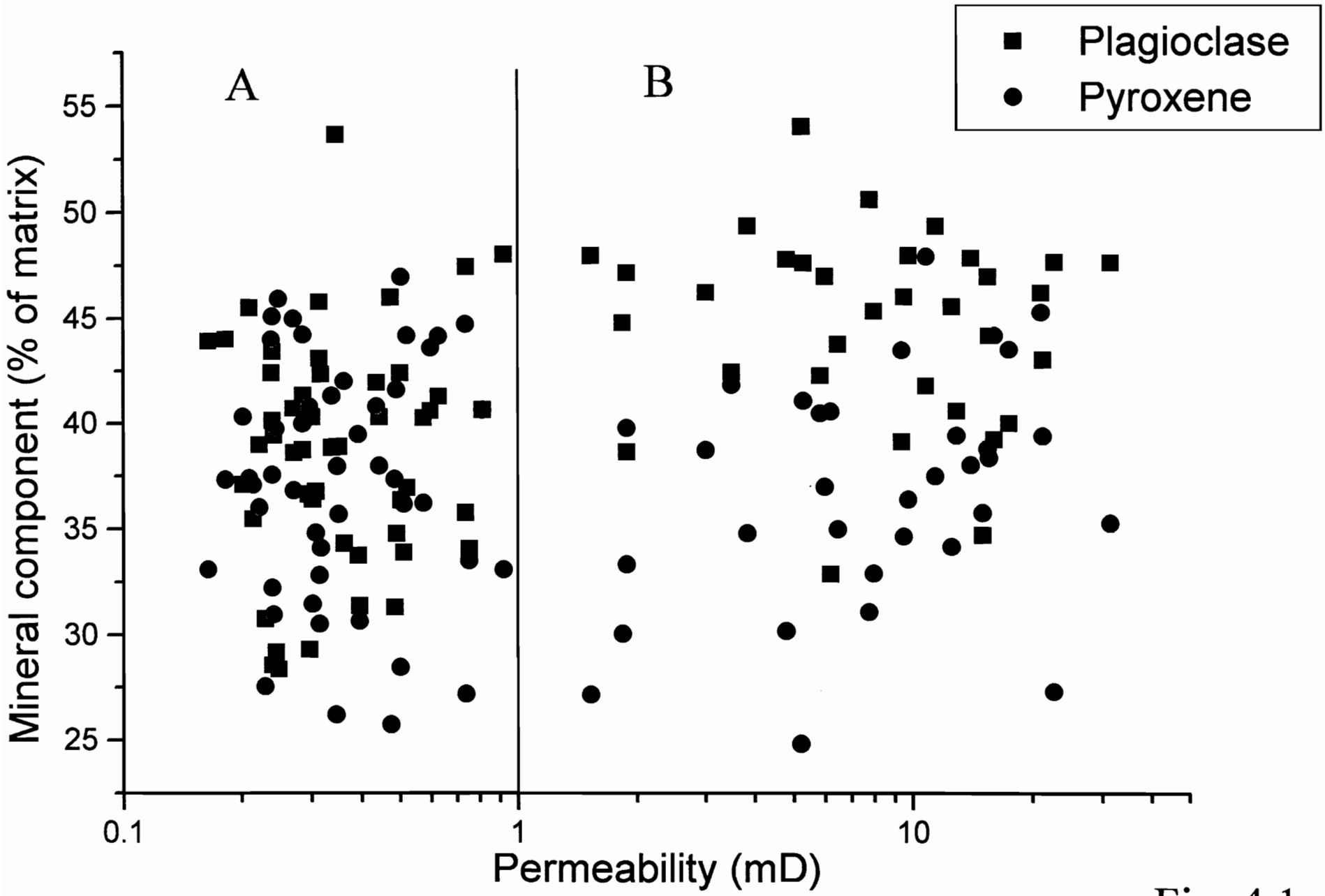
Plagioclase
Pyroxene
A
B
Mineral component (% of matrix)
55
50
45
40
35
30
25
0.1
1
10
Permeability (mD)

Fig. 4.1

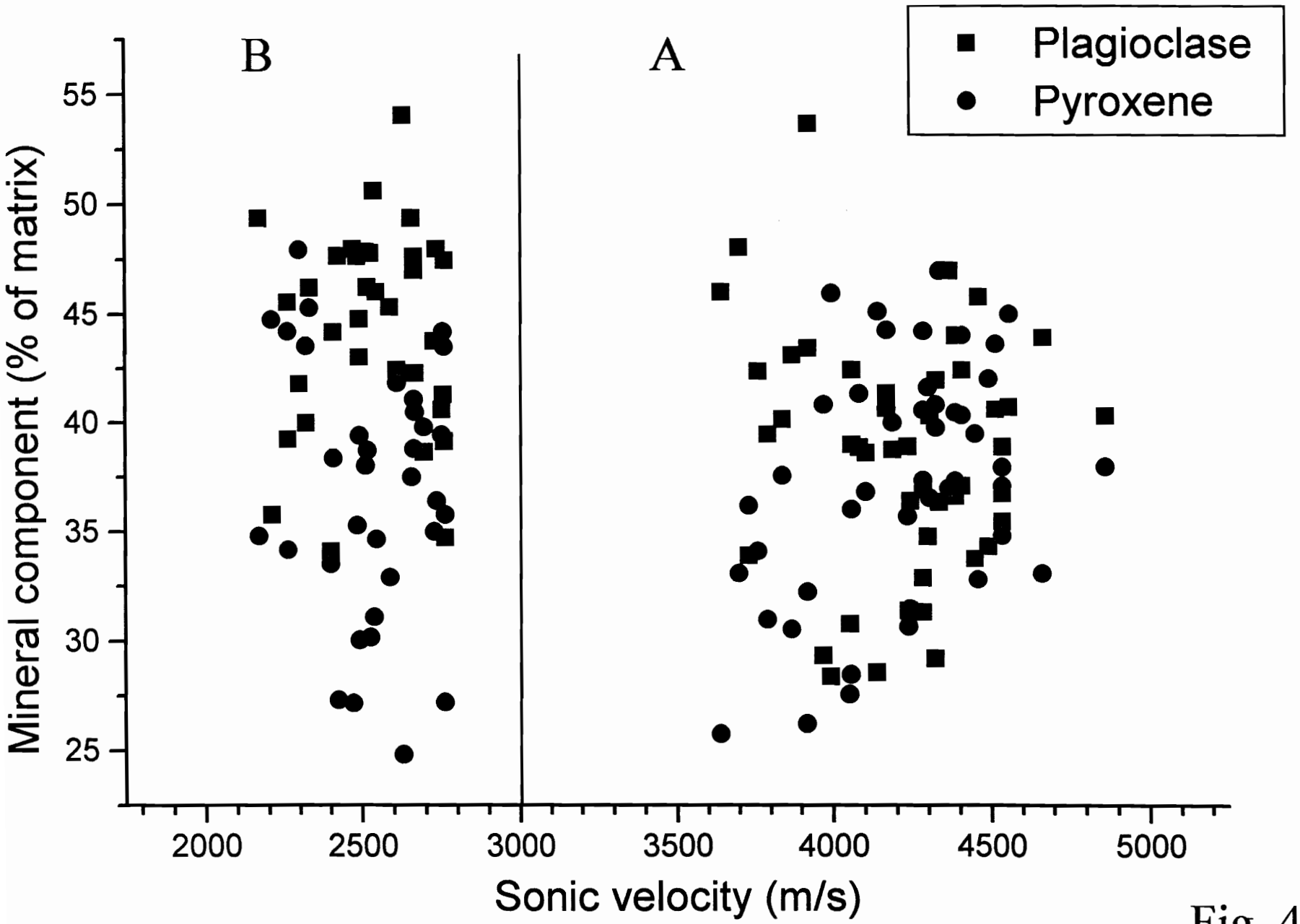
B
A
Plagioclase
Pyroxene
Mineral component (% of matrix)
55
50
45
40
35
30
25
2000
2500
3000
3500
4000
4500
5000
Sonic velocity (m/s)

Fig. 4.2

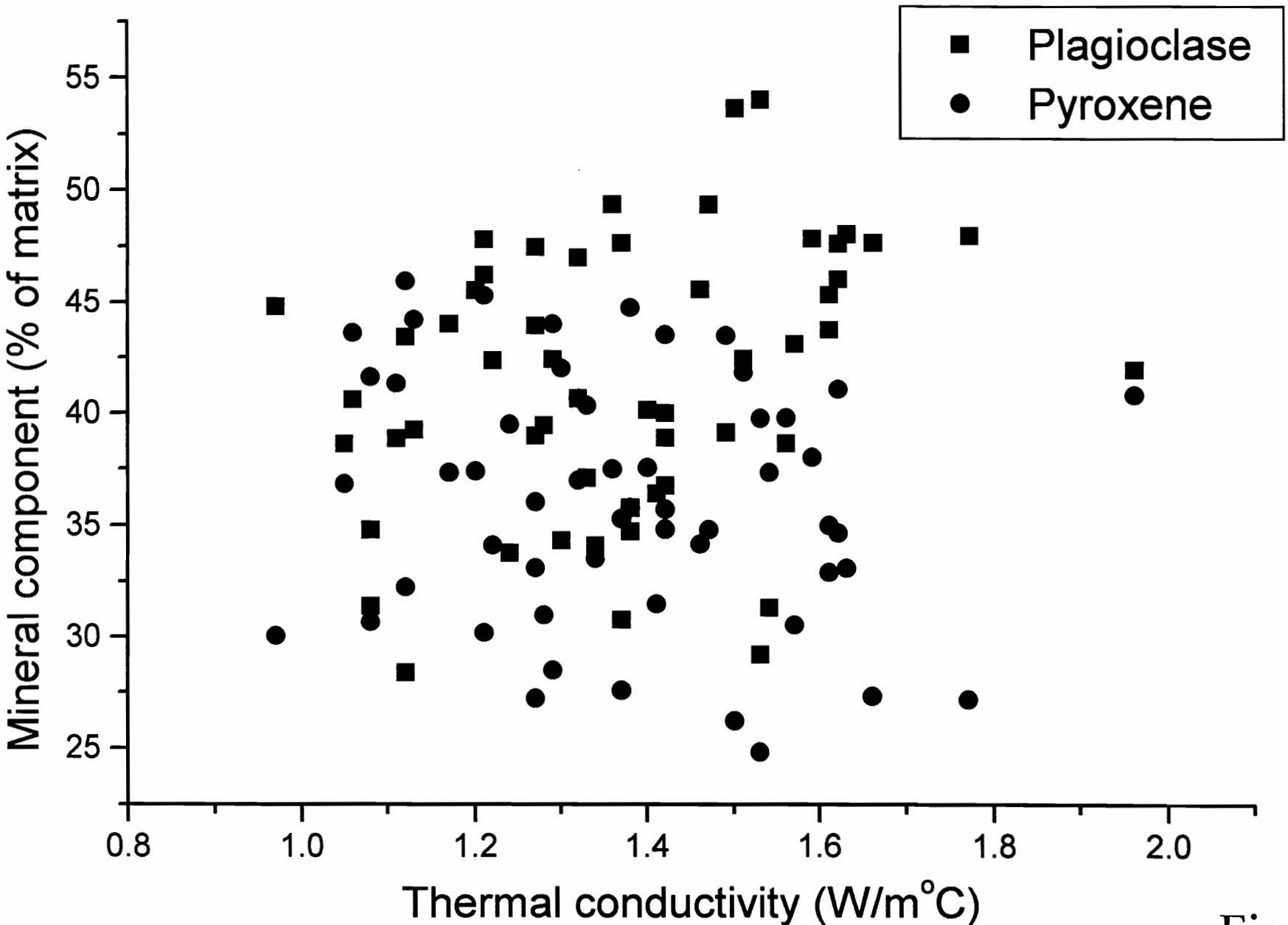
Plagioclase
Pyroxene
Mineral component (% of matrix)
55
50
45
40
35
30
25
0.8
1.0
1.2
1.4
1.6
1.8
2.0
Thermal conductivity (W/m°C)

Fig. 4.3

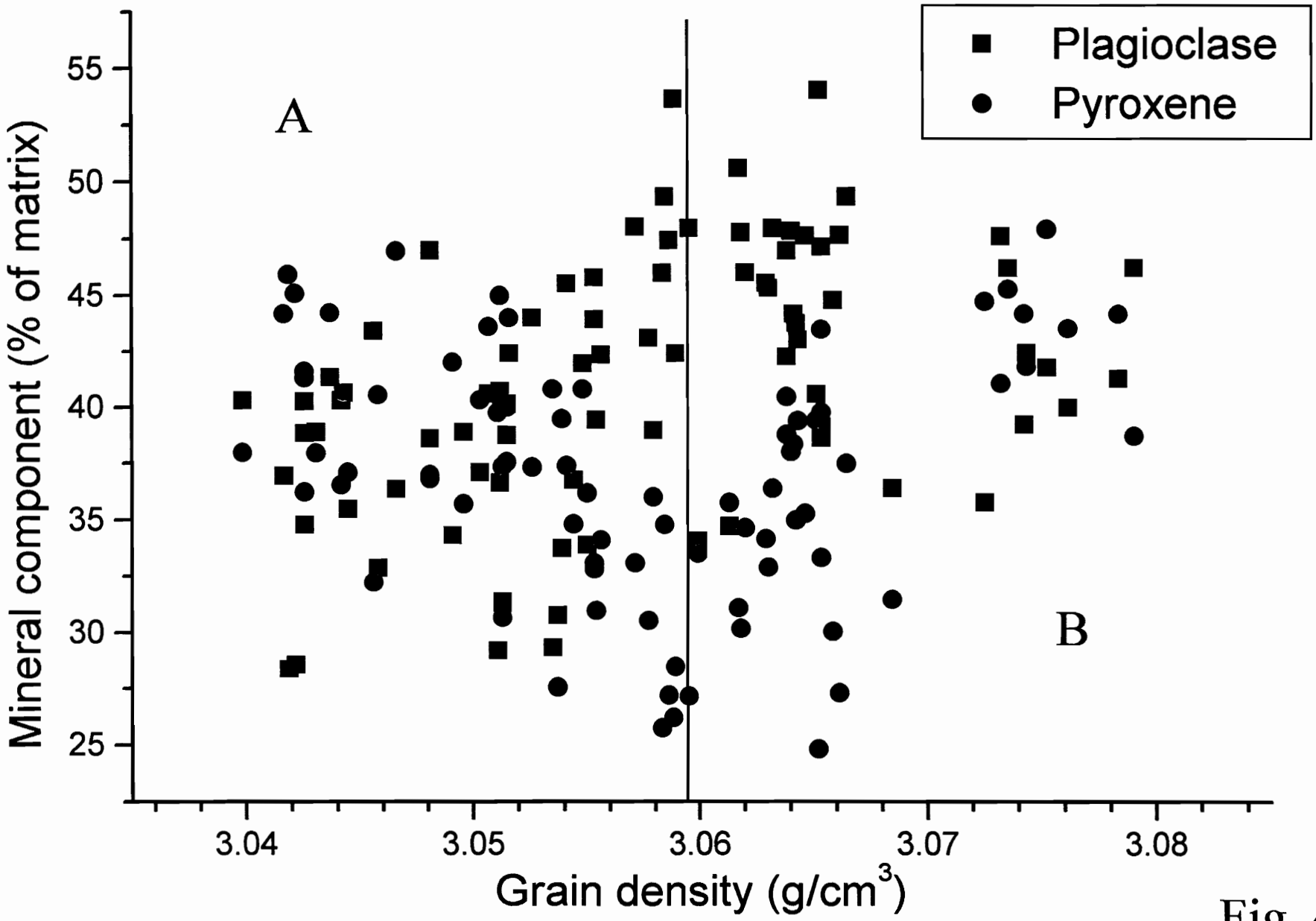
Plagioclase
Pyroxene
A
B
Mineral component (% of matrix)
55
50
45
40
35
30
25
3.04
3.05
3.06
3.07
3.08
Grain density (g/cm3)

Fig. 4.4

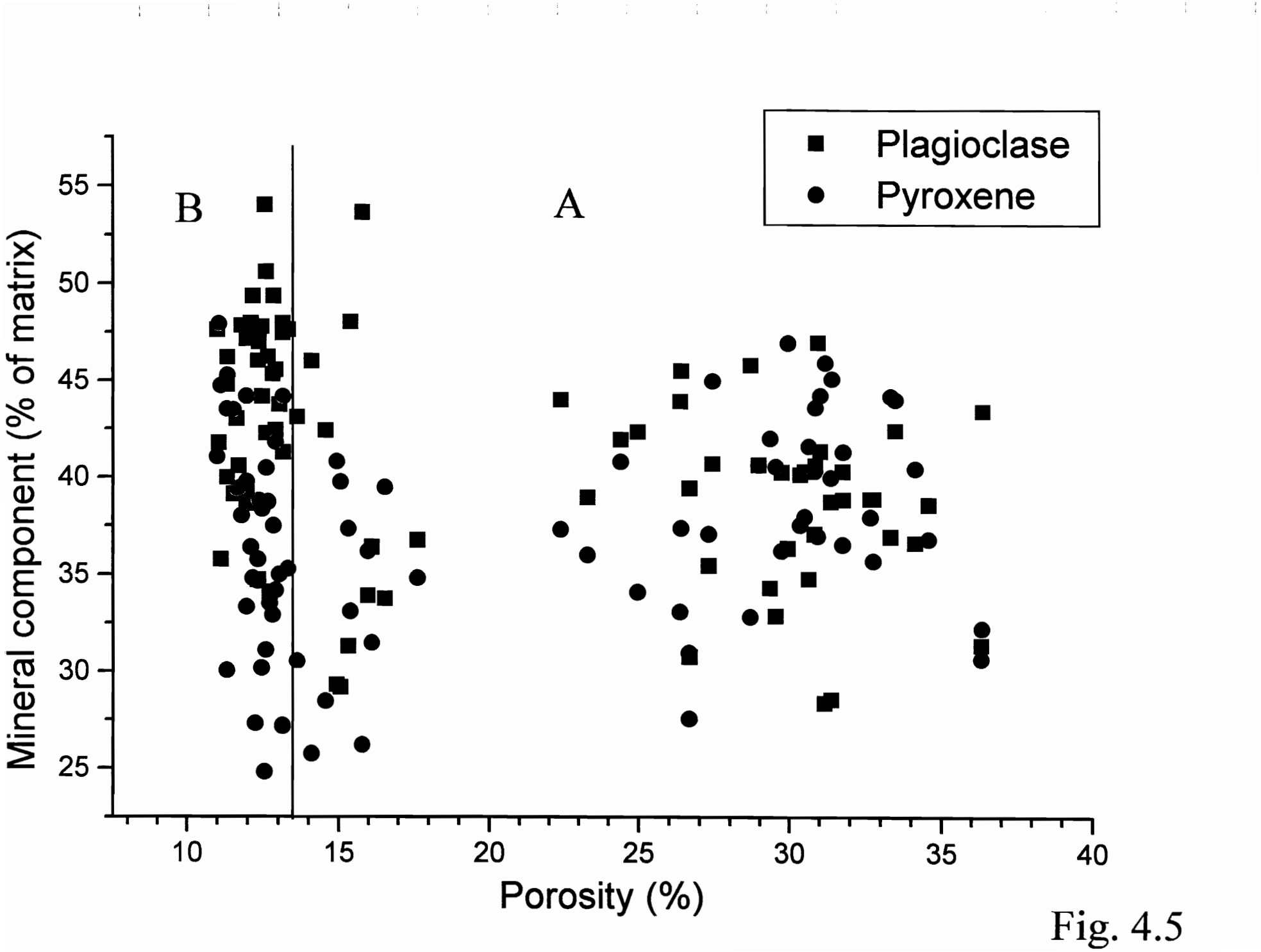
Plagioclase
Pyroxene
B
A
Mineral component (% of matrix)
55
50
45
40
35
30
25
10
15
20
25
30
35
40
Porosity (%)

Fig. 4.5

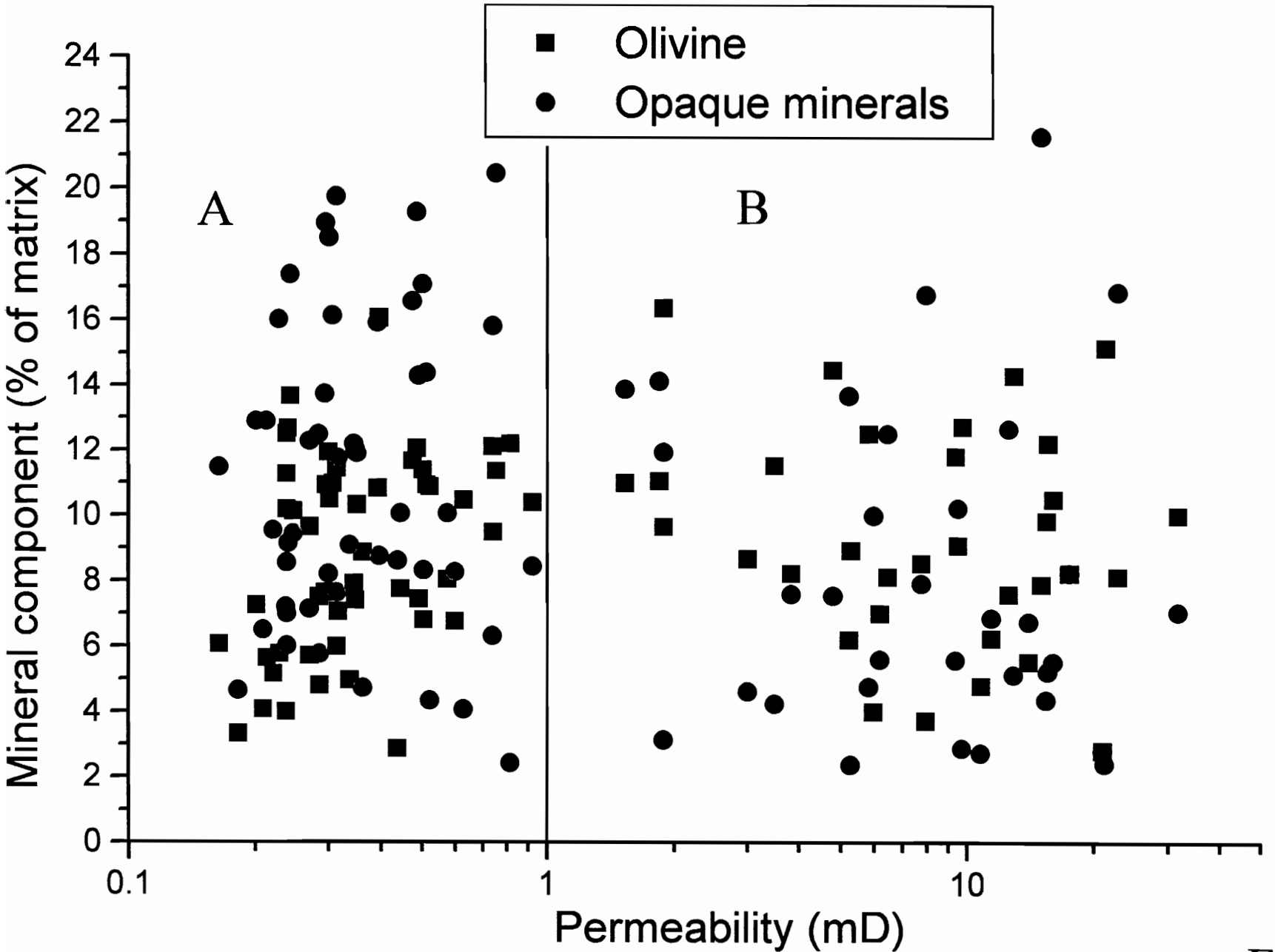
Olivine
Opaque minerals
A
B
Mineral component (% of matrix)
Permeability (mD)
0
2
4
6
8
10
12
14
16
18
20
22
24
0.1
1
10

Fig. 4.6

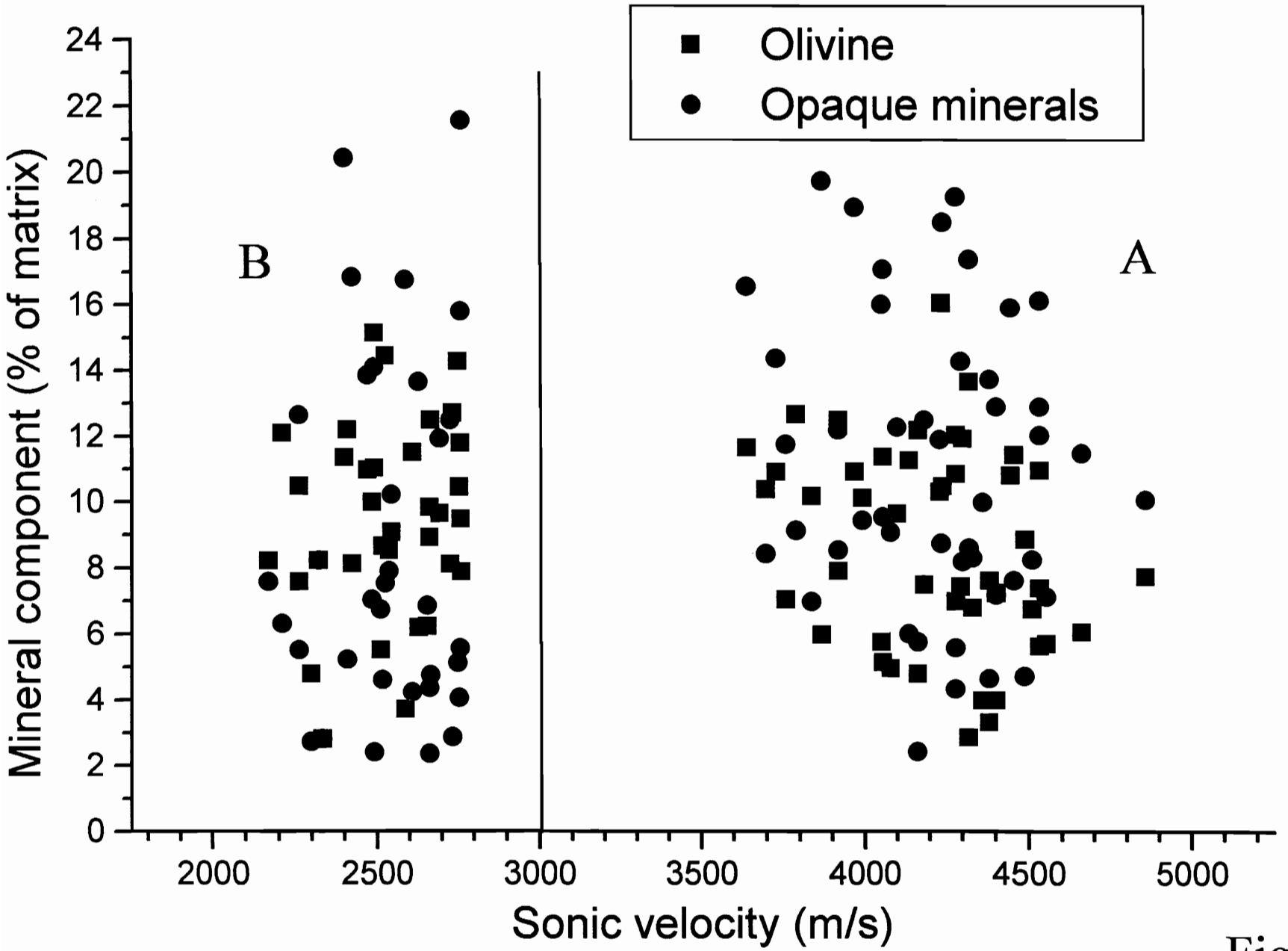
Olivine
Opaque minerals
B
A
Mineral component (% of matrix)
Sonic velocity (m/s)
0
2
4
6
8
10
12
14
16
18
20
22
24
2000
2500
3000
3500
4000
4500
5000

Fig. 4.7

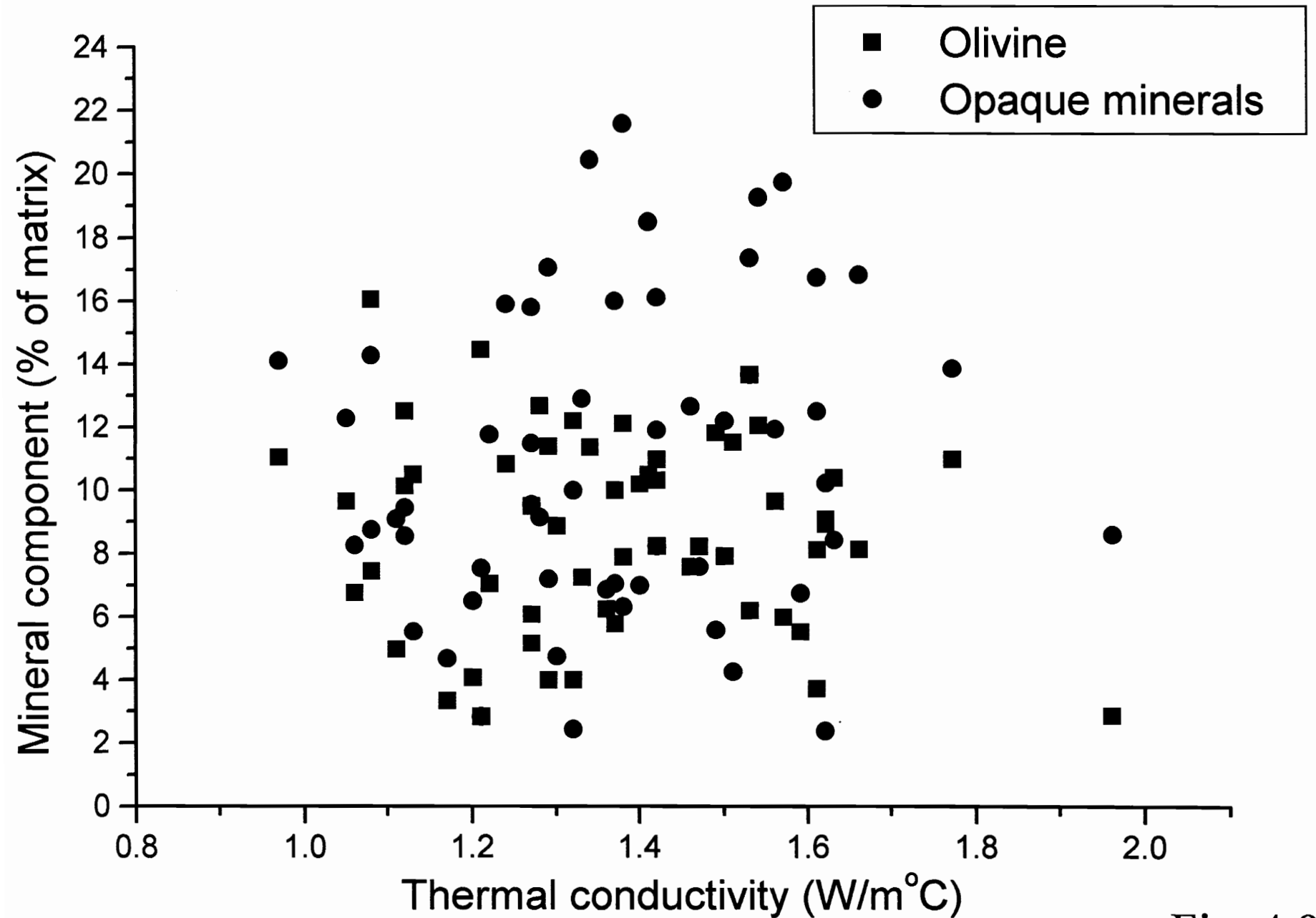
Olivine
Opaque minerals
Mineral component (% of matrix)
0
2
4
6
8
10
12
14
16
18
20
22
24
0.8
1.0
1.2
1.4
1.6
1.8
2.0
Thermal conductivity (W/m°C)

Fig. 4.8

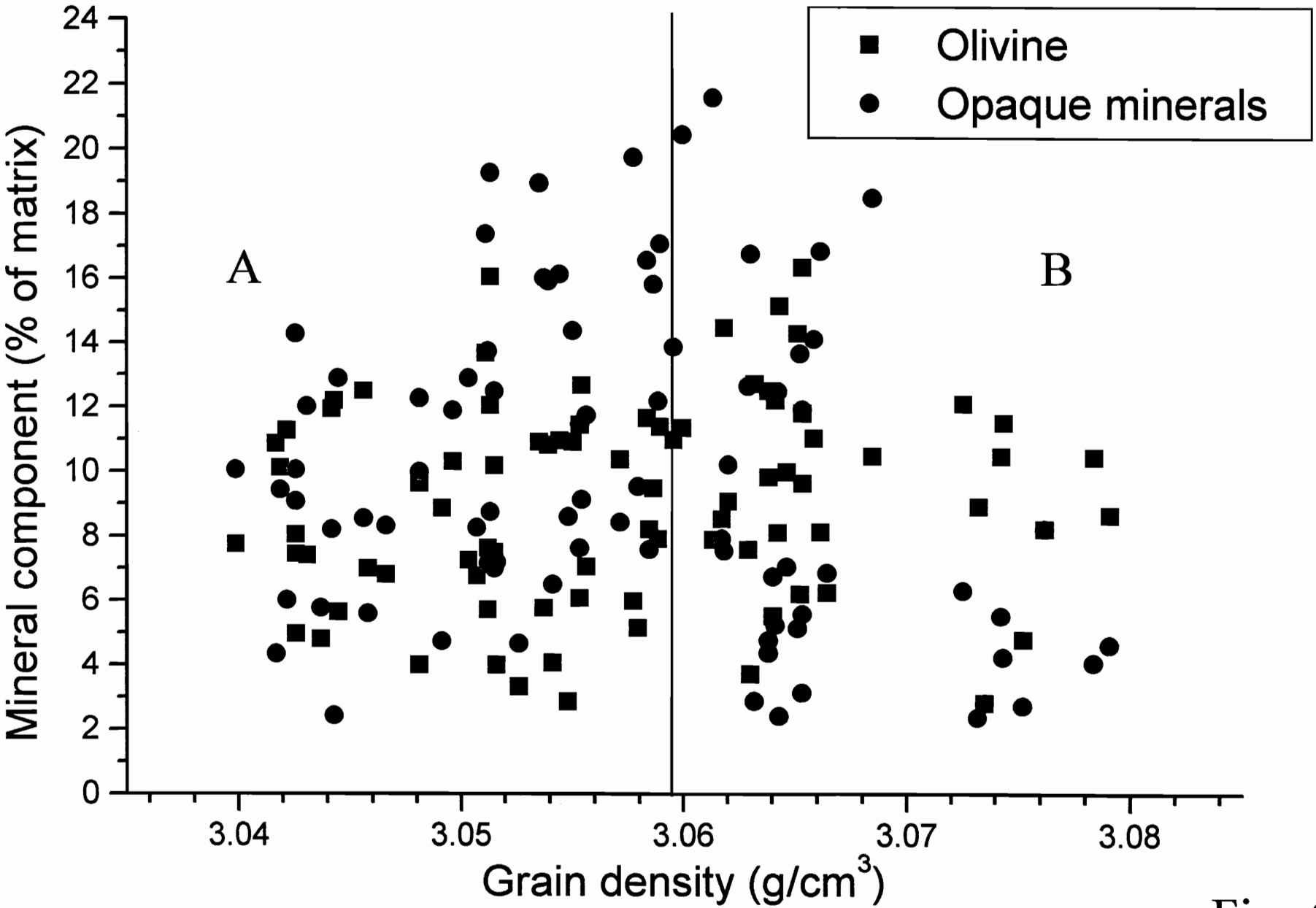
Olivine
Opaque minerals
A
B
Mineral component (% of matrix)
0
2
4
6
8
10
12
14
16
18
20
22
24
3.04
3.05
3.06
3.07
3.08
Grain density (g/cm3)

Fig. 4.9

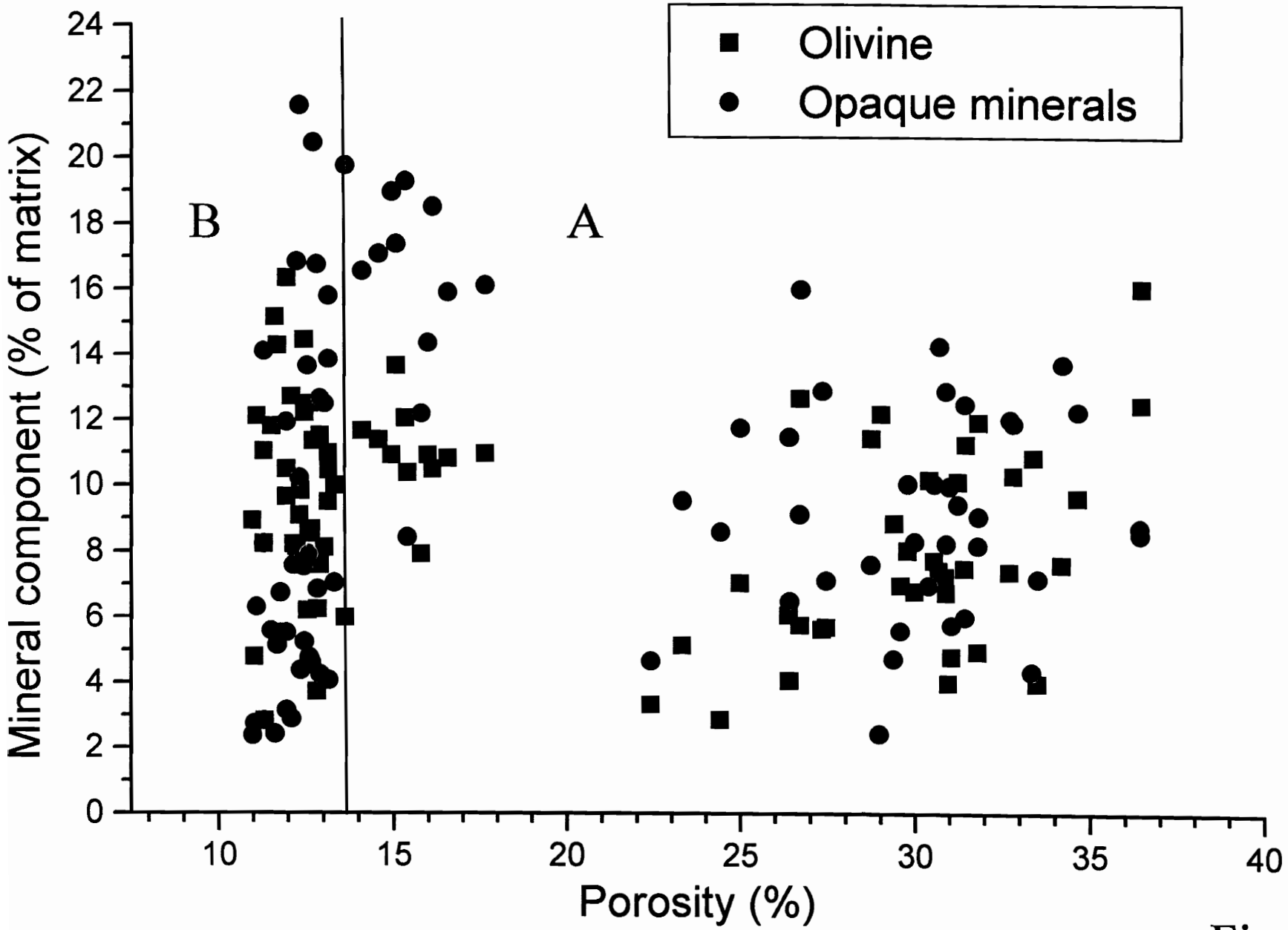
Olivine
Opaque minerals
B
A
Mineral component (% of matrix)
Porosity (%)
0
2
4
6
8
10
12
14
16
18
20
22
24
10
15
20
25
30
35
40

Fig. 4.10

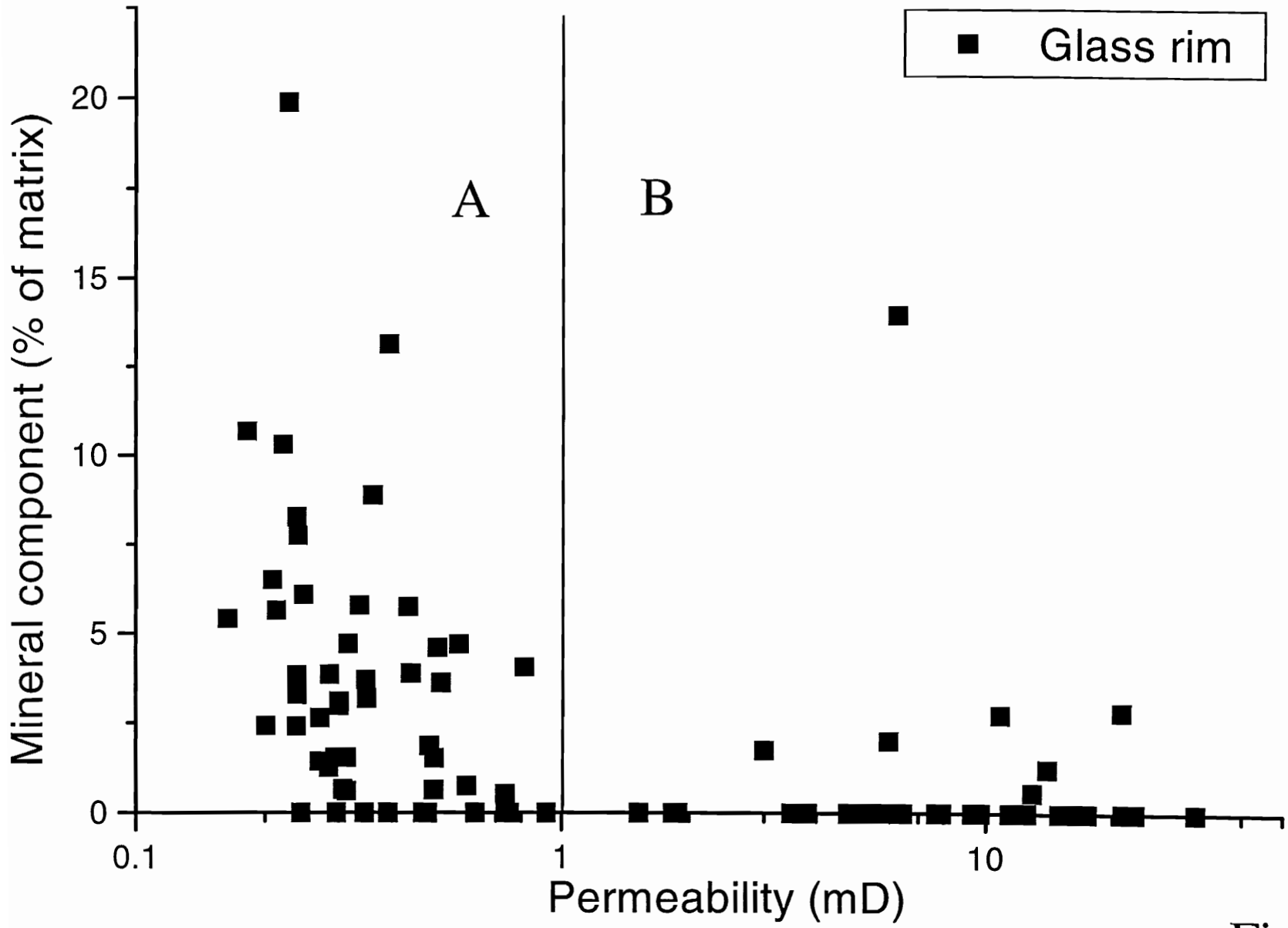
Glass rim
A
B
Mineral component (% of matrix)
20
15
10
5
0
0.1
1
10
Permeability (mD)

Fig. 4.11

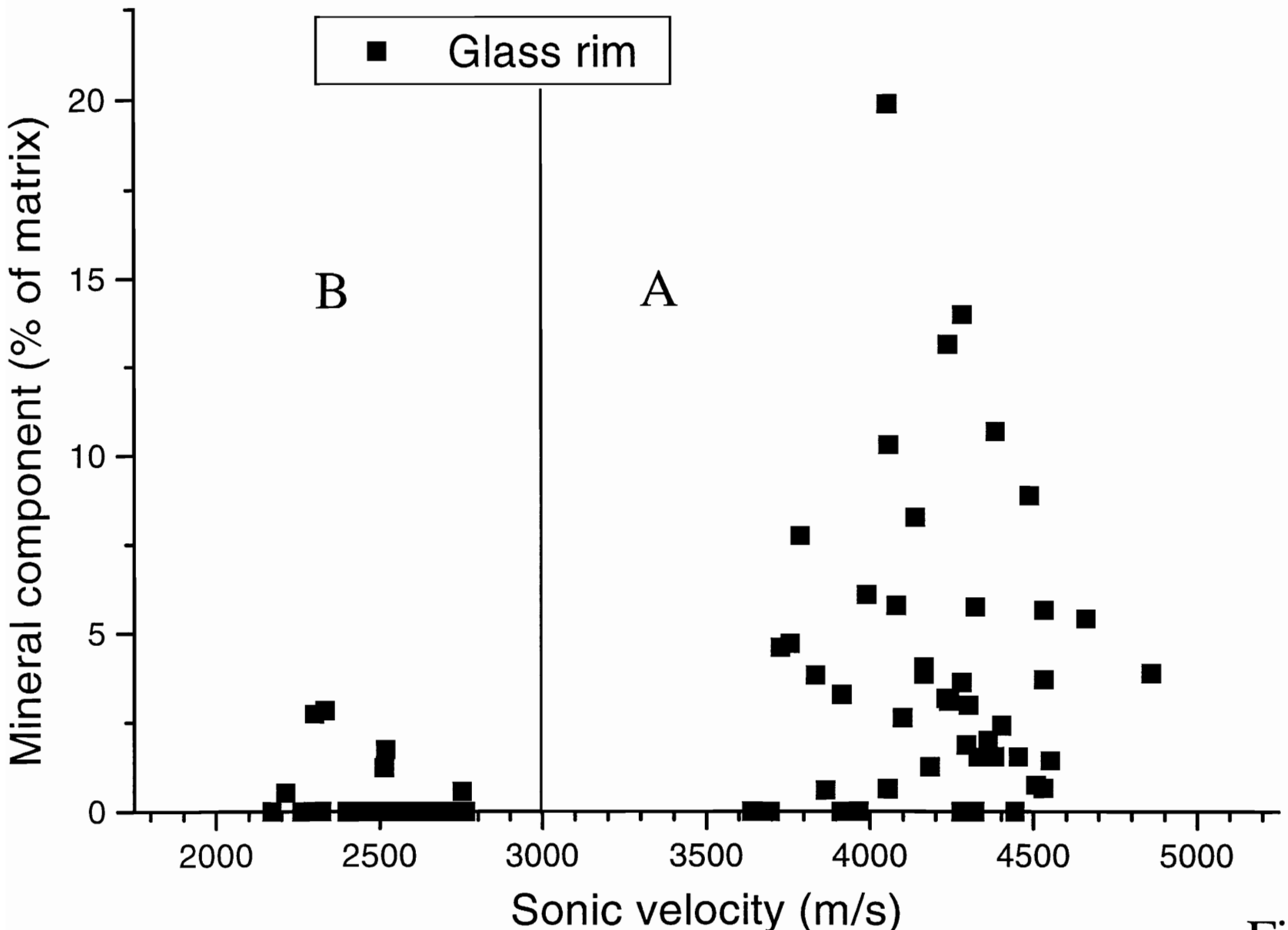
Glass rim
B
A
Mineral component (% of matrix)
0
5
10
15
20
2000
2500
3000
3500
4000
4500
5000
Sonic velocity (m/s)

Fig. 4.12

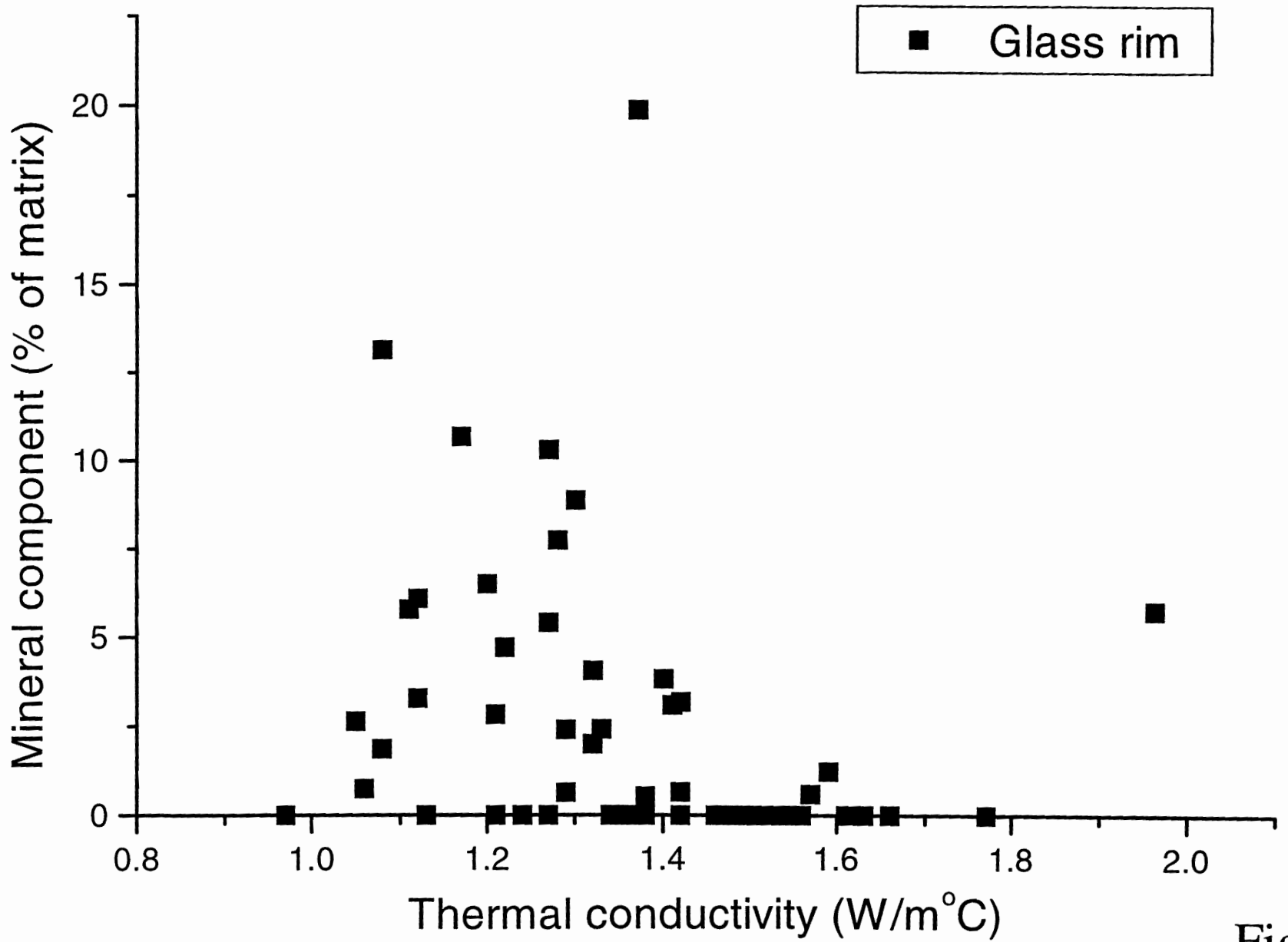
Glass rim
Mineral component (% of matrix)
0
5
10
15
20
0.8
1.0
1.2
1.4
1.6
1.8
2.0
Thermal conductivity (W/m°C)

Fig. 4.13

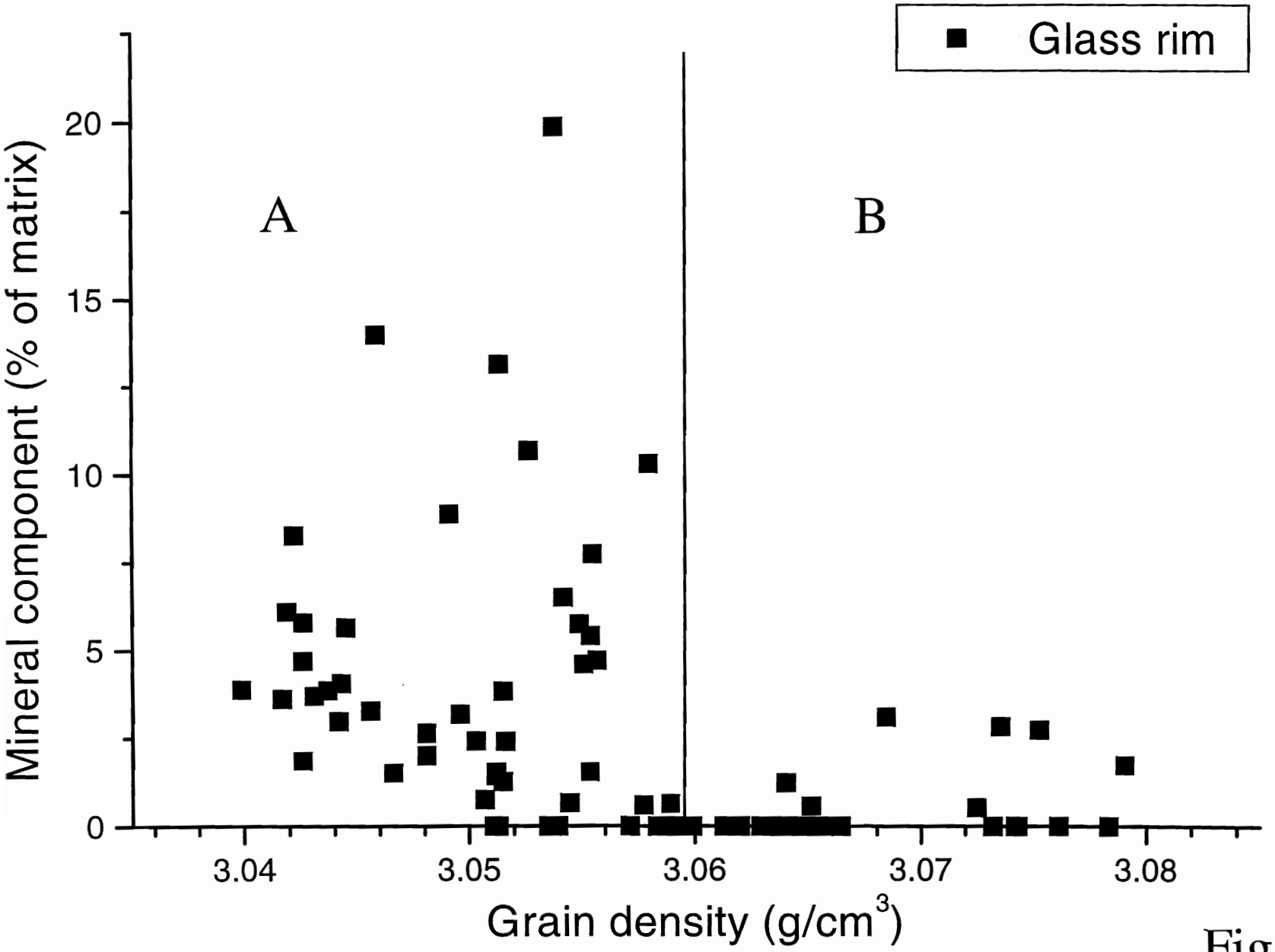
Glass rim
A
B
Mineral component (% of matrix)
0
5
10
15
20
3.04
3.05
3.06
3.07
3.08
Grain density (g/cm3)

Fig. 4.14

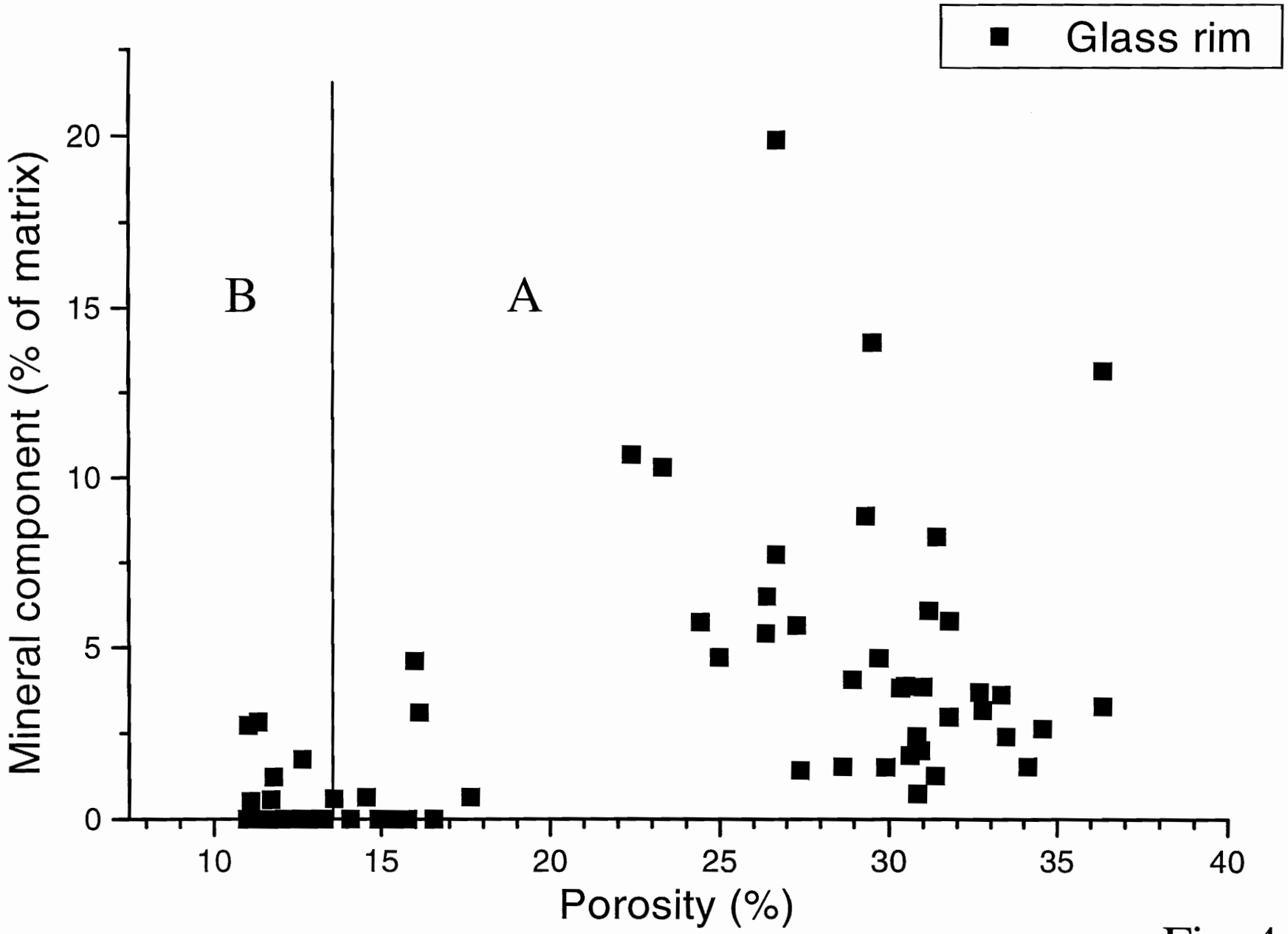
Glass rim
Mineral component (% of matrix)
Porosity (%)
B
A
0
5
10
15
20
10
15
20
25
30
35
40

Fig. 4.15

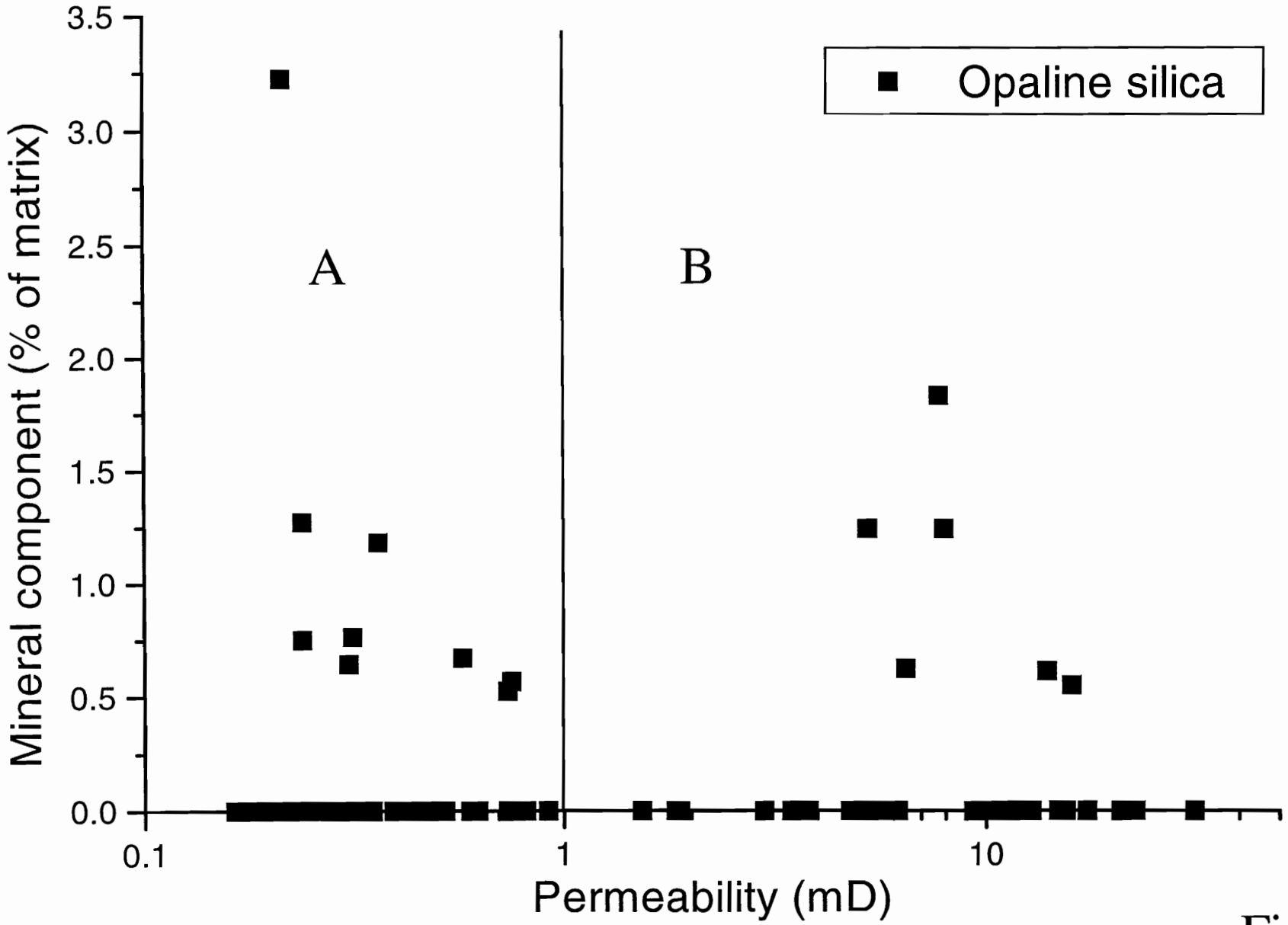
Opaline silica
A
B
Mineral component (% of matrix)
3.5
3.0
2.5
2.0
1.5
1.0
0.5
0.0
0.1
1
10
Permeability (mD)

Fig. 4.16

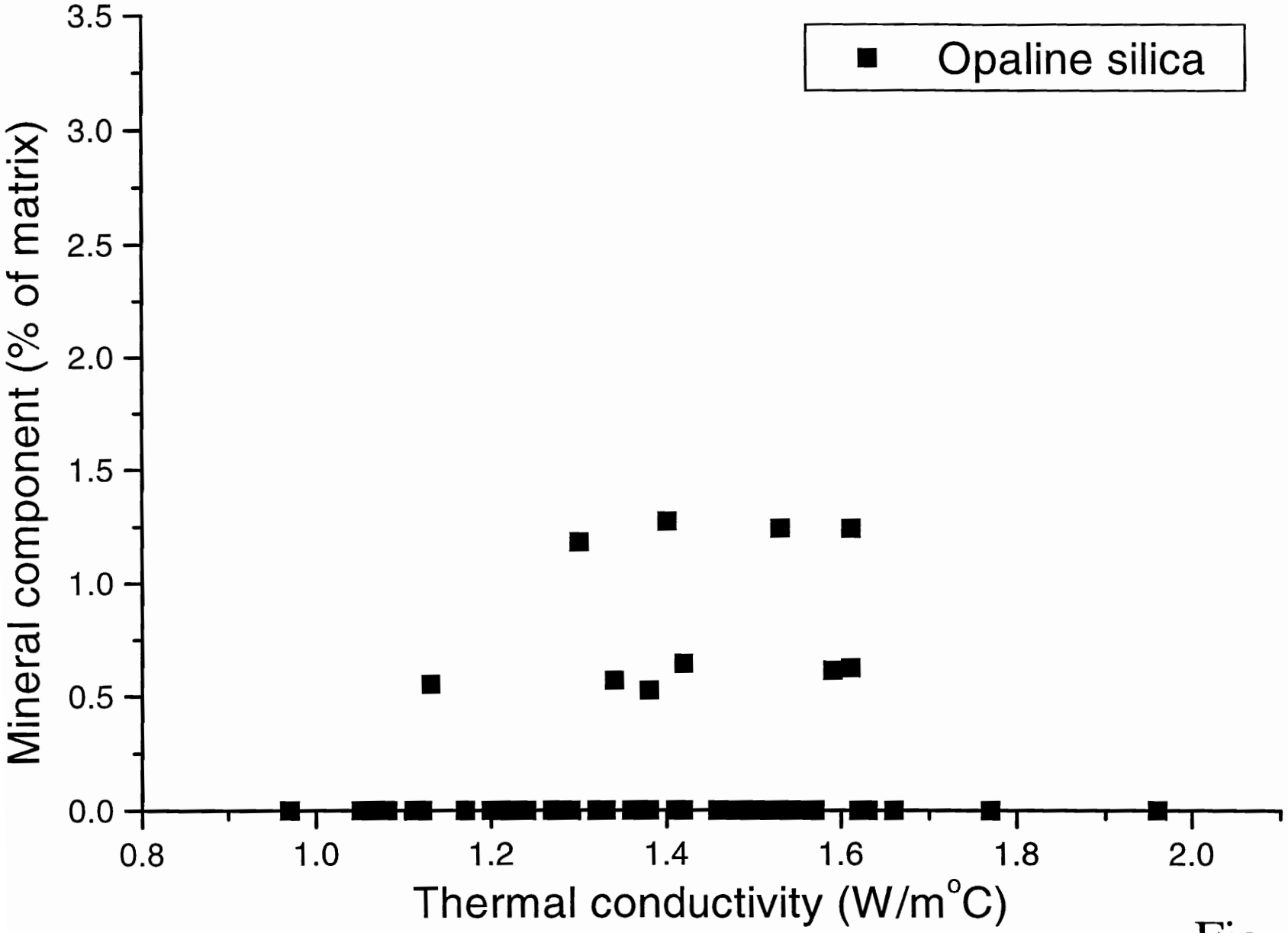
Opaline silica
Mineral component (% of matrix)
3.5
3.0
2.5
2.0
1.5
1.0
0.5
0.0
0.8
1.0
1.2
1.4
1.6
1.8
2.0
Thermal conductivity (W/m°C)

Fig. 4.18

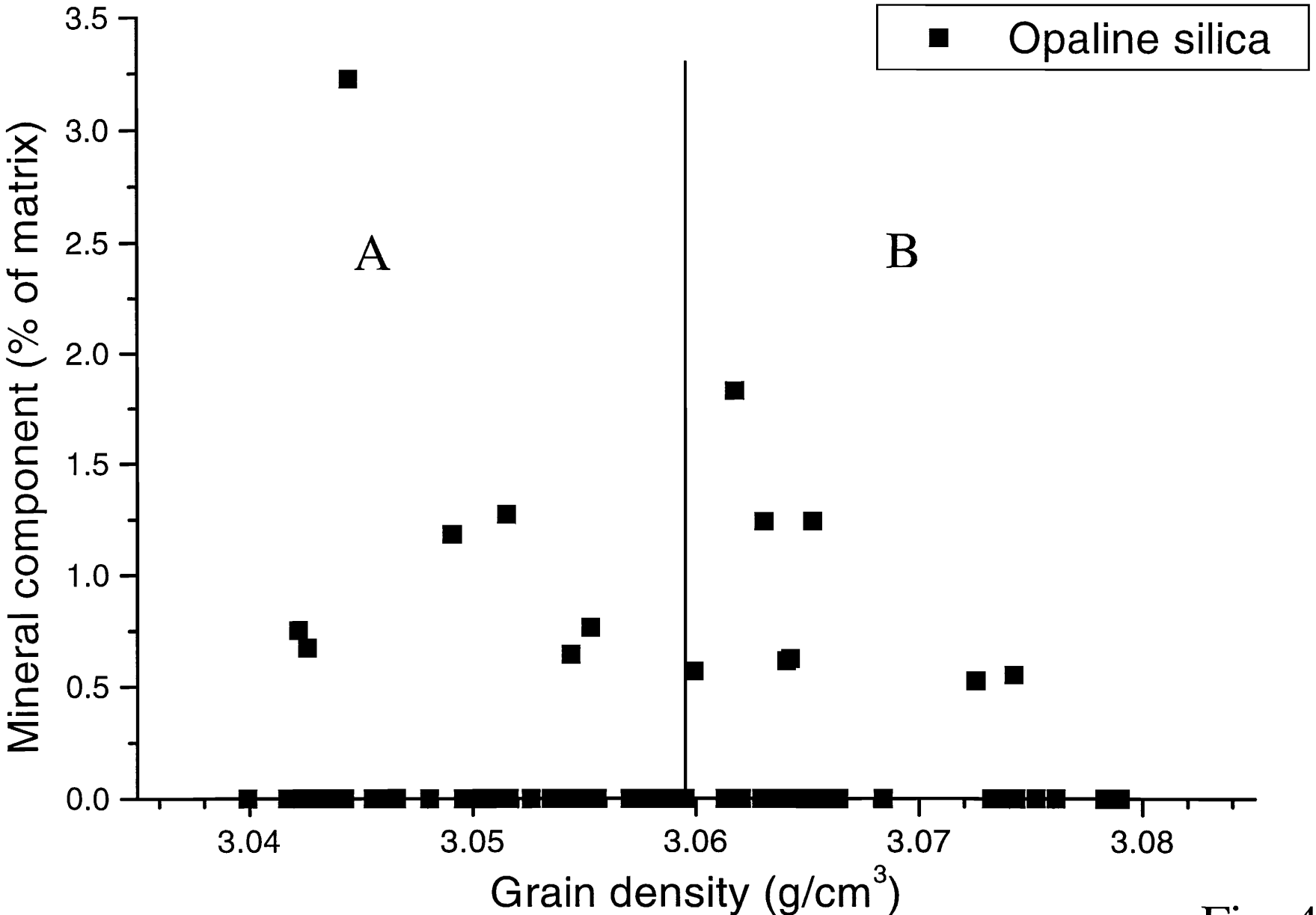
Opaline silica
A
B
Mineral component (% of matrix)
3.5
3.0
2.5
2.0
1.5
1.0
0.5
0.0
3.04
3.05
3.06
3.07
3.08
Grain density (g/cm3)

Fig. 4.19

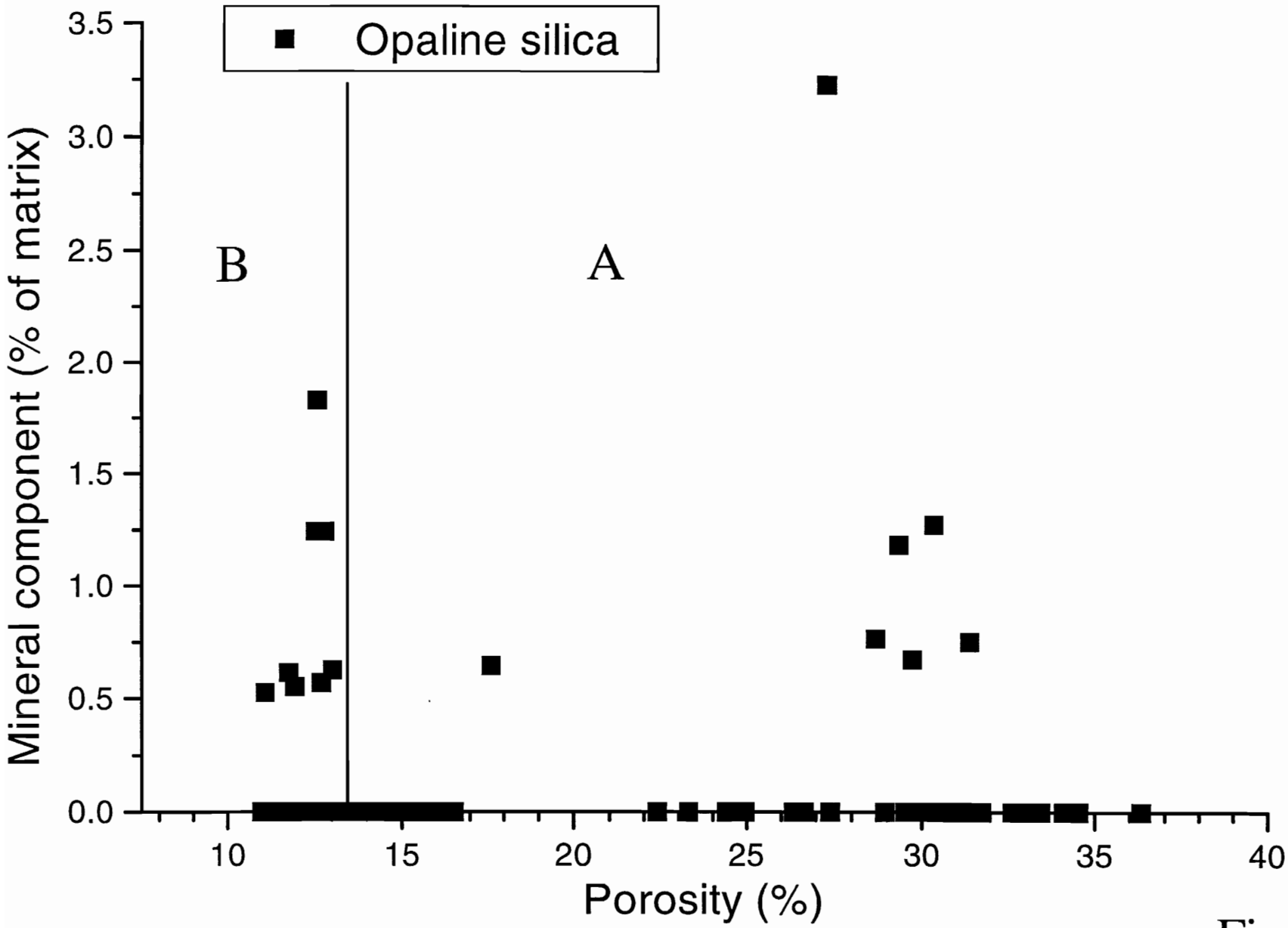
Opaline silica
Mineral component (% of matrix)
Porosity (%)
B
A
0.0
0.5
1.0
1.5
2.0
2.5
3.0
3.5
10
15
20
25
30
35
40

Fig. 4.20

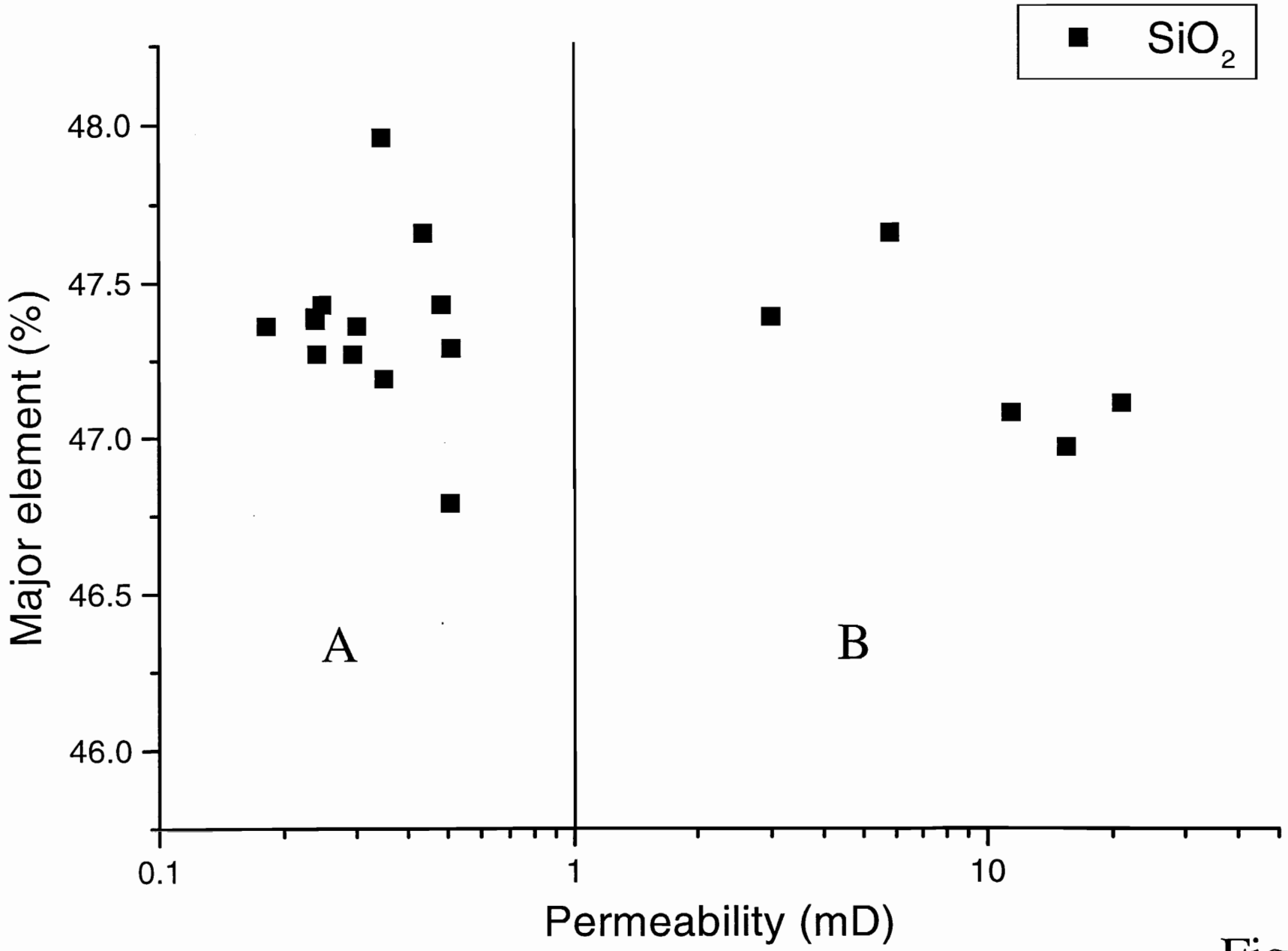
SiO2
48.0
47.5
47.0
46.5
46.0
Major element (%)
A
B
0.1
1
10
Permeability (mD)

Fig. 5.1

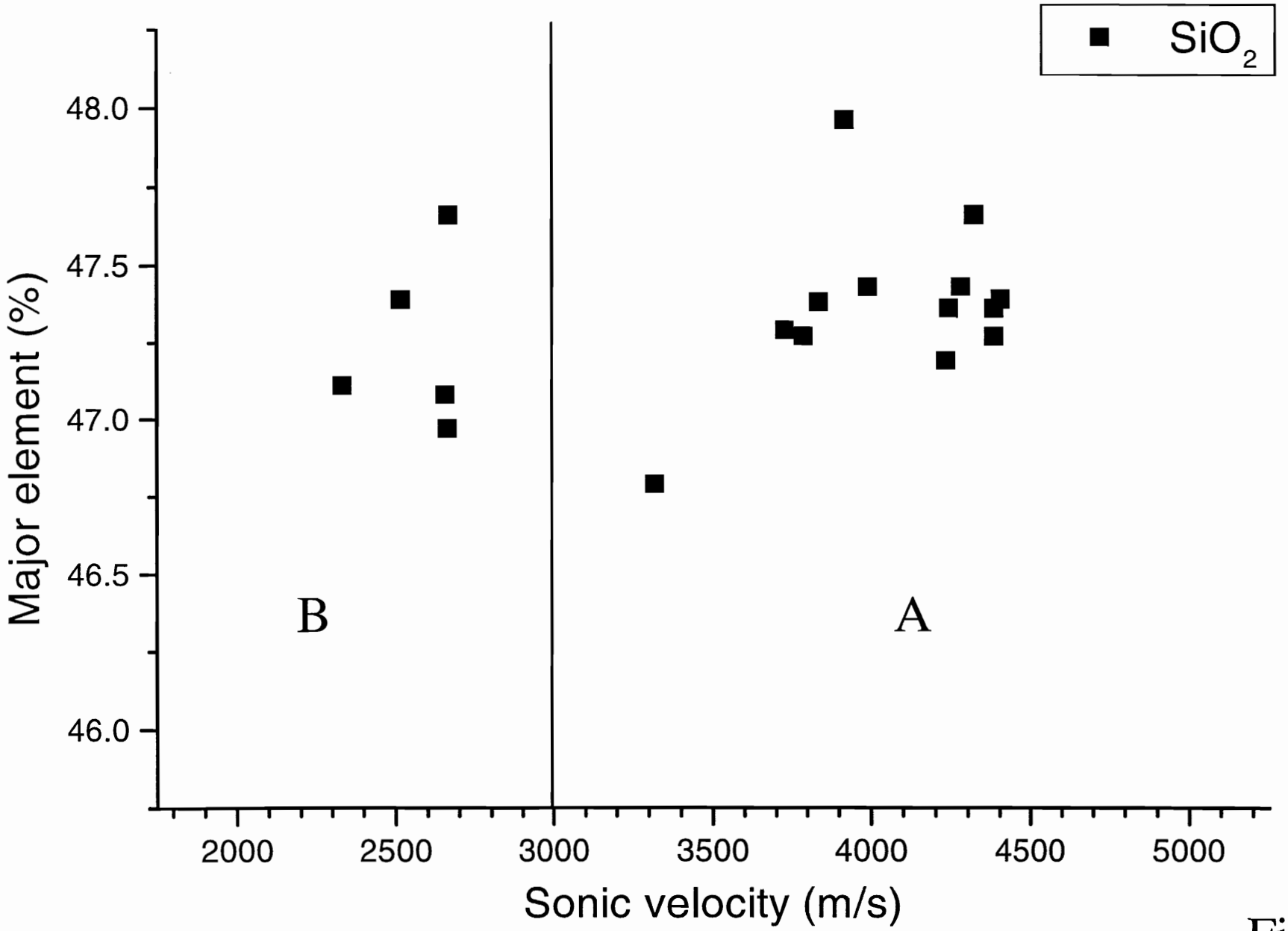
SiO2
48.0
47.5
47.0
46.5
46.0
Major element (%)
B
A
2000
2500
3000
3500
4000
4500
5000
Sonic velocity (m/s)

Fig. 5.2

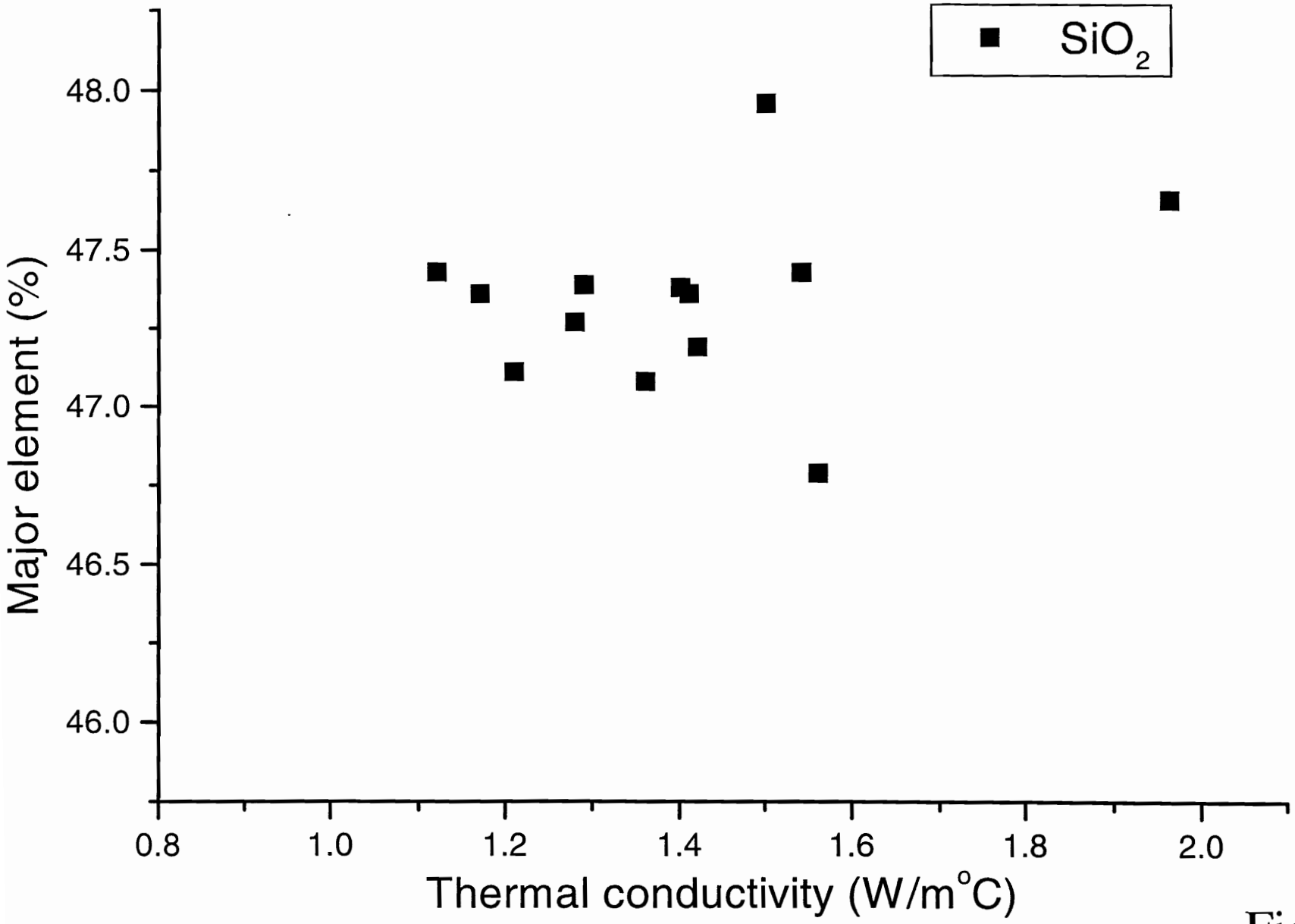
SiO2
48.0
47.5
47.0
46.5
46.0
Major element (%)
0.8
1.0
1.2
1.4
1.6
1.8
2.0
Thermal conductivity (W/m°C)

Fig. 5.3

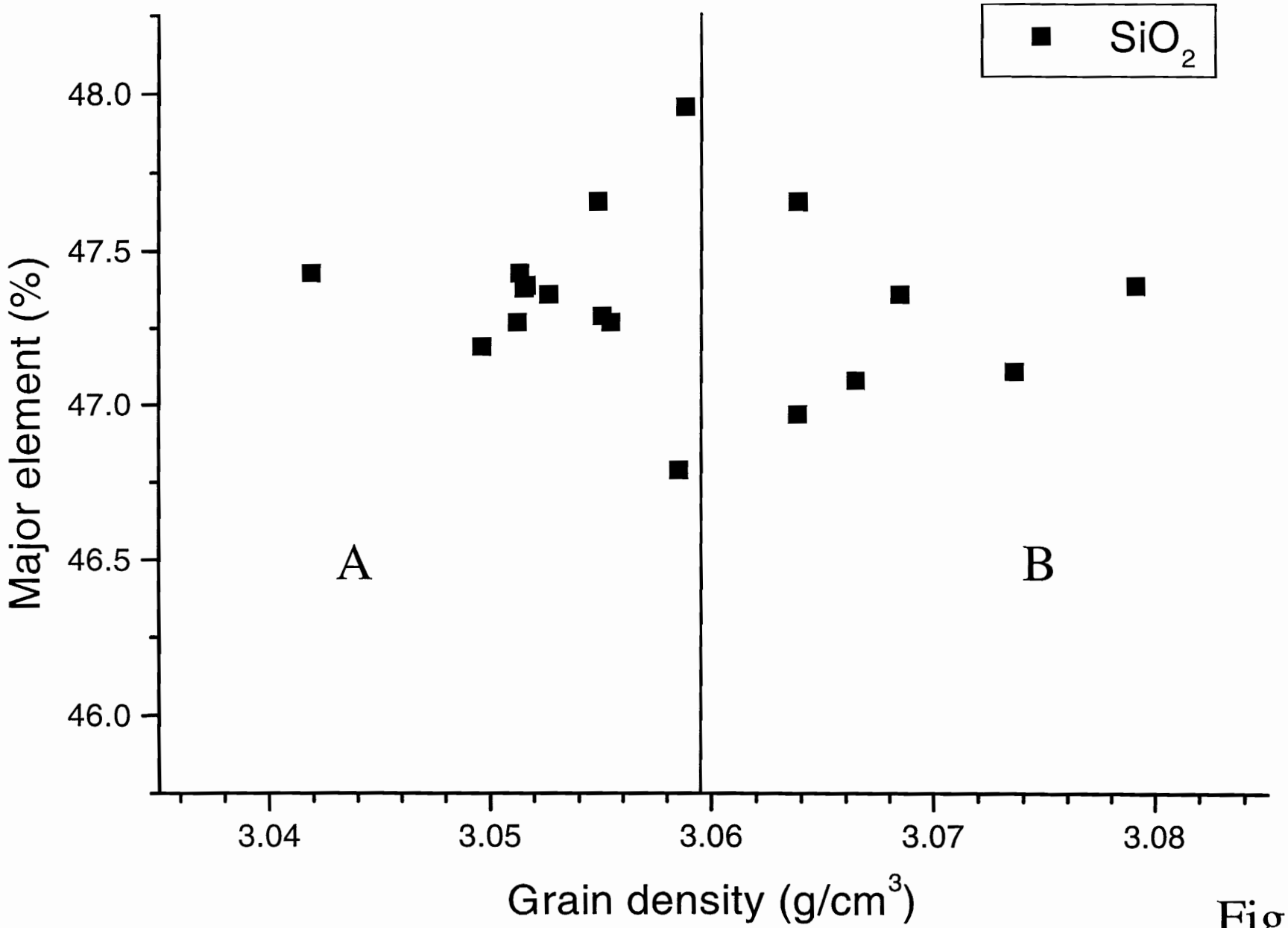
SiO2
48.0
47.5
47.0
46.5
46.0
Major element (%)
A
B
3.04
3.05
3.06
3.07
3.08
Grain density (g/cm3)

Fig. 5.4

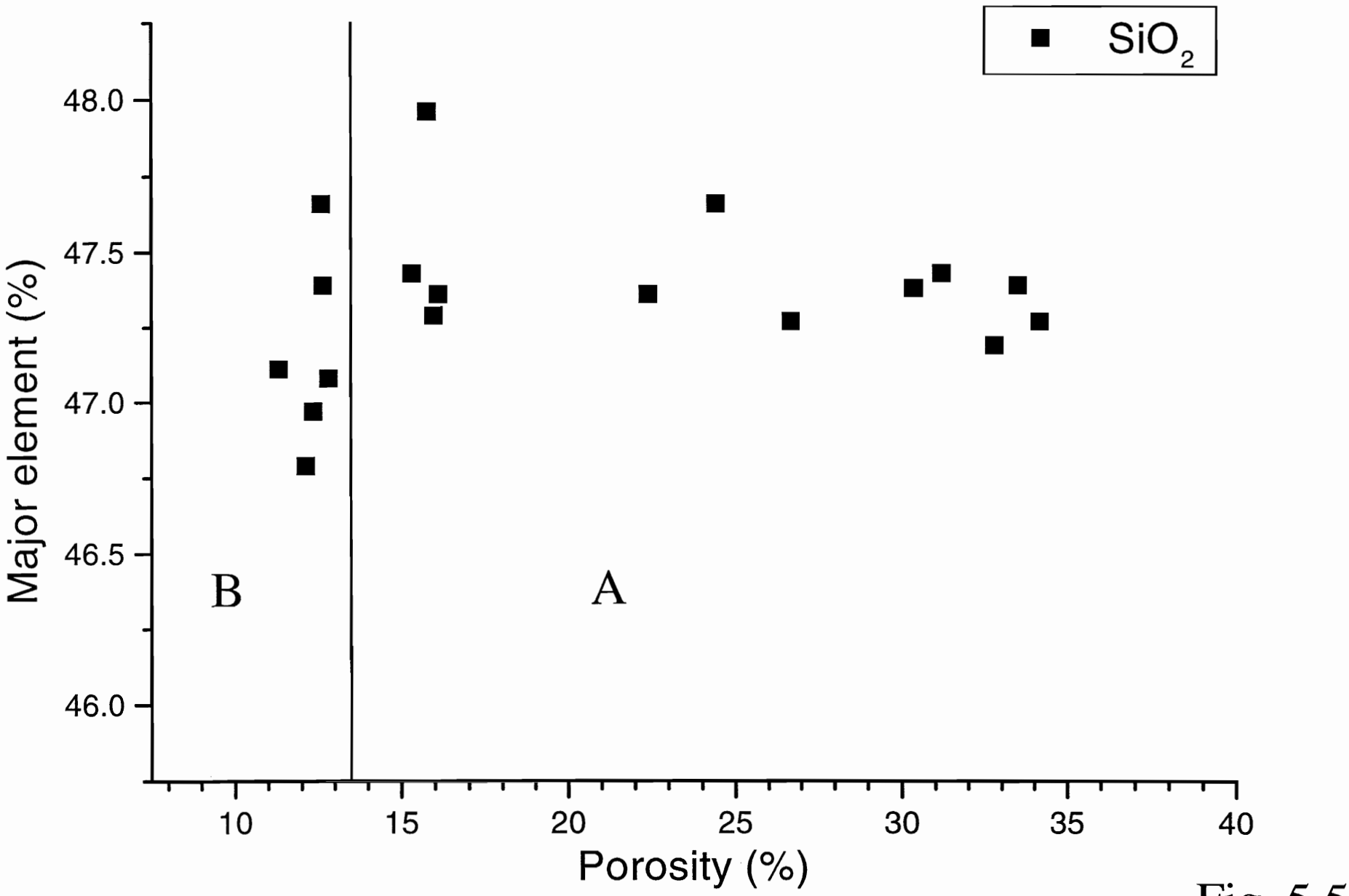
SiO2
48.0
47.5
47.0
46.5
46.0
Major element (%)
B
A
10
15
20
25
30
35
40
Porosity (%)

Fig. 5.5

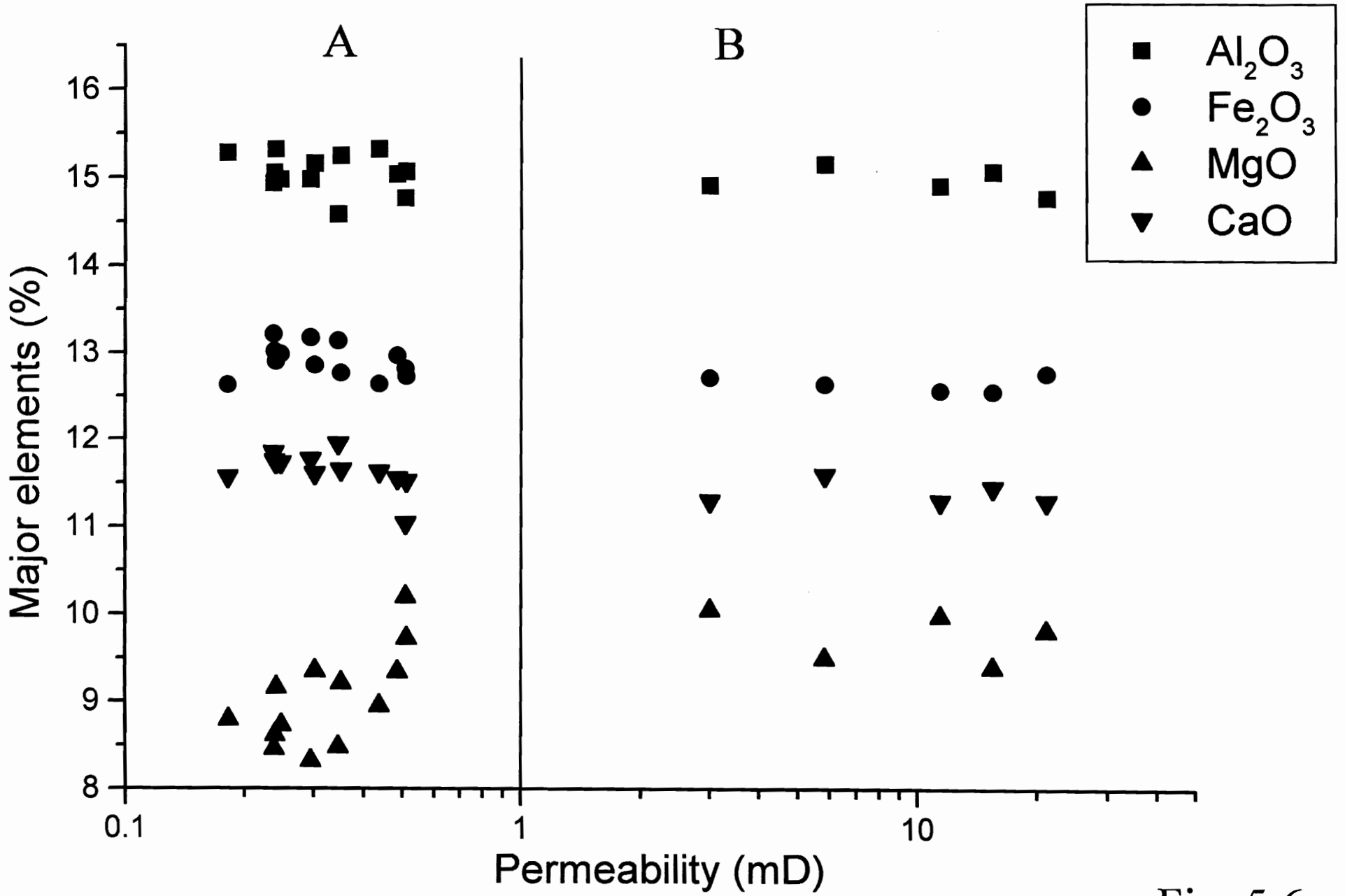
A
B
Al_2O_3
Fe_2O_3
MgO
CaO
Major elements (%)
16
15
14
13
12
11
10
9
8
0.1
1
10
Permeability (mD)

Fig. 5.6

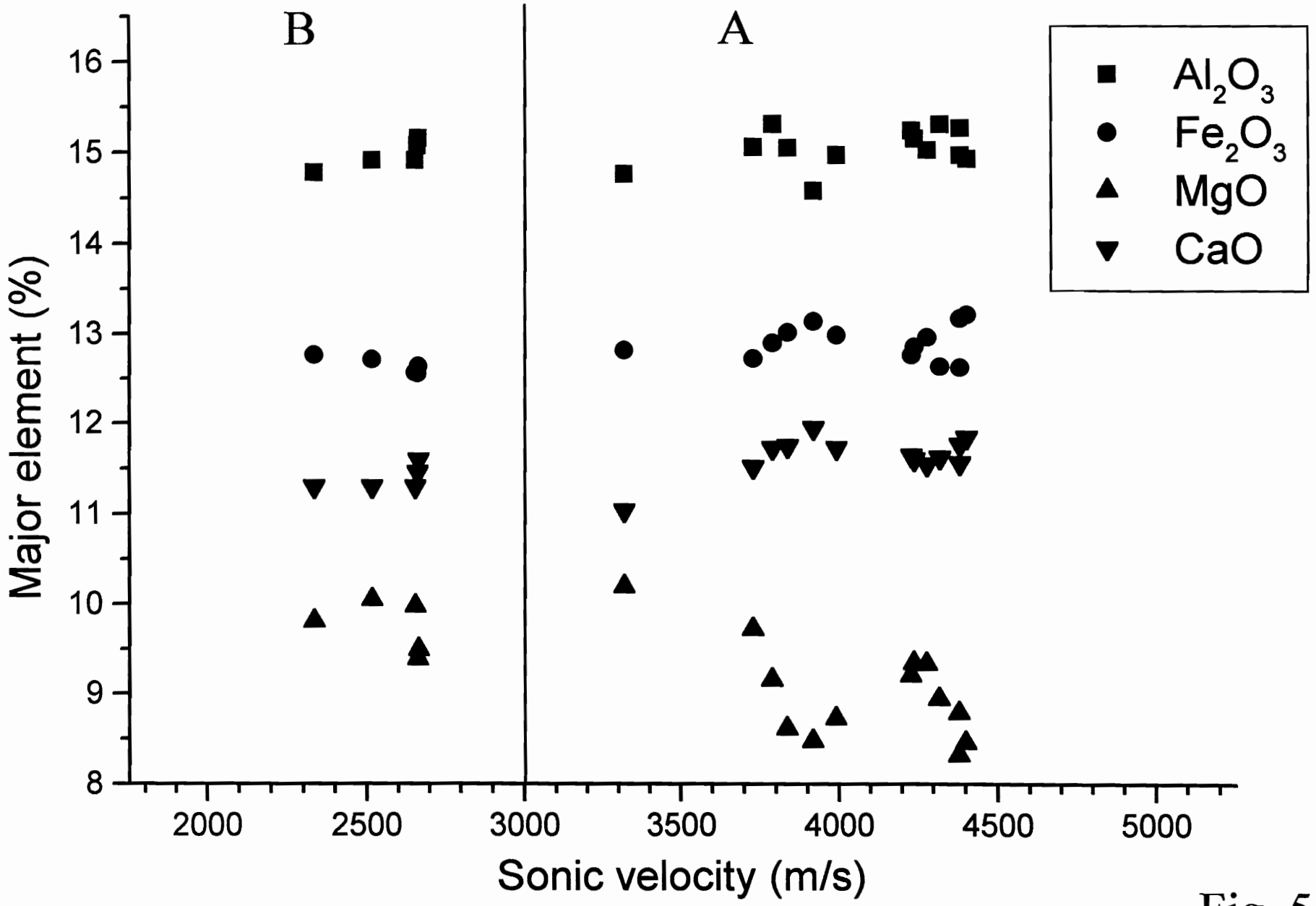
B
A
Al2O3
Fe2O3
MgO
CaO
Major element (%)
16
15
14
13
12
11
10
9
8
2000
2500
3000
3500
4000
4500
5000
Sonic velocity (m/s)

Fig. 5.7

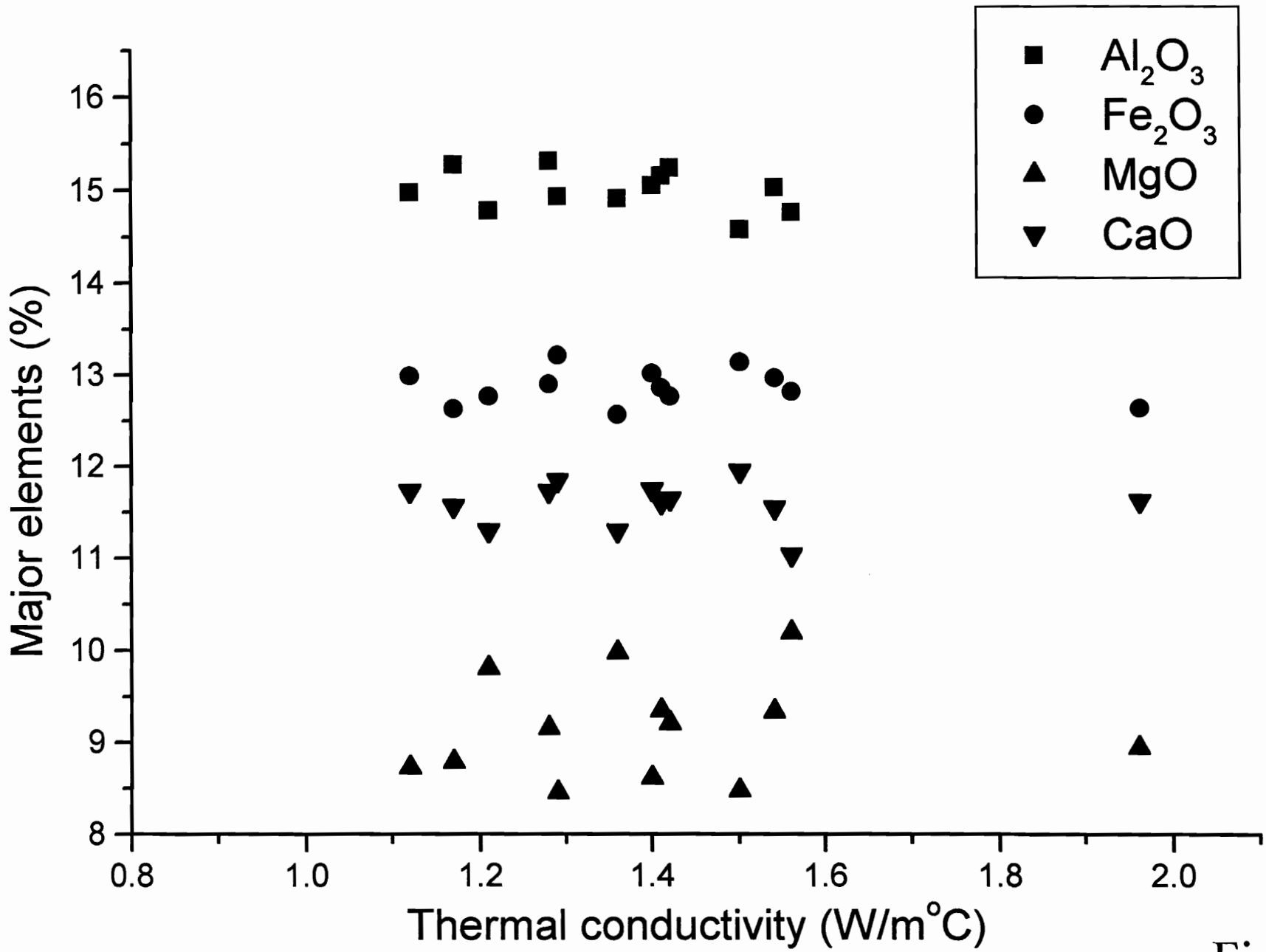
Major elements (%)
16
15
14
13
12
11
10
9
8
0.8
1.0
1.2
1.4
1.6
1.8
2.0
Thermal conductivity (W/m°C)
Al2O3
Fe2O3
MgO
CaO

Fig. 5.8

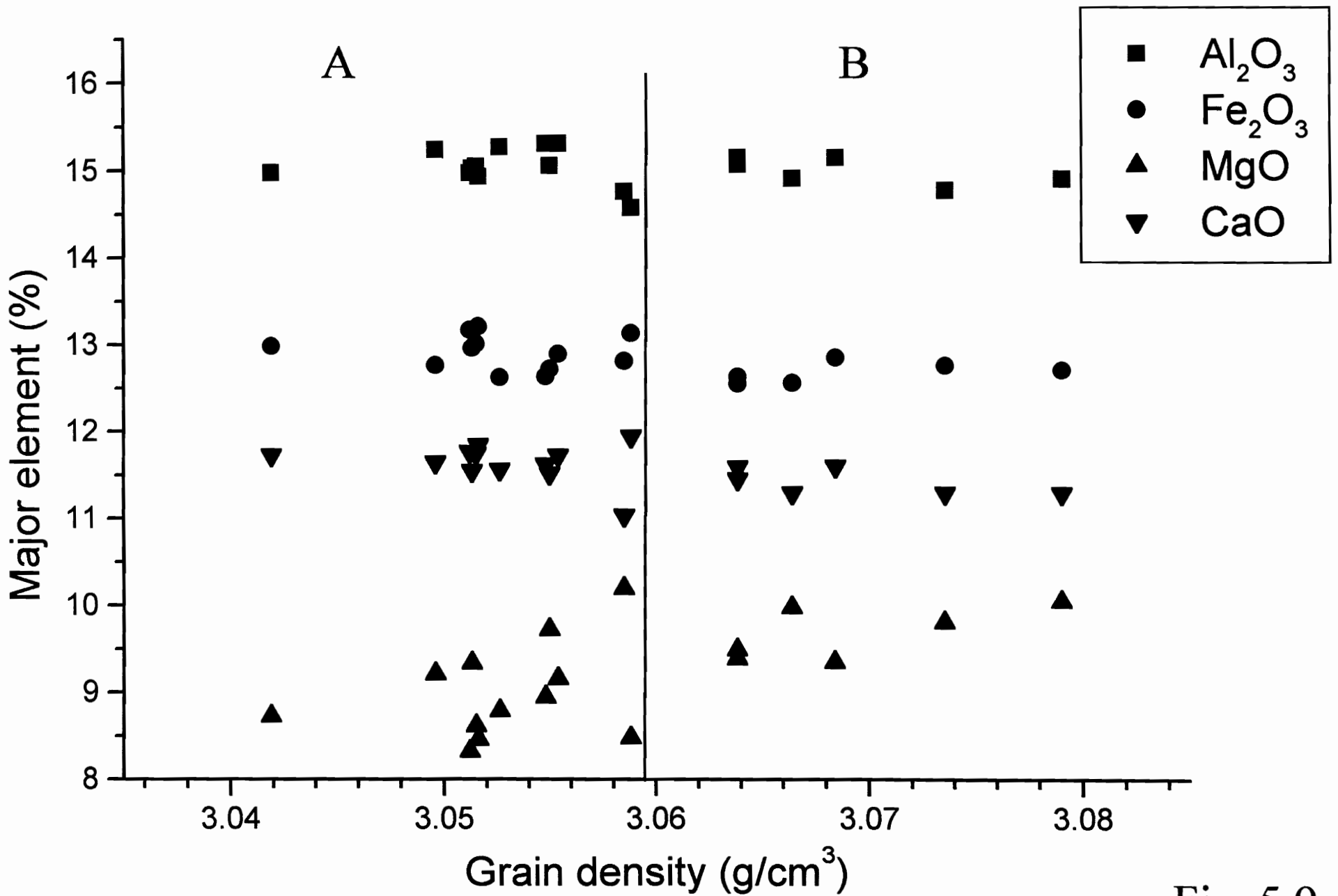
A
B
Al_2O_3
Fe_2O_3
MgO
CaO
Major element (%)
16
15
14
13
12
11
10
9
8
3.04
3.05
3.06
3.07
3.08
Grain density (g/cm^3)

Fig. 5.9

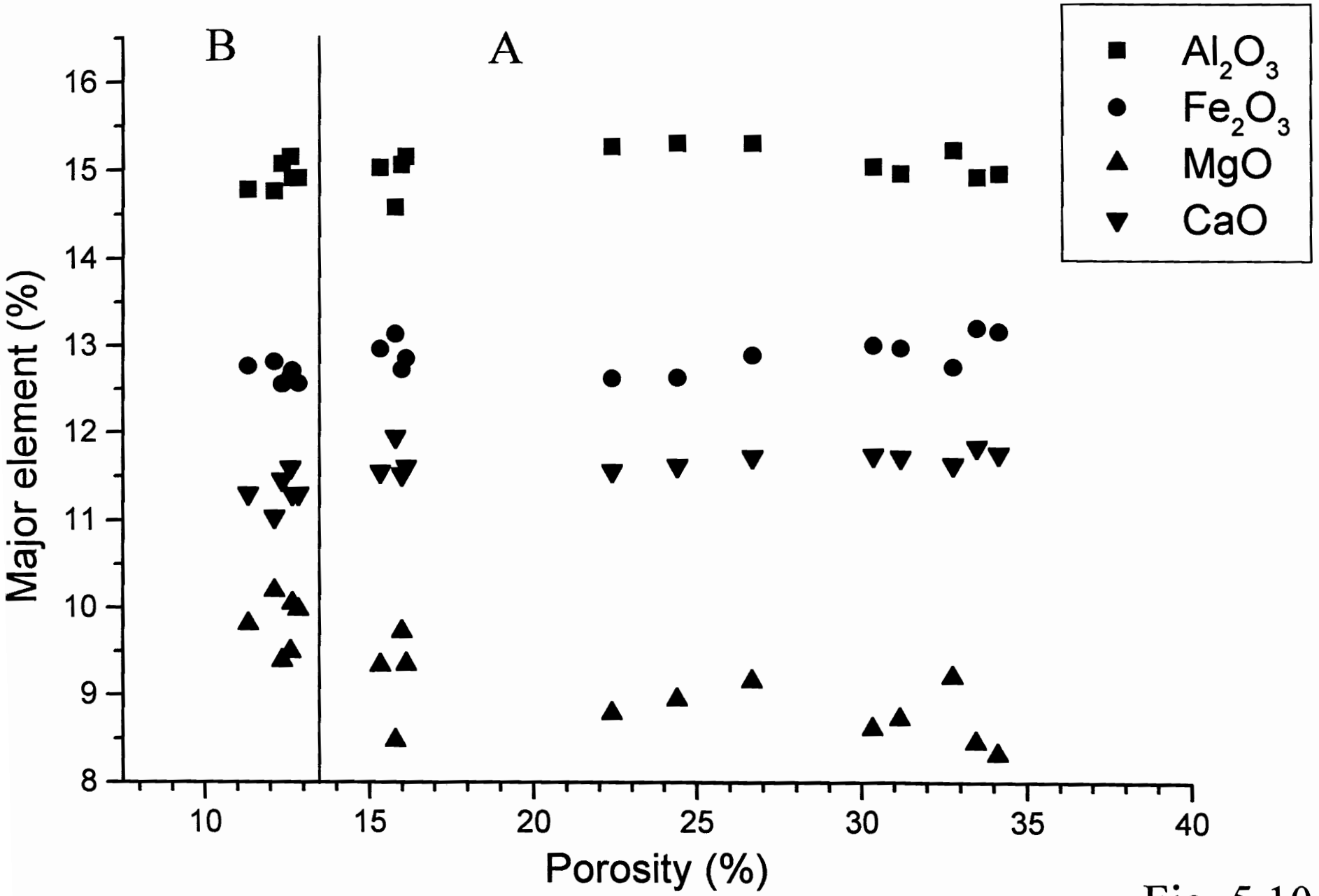
B
A
Al_2O_3
Fe_2O_3
MgO
CaO
Major element (%)
Porosity (%)
16
15
14
13
12
11
10
9
8
10
15
20
25
30
35
40

Fig. 5.10

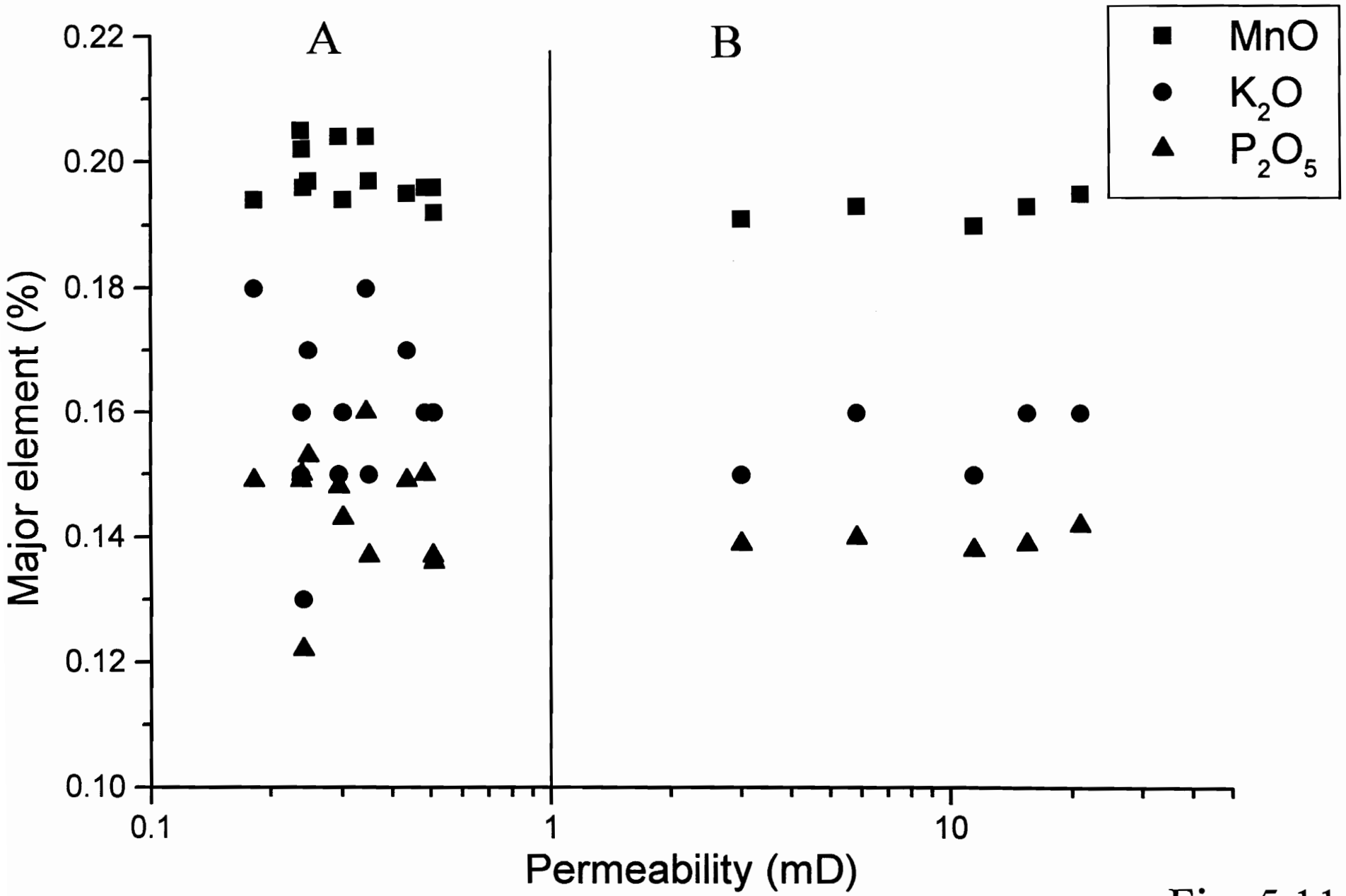
A
B
MnO
K_2O
P_2O_5
Major element (%)
0.22
0.20
0.18
0.16
0.14
0.12
0.10
0.1
1
10
Permeability (mD)

Fig. 5.11

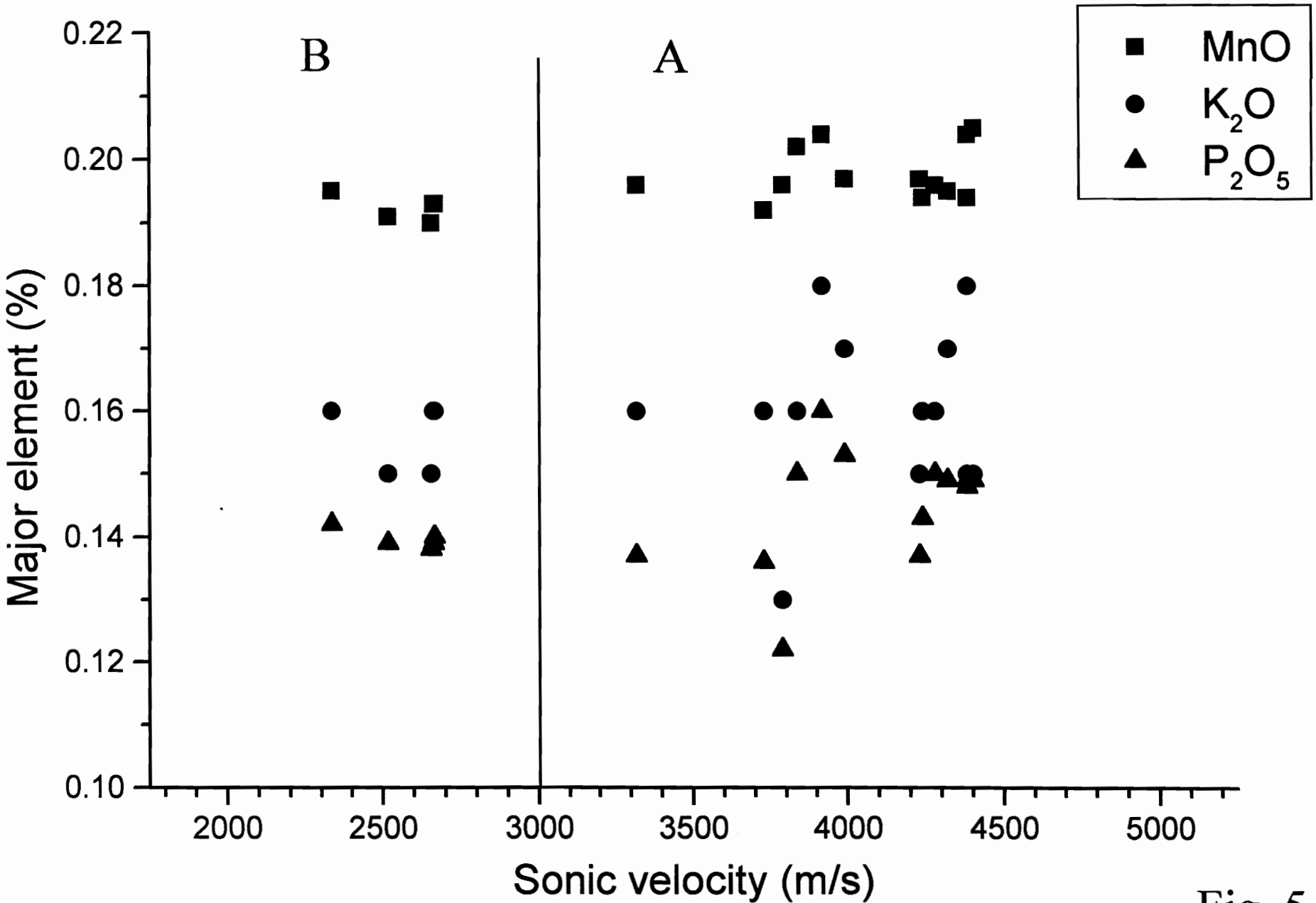
B
A
MnO
K_2O
P_2O_5
Major element (%)
0.22
0.20
0.18
0.16
0.14
0.12
0.10
2000
2500
3000
3500
4000
4500
5000
Sonic velocity (m/s)

Fig. 5.12

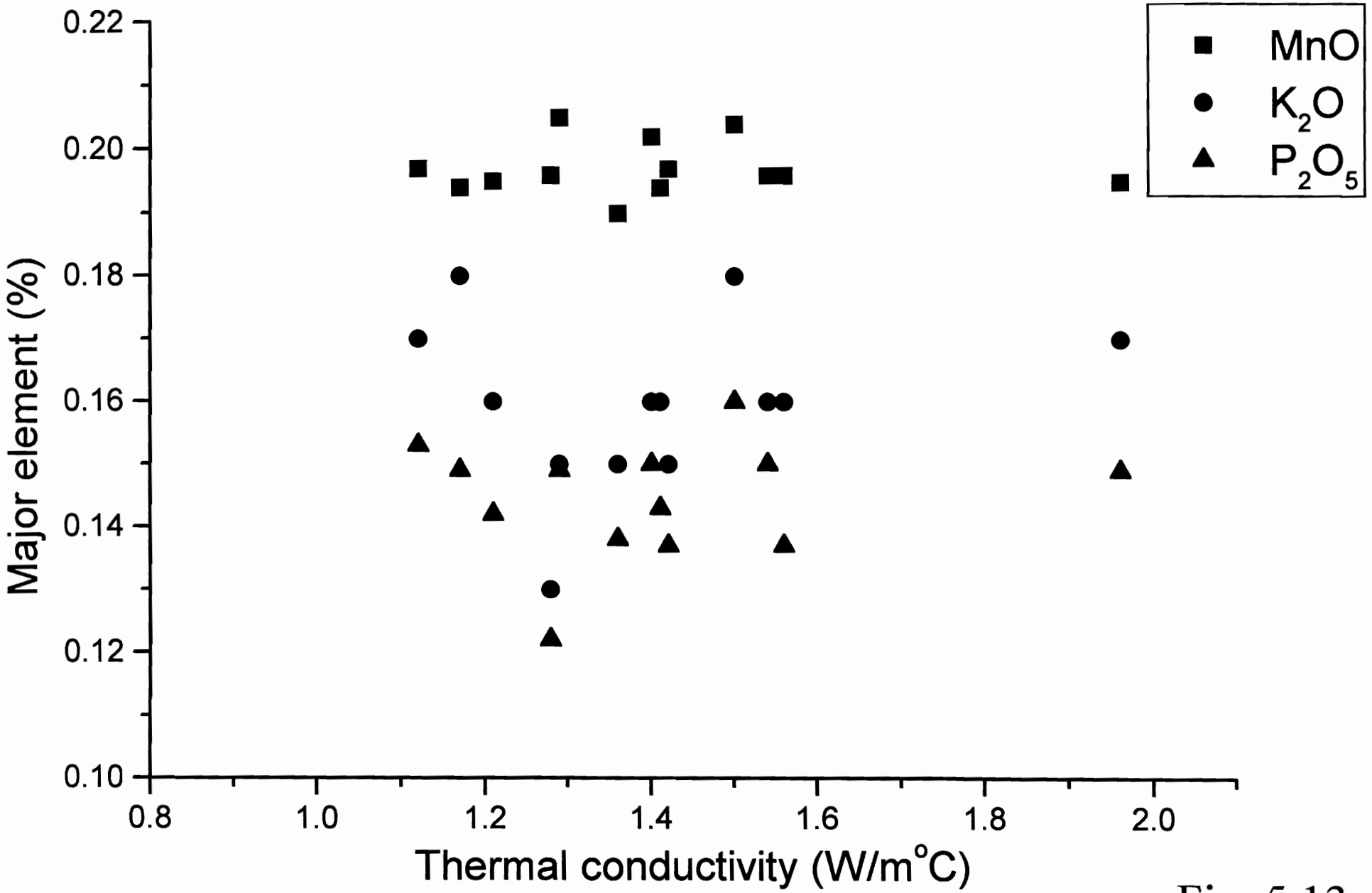
MnO
K2O
P2O5
Major element (%)
0.22
0.20
0.18
0.16
0.14
0.12
0.10
0.8
1.0
1.2
1.4
1.6
1.8
2.0
Thermal conductivity (W/m°C)

Fig. 5.13

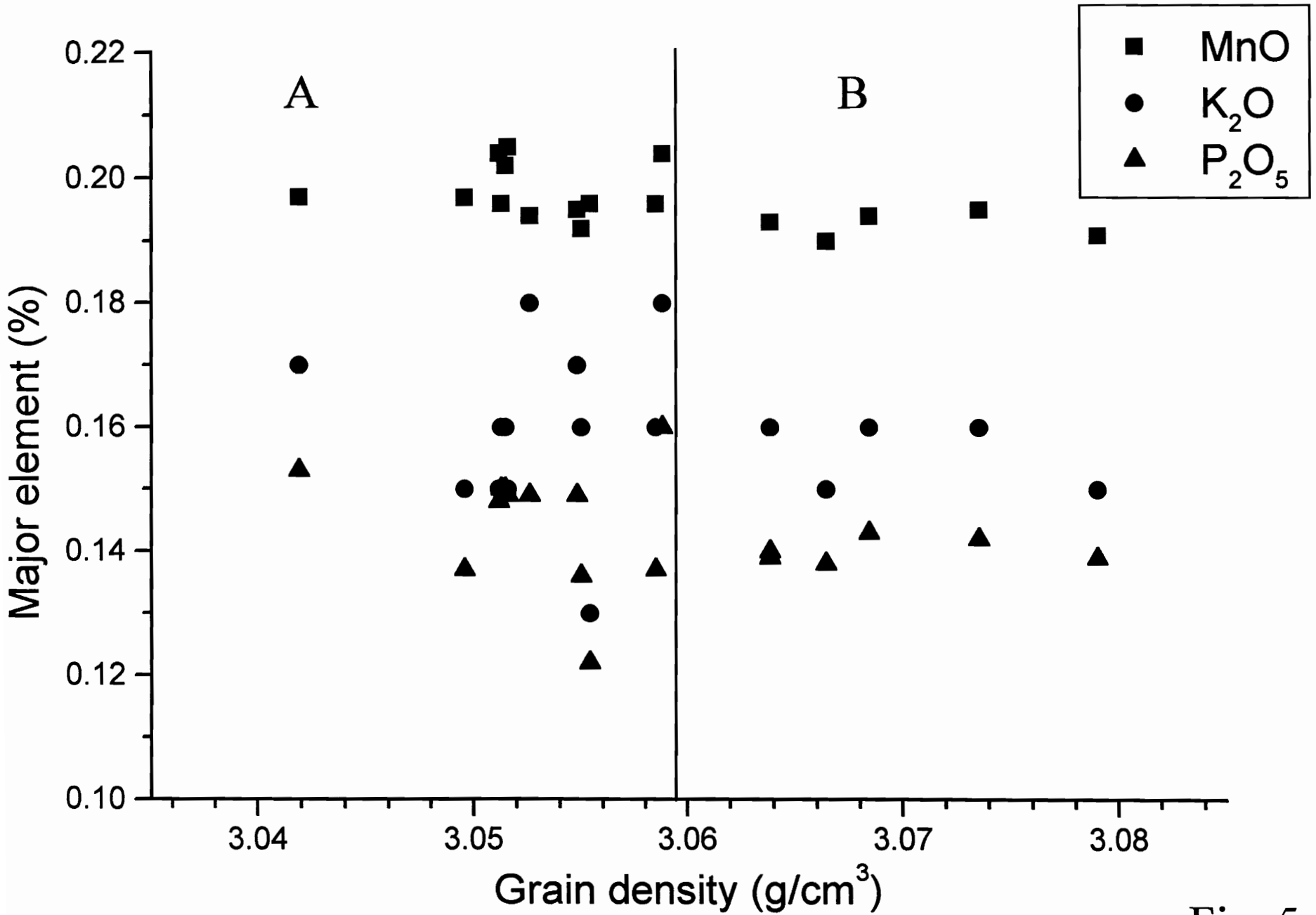
A
B
MnO
K_2O
P_2O_5
Major element (%)
0.22
0.20
0.18
0.16
0.14
0.12
0.10
3.04
3.05
3.06
3.07
3.08
Grain density (g/cm^3)

Fig. 5.14

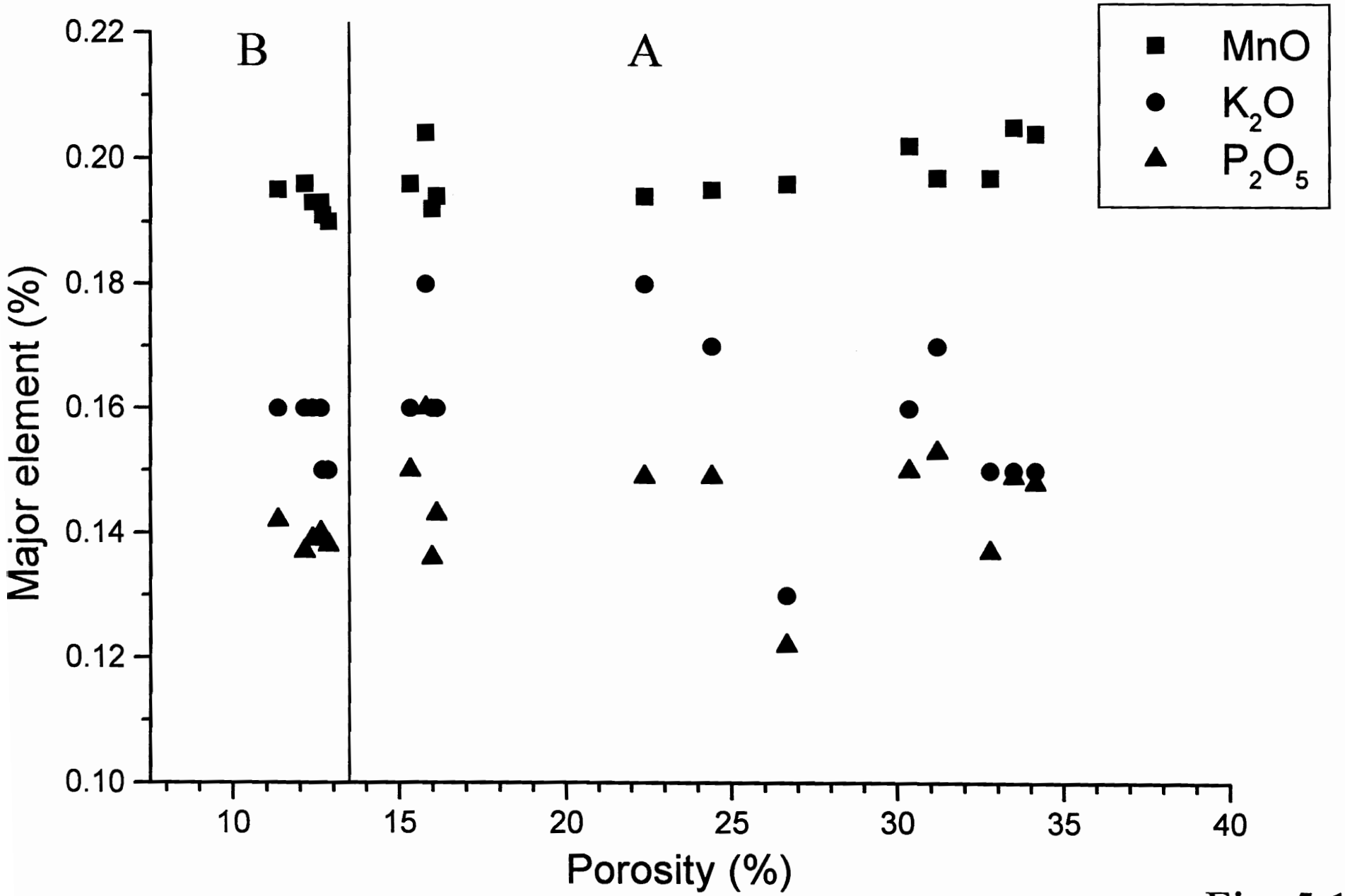
B
A
MnO
K_2O
P_2O_5
Major element (%)
0.22
0.20
0.18
0.16
0.14
0.12
0.10
10
15
20
25
30
35
40
Porosity (%)

Fig. 5.15

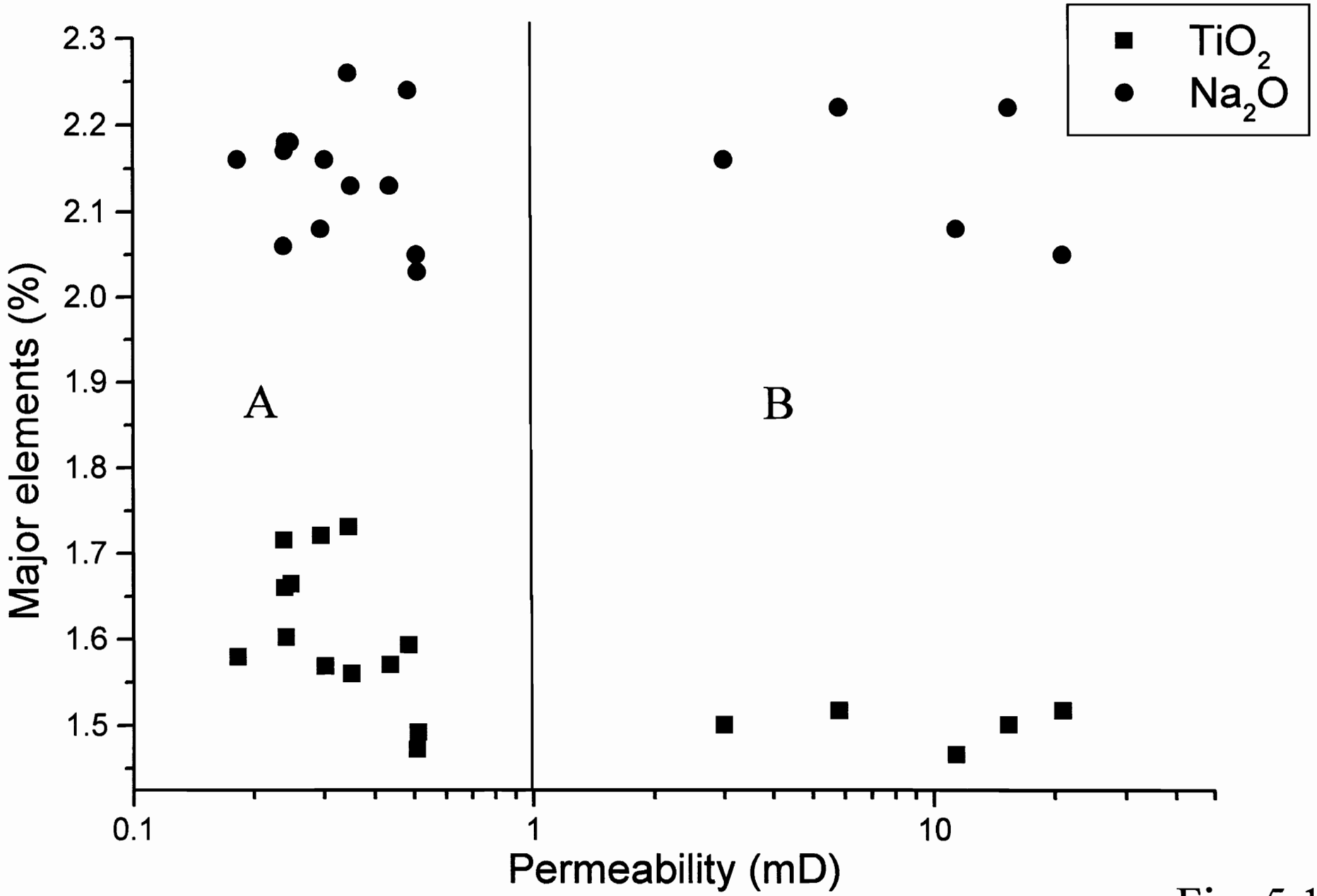
TiO2
Na2O
Major elements (%)
2.3
2.2
2.1
2.0
1.9
1.8
1.7
1.6
1.5
A
B
0.1
1
10
Permeability (mD)

Fig. 5.16

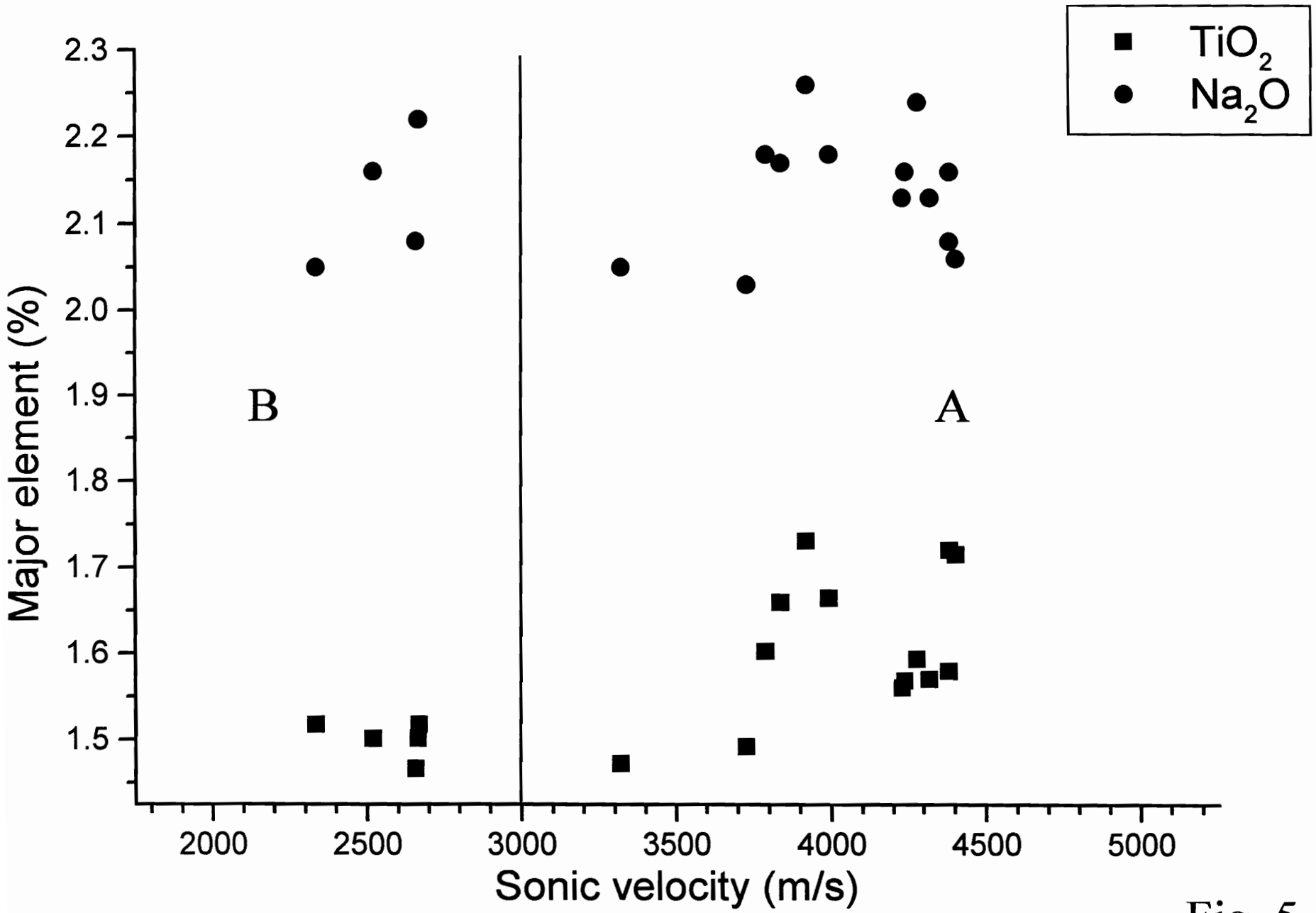
TiO2
Na2O
Major element (%)
2.3
2.2
2.1
2.0
1.9
1.8
1.7
1.6
1.5
B
A
2000
2500
3000
3500
4000
4500
5000
Sonic velocity (m/s)

Fig. 5.17

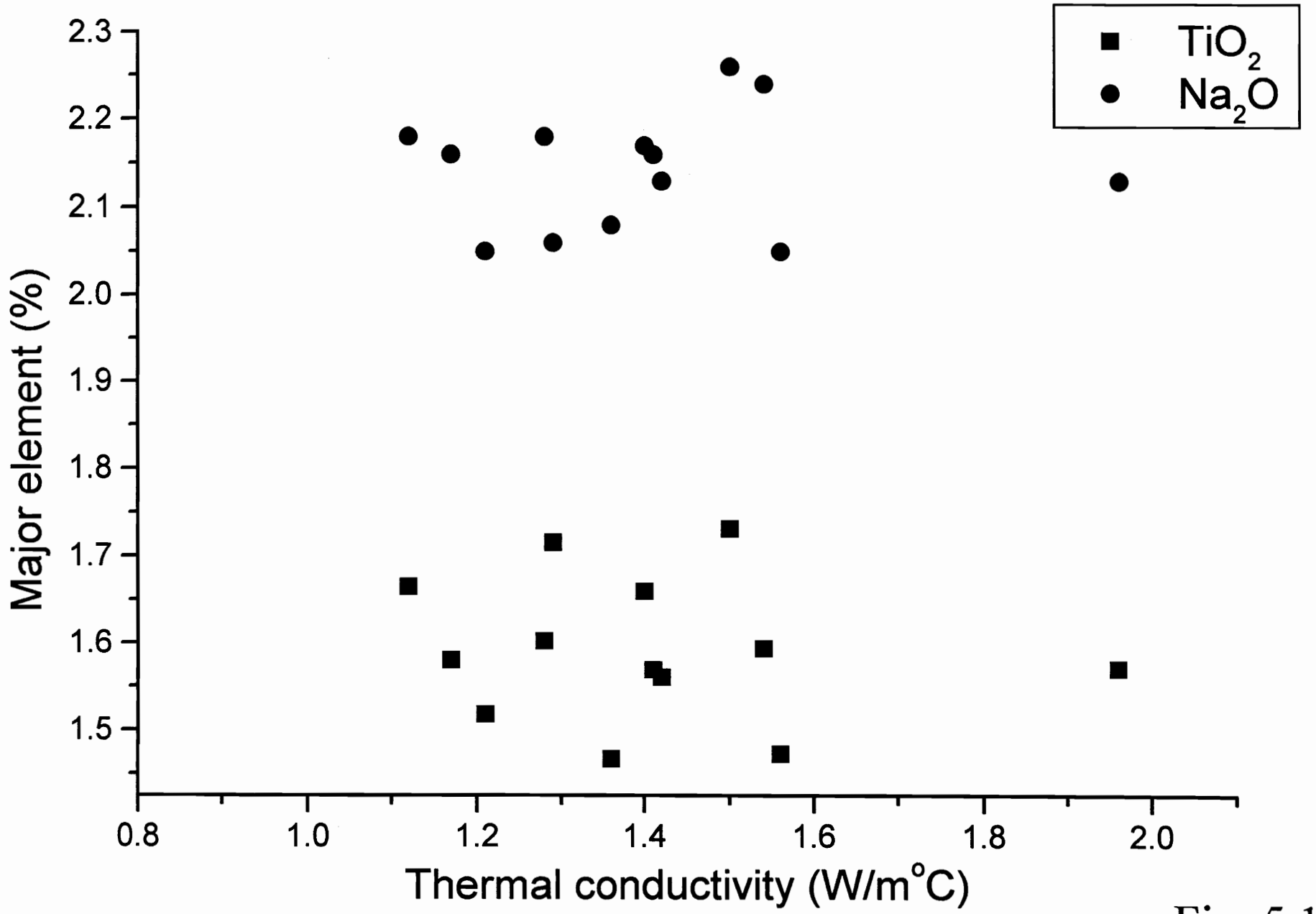
TiO2
Na2O
Major element (%)
2.3
2.2
2.1
2.0
1.9
1.8
1.7
1.6
1.5
0.8
1.0
1.2
1.4
1.6
1.8
2.0
Thermal conductivity (W/m°C)

Fig. 5.18

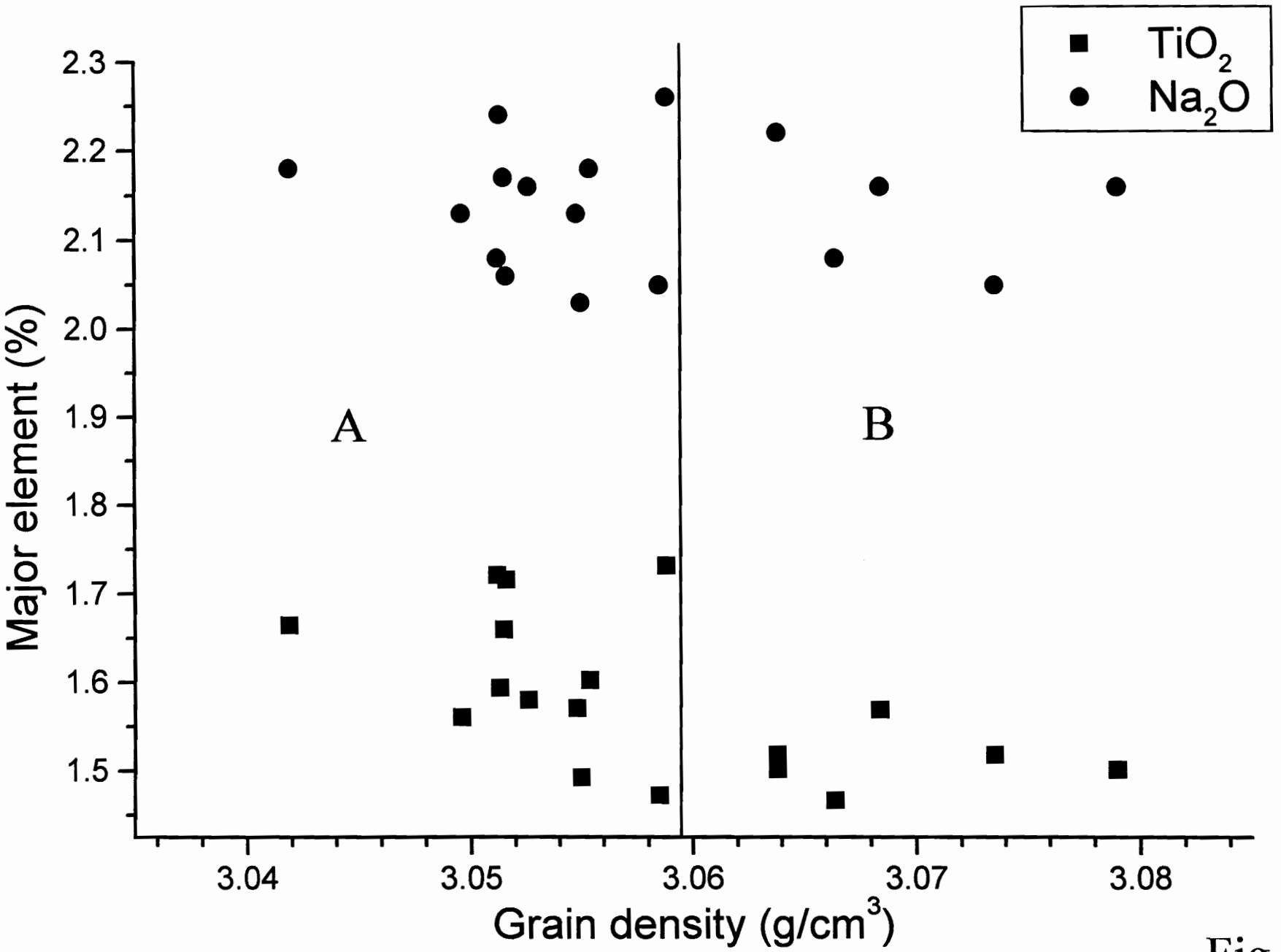
TiO2
Na2O
Major element (%)
2.3
2.2
2.1
2.0
1.9
1.8
1.7
1.6
1.5
A
B
3.04
3.05
3.06
3.07
3.08
Grain density (g/cm3)

Fig. 5.19

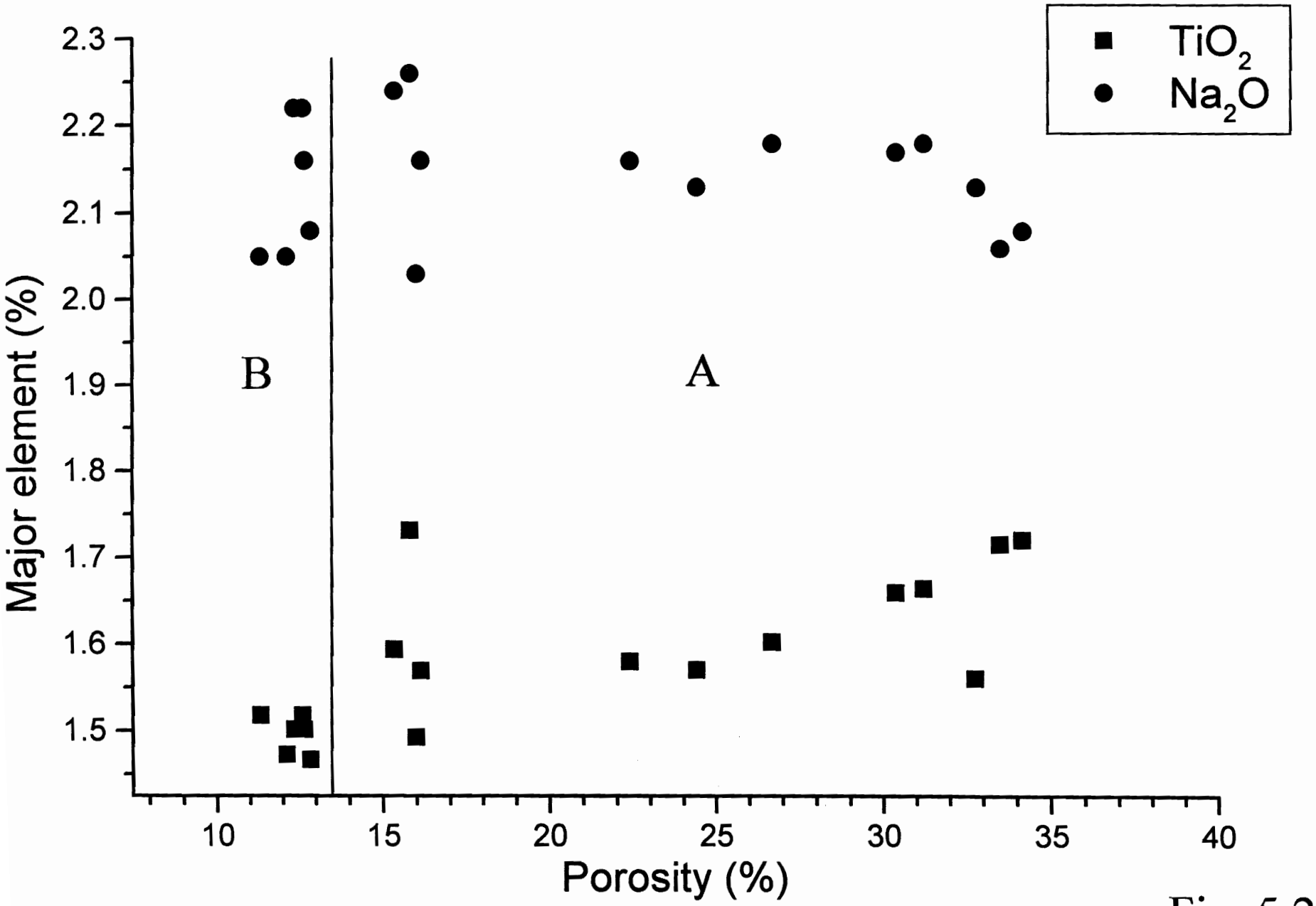
TiO2
Na2O
Major element (%)
Porosity (%)
B
A
2.3
2.2
2.1
2.0
1.9
1.8
1.7
1.6
1.5
10
15
20
25
30
35
40

Fig. 5.20

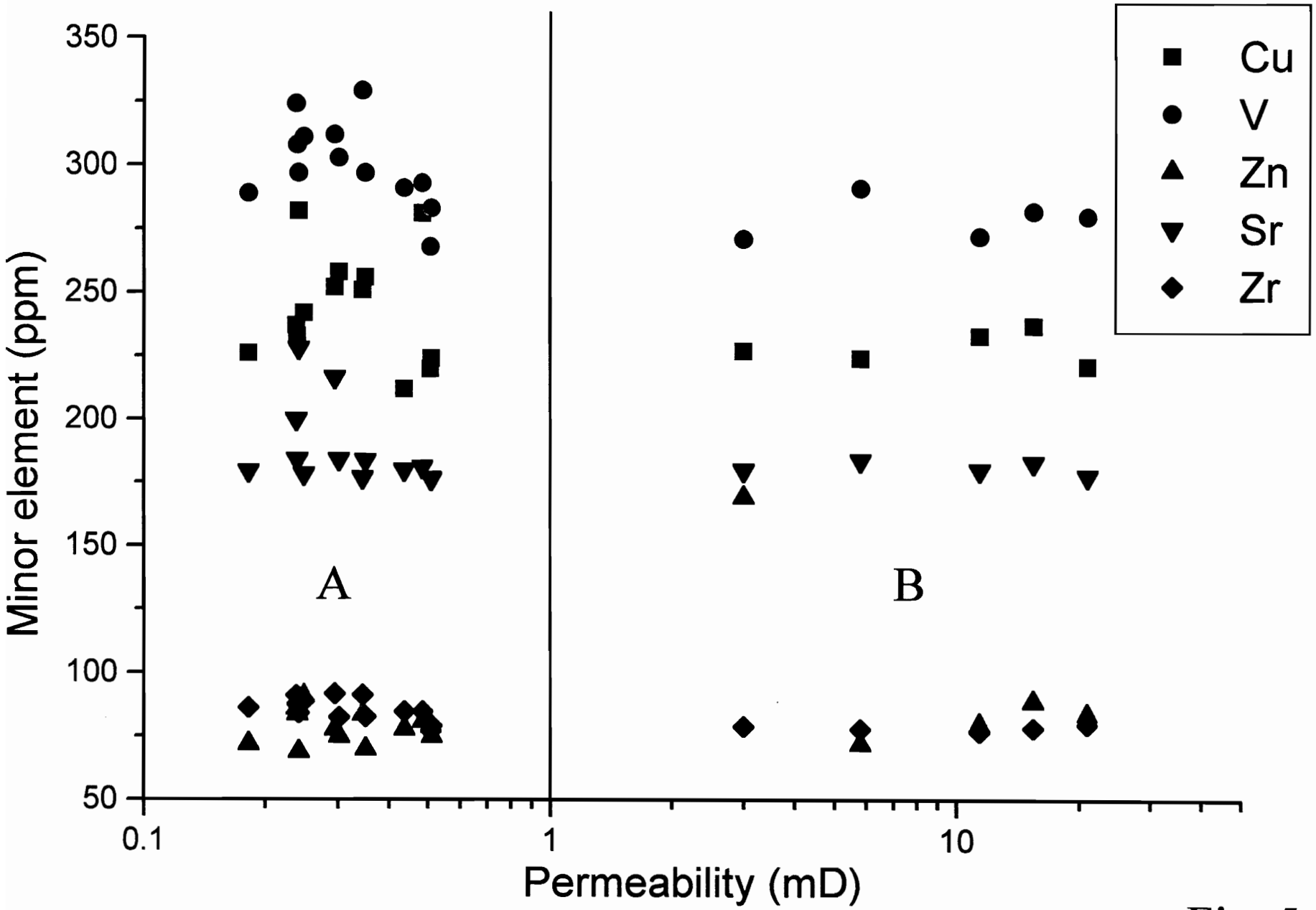
Minor element (ppm)
350
300
250
200
150
100
50
0.1
1
10
Permeability (mD)
A
B
Cu
V
Zn
Sr
Zr

Fig. 5.21

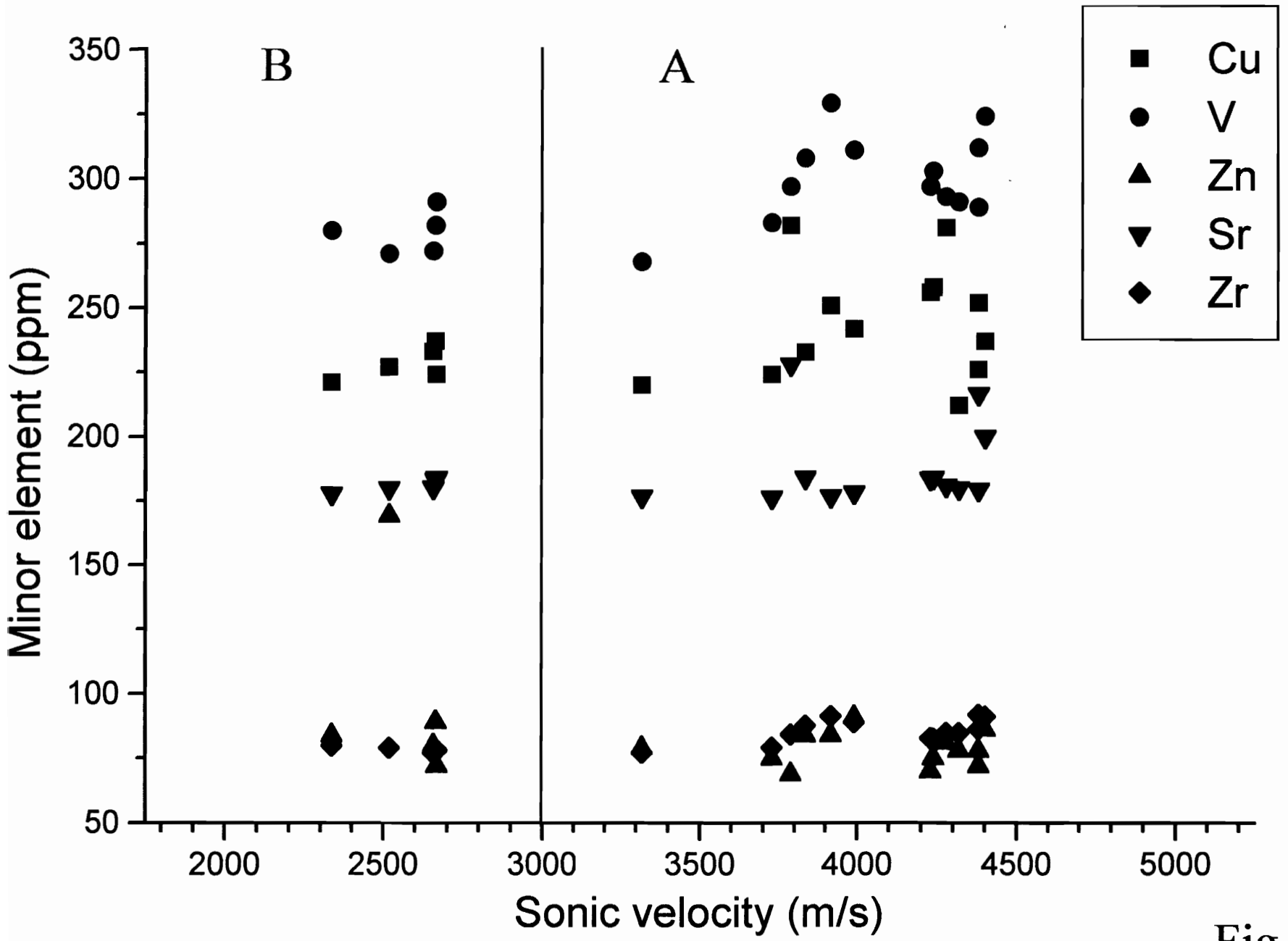
B
A
Cu
V
Zn
Sr
Zr
Minor element (ppm)
350
300
250
200
150
100
50
2000
2500
3000
3500
4000
4500
5000
Sonic velocity (m/s)

Fig. 5.22

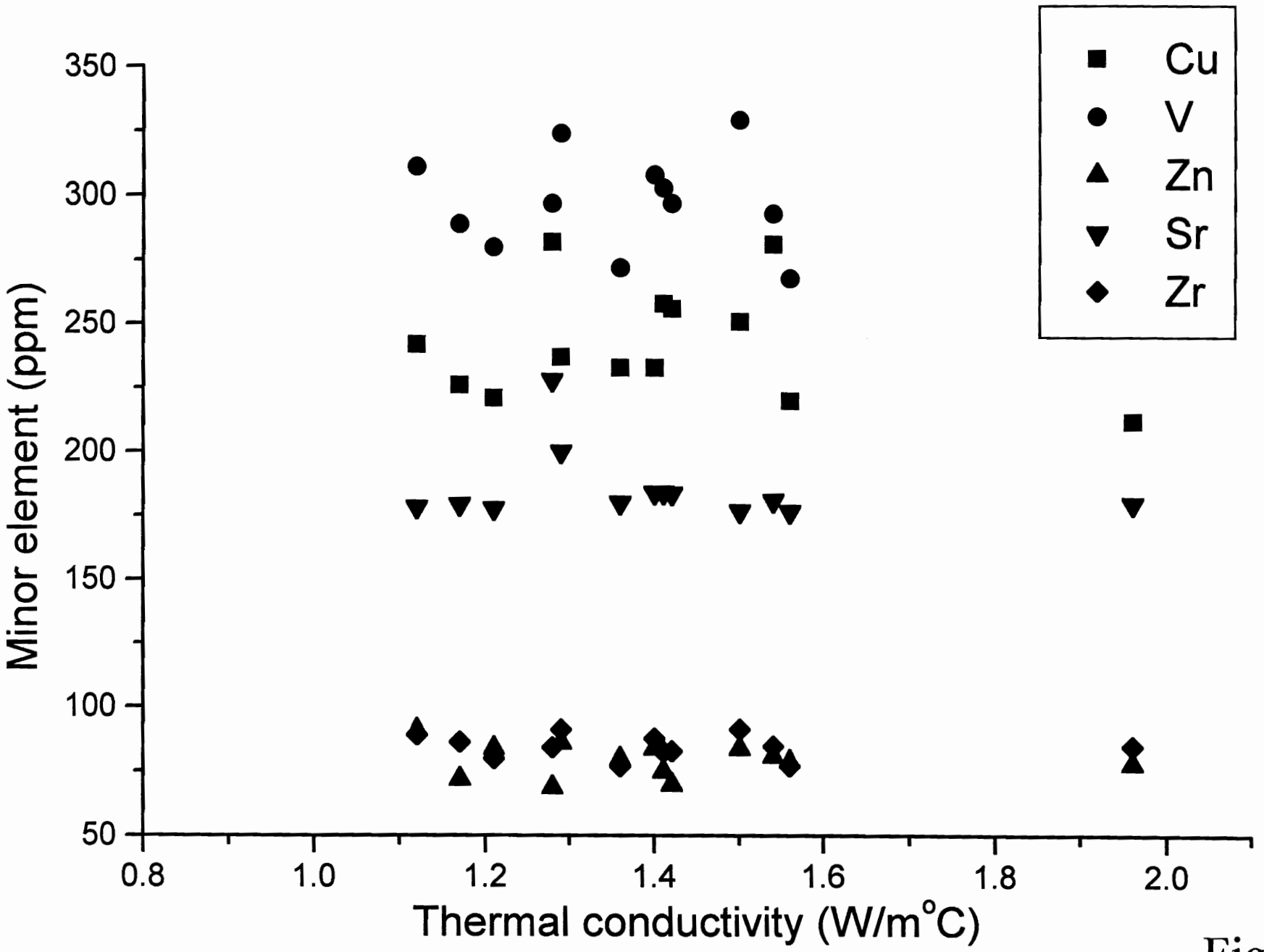
Cu
V
Zn
Sr
Zr
Minor element (ppm)
350
300
250
200
150
100
50
0.8
1.0
1.2
1.4
1.6
1.8
2.0
Thermal conductivity (W/m°C)

Fig. 5.23

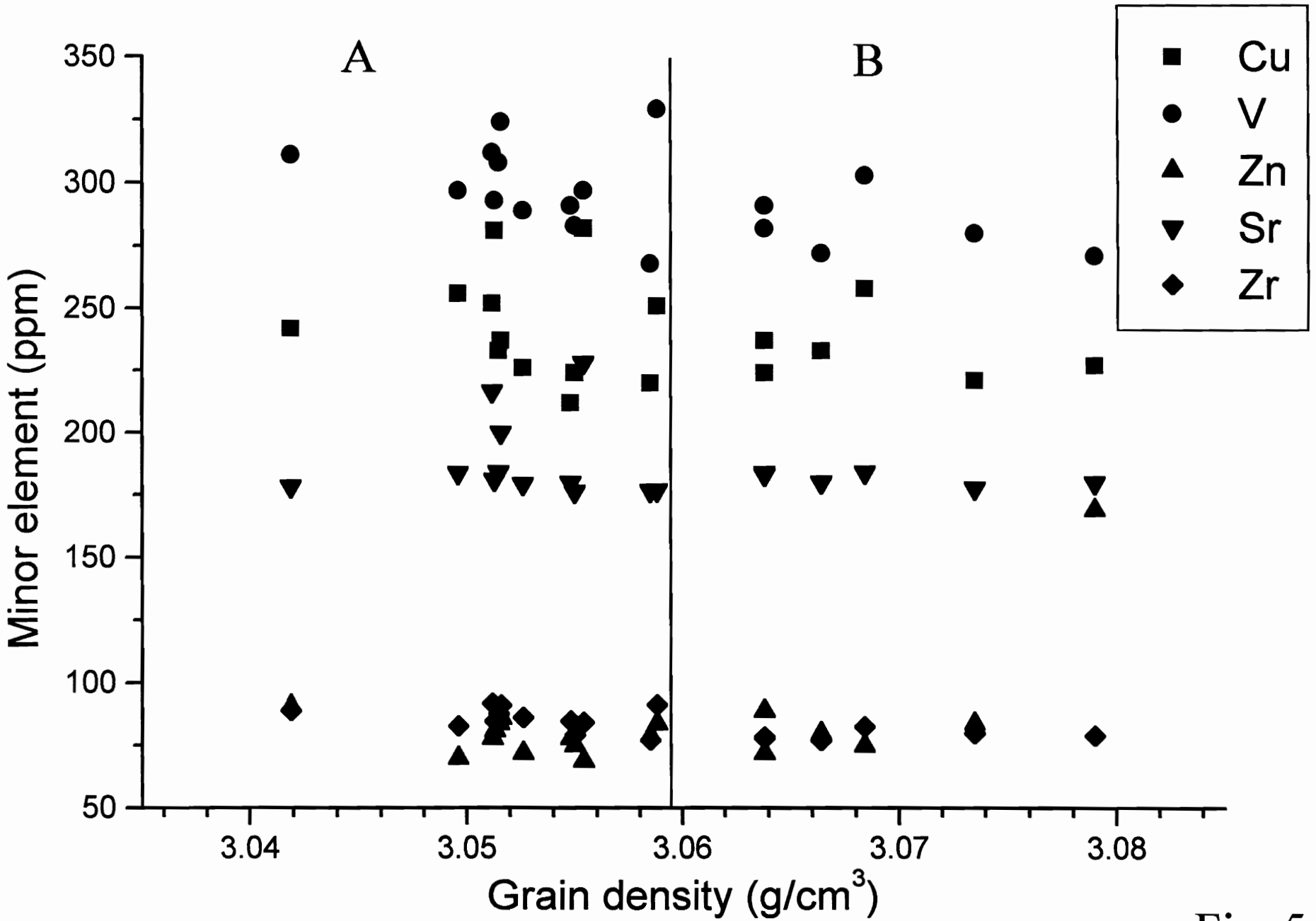
A
B
Cu
V
Zn
Sr
Zr
Minor element (ppm)
350
300
250
200
150
100
50
3.04
3.05
3.06
3.07
3.08
Grain density (g/cm3)

Fig. 5.24

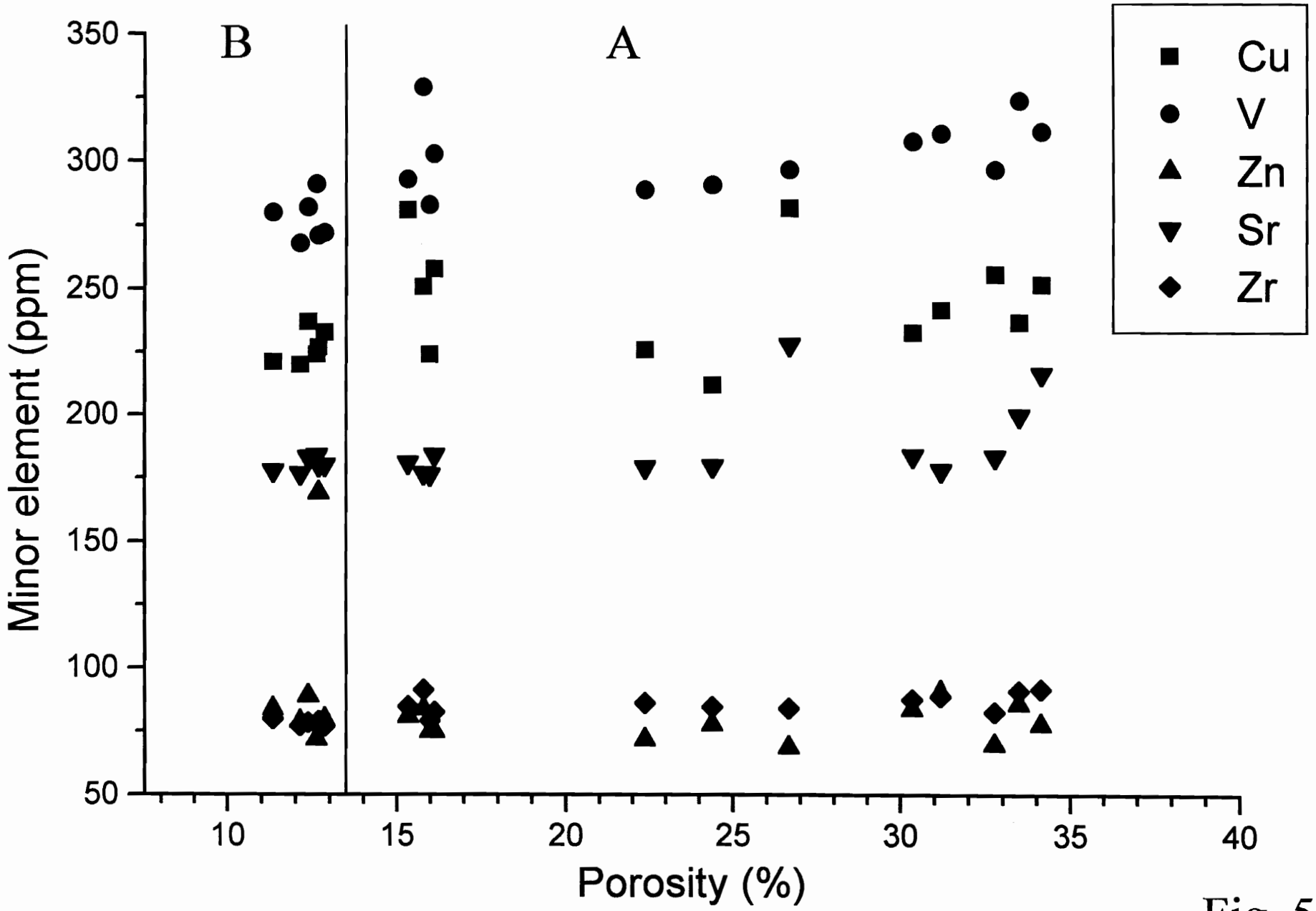
B
A
Cu
V
Zn
Sr
Zr
Minor element (ppm)
350
300
250
200
150
100
50
10
15
20
25
30
35
40
Porosity (%)

Fig. 5.25

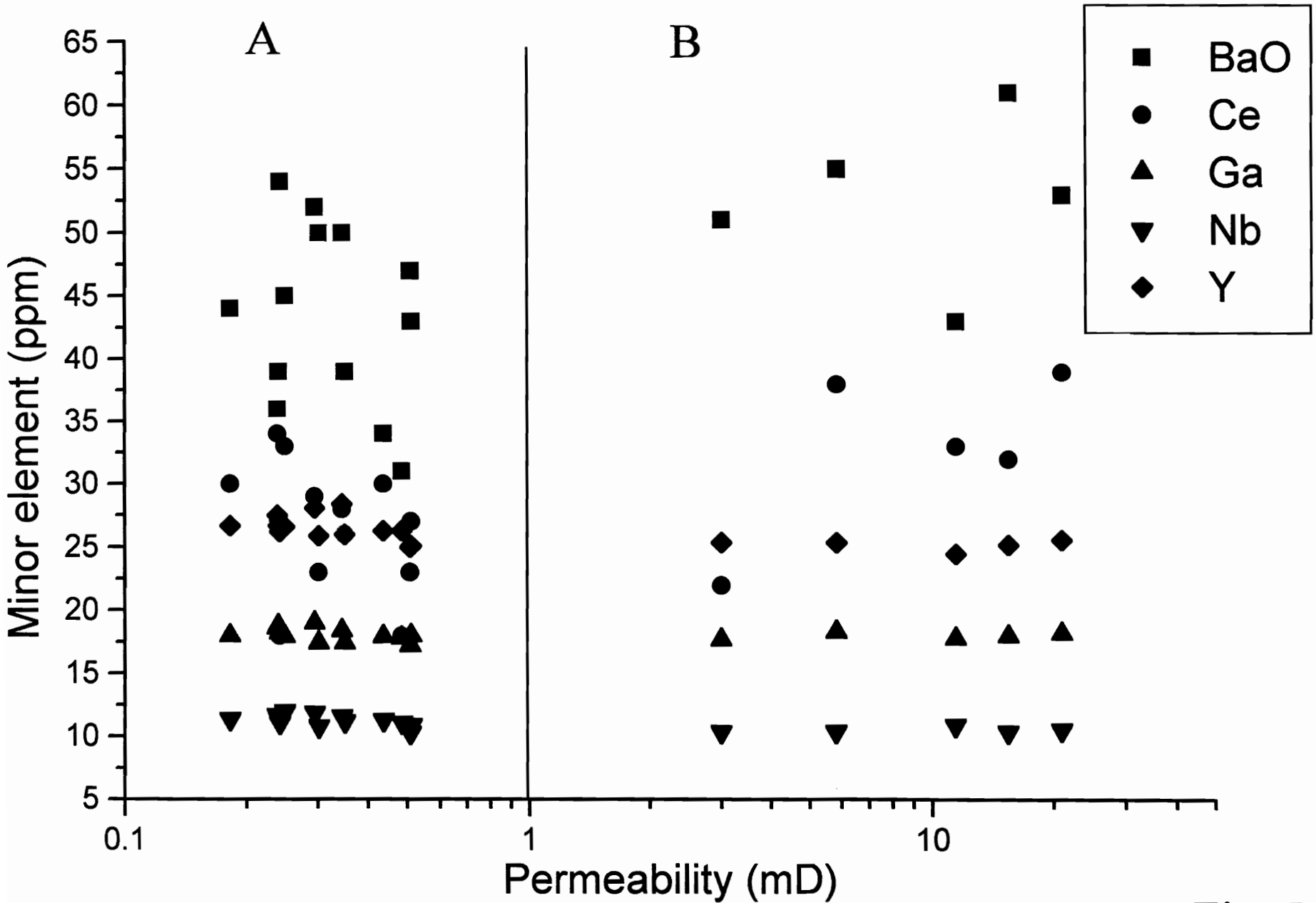
A
B
BaO
Ce
Ga
Nb
Y
Minor element (ppm)
65
60
55
50
45
40
35
30
25
20
15
10
5
0.1
1
10
Permeability (mD)

Fig. 5.26

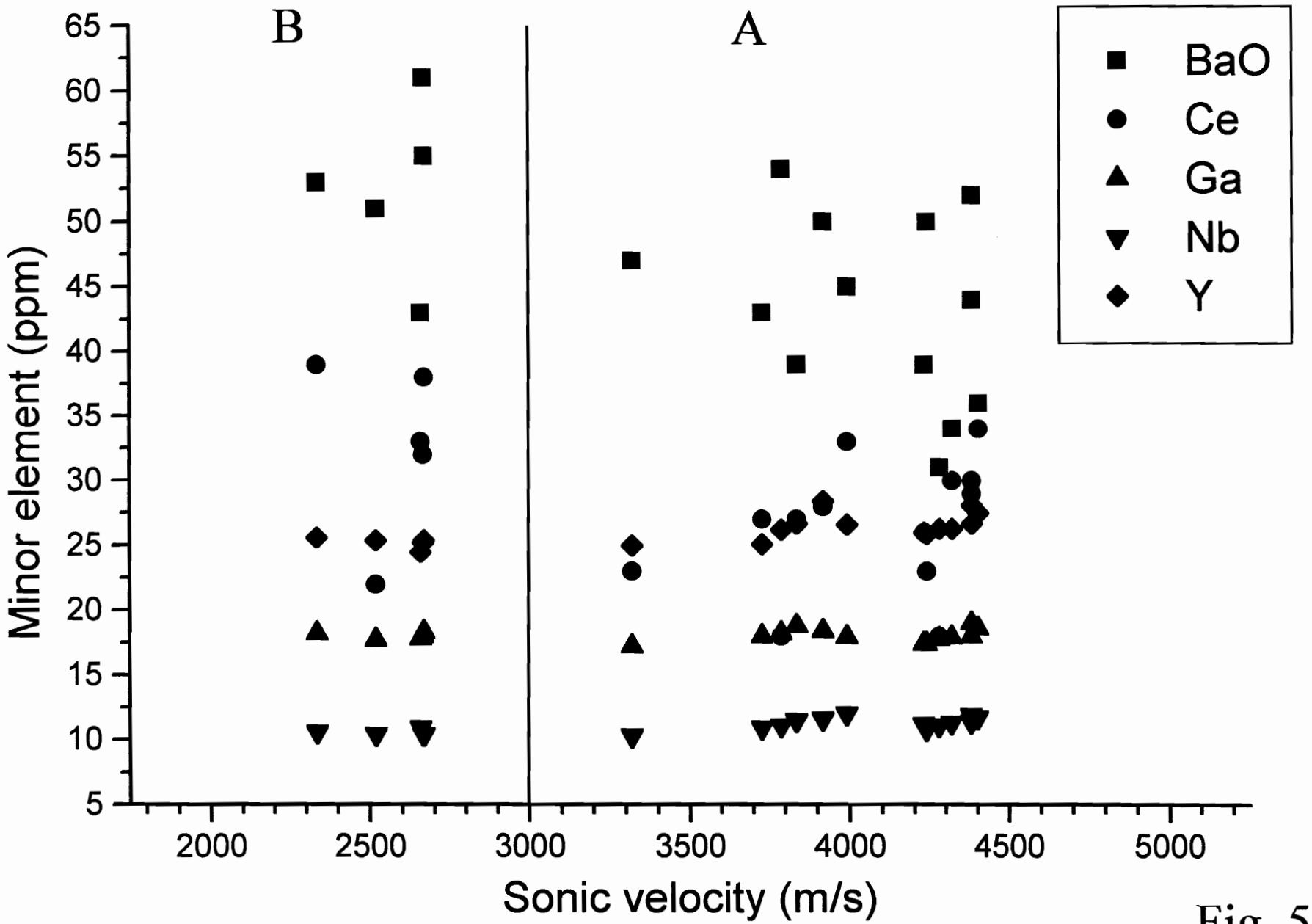
B
A
BaO
Ce
Ga
Nb
Y
Minor element (ppm)
65
60
55
50
45
40
35
30
25
20
15
10
5
2000
2500
3000
3500
4000
4500
5000
Sonic velocity (m/s)

Fig. 5.27

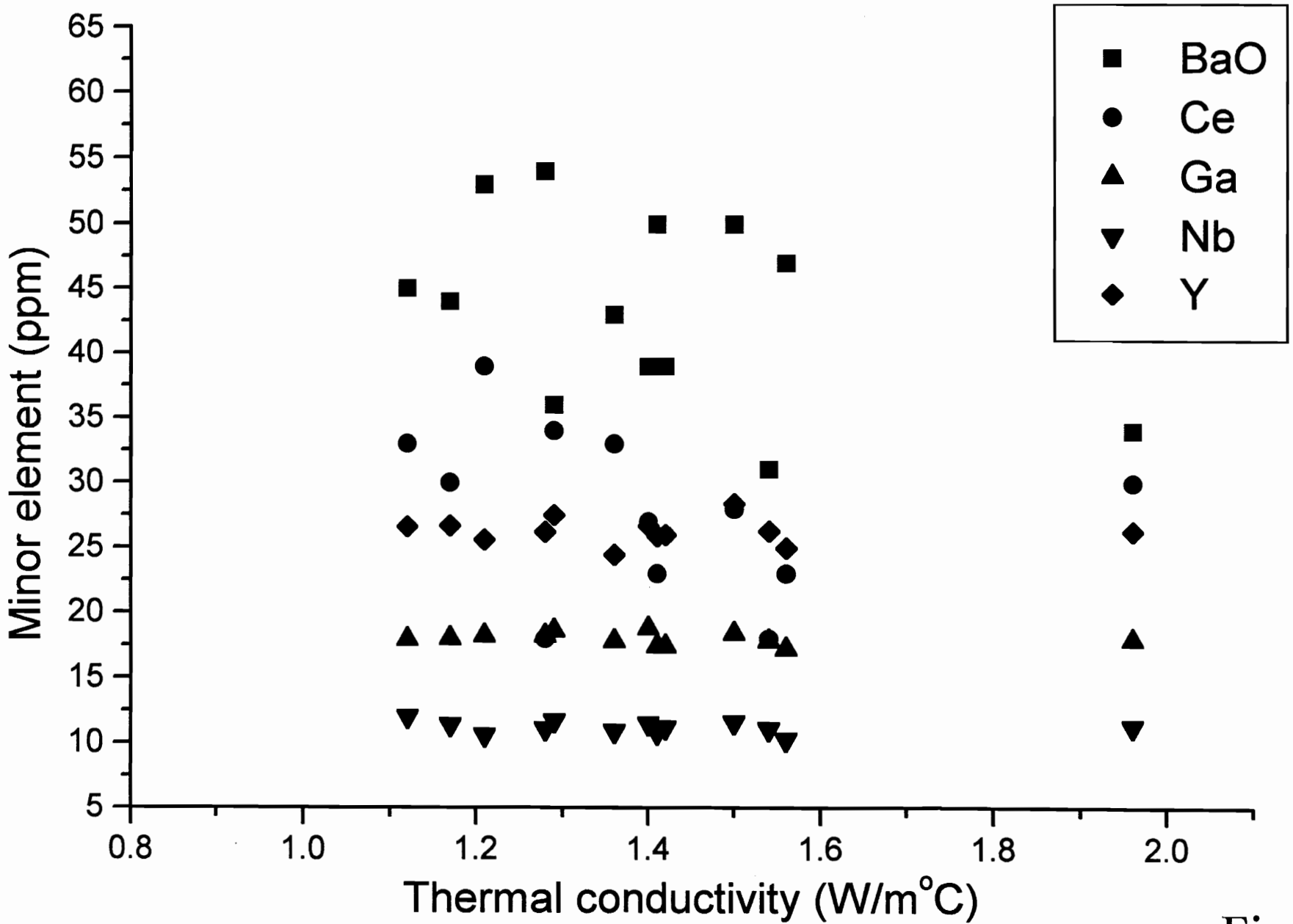
BaO
Ce
Ga
Nb
Y
Minor element (ppm)
65
60
55
50
45
40
35
30
25
20
15
10
5
0.8
1.0
1.2
1.4
1.6
1.8
2.0
Thermal conductivity (W/m°C)

Fig. 5.28

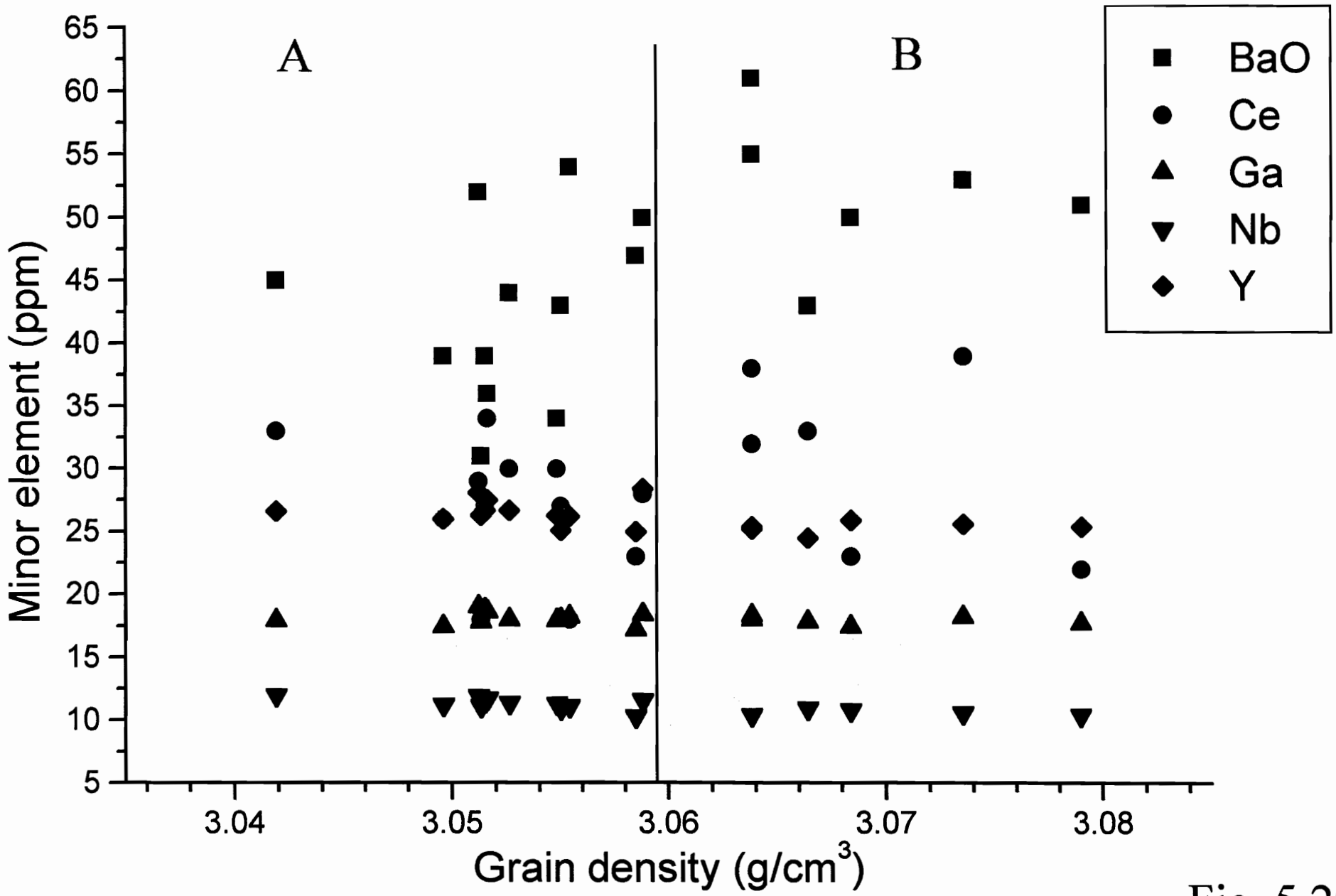
A
B
BaO
Ce
Ga
Nb
Y
Minor element (ppm)
65
60
55
50
45
40
35
30
25
20
15
10
5
3.04
3.05
3.06
3.07
3.08
Grain density (g/cm3)

Fig. 5.29

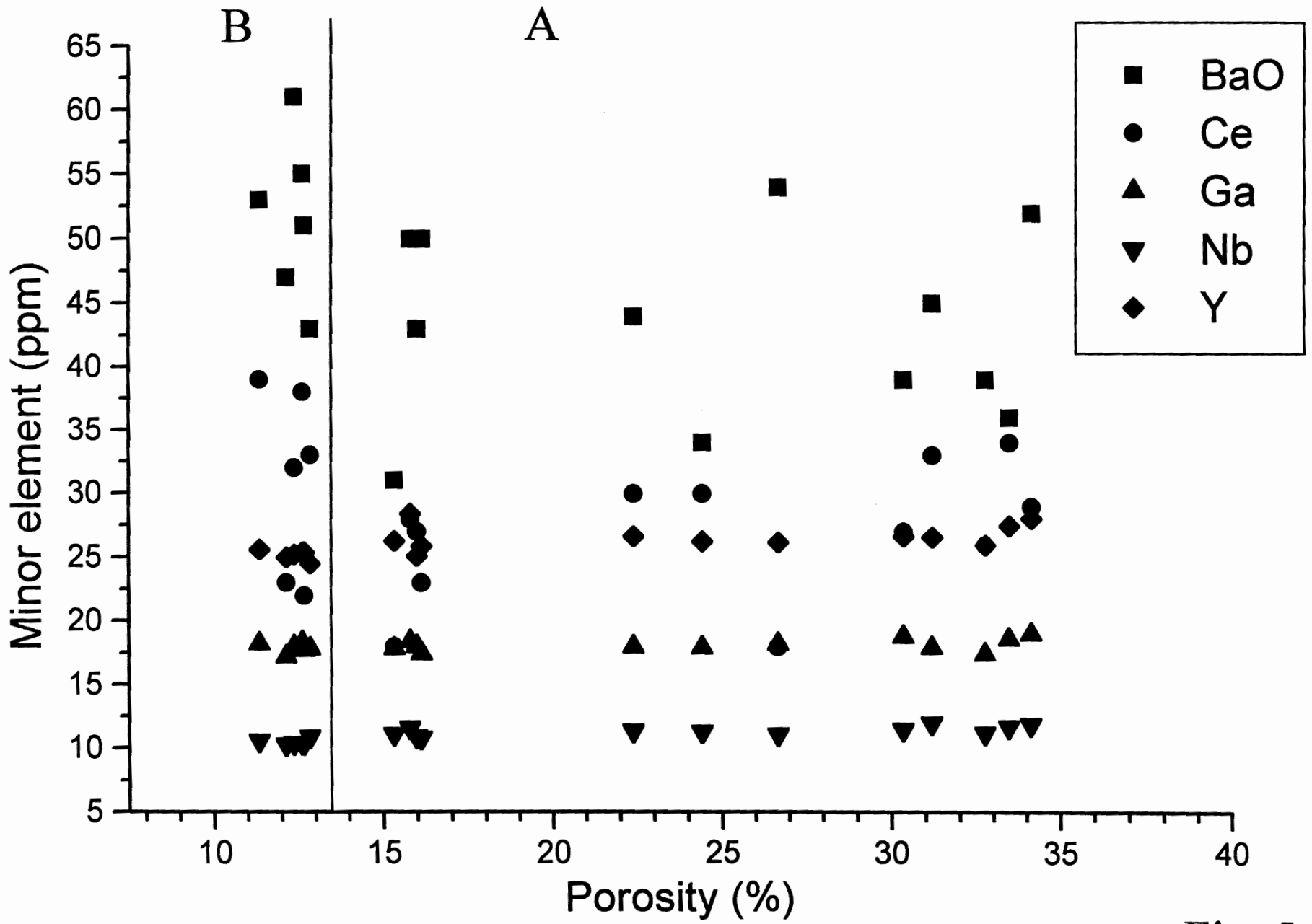
B
A
BaO
Ce
Ga
Nb
Y
Minor element (ppm)
Porosity (%)
65
60
55
50
45
40
35
30
25
20
15
10
5
10
15
20
25
30
35
40

Fig. 5.30

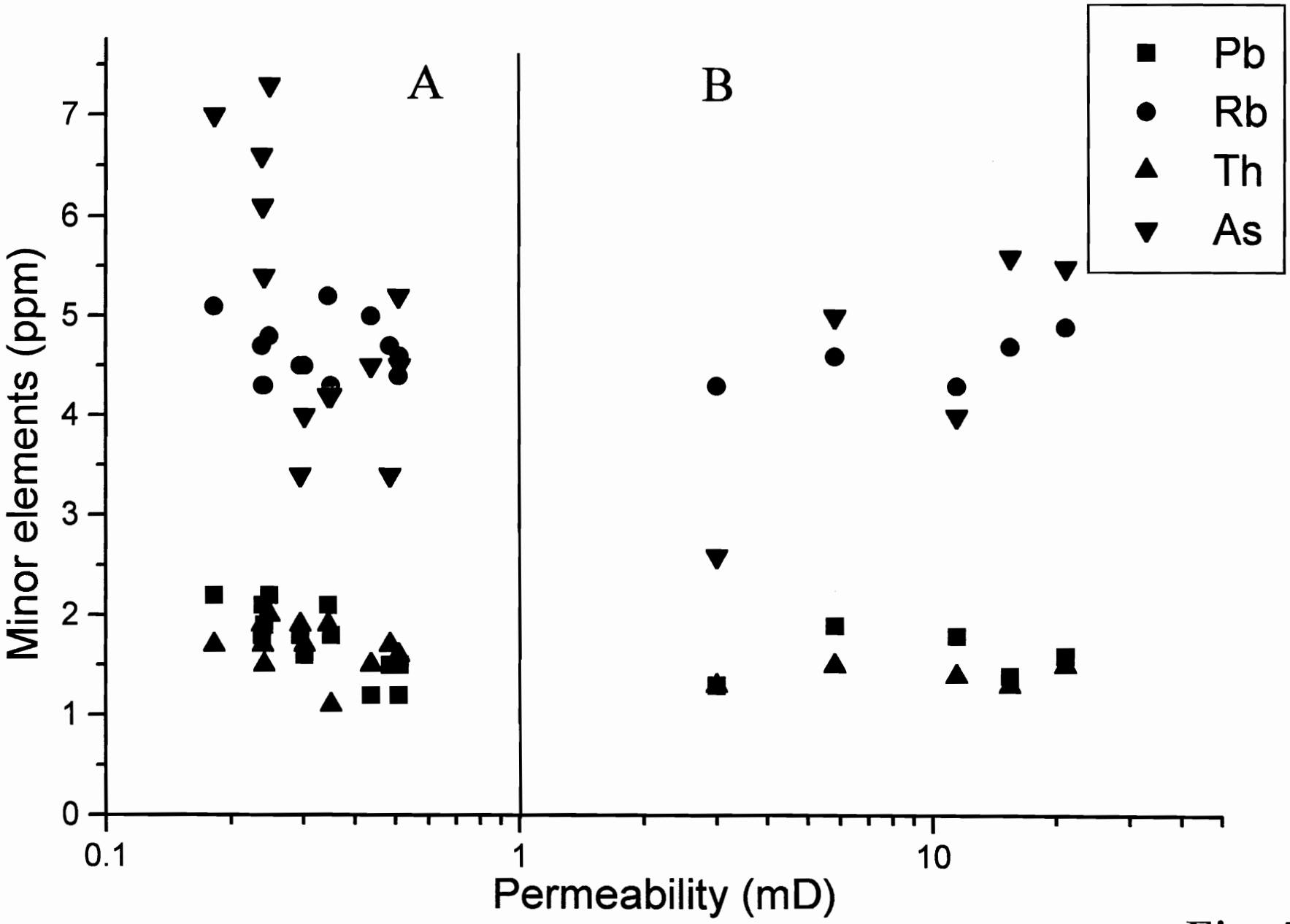
A
B
Pb
Rb
Th
As
Minor elements (ppm)
0
1
2
3
4
5
6
7
0.1
1
10
Permeability (mD)

Fig. 5.31

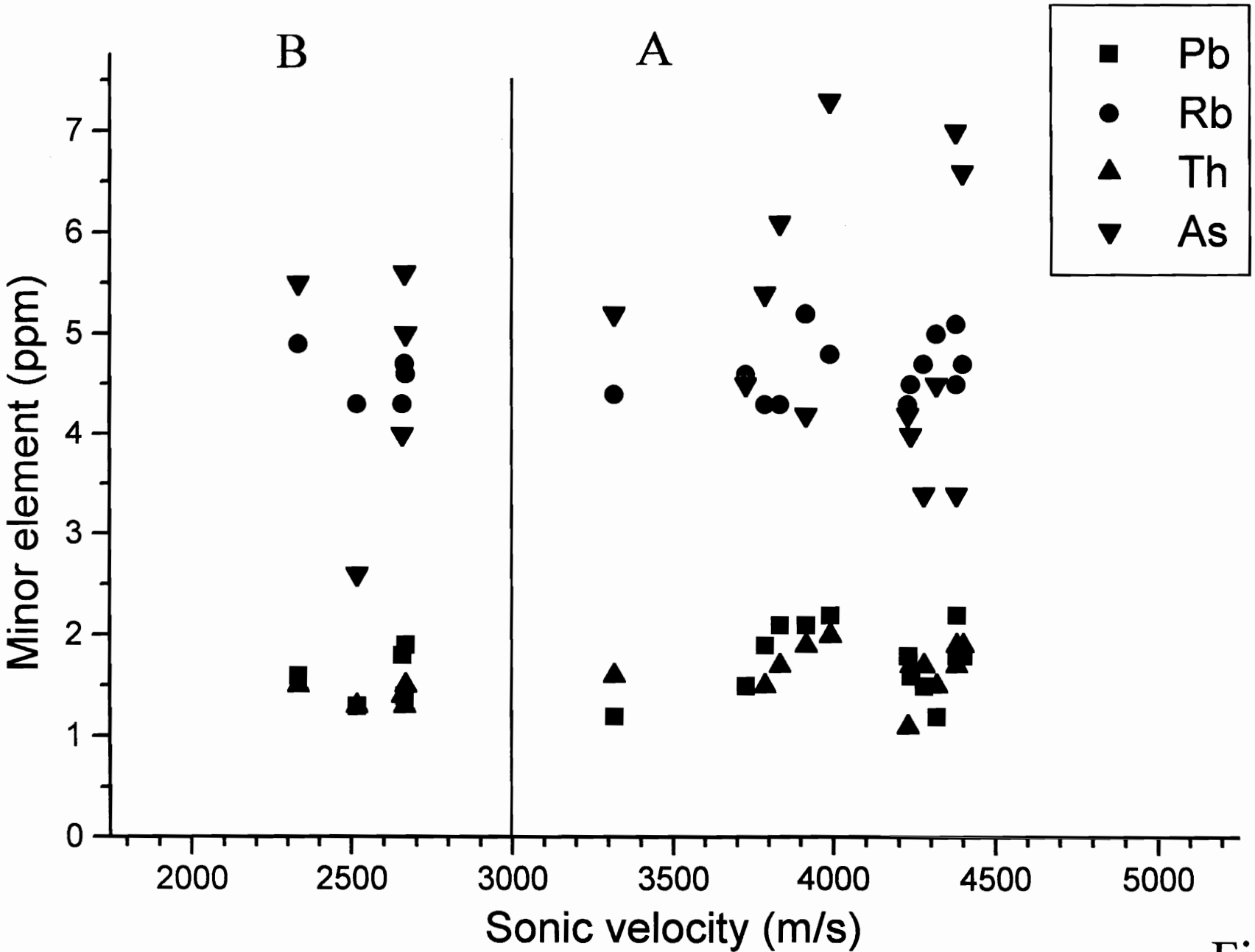
B
A
Pb
Rb
Th
As
Minor element (ppm)
0
1
2
3
4
5
6
7
2000
2500
3000
3500
4000
4500
5000
Sonic velocity (m/s)

Fig. 5.32

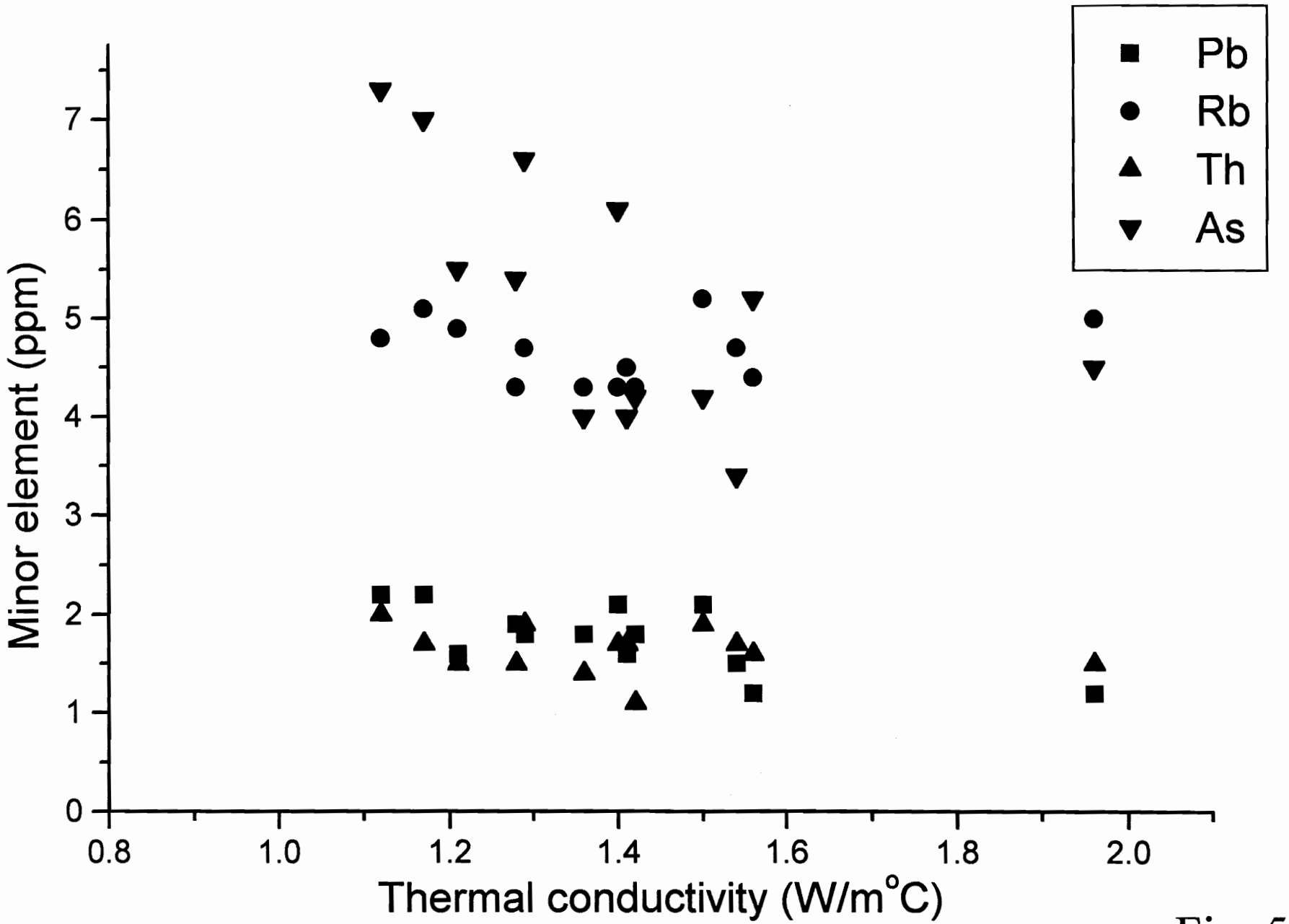
Pb
Rb
Th
As
Minor element (ppm)
0
1
2
3
4
5
6
7
0.8
1.0
1.2
1.4
1.6
1.8
2.0
Thermal conductivity (W/m°C)

Fig. 5.33

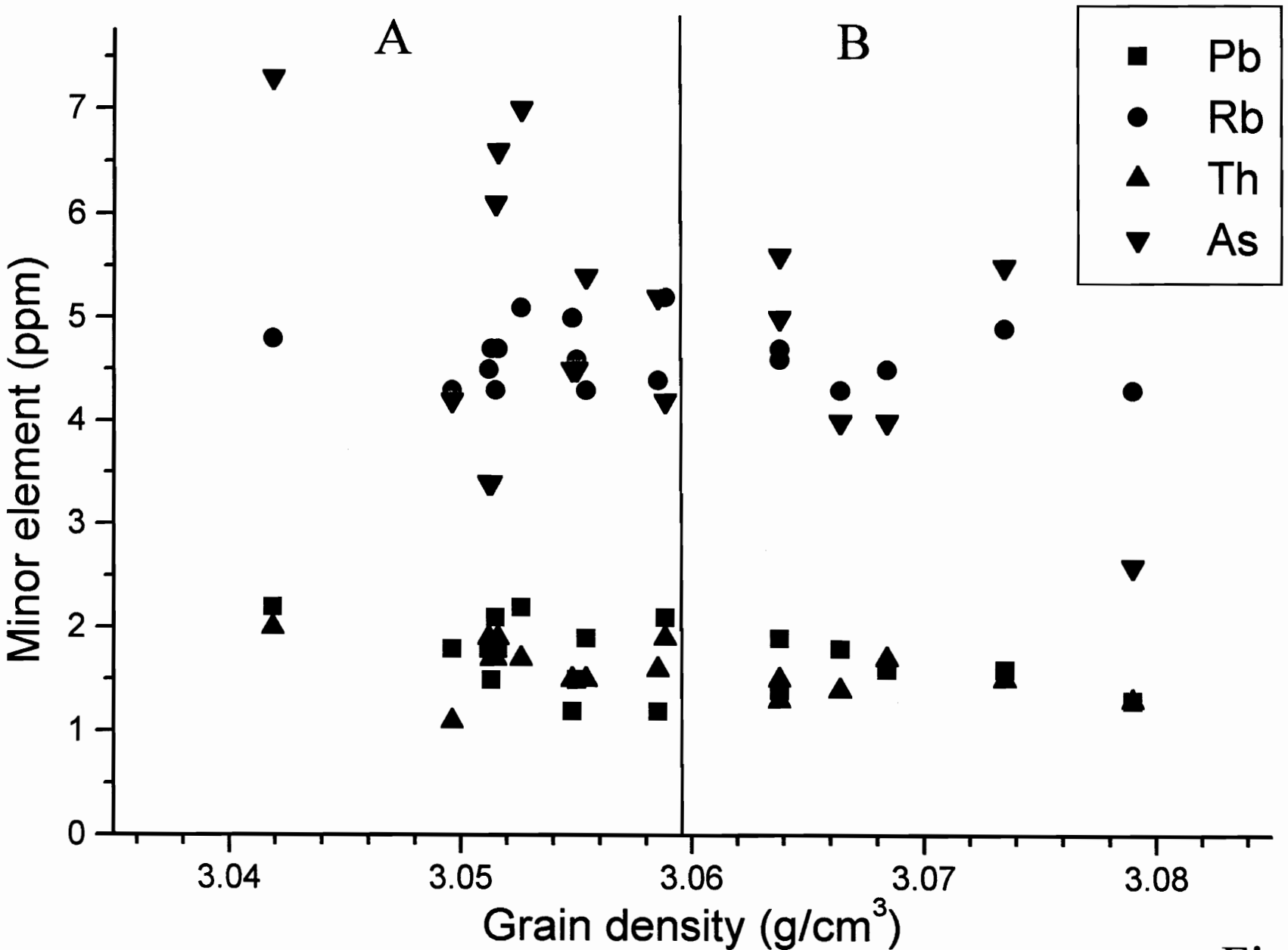
A
B
Pb
Rb
Th
As
Minor element (ppm)
0
1
2
3
4
5
6
7
3.04
3.05
3.06
3.07
3.08
Grain density (g/cm3)

Fig. 5.34

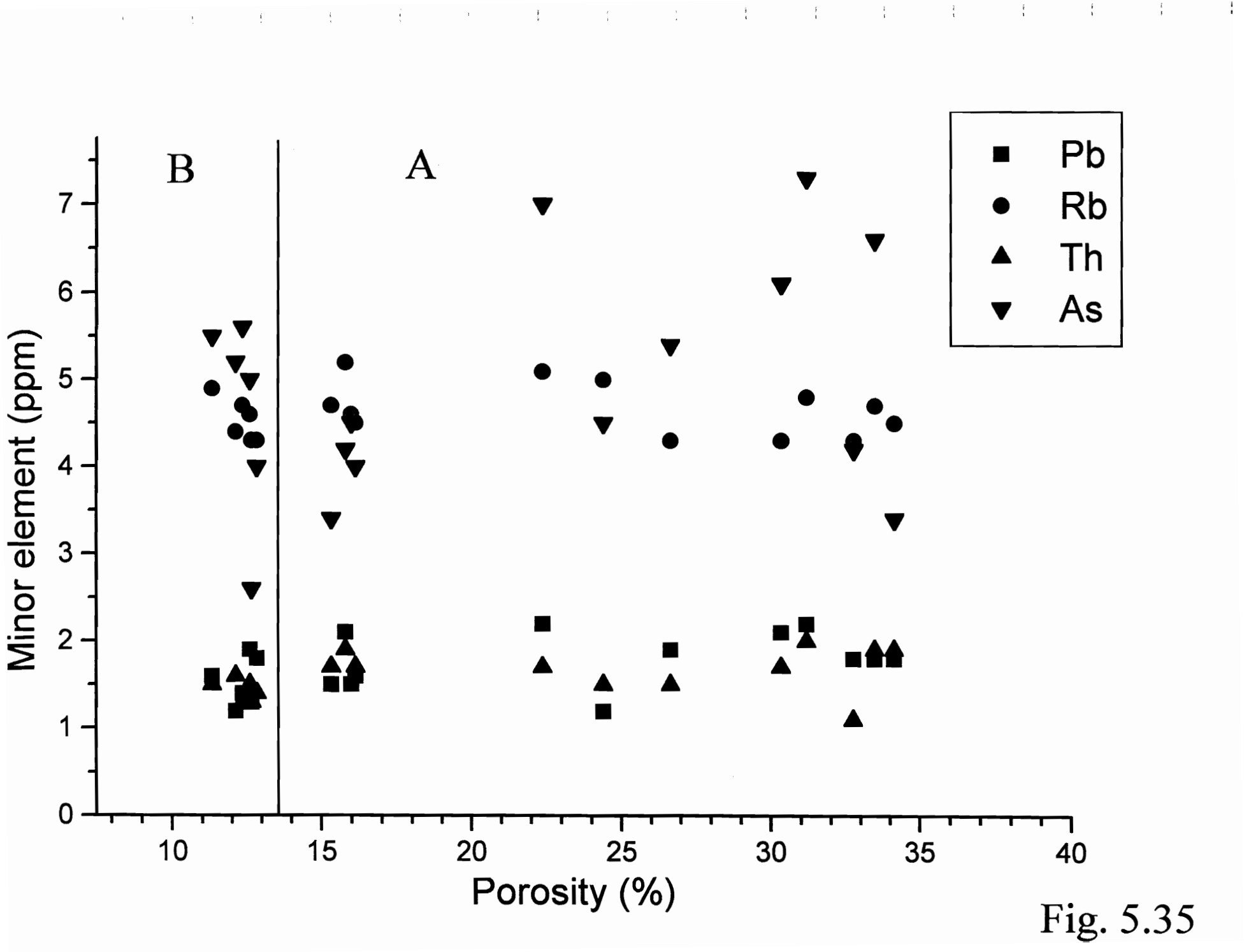
B
A
Pb
Rb
Th
As
Minor element (ppm)
Porosity (%)
0
1
2
3
4
5
6
7
10
15
20
25
30
35
40

Fig. 5.35